NUCARS Modeling of a Freight Locomotive with Steerable Trucks

by

Michael DeLorenzo

Thesis submitted to the Faculty of the

Virginia Polytechnic Institute and State University

in partial fulfillment of the requirements for the degree of

Master of Science

in

Mechanical Engineering

APPROVED:

_____

Mehdi Ahmadian, Chairman

_____ _____

Harry H. Robertshaw Norman S. Eiss

May 20, 1997
Blacksburg, Virginia

Keywords: NUCARS, Locomotive, Steerable, Trucks, Bogies, Parametric

NUCARS Modeling of a Freight Locomotive with Steerable Trucks

by

Michael DeLorenzo

Mehdi Ahmadian, Chairman

Mechanical Engineering

The rail dynamics modeling package NUCARS has been used extensively to model freight cars. We have found that it can also be used effectively to model freight locomotives. This thesis discusses the development of a NUCARS model to represent a six-axle freight locomotive equipped with steerable trucks. This includes separating it into a set of individual bodies, representing the suspension components as inter-body connections, and validation of the computer model. This model is then used to conduct a study of the impact on tangent track stability and curving performance of varying suspension parameters. It is found that the presence of damping in the system improves hunting stability, while increasing wheel conicity is harmful to stability and varying the flexicoiling stiffness has little effect. In curving, the clearances between the axles and truck frame are very important. Limiting these clearances in the steerable truck causes it to curve similar to a conventional straight locomotive truck and increases both the track force ratios and angles of attack. Increasing the wheel conicity increases an axle's tendency to align with the track and improves the locomotive's curving performance. The lateral stiffness of the inter-axle links and inter-motor links has little effect on the curving of the locomotive.

Acknowledgments

I would like to thank my advisor, Dr. Mehdi Ahmadian, for his guidance and time in teaching me about rail vehicles. I would also like to thank Dr. Harry Robertshaw and Dr. Norm Eiss for serving on my graduate committee and Dr. Charles Reinholtz for filling in on my defense. The financial support of the Department of Mechanical Engineering and GE Transportation Systems are greatly appreciated. I am grateful for both the financial support and the technical assistance provided by the Association of American Railroads. In addition, I appreciate Kim Jessup, Alison Eddy, and Alex Adler for supplying me with a place to live while I finished writing this thesis. I am also indebted to Stephanie Tepper, Doug Patterson, Kevin Philip, David and Truc DeLorenzo, Todd Manley and my parents for the support and distractions necessary to finish this work.

Contents

List of Figures

List of Tables

List of Variables

α = flange angle; angle of attack

μ = rail frictional coefficient

λ = wheel tread angle

Θ = Yaw angle

ω = yaw velocity

a = half the track gage or taping line width

d = width of rail base

f_H = hunting frequency

h = rail height

L = rail contact lateral force

N = rail contact normal force

R = wheel rolling radius

dR = change in rolling radius

V = longitudinal velocity; rail contact vertical force

V_{LAT} = lateral velocity

V_1, V_2 = longitudinal wheel velocity

x = longitudinal position

y = lateral displacement

Y = lateral displacement

Chapter 1

Introduction

Rail transportation remains the most cost effective method for moving passengers or freight between two locations connected by land. This is due to the low energy loss of the metal on metal contact between the wheels and rail. Since both surfaces are fairly rigid, there is little deformation. This allows the surfaces to roll past each other with little dissipation of energy. Once the vehicle has reached its traveling speed, little power is required to maintain that speed on tangent track; as a result, much of the energy loss of rail travel occurs during curving. In curving, when an axle is not positioned radial to the track, the velocity vectors of its wheels differ from the track direction by the angle of attack. The wheels are constrained to move along the track, however, so the actual velocities must be oriented tangential to the curve. This difference is accounted for by the wheels slipping sideways across the rail. This results in friction between the wheels and rail and removes kinetic energy from the locomotive. As a result, for the locomotive to curve at a continuous speed, energy must be added through its motors.

1.1 Steerable Locomotive Trucks

Steerable trucks attempt to reduce the frictional energy loss associated with curving. By forcing the end axles to yaw in opposite directions relative to the truck frame, they reduce the angles of attack and achieve improved radial alignment. This improves the velocity

orientation and reduces the amount of cross-track motion. As a result, less force resists the locomotive's motion through the curve.

In addition to reducing frictional energy loss, decreasing the axle angle of attack allows the wheels to safely achieve higher rail forces. This increases the range of safe curving speeds and reduces the likelihood of derailment.

1.2 Locomotive Modeling

The use of computers with fast processors has allowed real-time simulation of rail vehicle dynamic models. This allows a model's states to be determined at all times and on all sections of a track. Due to the complexity of the dynamic equations that describe rail vehicle motion, most computer models have focused on the dynamics of an individual wheelset or of an individual truck [1-4]. These include models focusing on tangent track dynamics [1] and accounting for nonlinear effects [2,4]. Some projects have attempted to model the dynamics of an entire locomotive [5,6]. These models have been limited, however, as they omit many types of motion from the different bodies.

One software package that was developed specifically to model rail vehicles is NUCARS (New and Untried Car Analytic Regime Simulation) [7]. It was created by the Association of American Railroads (AAR) for freight car modeling and has become the industry standard for doing so. Until recently, however, NUCARS has not been used to model freight locomotives. One of the first NUCARS locomotive models was developed by Ahmadian in 1993. His model was of a six-axle freight locomotive with conventional trucks and featured 15 bodies and 69 degrees of freedom. Since then, we have established

guidelines for using NUCARS to model freight locomotives [8]. In addition, I have developed a NUCARS model of a freight locomotive equipped with steerable trucks. This model includes kinematic suspension links between the axles and truck frames, and is the first one to do so.

1.3 Parametric Testing

One use of computer modeling is in determining a system's parametric sensitivity. By varying a specific parameter while repeatedly running the model over a section of track, the effect of that parameter on the vehicle's performance is determined. This information can then be used to select the suspension characteristics that give the desired performance.

A few projects have investigated parametric sensitivity [9-11]. They determined parametric effects on performance by analyzing the system dynamic equations [9,10] or experimental test data [11]. Due to the complexity of the dynamic equations and the costs of experimental testing, only a few parameters were investigated. Using a validated computer model to perform the parametric testing allows simplified parametric variation. This greatly reduces the costs associated with experimental testing. In addition, the model complexity can be much greater than for using the system dynamic equations. This allows more parametric values to be tried and can achieve improved component tuning.

1.4 Thesis Topic

This thesis will discuss the development of a NUCARS model for a six-axle freight locomotive equipped with steerable trucks. It will also cover the use of this model to investigate the locomotive's parametric sensitivity. Chapter 2 will discuss rail dynamics on tangent and curved track. This includes axle and truck hunting, derailment, curving, and truck components. Chapter 3 will deal with the development of the NUCARS steerable model. It will include representation of the different components as individual bodies and connections, input due to track shape, and the geometry of the wheel/rail connections. Chapter 4 will cover the validation of the NUCARS model. This includes the tangent and curved track runs and how they demonstrate that the model is a good representation of the locomotive. Chapter 5 deals with the parametric sensitivity analysis conducted on tangent and curved sections of track. It discusses different parameters' effect on the locomotive's stability and curving performance.

Chapter 2

Truck Dynamics

The contact that occurs between the wheels and the rail is the principal driving force in rail dynamics. The wheels follow the path of the track as it goes through straight sections and curves. Derailment occurs when the wheels are no longer able to follow the path of the track and contact with the rails is broken. This chapter will discuss how a rail vehicle, in particular a locomotive bogie or truck, behaves on straight and curved track sections and the paths to derailment.

2.1 Tangent Track Dynamics

A locomotive traveling on a tangent (or straight) section of track exhibits a unique behavior. This is due to the conical shape of its wheels, which taper toward the outside of the track, causing a wheel's rolling radii to increase as it moves toward the outside of the track. Figure 2.1 shows a railway wheelset, displaying the conical wheel profiles and the wheel flanges.

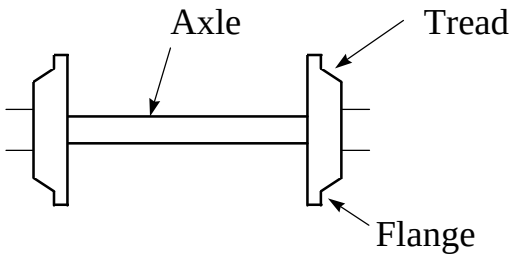

Figure 2.1 Locomotive wheelset with profiled wheels

2.1.1 Axle Hunting

Figure 2.2 shows the path of an axle experiencing coupled lateral and yaw oscillation, commonly referred to as hunting. Hunting occurs due to the conical profile of railway wheels, which is used to maintain the vehicle in the center of the rails and to assist it in negotiating curves.

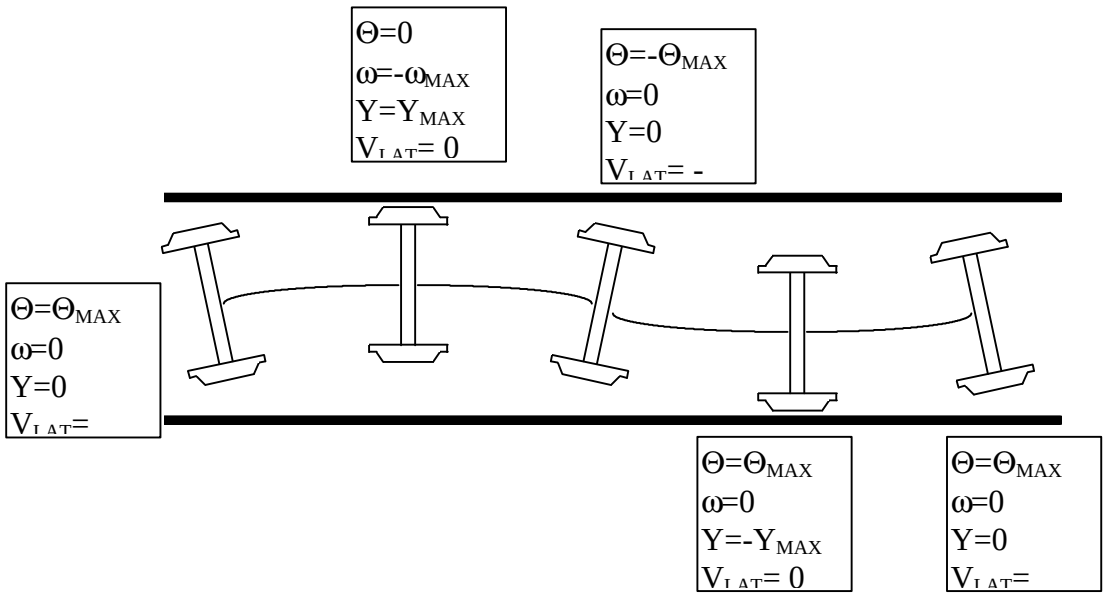

Figure 2.2 Path of axle hunting

When a wheelset is displaced to one side, the wheel on that side increases its rolling radius by moving outward on the track. The wheel on the other side travels toward the center of the track, decreasing its rolling radius. This produces a difference in the rolling radii of the two wheels. Since they are rigidly connected together through the axle and must spin at the same rate, the forward velocity of the first wheel is larger than the forward velocity of the second wheel. This causes a rotation (yaw) of the axle toward the

center of the track, with the yaw angle continuing to increase until the axle center moves back to the middle of the track.

Once there, the wheel radii are again equal, so that axle rotation ceases and the yaw angle is a maximum. This yaw angle keeps the axle moving across the track center and toward the opposite side. A reversed difference in wheel radii is produced, causing the axle to yaw in the opposite direction. This counter yaw reduces the axle's angle of attack until the axle is perpendicular to the track. This is the axle's maximum lateral displacement. This is also the maximum difference between the rolling radii, and the axle again turns toward the center of the track. It moves laterally back to the middle of the track, where the yaw angle is again a maximum. This causes the axle to again move laterally, yaw due to difference in rolling radii, and return to the center of the track. This motion continues, with the axle oscillating from side to side in coupled lateral and yaw motion.

The type of motion described above is referred to as axle hunting. Below a certain speed, called the critical speed, it appears as a damped sinusoidal oscillation along the track centerline. Above this critical speed, the motion is undamped and the displacement increases until the wheel flanges contact the rails. At this point, the axle slams back and forth between the wheel flanges creating large contact forces with the track. As the speed increases, the force of the wheels hitting the rails becomes large enough to cause rail damage and eventually can lead to derailment.

2.1.2 Hunting Frequency

Axle hunting appears as an oscillation of the axle back and forth across the track in a nearly sinusoidal path. If this motion is assumed to be sinusoidal, the motion can be described with two harmonic equations. Solution of these equations leads to a formula for the frequency of the hunting motion in terms of the vehicle speed and track parameters. Figure 2.3 shows a locomotive wheelset and the sign convention used to model the harmonic hunting motion, and is followed by a derivation of the axle hunting frequency.

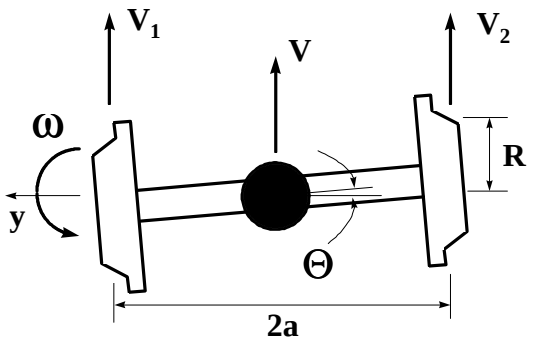

V = velocity of axle c.g.
V_1, V_2 = velocities of wheels
y = lateral displacement
Θ = axle yaw angle relative to track
ω = angular velocity about y-axis
a = half the taping line width
R = wheel rolling radius

Figure 2.3 Sign convention used to describe axle hunting motion

The forward velocity of the axle center of gravity is the product of its angular velocity, ω, and the wheel nominal radius, R, i.e.,

$$V = Rw \qquad (2.1)$$

For a positive axle yaw velocity, ω, the velocity of the left wheel decreases and the velocity of the right wheel increases due to lever arm, a, which is half of the distance between the wheel taping lines (the lines of rail contact on the wheels).

$$V_1 = V - \dot{\Theta}a \quad \textbf{(2.2a)}$$

$$V_2 = V + \dot{\Theta}a \quad \textbf{(2.2b)}$$

Due to the wheel conicity, a lateral shift of the axle center of gravity in the positive y direction increases the rolling radius of the left wheel, shown in Figure 2.4, and decreases the rolling radius of the right wheel.

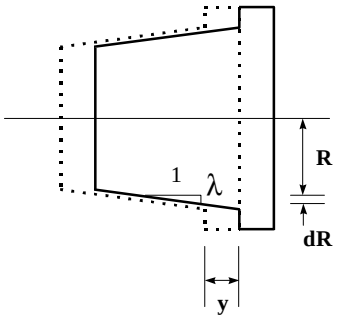

λ = wheel tread angle
y = lateral displacement
R = wheel rolling radius
dR = change in rolling radius

Figure 2.4 Wheel radius change due to lateral wheel shift

This increases the velocity of the left wheel, and decreases the velocity of the left wheel.

$$V_1 = (R + l\ y)w \quad \textbf{(2.3a)}$$

$$V_2 = (R - l\ y)w \quad \textbf{(2.3b)}$$

Substituting Eq. 2.1 into Eq. 2.3 yields

$$V_1 = (R + l\ y)\ V/R \quad \textbf{(2.4a)}$$

$$V_2 = (R - l\ y)\ V/R \quad \textbf{(2.4b)}$$

Then, setting Eq. 2.2b equal to Eq. 2.4b results in

$$V_2 = V + \dot{\Theta}\, a = (R - l\ \ a)\, V/R$$

$$V + \dot{\Theta}\, a = V - \frac{V l\ \ y}{R}$$

$$\dot{\Theta} = -\left(\frac{V l}{aR}\right) y \qquad \textbf{(2.5)}$$

Next, we assume that the hunting motion is sinusoidal, as shown in Figure 2.2, and we note that the lateral position, y, lags the yaw angle, θ, by ¼ wavelength or 90°. This allows us to define these variables as

$$y = Y_{MAX} \sin(2\pi f_H x) \qquad \textbf{(2.6a)}$$

$$\Theta = \Theta_{MAX} \cos(2\pi f_H x) \qquad \textbf{(2.6b)}$$

where f_H is the hunting frequency.

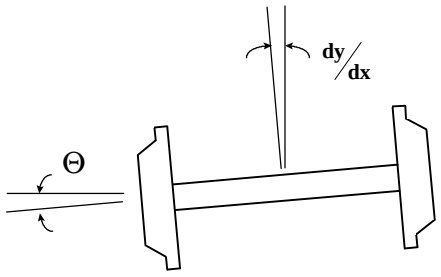

Figure 2.5 Trajectory of wheelset

We note in Figure 2.5 that the trajectory of the axle, dy/dx, is equal to the axle yaw angle, Θ.

$$dy/dx = \Theta \qquad \textbf{(2.7)}$$

But, Eq. 2.5 is in terms of the time derivative of the axle yaw angle $d\Theta/dt$. We can put Eq. 2.7 in terms of its time derivative using the velocity relationship

$$\mathbf{V = dx/dt} \tag{2.8}$$

Starting with Eq. 2.7, we use the chain rule to express the axle yaw angle in terms of the time derivative of lateral displacement

$$\Theta = \mathbf{dy/dx}$$
$$\Theta = \mathbf{dy/dt}\ \mathbf{dt/dx}$$
$$\Theta = \frac{1}{\mathbf{V}}\mathbf{dy/dt} \tag{2.9}$$

Taking the time derivative of this equation and equating it to Eq. 2.5, we arrive at a dynamic equation describing axle hunting.

$$\dot{\Theta} = \frac{1}{\mathbf{V}}\mathbf{d^2y/dt^2}$$
$$\dot{\Theta} = \frac{1}{\mathbf{V}}\mathbf{d^2y/dt^2} = -\left(\frac{\mathbf{Vl}}{\mathbf{aR}}\right)\mathbf{y}$$

$$\mathbf{d^2y/dt^2} + \left(\frac{\mathbf{V^2l}}{\mathbf{aR}}\right)\mathbf{y} = \mathbf{0} \tag{2.10}$$

Returning to the equation for the assumed lateral motion (Eq. 2.6a), we take the second derivative with respect to time.

$$\mathbf{y} = \mathbf{Y_{MAX}}\ \mathbf{sin}\left(2\,\pi\ f_H\ \mathbf{x}\right)$$
$$\mathbf{dy/dt} = \left(2\,\pi\ f_H\right)\mathbf{Y_{MAX}}\ \mathbf{cos}\left(2\,\pi\ f_H\ \mathbf{x}\right)$$
$$\mathbf{d^2y/dt^2} = -\left(2\,\pi\ f_H\right)^2\ \mathbf{Y_{MAX}}\ \mathbf{sin}\left(2\,\pi\ f_H\ \mathbf{x}\right) \tag{2.11}$$

This second derivative (Eq. 2.11) and the lateral displacement equation (Eq. 2.6a) are substituted into the axle hunting dynamic equation (Eq. 2.10). The resulting relation is then solved to determine an expression for the frequency of the hunting motion in terms of the forward velocity and track parameters (Eq. 2.12).

$$-\left(2\pi f_{HX}\right)^2 Y_{MAX} \sin\left(2\pi f_{HX}\right) + \left(\frac{V^2 l}{aR}\right) Y_{MAX} \sin\left(2\pi f_{HX}\right) = 0$$

$$\left(2\pi f_{HX}\right)^2 = \frac{V^2 l}{aR} \qquad \textbf{(2.12)}$$

$$f_H = \frac{V}{2\pi}\sqrt{\frac{l}{aR}}$$

2.1.3 Truck Hunting

The hunting motion of the axles generates forces on the truck frames at the coil spring locations. This causes the truck frames to displace laterally and in yaw relative to the locomotive platform. As a result, displacements in the truck frame/platform connections generate restraining forces on the truck frames. These forces accelerate the truck frames back to their nominal positions, where the non-zero velocities carry them past equilibrium and to the opposite side. They are then slowed by new restorative forces in the opposite directions, and are again accelerated back to their nominal positions. In this way, the truck frames also experience coupled oscillatory motion, or hunting. For low speeds, this appears as decaying harmonic motion due to the damping present in the connections. Above the critical speed, however, the damping isn't able to remove energy from the system quickly enough and the motion becomes unstable. The truck frames jolt back and

forth between the suspension stops causing damage to these elements and rider discomfort.

2.2 Curving Dynamics

2.2.1 Conventional Curving

Rail vehicles use two different methods for negotiating curved sections of track. Shallow curves are negotiated with lateral wheel displacement, which produces a difference in the rolling radii of the right and left wheels and generates a turning motion. For sharper curves, the trucks use wheel flange contact to generate large wheel contact forces and increase the turning moments about their centers of gravity.

Since the wheels have a conical shape and taper toward the outside of the track, an axle's lateral displacement causes a difference in the rolling radii of the left and right wheels. This causes a difference in the wheels' velocities and leads to a yawing of that axle. If all of the axles displace to one side, a common turning motion translates to a yawing of the truck and allows it to roll smoothly through the curve. Figure 2.6 shows the three axles of a locomotive truck displaced to the left to negotiate a shallow, right-hand curve.

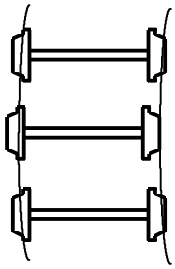

Figure 2.6 Truck negotiating a right hand curve through lateral displacement

Lateral movement of the wheels creates the rolling radii difference that brings the truck through the curve. As the curvature increases, the axle displaces more and generates a larger difference of the wheel radii, increasing the rate of yaw rotation. The yaw rotation rate, and hence the curvature that the axle can smoothly roll through, is limited by the maximum wheel radii difference. This in turn is limited by the clearance between the wheel flanges and rail (called the gage clearance). For tighter curves, the truck curves with flange contact, as shown in Figure 2.7 and discussed next.

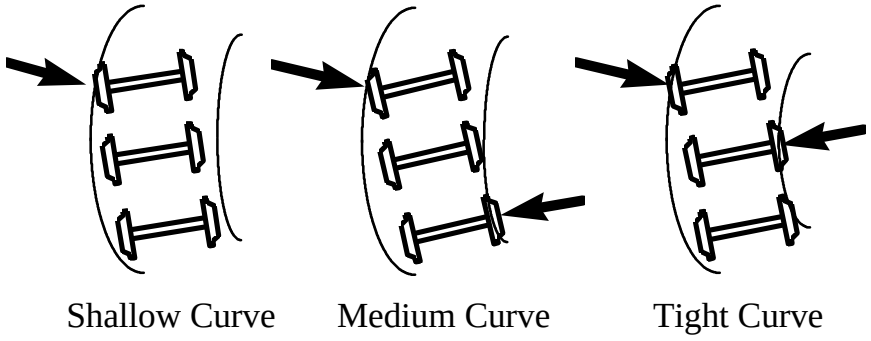

Figure 2.7 Flange contact in increasing curvature

Beyond a certain curvature, flange contact occurs at the outside wheel of the first axle. This generates a large wheel/rail contact force and increases the magnitude of the truck turning moment. This additional moment increases the truck yaw rate, allowing it to negotiate the tighter curve. As curvature increases, the truck yaws more into the outside rail to increase the contact force on the wheel flange. Eventually, the truck yaws enough for the inside wheel on the trailing axle to contact the rail. Now, flange forces at both the outside lead wheel and the inside trailing wheel generate turning moments about the truck center of gravity, producing a higher rate of yaw. For still sharper curves, the truck becomes pinched between the rails, with contact at the wheel flanges of the outside wheel

of the first axle and the inside wheel of the middle axle. This halves the length of the effective lever arm, doubling the magnitudes needed to generate the turning moment. The magnitudes of the flange contact forces increase with increasing curvature, first causing rail damage and eventually leading to the wheels climbing the rail.

2.2.2 Steerable Trucks

Shallow curves are negotiated through a lateral shift of the axles. Assuming that the center axle is oriented radially to the curve, then the outside axles sit slightly off-radial and have an angle of attack with the rail. This causes their forward velocities to not be tangential to the curve, but rather into and away from the outside rail for the lead and trail axles, respectively. As a result, the wheels have a tendency to roll somewhat laterally instead of directly following the curve's path. Since the axle is constrained to move along the track, this lateral tendency is compensated for through lateral wheel slip. Wheel slip, however, leads to the dissipation of energy through frictional forces and causes inefficiency in the curving of the truck. To reduce this effect, steerable trucks use an axle's natural tendency to align with the track to improve the radial alignment of the end axles and reduce their angles of attack. This improves both curving performance and resistance to wheel-climb derailment.

2.3 Derailment Measures

In the last few decades, extensive research has been done by the railroad industry to determine the best criteria for predicting derailment of locomotives or rolling stock. These studies date back to Nadal's work in 1908, with more recent work being done by Weinstock, Blader, Elkins and many others [12-18]. Three criteria are traditionally used for predicting rail vehicle derailment. These are the maximum lateral-to-vertical force ratios (commonly called "L/V ratios") on an individual wheel, on an axle, and on one side of a truck. The first two, the wheel L/V ratio and axle sum L/V ratio, are used to predict derailment through wheel flange climbing. The third criterion, the truckside L/V ratio, predicts derailment through rail rollover.

Due to the importance of preventing derailment in railway operation, the Association of American Railroads (AAR) has supported outside research, and conducted their own, to establish the most reliable and accurate derailment criteria. These criteria are outlined in their Manual of Standards and Recommended Practices in Chapter XI, titled "Service Worthiness and Analysis for New Freight Cars" (Appendix A). These derailment limits are summarized below in Table 2.1.

Table 2.1 AAR limits on L/V ratios

maximum wheel L/V ratio	1.0
maximum axle L/V ratio	1.5
maximum truckside L/V ratio	0.6

Next, we will examine each of the above criteria and provide a summary on some of the work that has been done to establish them as the industry standards.

2.3.1 Wheel L/V Ratio

The original estimate of the critical wheel L/V ratio was made in 1908 by Nadal, who assumed two point contact between the wheel and rail at impending derailment. He further assumed that the first contact point, located on the tread, serves as an instantaneous point of rotation. He then equated the friction and normal forces at the second point, located on the wheel flange, with the lateral and vertical forces occurring at the wheel/rail interface, as shown in Figure 2.8. This resulted in his classic expression for critical wheel L/V ratio:

$$\frac{L}{V} = \frac{\tan\alpha - \mu}{1 + \mu\tan\alpha} \qquad \textbf{(2.13)}$$

where α is the flange angle and μ is the coefficient of friction at the wheel/rail interface. For his work, Nadal used a flange angle of 65° and a coefficient of friction of 0.5, which resulted in a critical L/V ratio of 0.79. As a result, he suggested a limit of 0.80 for single wheel L/V ratios.

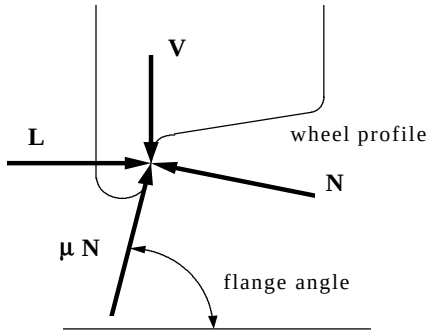

Figure 2.8 Forces at wheel/rail interface

Since Nadal's pioneering work nine decades ago, many studies have shown that Nadal's limit is extremely conservative for most practical cases [12 - 14]. In his model,

Nadal assumed that the friction force at the contact point between the wheel flange and rail is oriented in the lateral direction (perpendicular to the track). In reality, however, there are components in both the longitudinal (along track) and lateral directions, causing the lateral friction force to be somewhat less than μN. For high angles of attack, the longitudinal friction force is small, and Nadal's limit is a reasonably conservative estimate of the critical L/V ratio. For low angles of attack, however, increased longitudinal creep reduces the lateral component of the friction force, and makes Nadal's limit excessively conservative. Figure 2.9 shows this relationship between the critical L/V ratio and the angle of attack for a flange angle of 65° and a coefficient of friction of 0.5.

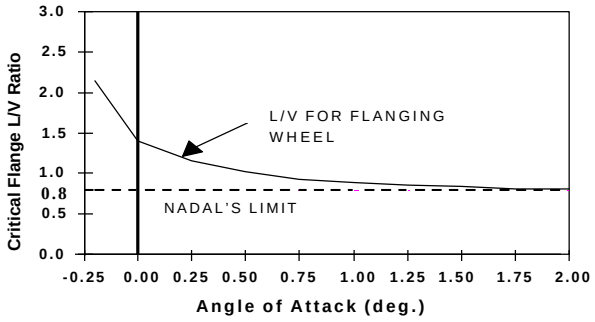

Figure 2.9 Variation of Critical Flange L/V Ratio With Angle of Attack

Another concern with Nadal's limit is his choice of values for the flange angle and coefficient of friction. Nadal performed his calculations using a flange angle of 65° and a coefficient of friction of 0.5 to arrive at a critical L/V ratio of 0.8. In practice, however, the flange angle of the wheel ranges from 70° to 75°, as documented in Appendix B. Furthermore, the coefficient of friction between the wheel and rail in the field is much lower than 0.5; in most cases, it ranges from 0.15 to 0.40.

Assuming the conservative limits

$\mu = 0.40$ (the largest coefficient of friction)
$\alpha = 70°$ (the smallest flange angle)

the critical wheel L/V becomes

$$\frac{L}{V} = \frac{\tan(70°) - 0.40}{1 + 0.40 * \tan(70°)} = 1.05 \qquad \textbf{(2.14)}$$

which is in-line with the recommendation made by AAR and many other researchers.

Reflecting these modern values, AAR established the limit on wheel L/V values at 1.0. Although this value is still believed to be a conservative estimate by many, it is widely accepted as a much more realistic limit than the 0.8 limit suggested by Nadal.

2.3.2 Axle Sum L/V Ratio

When Weinstock plotted the critical L/V ratios of the flanging and non-flanging wheels as a function of angle of attack (Figure 2.10), he noticed that the difference between the two values remained nearly constant [1]. Using this fact, he hypothesized that derailment occurs when the difference in the L/V forces for the flanging and non-flanging wheels is greater than the sum of Nadal's criteria and the coefficient of friction for the wheel/rail interface.

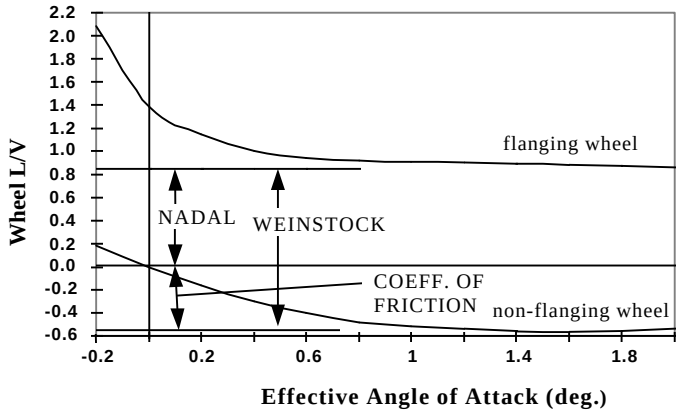

Figure 2.10 Critical L/V Ratio of Flanging and Non-flanging wheels for different angles of attack

This led to a second derailment criterion, the axle sum L/V ratio. It is calculated as the sum of the absolute values of the L/V ratios for both wheels on an individual axle.

$$\text{Axle Sum L / V} = \left|\text{L / V}\right|_{\text{left wheel}} + \left|\text{L / V}\right|_{\text{right wheel}} \qquad \textbf{(2.15)}$$

The main advantage of using the critical L/V ratio of an axle over that of a single wheel is a reduced dependence on the coefficient of friction. This is shown by the more level curve of the Weinstock criteria in Figure 2.11. This simplifies field testing, where the coefficient of friction over a section may change or be difficult to measure.

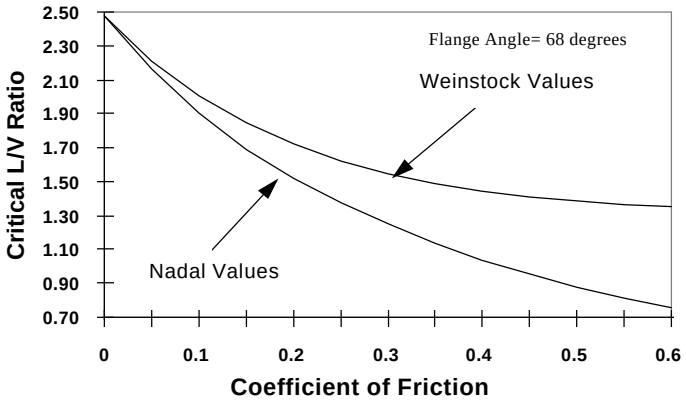

Figure 2.11 Dependence of Weinstock and Nadal criteria on the coefficient of friction

2.3.3 Truckside L/V Ratio

The third derailment measure is the truckside L/V ratio. This is the ratio of the sum of the lateral forces to the sum of the vertical forces for the wheels on one side of a truck.

$$\text{Truckside } \frac{L}{V} = \frac{\sum L \text{ (truck side)}}{\sum V \text{ (truck side)}} \tag{2.16}$$

Derailment is assumed to occur through rail rollover, and the L/V ratio is calculated from the moments of the lateral and vertical forces about a pivot point at the bottom of the rail, as shown in Figure 2.12 [14].

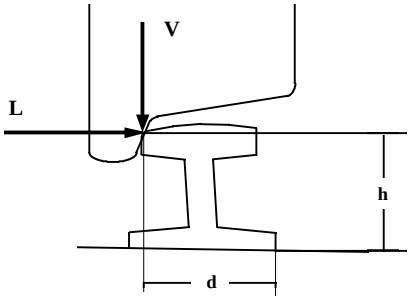

Figure 2.12 Rail Rollover geometry

This gives the critical L/V ratio as the lever arm of the vertical force (the rail width, d), divided by the lever arm of the lateral force (the rail height, h), i.e.,

$$\frac{L}{V}_{\text{critical}} = \frac{d}{h} \tag{2.17}$$

Blader calculated the critical truckside L/V values for some common rail shapes, shown in Table 2.2, to be in the range of 0.66 to 0.70 [13].

Table 2.2 Ratios of d/h for Common Rail Shapes (using an assumed tie plate cant of 1/40)

Rail Type	Rollover Ratio d/h
115 RE	0.67
119 RE	0.66
132 RE	0.70
136 RE	0.69
140 RE	0.67

2.3.4 AAR L/V Limits

Based on the work done by AAR researchers and others on derailment, AAR has set limits on the allowable levels of these L/V ratios. For an individual wheel, the L/V ratio is limited to 1.0. This reflects the critical L/V ratios calculated with Nadal's formula for the flange angles of modern wheel profiles. The limit on the axle sum L/V ratio is 1.5. This is equivalent to Weinstock's criteria for the single wheel AAR limit and a coefficient of friction of 0.5. Finally, the AAR limit for truckside L/V ratio is 0.6. This is slightly lower than any of the critical values that Blader calculated for common rail profiles. Table 2.3 gives a summary of these values.

Table 2.3 AAR limits on maximum L/V ratios

AAR Standards	
	Max L/V Ratio
Wheel	1.0
Axle Sum	1.5
Truckside	0.6

2.3.5 Angle of Attack

In addition to the L/V ratios, another factor that is important in assessing derailment is the angle of the wheel with respect to the rail (called the “angle of attack”). For the same L/V ratios, the wheel with a larger angle of attack has more likelihood of derailment.

The steering ability of a steerable truck aligns the axles with the radius of a curve, which reduces the angle of attack at the wheel/rail interface as compared to a straight (non-steering) truck. The angle of attack is defined, in its simplest form, as the angle between a line perpendicular to the axle and the center-line of the track, as shown in Figure 2.13.

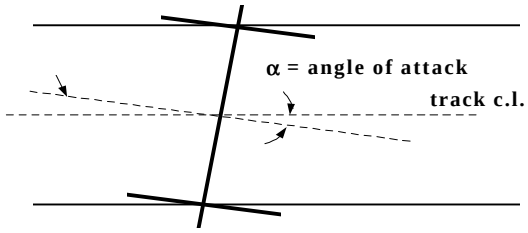

Figure 2.13 Angle of attack at wheel/rail interface

This implies that the angle of attack can equally be defined as the difference between the curve angle and the axle yaw, as shown in Figures 2.14. This figure shows a three-axle truck in a curve with the lead axle yawed relative to the truck frame.

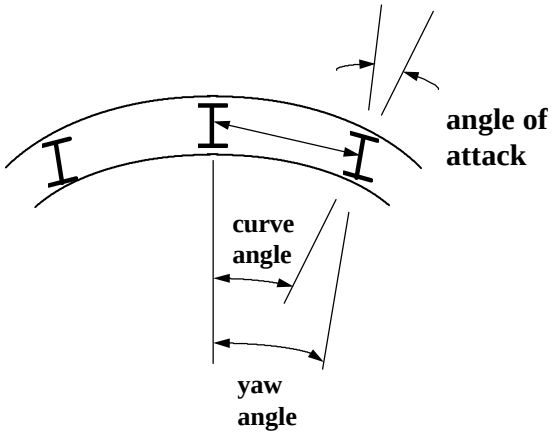

Figure 2.14 Relationship of angles in curve

The benefit of steerable trucks (which allow the end axles to yaw) is that the are able to align themselves with the curve, reducing the angles of attack between the wheels and rail. This allows steerable trucks to safely experience a larger range of L/V values.

The angles of attack for a typical two-axle, straight truck with pedestal legs and a three-axle, steerable truck are calculated in Appendix B, and the results are summarized below in Table 2.4. As the Table shows, the steerable truck has a much lower angle of attack than the B-truck with new pedestal liners. With worn pedestal liners, the angle of attack is reduced for the B-truck, but is still significantly larger than for the steerable truck. As a result, the steerable truck has a higher critical L/V ratio than the B-truck

Table 2.4 Angle of Attack Comparison for Steerable and B-Trucks

	Angle of Attack		Critical L/V Ratio
	New Pedestal Liners	Worn Pedestal Liners	
Steerable Truck	**0.33**	**0.33**	**1.10**
B-Truck	**0.80**	**0.51**	**0.95 - 1.05**

2.4 Purpose of Locomotive Trucks

The trucks are essential to the motion of a locomotive. They transmit vertical loads between the platform and the track. Additionally, they transmit longitudinal traction and braking forces, as well as lateral forces due to hunting and curving. The rotation of the trucks allows the wheels to follow the track shape and assists the vehicle in negotiating curves. By connecting the axles together, and allowing the addition of stiffness between the axles, they can improve hunting stability, which increases the range of safe operating speeds. The truck frames also allow the mounting of steering mechanisms to control axle orientation and improve curve negotiation.

2.5 Truck Components

Locomotive trucks (like the three-axle truck shown in Figure 2.15) incorporate several components, each one performing a specialized function. These components include the truck frames, motor combos, and primary and secondary suspensions. Steerable trucks additionally have steering linkages that control the yaw rotation of the axles. This section will discuss the dynamics of these individual components.

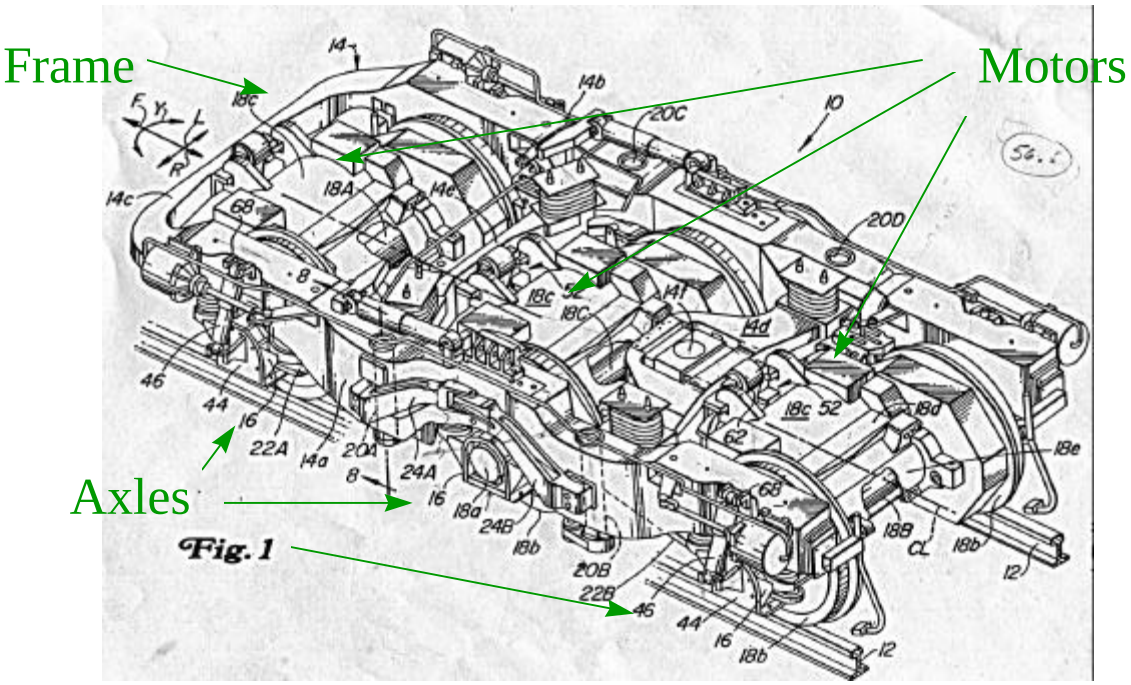

Figure 2.15 Three-axle locomotive truck

2.5.1 Truck Frames

The truck frames distribute the weight from the locomotive platform to the individual axles. This is done through coil springs sitting between the ends of each axle and the truck frames, and rubber pads between the truck frames and platform. The rubber pads sit close to the center pins and provide a small support area. The distance from this support area to the coil springs above the lead and trail axles is large. As a result, the truck frame must be very stiff in order to transfer the platform load onto the axles and resist vertical deflection. The truck frames also transmit lateral curving and longitudinal traction and braking forces from the axles to the platform. This requires the truck frame to also be stiff in these directions.

2.5.2 Axle Set

An axle set, as shown in Figure 2.1, consists of two wheels rigidly fixed onto an axle. This causes the wheels to rotate about the y-axis at the same rate and, due to the conical wheel profiles, leads to the axle hunting and curving dynamics previously discussed. The axle rides directly on the rails and sits below the coil springs. As a result, there is little change in its vertical position relative to the track. Thus, the axle is composed entirely of unsprung mass and has little effect on the vertical dynamics of the locomotive. Laterally, the axle transmits force due to hunting and curving through the traction links and coil springs. This allows axle hunting to drive the motion of the truck, increasing the displacement above that due solely to truck hunting. In turn, the stiffness between the axles and truck frame reduces the displacements due to axle hunting.

2.5.3 Motors

In each motor combo, the electric motors (AC or DC) generate torque, which is transferred through a gear and pinion to the axles to produce tractive effort. Additionally, the gearing between the motor and axle allows the motor to be used as a generator to provide dynamic breaking (a counter-torque to the rotation of the axle). Since the rotation of the axle and motor gears are coupled, the roll moment of inertia of each axle must include a contribution due to the internal gearing of that motor.

The motor bolts to the axle u-tube, enclosing the axle and rigidly connecting the two bodies together in all directions. The axle is able to rotate inside the u-tube, however, so there is no connection in the roll direction. Rotation of the motor relative to the truck

frame is prevented by a suspension link between the truck and motor nose called a dog-bone. The dog-bone includes a rigid link extended vertically between the motor nose and truck frame, with resilient bushings at each end. Lateral motion of the motor relative to the frame causes cocking of the dog-bone, which compresses rubber bushings and generates a resistive force. As a result, the dog-bone provides both vertical and lateral stiffnesses between the motor and truck frame.

2.5.4 - Steering Mechanism

To improve curving, steerable trucks connect the outside axles together and force them to yaw in opposite directions from each other. This allows the axles to conform to the shape of the curve, reducing the resistive friction forces and improving curving performance. The steering mechanism connects to the truck frame, and reacts against the motion of one end axle to generate a force on the other end axle. The steering links are relatively light compared to other components on the truck. Furthermore, their movements are small and relatively slow. Therefore, their inertial dynamics can be ignored relative to the dynamics of the other components, such as the axle, truck frame and locomotive platform.

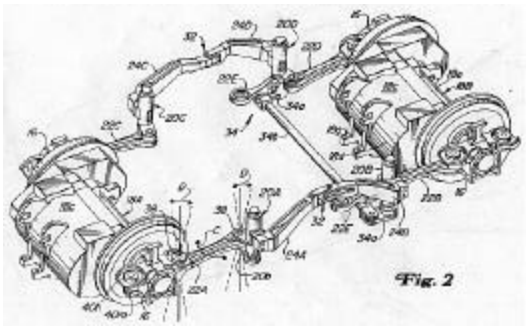

Figure 2.16 Steering linkage

Chapter 3

Steerable Truck Modeling in NUCARS

For this project, we developed a NUCARS model for a six-axle locomotive with steerable trucks. The first step in constructing the model was representing the locomotive in a multi body form. A multi body model lumps physical components into individual bodies with defined positions and inertial properties. The model shows inter-body connections as lines running between the bodies. The inter-body connections are used to represent the stiffness and damping that exist between physical components of the locomotive. Figure 3.1 shows a multi body model for a six-axle locomotive, similar to the one used in this study. The following sections describe the bodies and connections used in our model, as well as the general assumptions that we made.

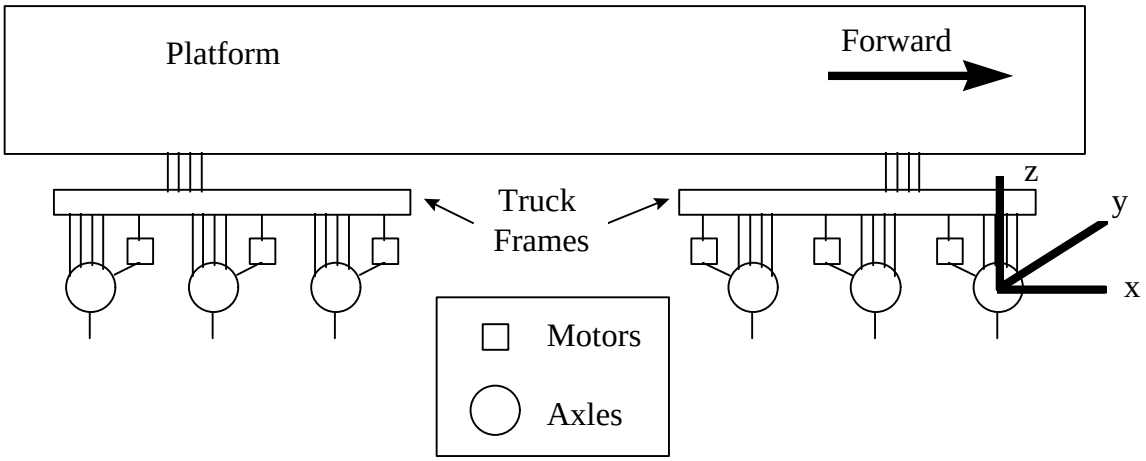

Figure 3.1 Multi-body figure of six-axle locomotive

3.1 Assumptions

The speed that the locomotive travels along the track is specified in the NUCARS RUN file. This translates to a forward speed for a local coordinate system that moves along with the locomotive in the longitudinal direction. The longitudinal speed of this local coordinate frame can be used as the longitudinal speed of each body, since little longitudinal motion occurs between bodies. This allows the longitudinal degrees of freedom to be removed from the model, constraining the bodies to move along the x-axis with the reference frame.

In the model, vertical measurements are made from the center of the front axle, as shown in Figure 3.2. As a result, the positions of the track and locomotive components are specified relative to the center of the first set of wheels. This allows a change in the wheel radius to be made without affecting the vertical position of other components. The only changes that are required in using different wheels on the model are changing the vertical position of the wheel/rail connections and using a new wheel/rail geometry (WRG) file.

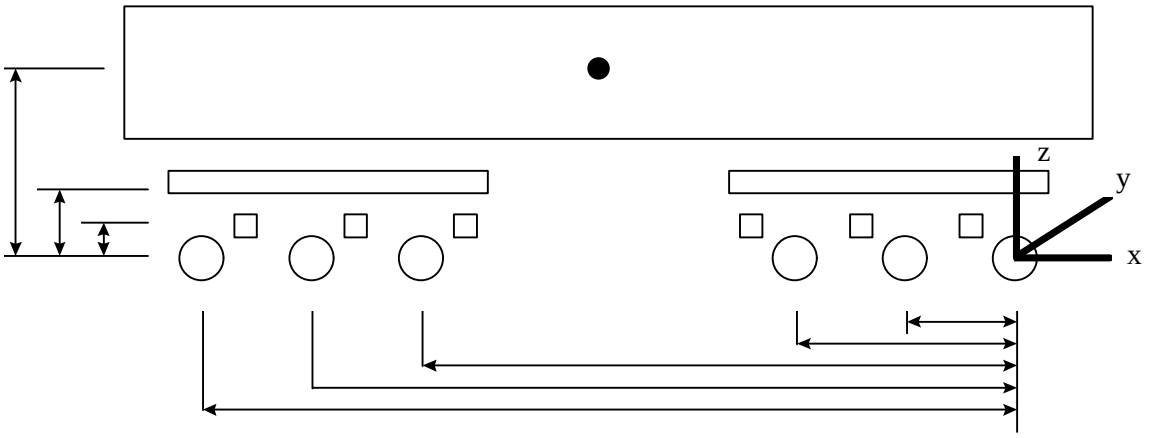

Figure 3.2 Sample of measurements for multi body model

At the beginning of each model run, an equilibrium calculation is performed to determine the position of the bodies when the suspension components are loaded with weight. This results in the loaded equilibrium position of each suspended body to be at a lower height than the unloaded (free) height originally specified in the model. This causes the connection locations to be different than their intended positions. To include the unloaded heights, the initial position of each body is raised by the suspension deflection at its center of gravity due to the sprung weight. Since the axles are unsprung components, they do not need to be raised. For the motors, however, only half of their weight is sprung mass, with the other half supported by the axles. As a result, their centers of gravity have half of the drop that occurs for the truck frames. To calculate the amount of truck frame drop, the weight of one truck frame is added to half of the weight of three motors and divided by the stiffness of twelve coil springs. This gives the compression in the coil springs, by which the truck frame centers of gravity must initially be raised. The motor centers of gravity are then raised by half of this, since no vertical movement occurs at the axle connections. The amount that the platform lowers due to the equilibrium calculation will be due to the sum of the lowering of the truck and the compression of the side bearer pads. To calculate this, the weight of the platform is divided by the stiffness of the four pads and added to the amount that the trucks are raised. The cumulative deflection due to the side bearer pads and primary coil springs is the height that the platform must be raised initially.

3.2 Bodies

The locomotive is modeled as 19 separate bodies. Only bodies with significant contributions to the locomotive dynamics are included in the model. The masses and inertial properties of other components, whose dynamics are not important, are incorporated into these 19 bodies. Table 3.1 summarizes the bodies in the NUCARS model, and includes the orientation and degrees of freedom for each body. These degrees of freedom are shown in Figure 3.3. These bodies are discussed in the following sections

Table 3.1 Bodies used in NUCARS model

Body	# of Bodies	DOF	DOF Axes/Orientation
Platform	1	5	2,3,4,5,6
Bogies (Trucks)	2	5	2,3,4,5,6
Axles	6	4	2,3,4,6
Motors	6	5	2,3,4,5,6
Dog Ears	4	1	6
	19	73	

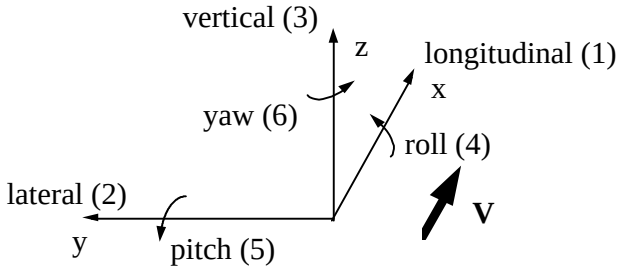

Figure 3.3 Degree of freedom convention

3.2.1 Platform

One body is used to model the platform and all of the components which are mounted to it. These components include the locomotive cab, diesel engine, electric generator and all other mechanical and electrical accessories of the locomotive. The motion of these components relative to each other is negligible, and does not contribute to the dynamics of the locomotive. As a result, they can be combined into one body in the model without changing the system dynamics. The platform mass then includes the sum of the masses of all of these components. The inertial properties and location of the center of gravity are calculated as the aggregate of the heaviest components. Due to compression of the side bearer pads and coil springs, the initial position of the center of gravity is initially raised. This allows the platform to ride at the correct height during simulation. The platform body is assumed rigid, eliminating flexible modes from the model. It has rigid modes, however, allowing it to move in any of the two translational and three rotational directions. The longitudinal degree of freedom is removed because the speed of the local coordinate frame in that direction is specified in the model.

3.2.2 Truck Frames

The truck frames are modeled similar to the platform in the sense that the bodies include all mounted components. For the truck frames, these components include the braking system and steering linkage. The inertial properties and center of gravity of the truck frames have contributions from these components. The centers of gravity are raised by the

amount of static compression in the coil springs. Similar to the platform, these bodies are assumed rigid and have all degrees of freedom except for in the longitudinal direction.

3.2.3 Axles

The axles and motors of the motor combos are modeled separately. This eliminates the need to divide the motor mass to include it with the masses of the axles and truck frames. The axle bodies include the wheels, which are rigidly mounted to them. As such, the mass and inertial properties include contributions from them. Since the axle rotation about the y-axis is governed by the contact conditions specified in the WRG file, the roll degree of freedom is removed in addition to the longitudinal degree of freedom. Since the axles are not supported by any suspension components, they are unsprung weight; therefore, their center of gravity remain at the original heights.

3.2.4 Motors

The gear and pinion that is used at the interface between the axle and motor affects the motor's inertial properties. This requires the motor's pitch moment of inertia to include a contribution from the internal gearing. For the model, the motors are allowed to move independently in all directions and have all degrees of freedom, other than in the longitudinal direction. Although in practice the center of gravity of the motors are offset laterally, in the model they are assumed to have no offset in order to eliminate forces that would cause the axles to roll off center on tangent track. The motors are mounted to the unsprung axles on one end and to the sprung truck frame on the other end. As a result,

the centers of gravity, which is roughly halfway between these points, are raised by half as much as the truck frames.

3.2.5 Dog Ears

The non-parallel traction links define the relationship between the lateral and yaw positions of the outside axles. These axles, however, can yaw independent of lateral motion. This is because the traction links are connected to dog ears, shown in Figure 3.4, which can yaw relative to the truck frame. This freedom of motion requires the model to include the dog ear kinematics. The dog ears are represented by a centrally-mounted body that can yaw relative to the truck frame and accommodate the opposing yaw rotation of the axles. They are mounted so that the center of mass and center of rotation are coincident, eliminating inertial effects due to mass. Yaw inertia and connection stiffness for these bodies are small and are chosen to place dynamic frequencies outside the range of interest.

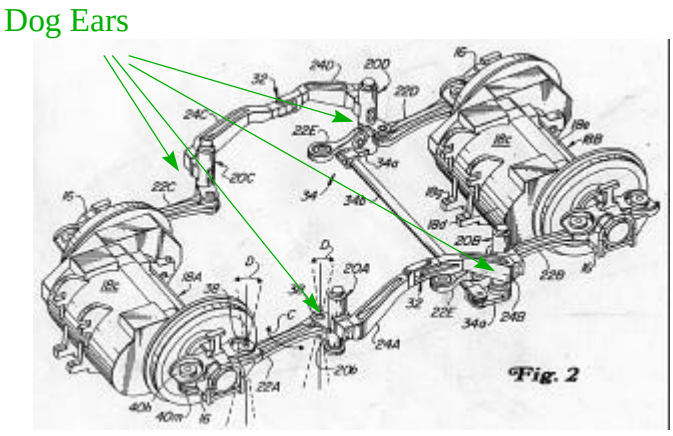

Figure 3.4 Steering linkage and dog ears

3.3 Inter-Body Connections

The NUCARS model uses connection elements between the different bodies to represent the stiffness and damping that exist between various components. The connection elements are chosen to represent the inter-body dynamics that exist in practice. In some cases, a physical connection is represented by more than one connection element, giving correct motion in all directions.

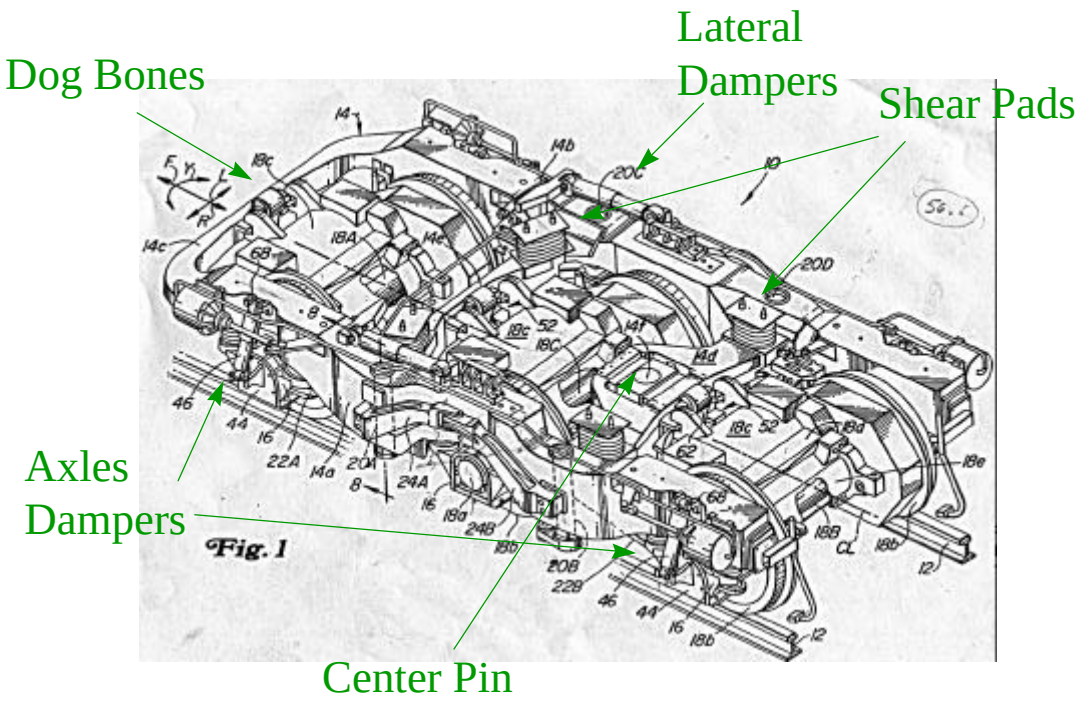

Figure 3.5 Some connections in the steerable locomotive truck

Connection elements in the model represent both the primary and secondary suspensions. The primary suspension connects the motor combos to the truck frame and transmits tractive, braking, curving and vertical forces. These components include the axle vertical dampers, coil springs, and the traction and center links (suspension links which transfer longitudinal forces between the end and center axles and the truck frame,

respectively). Figure 3.5 shows the steerable locomotive truck with some of the suspension elements labeled. The secondary suspension transmits longitudinal, lateral and vertical forces between the platform and the truck frames. It consists of the center pins (pins connected to the platform that transfer lateral and longitudinal forces between the platform and truck while allowing relative yaw rotation), lateral and yaw dampers, and the side bearer pads (rubber pads sandwiched between the platform and truck that support the vertical load in compression, while shearing under horizontal loads). Table 3.2 summarizes the connection elements included in the NUCARS model, and includes which bodies they connect, the connection type and the connection orientation.

Table 3.2 Connections for NUCARS Locomotive Model

Bodies	Sub-System	Component	Bodies		Type	Axis/DOF #	Purpose
Platform/Bogie Connections	Secondary Suspension	Sidebearer Pads	Platform	Bogie	1.1	1,2,3	to accommodate platform/bogie relative motion
		or					
		Bolster	Bolster	Platform	1.1	1,2,3	
		Body Yaw Damper	Platform	Bogie	1	1	to control platform and bogie motion; increase critical hunting speed
		Body Lateral Damper	Platform	Bogie	1	2	
	Buff Mechanism	Center Pin	Platform	Bogie	1	2	to transfer tractive effort from bogie to platform
		or					
		Fifth Wheel	Platform	Bolster	1.1	2,6	
Bogie/Axle Connections	Primary Suspension	Coil Springs	Bogie	Axle	1.1	1,2,3	to resiliently connect axle to the bogie frame
		Axle Damper	Bogie	Axle	1 or -1	3 or 1	to control axle motion
	Traction Tranfer Mechanism	Pedestal Legs	Bogie	Axle	6.4	1	to transfer tractive effort from axle to bogie frame
		or					
		Traction Links	Bogie	Axle	1 or -1	1	
Motor/Axle and Motor/Bogie Connections	Motor Suspensions	Motor/Axle Suspension	Motor	Axle	1.1	2,3,4,6	to connect axle to motor
		Motor Nose Suspension	Motor	Bogie	1.1	2,3	to connect motor to bogie frame
Wheel/Rail Connections	Wheel/Rail Interface	Wheel/Rail Contact	Wheel	Rail	4		to model wheel/rail interface

3.3.1 Axle Vertical Dampers

The axle vertical dampers control the vertical motion of the axles due to roughness in the rails and unevenness in the joints between rail sections. The axle dampers provide damping force along one axis. As such, they are modeled with off-axis, uni-axial (type "-1") parallel spring dampers, with the stiffness terms set to zero. The connection bodies are the axles and the truck frame. The truck frame is assigned as the first body in all cases, since raising them in relation to the axles stretches each of the vertical dampers. Figure 3.6 shows the vertical dampers connecting an axle and truck.

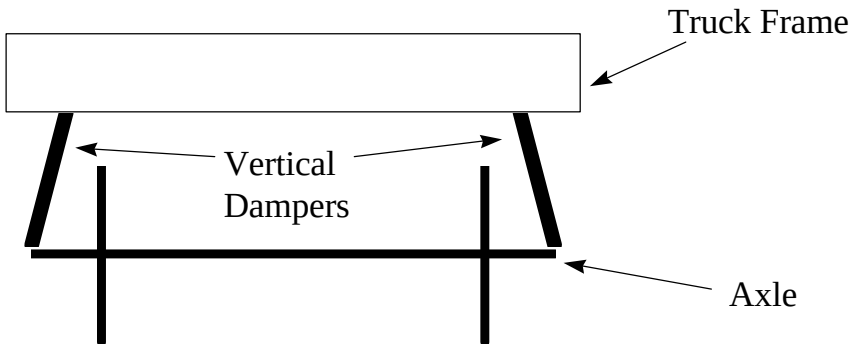

Figure 3.6 Axle vertical dampers

3.3.2 Coil Springs

The coil springs allow motion between the axles and truck frames and set the static position between these elements. Vertically, the springs allow movement through axial compression and extension, and are very stiff. Longitudinally and laterally, however, displacement is through flexicoiling, resulting in much lower stiffness. To model these connections, on-axis, multi-axial (type "1.1") elements are used. Rotation of the axle

journal boxes about the y-axis does not significantly affect the wheelset dynamics. This allows the two springs on either side of a journal box to be combined into one stiffness element and placed above the axle center line. The stiffness characteristics for the connections are then twice the values for an individual spring. Figure 3.7 shows coil springs as they exist on the locomotive and in the model.

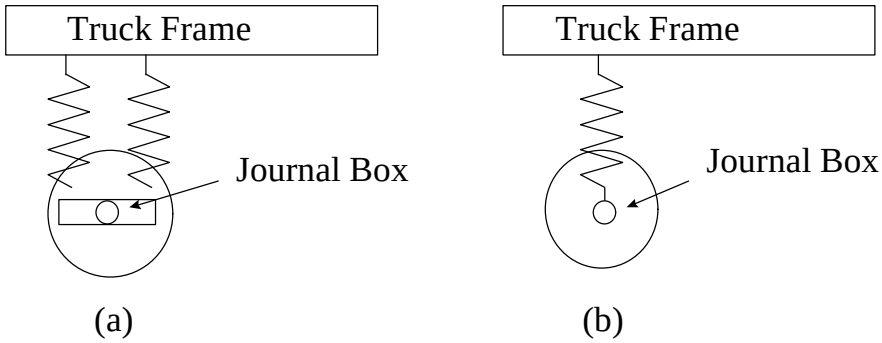

Figure 3.7 Coil springs, as they appear (a) on the locomotive, and (b) in the model

3.3.3 Traction Links

The outside axles of the truck transmit traction and braking forces from the axles to the truck frames through traction links. These links are shown in Figure 3.8 and can be parallel to the truck center line or at a slight angle. Angled traction links couple the yaw and lateral motion of the outside axles with respect to the truck frames. To model the traction links, off-axis, uni-axial (type "-1") connection elements are used, with no damping and very large stiffness. This allows the links to behave as nearly rigid rods and move the axles by rotating about their mounts on the truck frames. The bodies for the

connections are the axles and dog ears, with the order changing for the leading and trailing axles due to the rotated configuration.

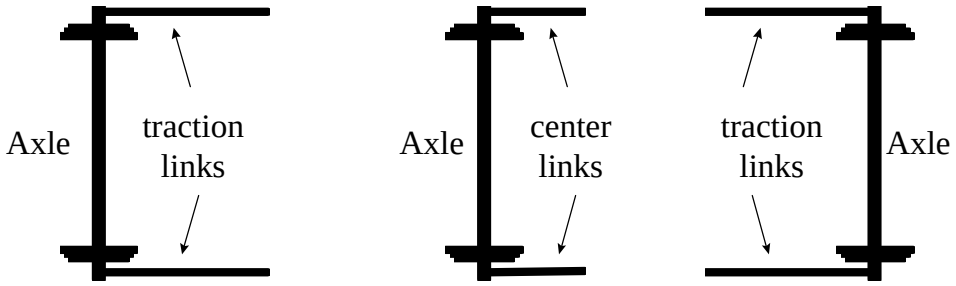

Figure 3.8 Orientation of traction links and center links in a truck

Vertical motion of the axles causes the traction links to cock, compressing the end bushings and generating a resistive force. This provides a vertical stiffness between the axles and truck frames due to the traction links. Off-axis connections can provide stiffness in only one direction, requiring the use of separate connection elements to model the cocking of the traction links. This is done with on-axis, uni-axial (type "1") elements with the stiffness oriented vertically. Body 1 for these connections is the truck frame in all cases, since the truck frame sits above the axles and raising the truck frame stretches the connection.

3.3.4 Center Links

The connections between the middle axles and truck frames are similar to the traction links and are also shown in Figure 3.5. These center links, however, are always oriented parallel to the truck frame center lines, allowing the center axle to move only in lateral motion. Cocking of the center links provides stiffness in both the lateral and vertical directions. Unlike the traction links, which lie at an angle from the longitudinal axis, the

center links are parallel to this axis and their stiffness in all directions can be modeled by a single on-axis multi-axial element. The longitudinal characteristic represents the axial stiffness of the center links. The stiffness due to shear of the rubber end bushings is represented with the lateral and vertical stiffnesses. The connection bodies are the axles and truck frames, with the body order changing for the front and rear trucks due to the end-to-end configuration of the truck frames when they are installed under the platform.

3.3.5 Inter-Axle Yaw Connections

The outside axles of a steerable truck yaw in opposite directions to each other. This helps them to conform to the shape of a curve and aids the wheels in negotiating the curve smoothly. Figure 3.9 shows a steerable truck in a right hand curve, with the end axles yawed in opposite directions from each other. The counter-yaw of the end axles is caused by a steering linkage between them, as shown in Figure 3.10. The lateral or yaw motion of one axle moves the steering arms, causing them to push against the steering arms of the other axle and yaw it in the opposite direction. To model the steering linkage, off-axis (type "-1") elements are used to connect the ends of the leading axle (axle 1 or 4) to the opposite ends of the trailing axle(axle 3 or 6). This causes the rotation of one axle to impose a torque on the other axle and rotate it in the opposite direction. The position and orientation of the steering links are specified by connections ends located at the journal boxes on the end axles. The lead and trail axles are specified as the bodies for the connection. Body 1 is assigned as the lead axle in all cases, since moving it in the longitudinal direction in relation to the trail axle stretches the connection.

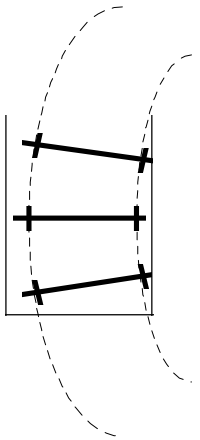

Figure 3.9 A steerable truck in a right hand curve

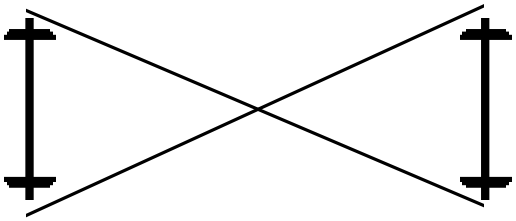

Figure 3.10 Steering linkage between outside axles

3.3.6 Axle to Motor Connections

Each motor is rigidly connected to the axle via a housing called a U-tube, that is pressed onto the axle bearings. The U-tube serves to protect the axle, in addition to the connection it provides between the motor and axle. The axle is able to rotate inside the U-tube, but the connection is rigid in all other directions. The connection represents four degrees of freedom (in the lateral, vertical, roll, and yaw directions) The longitudinal and pitch degrees of freedom have been ignored due to the forward and rotational motion of the wheelset-motor combination (called a motor combo). The motor/axle connection is modeled as an on-axis, multi-axial (type “1.1”) connection. One stiffness characteristic is

used for the translational degrees of freedom and another is used for the rotational degrees of freedom. Each connection is located at the center of the U-tube, which is the center of that particular axle.

3.3.7 Dog-Bones

The motors are kept from rotating about the axles by vertical links, called dog bones, connecting the nose of the motor to the truck frame. In addition to providing a vertical stiffness, cocking of the dog-bone due to lateral motion compresses rubber bushings at the ends, providing lateral stiffness between the motor and truck frame. Since the dog bone acts in both the vertical and lateral directions, it is modeled as a multi-axial (type "1.1") element. The connection location is defined as being halfway between the motor nose and truck frame connections. The connected bodies are the truck frame and motor. The truck frame is located above the motor and moving the truck frame positively along the z-axis stretches the connection. As a result, in each connection the truck frame is assigned as the first body and the motor as the second.

3.3.8 Inter Motor Links

The inter motor links, as shown in Figure 3.11, connect the three motors in a truck laterally, causing them to move together relative to the truck. This common displacement aids the truck in negotiating shallow curves where the difference in rolling radii of the wheels results in a velocity difference and causes the truck to rotate. These components

are modeled with on-axis, uni-axial (type "1") parallel spring dampers connected in the lateral direction.

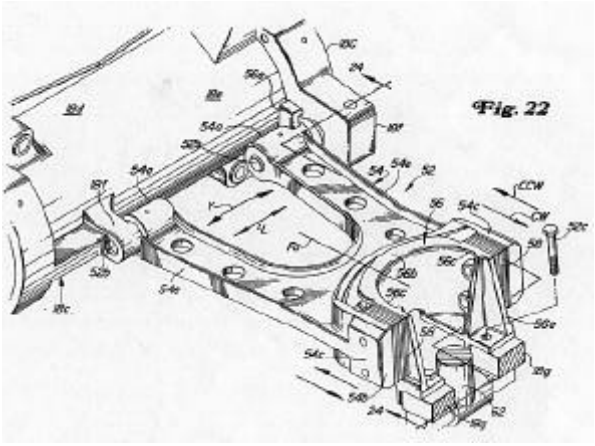

Figure 3.11 Inter motor connection mounted on U-tube

3.3.9 Center Pins

The tractive effort, braking and lateral forces are transferred between the trucks and platform through center pins. The center pin is a solid steel column that is welded to the platform and sits in a ring mounted to the truck frame with rubber shear pads. The longitudinal connection is not modeled, since this degree-of-freedom has been removed from the trucks and platform. This leaves the center pin connection acting only in the lateral direction; therefore, it can be modeled with an on-axis, uni-axial (type “1”) element. The truck frame is assigned as body 1 and the platform as body 2, allowing a positive displacement of the connection to occur when the truck moves laterally to the left relative to the platform.

3.3.10 Side Bearer Pads

As shown in Figure 3.12, the platform sits on rubber pads on top of the trucks. These pads are very stiff vertically (in compression) but relatively soft horizontally (in shear). This allows the truck to yaw in relation to the platform as is needed in curves, while supporting the static weight of the platform. The side bearer pads are modeled using on-axis, multi-axial (type"1") parallel spring damper elements. Due to the natural damping of rubber elements, both damping and stiffness characteristics are retained. Since the pads have a rectangular base, the stiffness for the two horizontal directions is not equal. Additionally, the rear side bearer pads are angled to establish the truck center of rotation, which affects the longitudinal and lateral stiffness values. The characteristic data used in the model reflects this.

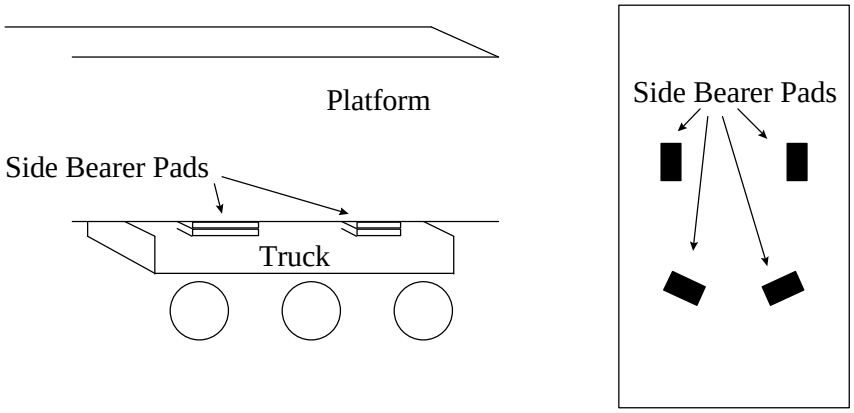

Figure 3.12 Side bearer pads: (a) between platform and truck and (b) orientation on truck

3.3.11 Lateral Dampers

Truck hunting is controlled through the use of lateral and yaw dampers mounted between the platform and truck frames. The lateral dampers are oriented parallel to the y-axis and control side-to-side motion. They have little effect on controlling the relative yaw between the truck and platform, since they are commonly mounted near the yaw center of rotation. The dampers operate in one direction, and therefore can be modeled with on-axis, uni-axial spring damper elements that are oriented laterally and have the stiffness component removed. The connection bodies are assigned as the platform and truck frames, with the order changing for the dampers to the left and right of the center pins.

3.3.12 Yaw Dampers

The dampers designed to limit the relative yaw between the platform and truck frames are similar to the lateral dampers, but are oriented longitudinally. They are located at the sides of the truck frames near the yaw center of rotation. An on-axis, uni-axial (type "1") elements is again used, with the stiffness characteristics set to zero.

3.3.13 Wheel/Rail Connections

The connection between the wheels and rail are modeled with special NUCARS elements. One connection is placed at each wheel where it contacts the rail. The connection characteristics specify the linear stiffness and damping inherent to a rail. The geometry of the contact is defined in a data file written from experimental test data and supplied with the NUCARS package. The connection locations are one wheel radius below the axle centers at the lateral spacing of the rails.

3.4 System Input

The model is run over two types of track shape, tangent track and curves. These were specified in input (INP) files as either measured data or track geometry. The track shapes are discussed in the following sections.

3.4.1 Tangent Track

Three different sections of tangent track are used. These included an undisturbed section to demonstrate that the model is running properly, a section with an initial disturbance to show system's free response, and a section modeling the AAR Tangent Track Hunting Zone. The first two files specify the track profile through its geometry. The track deviation is set to zero either initially, or after an initial variation. The AAR tangent section is specified through measured data stored in a TRK file. Runs made on this section are compared to field test data for model validation.

3.4.2 Curved Track

The model is run through several sections with various curvatures. These sections are designed to simulate test conditions on the AAR Wheel Rail Mechanism (WRM) Loop. This includes curve sections of 7.5, 10 and 12 degrees with super elevations of 3, 4 and 5 inches, respectively. Runs are also made on a 20 degree section having 2 inches of super elevation to test the models response in tight curves. The curve body and entry and exit spirals are specified in the INP file as sections with defined curvature and super elevation.

Additionally, the speeds for three different balance conditions are calculated and used for the runs. These are traveling through the curves at balanced speed, under-balanced by three inches and over-balanced by three inches. One inch of over balance and under balance are used for the 20 degree curve.

3.5 Wheel/Rail Geometry

The contact condition between the wheels and rail is specified in the WRG file. Most runs used a symmetric AAR-1B profile. It features a conicity of 0.05 (a 1:20 tread ratio), a gage of 56.5" and 136 lb. rail. This file is one of a group supplied by AAR and it has been created based upon field measurements. For the parametric wheel conicity tests, the values for the wheel radii and axle roll angle were changed. These new files, however, are only first-order approximations since they retain the original contact patch values.

Chapter 4

Model Validation

To validate the NUCARS model, the output from several runs is compared with the expected dynamic behavior and with the results from field testing. A similarity between the simulation output and the expected behavior or field test results suggests that the model is a good representation of the physical system. The validation runs are performed on both tangent and curved tracks. This chapter will discuss the runs used for validating the NUCARS model, including the run conditions and the significance of the results.

4.1 Tangent Track Tests

The hunting behavior of the model is investigated by running it on sections of tangent track. These track sections enable us to study both the free and dynamic responses, and to compare them with the model's expected behavior and with the results of field testing.

4.1.1 Description of Track

The tangent test track is a 2000 foot section of undisturbed tangent track that has an initial half-sine wave lateral disturbance, with a length of 39 feet and an amplitude of 0.5 inches. This initial disturbance excites the model's dynamics, which are then allowed to continue free from any future disturbances. This allows us to observe the model's free response. For runs below the critical hunting speed, there will be positive damping which leads to a

decay of the initial displacement. Beyond the critical speed, however, the initial displacement will not be damped out; it will continue to increase until the model reaches numerical saturation and stops.

4.1.2 Simulation Speeds

The modeling parameters we have selected belong to a locomotive that has proven to have a hunting critical speed of 75 mph. To verify this speed in the model and also study the hunting behavior above the critical speed, we chose speeds ranging from 50 to 100 mph. Up to 70 mph, the speeds are increased in 10 mph increments; beyond 70 mph, the speeds are changed in increments of 5 mph. This allows us to test a range of speeds around the critical speed and yet keep the number of runs manageable.

4.1.3 Criteria Used

The principal motion of interest for the tangent track runs is hunting of the truck frames and individual axles (called "primary" and "secondary" hunting, respectively). Hunting appears as coupled harmonic oscillation in both the lateral and yaw directions. As a result, accurate observation of hunting requires that both the lateral and yaw displacements be included in the measurements. For all tangent track runs, the relative axle displacements of the lead truck are used to observe hunting. As shown in Figure 4.1, relative axle displacements are measured as the lateral displacement between the platform and truck frame at the A-side of the leading and trailing axles. Measurement elements are placed laterally in the NUCARS model to record these values. The lateral orientation of these

elements allows them to directly measure the lateral component of truck hunting. Additionally, they measure the yaw of the truck frame, since these elements are offset from the center of rotation of the truck,

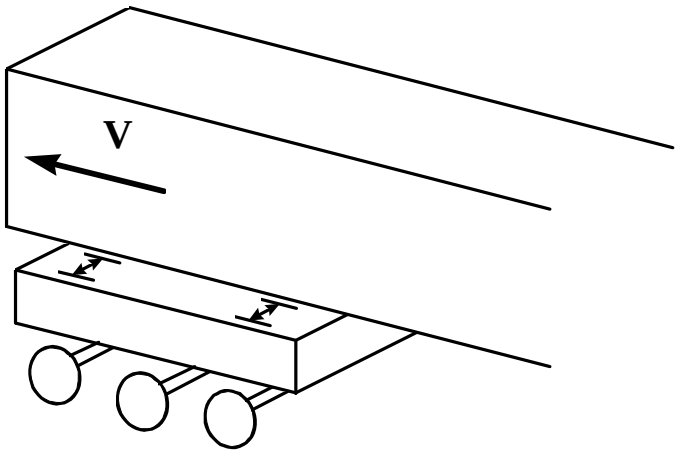

Figure 4.1 Location of transducer elements used for evaluating tangent track runs

Axle hunting causes relative lateral and yaw displacements between the axles and the truck frame. These displacements, in turn, generate forces and moments between the truck frames and axles, which drive the motion of the truck frames, and add to the hunting amplitude in a manner similar to a self-excited system. Since hunting of the axles drives the motion of the truck frame, truck hunting will always include a component due to axle hunting. This allows the same measurement that is used for observing hunting of the truck to also be used to observe hunting of the individual axles.

The relative axle displacements are examined in two ways. First, we look at the magnitude and shape of the decay in the time trace. As the truck and axle hunting becomes more unstable, the magnitude of the relative axle displacement increases. There is also a decrease in the damping of this motion and an increase in the decay time. Above

the critical speed, there will be no apparent decay in the motion of the truck. Thus, by looking at the shape and magnitude of the time response of the relative axle motion, we can determine if a run has exceeded the critical speed.

Truck and axle hunting occur as harmonic motion. This means that each hunting mode (e.g., axle lateral, truck yaw, etc.) has a certain resonance frequency. Additionally, the driving frequency of input from the track is a function of the forward speed of the locomotive, the wheel radius, conicity and track gage. The magnitude of each hunting component can be determined by examining the frequency content in the Fast Fourier Transform (FFT) of the relative axle displacement. This requires knowing the natural frequency for the lateral and yaw motion of the truck frame and axles, which are calculated according to

$$f = \sqrt{\mathbf{k}/\mathbf{m}} \text{ or } \sqrt{\mathbf{k}_\Theta/\mathbf{I}} \qquad \textbf{(4.1)}$$

where **k = equivalent linear stiffness**
$\mathbf{k}_\Theta$ = equivalent rotational stiffness
m = mass of axle or truck
I = inertia of axle or truck

Since each axle is rigidly connected to one of the motors to form a motor combo, the axle natural frequency is determined for the motor combo as a whole. The natural frequency for the truck is determined using the summed mass or inertia for the truck frame and motor combos and the sum of the stiffness values of all connections between the platform and truck. The frequencies calculated for the truck and axle hunting modes are shown in Table 4.1.

Table 4.1 Hunting mode frequencies

Hunting Mode	Frequency (Hz)
Axle Lateral	1.4
Axle Yaw	2.4
Truck Lateral	4
Truck Yaw	3.2

Since hunting is first noticed when the locomotive's crew becomes uncomfortable, the model's stability is also determined by placing a measurement connection element at the engineer's seat to determine the lateral acceleration of the car body. Plotting the time trace of this value shows the magnitude of the acceleration that the crew would feel, as well as the growth or decay in the platform acceleration. Stable simulation runs (ones below the critical speed) are characterized by a decay of the cab acceleration with time. Above the critical speed, the cab lateral acceleration grows with time; therefore, any speed that exhibits this behavior falls beyond the critical speed.

4.1.4 Results of Tangent Track Validation Runs

4.1.4.1 Time Traces of Relative Axle Displacement

Figures 4.2 to 4.7 show the relative axle displacements for model runs of 50 to 85 mph. At low speeds, the relative axle displacements are small. Figure 4.2 shows that the relative displacement of axle 1 for the run made at 50 mph has an amplitude of 0.35 inches. As the speed is increased in successive runs, the axle displacements grow in magnitude, and the peaks for axles 1 and 3 shift toward opposing positions. The plot for 70 mph (Figure 4.4) shows that the peaks are out of phase by approximately 90 degrees. At 75 mph, the relative axle displacement amplitudes for axles 1 and 3 are equal. At 85 mph (Figure 4.7), the axle displacements are consistently above 0.5 inches and the amplitude is larger for axle 3 than for axle 1. This shows that the truck has begun hunting by 85 mph.

The model is stable at low speeds (<50 mph). Additionally, the model becomes less stable as the speed increases, and is unstable by 85 mph. As such, the critical hunting speed lies somewhere between 50 and 85 mph.

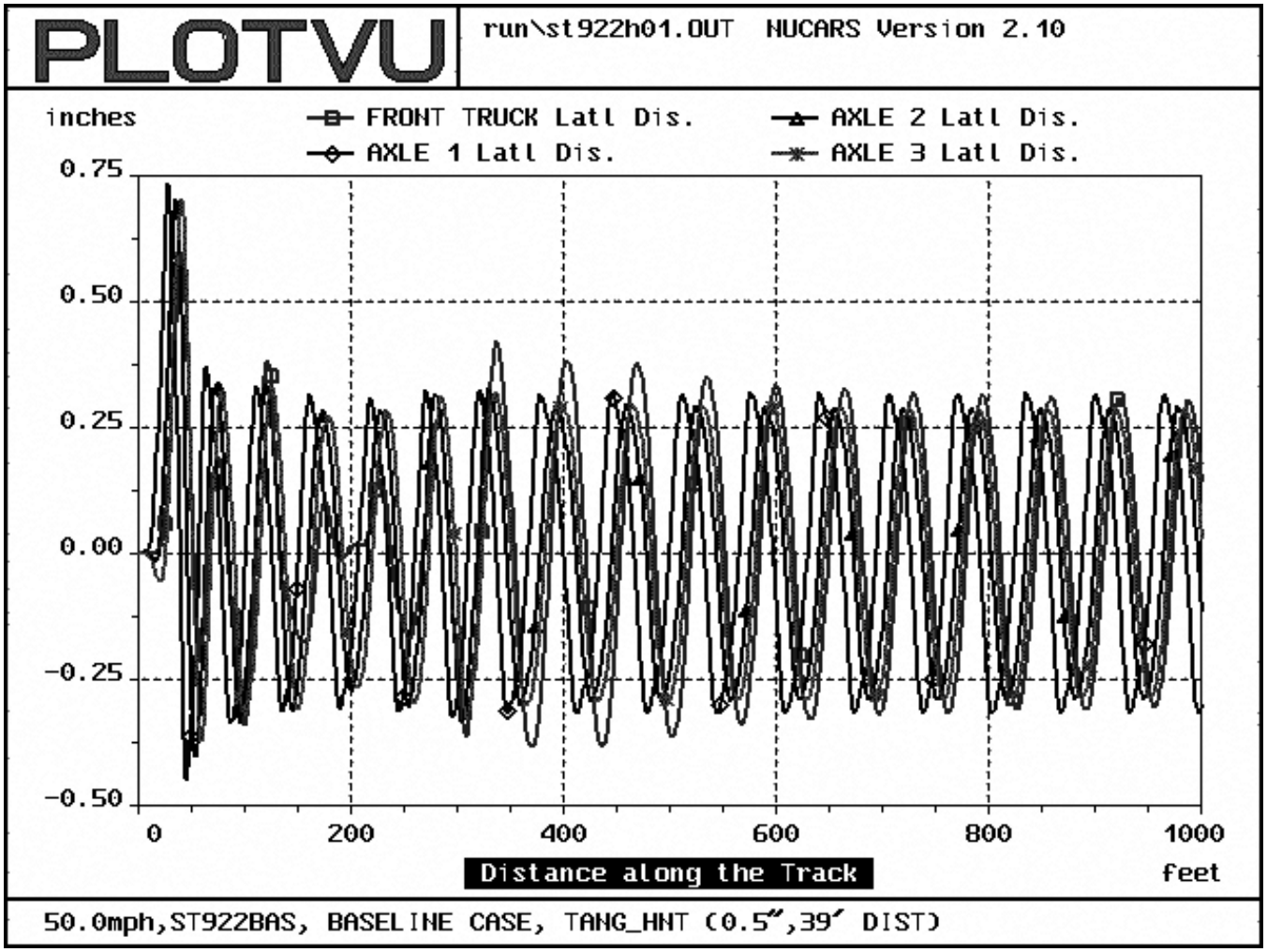

Figure 4.2 Time trace of relative axle displacement for 50.0 mph

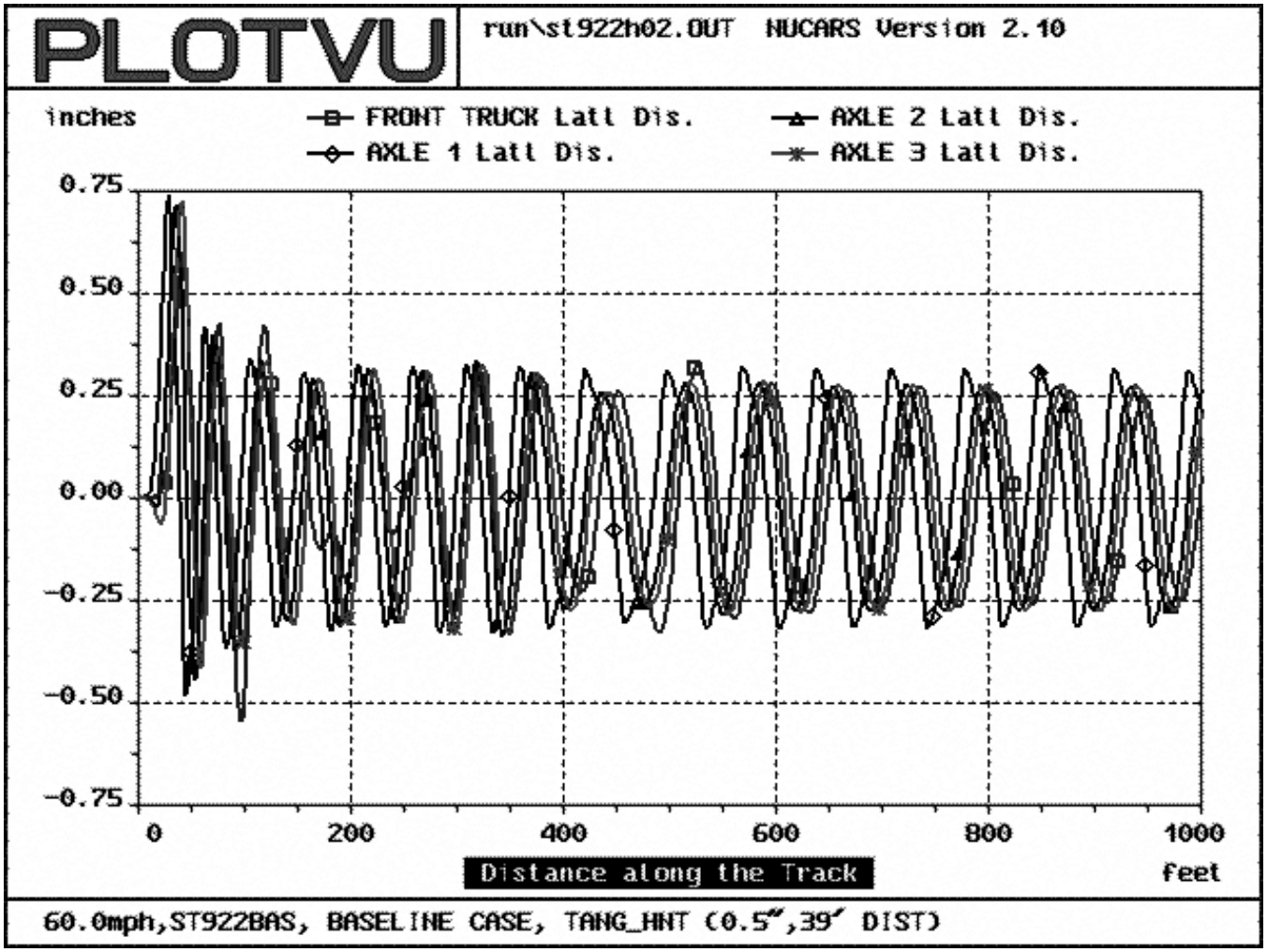

Figure 4.3 Time trace of relative axle displacement for 60.0 mph

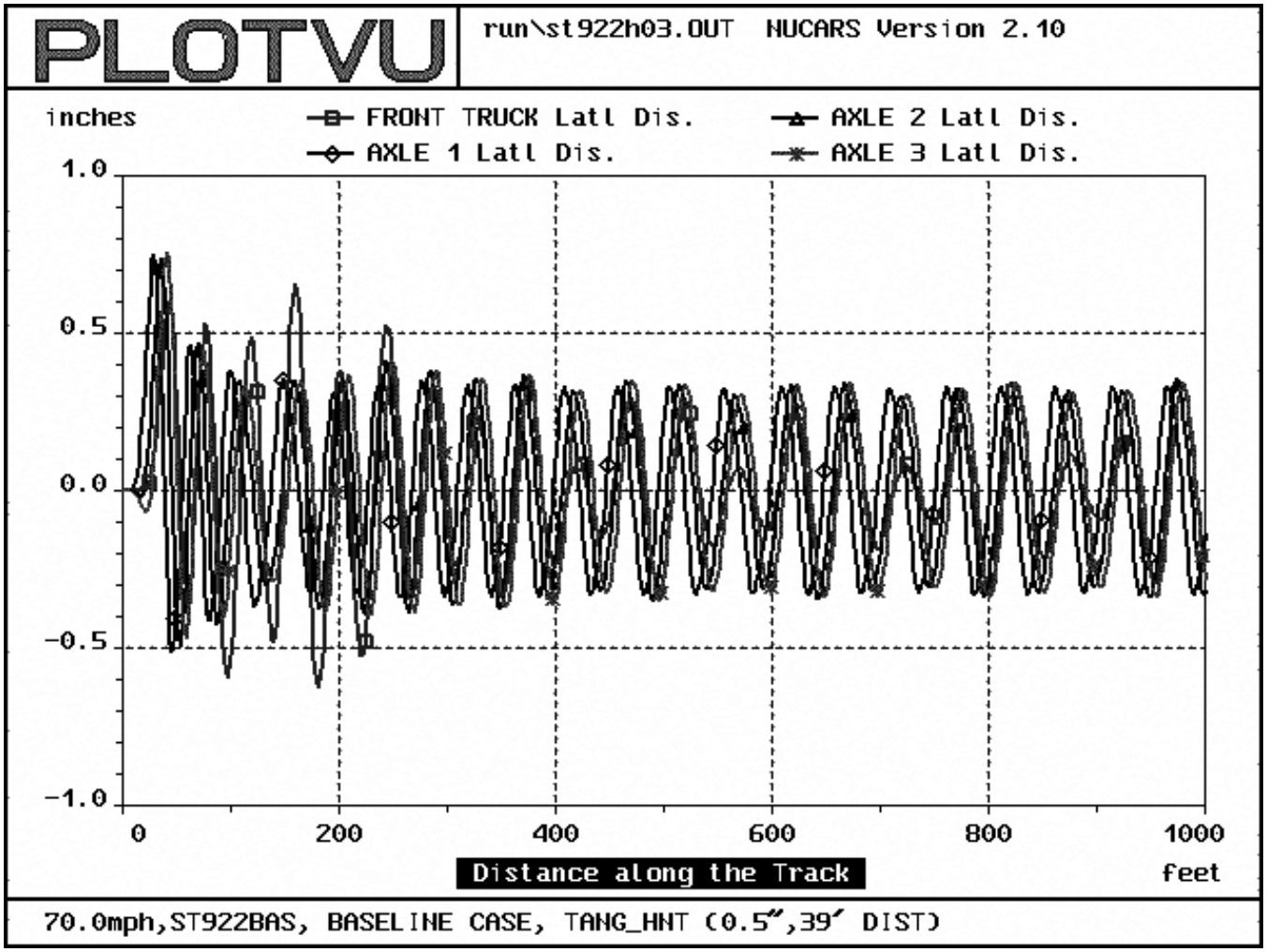

Figure 4.4 Time trace of relative axle displacement for 70.0 mph

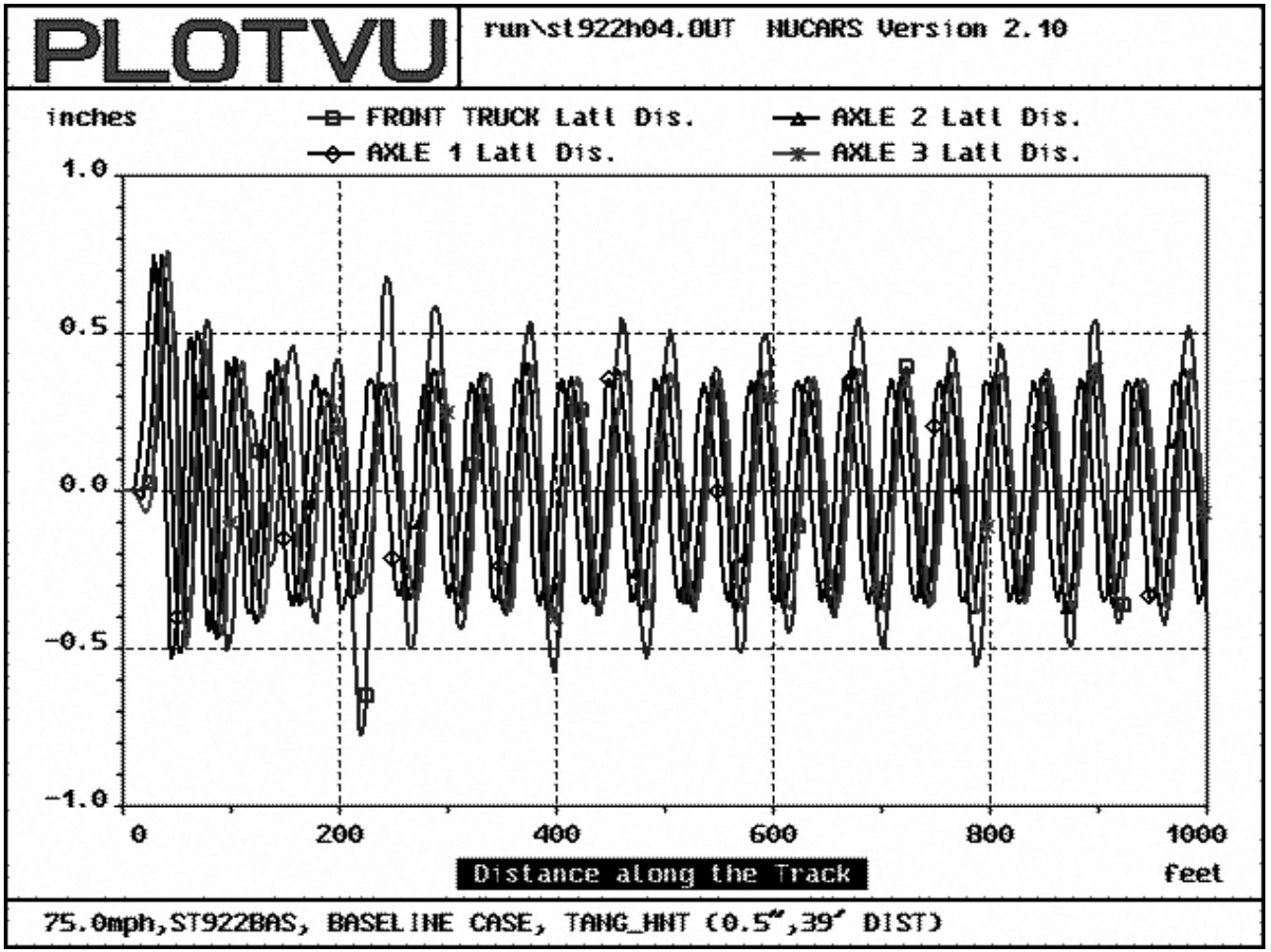

Figure 4.5 Time trace of relative axle displacement for 75.0 mph

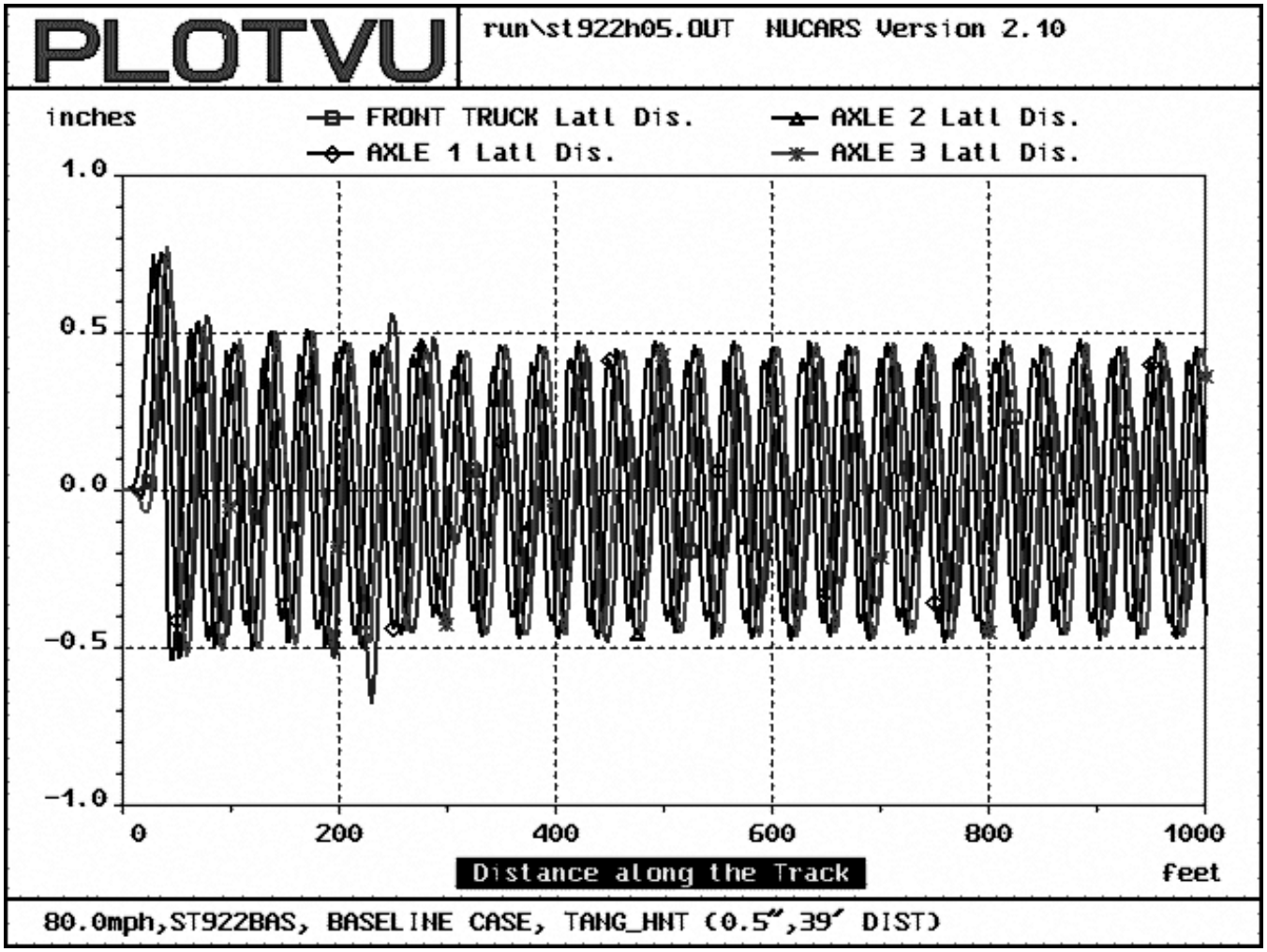

Figure 4.6 Time trace of relative axle displacement for 80.0 mph

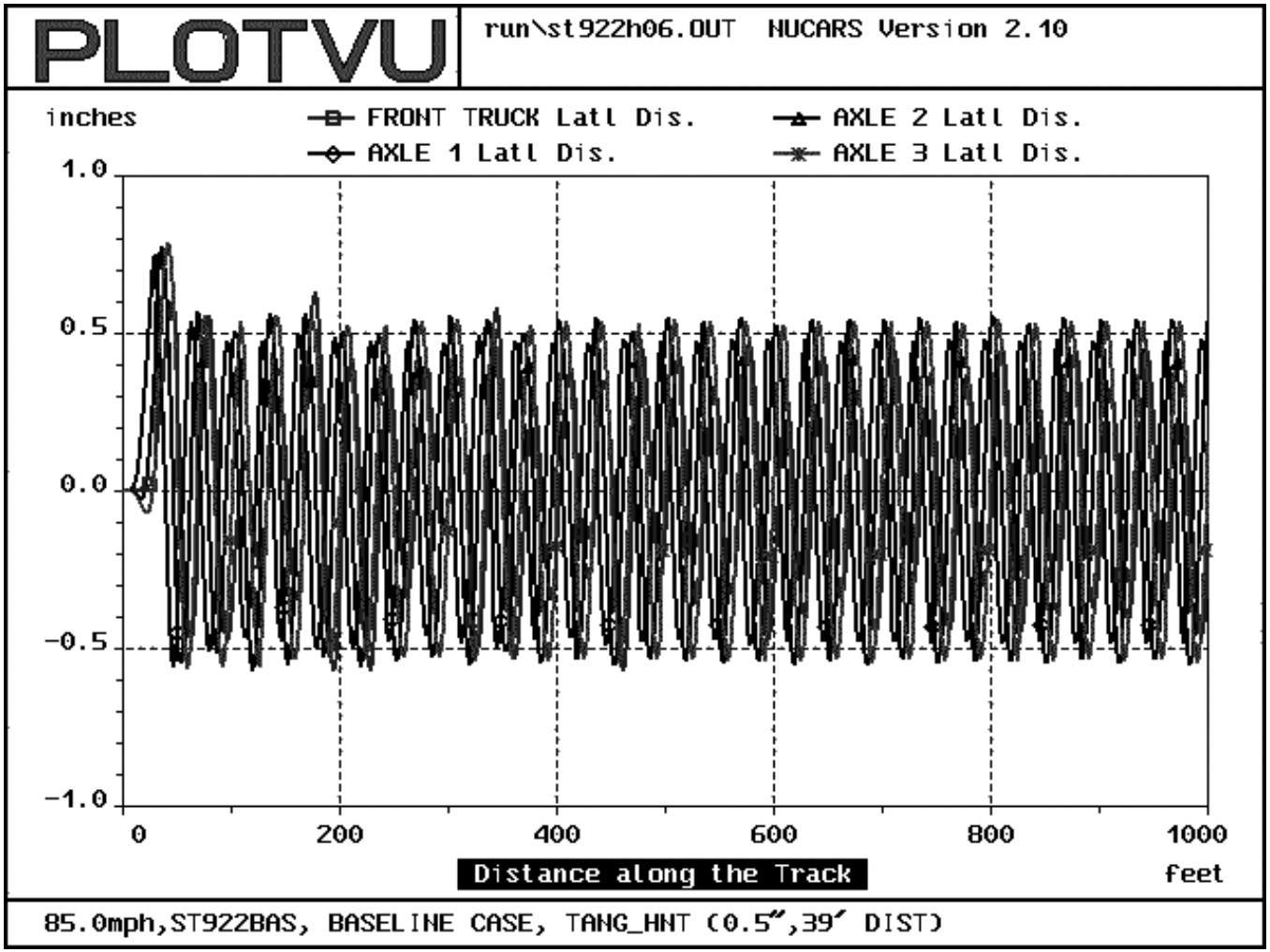

Figure 4.7 Time trace of relative axle displacement for 85.0 mph

The peaks of the relative axle displacement in the time traces, shown in Figures 4.2 to 4.7, occur closer together at higher speeds. This suggests that the frequency of the hunting oscillation is increasing with forward speed. The harmonic frequency in a plot can be determined by multiplying the number of oscillations observed in a 500 foot section by the velocity of the model and dividing this by the distance traveled (in this case 500 feet).

$$f = \frac{1}{T} = \frac{\left(\#\ \text{of oscillations} / 500\ \text{feet}\right)\left(\text{velocity} * 5280\ \text{fps} / 3600\ \text{mph}\right)}{(500\ \text{feet})} \qquad (4.2)$$

$$f = \frac{(7.5)\left(50\ \text{mph} * 5280\ \text{fps} / 3600\ \text{mph}\right)}{(500\ \text{feet})}$$

$$= 1.1\ \text{Hz}$$

For 50 mph, the relative axle displacement oscillates at 1.1 Hz. This frequency increases with speed, reaching 2.1 Hz at 70 mph, 3.3 Hz at 80 mph and 3.7 Hz at 85 mph.

4.1.4.2 Frequency Response of Relative Axle Displacement

Using the formulation for hunting frequency, shown in Eq. 2.12, we can determine the axle hunting frequency which drives the truck motion. The change in driving frequency is due to the velocity change, since all validation runs use the same parameters. These parameters are:

wheel radius: R=21"
wheel conicity: λ=1:20=0.05
track gage: a=59.5"

Using the above parameters, for 50 mph we obtain:

$$f_H = \frac{V}{2\pi}\sqrt{\frac{l}{aR}} = \frac{50\ \text{mph}}{2\pi}\sqrt{\frac{0.05}{29.75\text{"}*21\text{"}}}\left(\frac{5280*12}{3600}\right) \qquad \textbf{(4.3)}$$

$$f_H = \mathbf{1.25\ Hz} \quad \textbf{(50 mph)}$$

Table 4.2 shows the driving frequencies for speeds of 50 to 85 mph.

Table 4.2 Axle hunting frequencies for different speeds

Speed (mph)	Frequency (Hz)
50	1.25
60	1.50
70	1.75
75	1.88
80	2.00
85	2.13

Figure 4.8 shows the FFT's of the relative displacement of axle 1. By examining the figures, and referring Table 4.2, the onset of hunting can be identified as the speed where

1. a significant increase in the size of the resonance peak occurs, and
2. there is notable truck hunting (signified by a peak between 3 and 4 Hz).

This can be seen to happen at 75 mph, where there is a 50% increase in magnitude and the peak occurs at 2.6 Hz for a driving frequency of 1.9 Hz. This suggests that the critical speed is 75 mph, which agrees with the critical speed determined from the time traces of relative axle displacement.

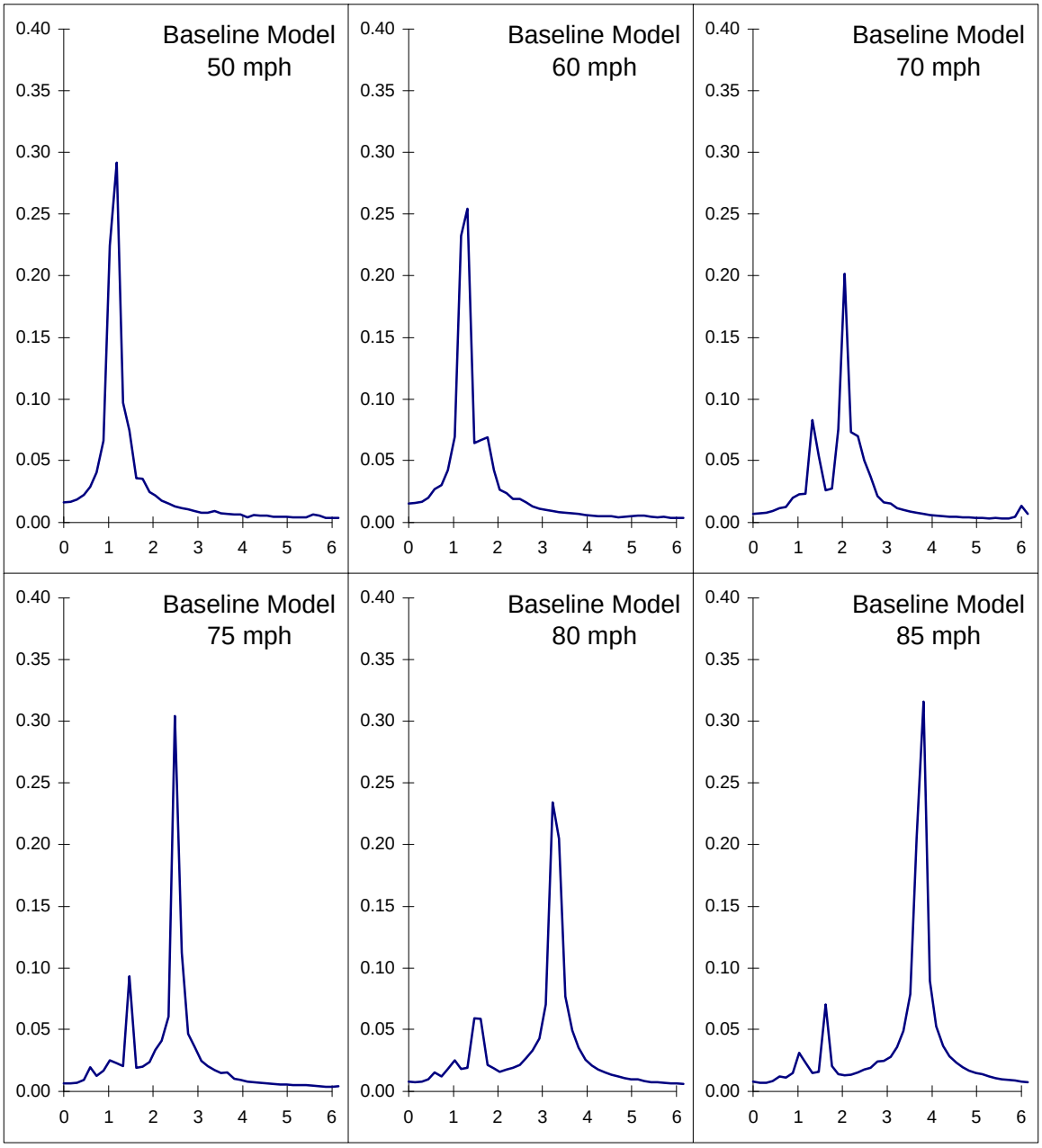

Figure 4.8 FFT's of axle 1 relative displacement for hunting tests

4.1.4.3 Time Traces of Cab Acceleration

Figures 4.9 to 4.11 show the time traces of the lateral cab acceleration that the crew would feel at a particular speed. The trend in these plots agrees with the time traces and frequency plots, shown in Figures 4.2 to 4.7 and Figure 4.8. At 50 mph (Figure 4.9), the lateral cab acceleration clearly decays with time, indicating that the model is stable at this speed. At 75 mph (Figure 4.10), the decay of the acceleration has been replaced with a constant amplitude oscillation whose center moves from side to side, showing that the model has begun to go unstable at that speed. At 85 mph (Figure 4.11), the amplitude is nearly 50 percent higher than for the 75 mph run. This suggests that the model has become unstable at this speed.

The critical speeds suggested by the three methods are all approximately 75 mph; the same critical speed was found in field testing of the locomotive. As such, we can conclude that the model provides a reasonably accurate estimation of critical hunting speed.

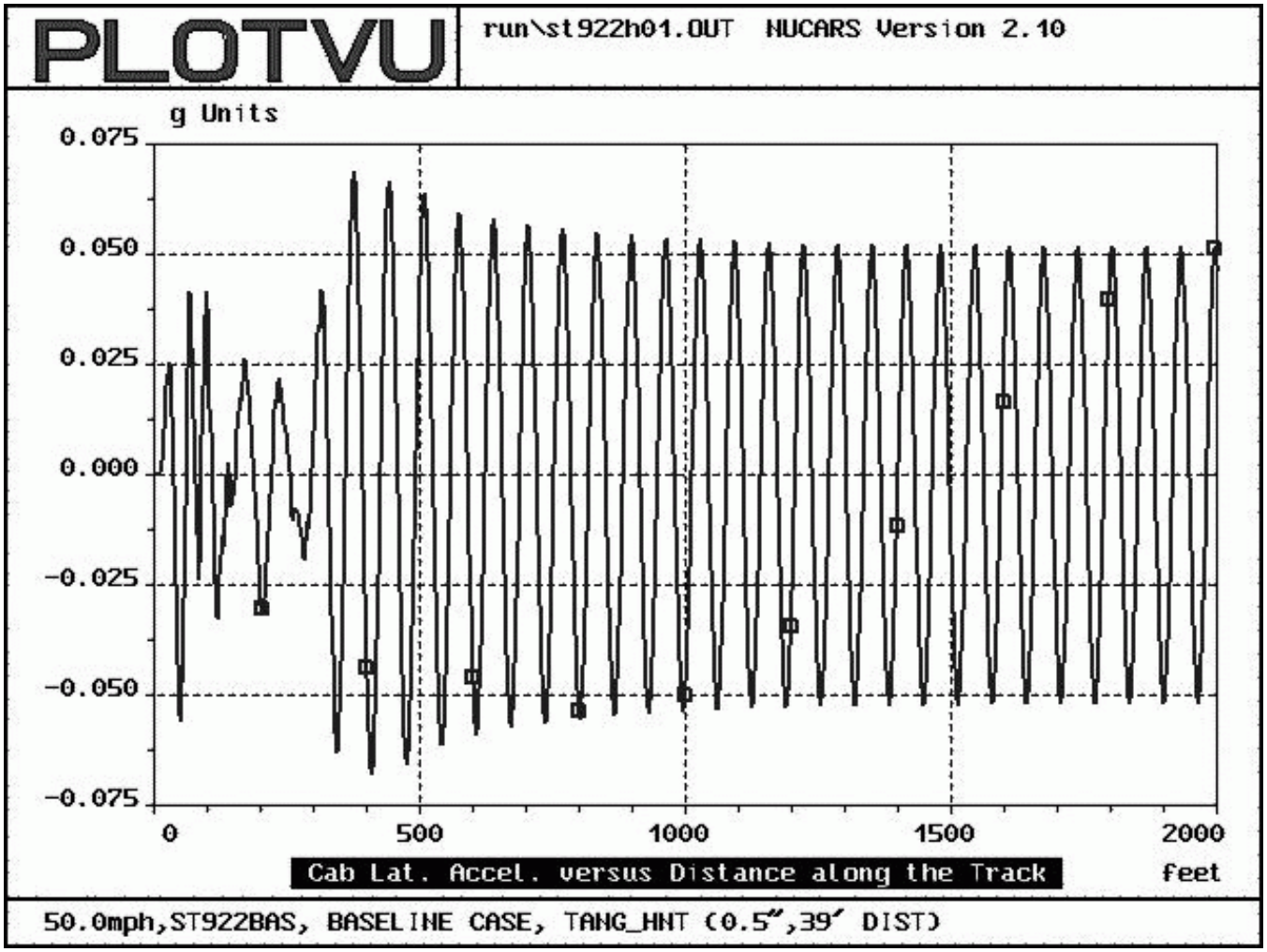

Figure 4.9 Time trace of cab lateral acceleration for 50.0 mph

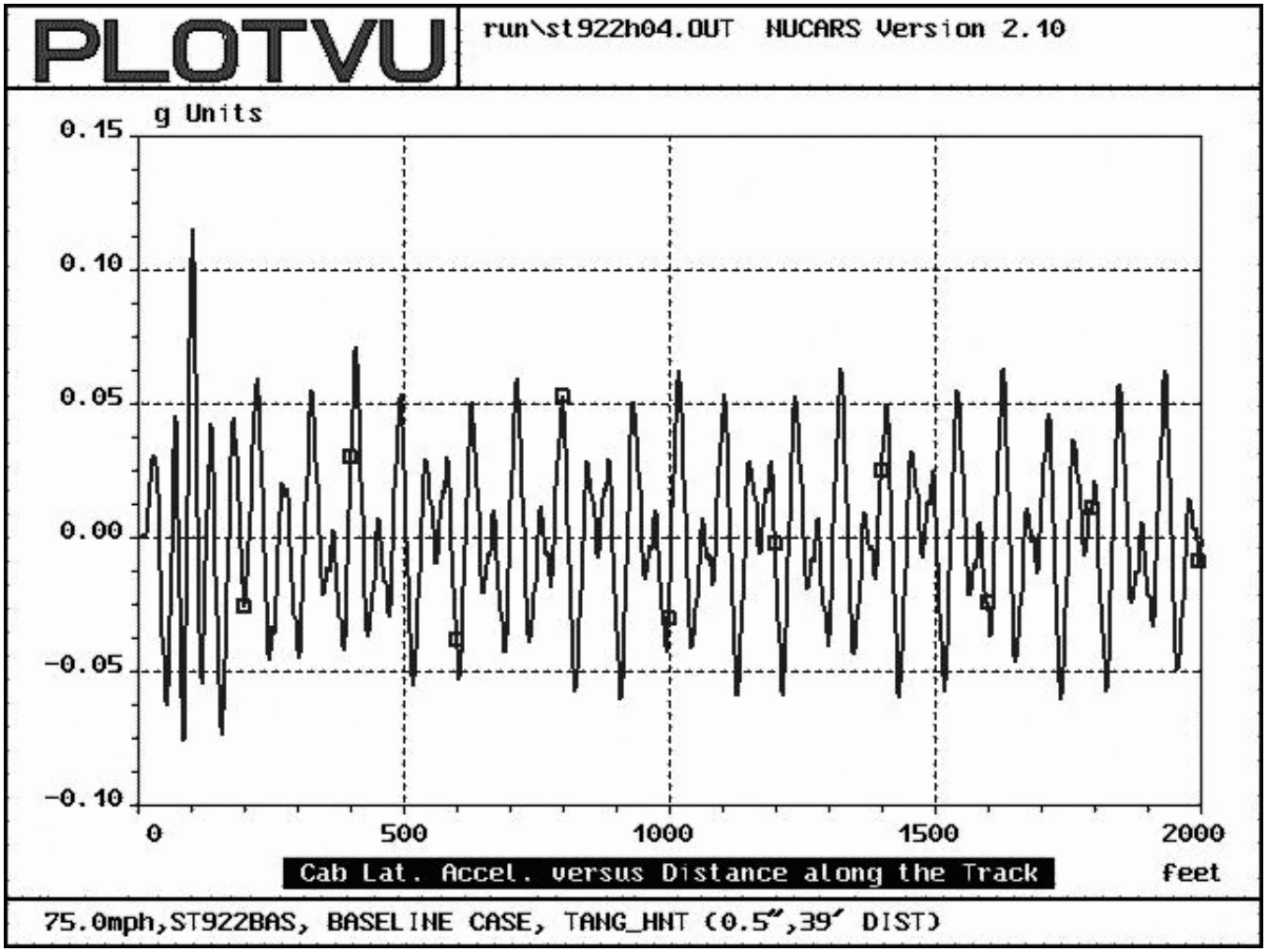

Figure 4.10 Time trace of cab lateral acceleration for 75.0 mph

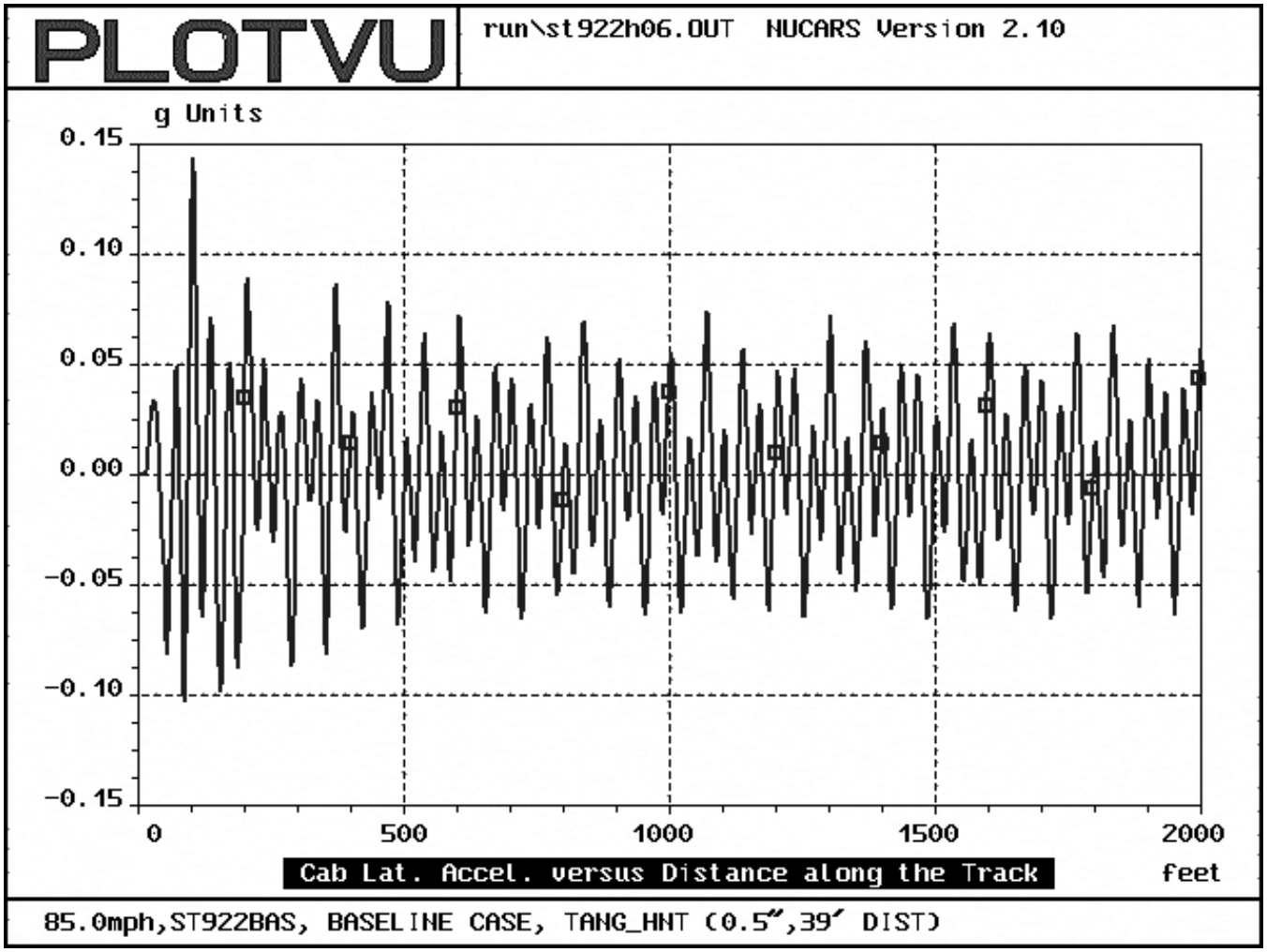

Figure 4.11 Time trace of cab lateral acceleration for 85.0 mph

4.2 Curved Track Tests

To check the model's curving behavior, several runs are made on curved track sections. The steady-state curving positions and the wheel/rail interactions are then used to show how well the model can predict curving behavior.

4.2.1 Description of Track

Four curved track files are used for the runs. Three of the curves (7.5, 10 and 12 degrees) represent portions of the Wheel Rail Mechanism (WRM) test loop at the Transportation Test Center in Pueblo, Colorado. This allows the simulation output to be compared with both the locomotive's expected behavior and with the results from field testing. The fourth curve file represents an extreme curvature of 20 degrees. Each of these curves features a 50-foot straight section to assure that the model is running correctly, a 900-foot curve body, and 100-foot entry and exit spirals to smooth the transition into and out of the body of the curve. The specified superelevation of the curve bodies matches the values in the WRM test loop; specifically, 3,4 and 5 inches for the 7.5, 10 and 12 degree curves, respectively. This sets the balance speeds for each curve at approximately 24 mph. To remain consistent, the 20 degree curve was given 8 inches of superelevation, which also set its balanced speed at 24 mph.

Over-balanced and under-balanced speeds, illustrated in Figure 4.12, refer to speeds where there is too much and too little track superelevation, which causes the resultant of the gravitational and centrifugal forces to be directed to the inside or outside

of the track center. This causes larger vertical loads on one side of the locomotive and for extremely under-balanced curves can lead to the vehicle rolling off of the track.

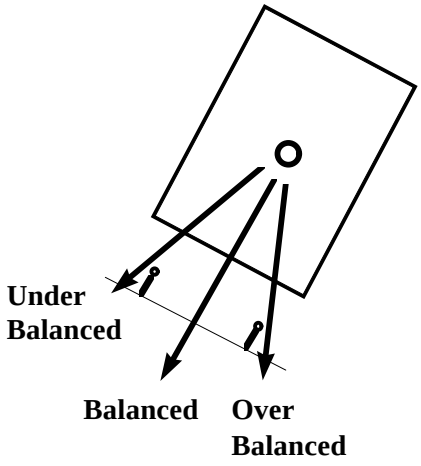

Figure 4.12 Body forces in a curve at balance speed

4.2.2 Simulation Speeds

The model is run for each of the curved track sections at three different speeds to investigate its behavior while balanced, over-balanced by 2 inches, and under-balanced by 2 inches. Runs on the 20° section were done with 3inches of over- and under-balance. The speeds in all curves corresponding to the three balance conditions are shown in Table 4.3.

Table 4.3 Speeds for validation curving runs

curvature	over-balanced	balanced	under-balanced
7.5 deg	12.0	24.0	34.0
10 deg	12.0	24.0	31.9
12 deg	15.5	24.5	31.1
20 deg	19.0	24.1	28.4

4.2.3 Criteria Used

The output values used to evaluate the curving runs include the lateral displacement of the axles and truck frame, their yaw angles and the wheel lateral-to-vertical force ratios. In the body of a curve, the axles and truck are in steady-state curving and assume quasi-static positions. The lateral displacement and the yaw rotation plots show these curving positions. The wheel L/V ratios are used to evaluate the locomotive's proximity to derailment, and to show the interaction between the wheels and the rail. These values are useful in evaluating curving forces at each wheel for the purpose of determining the risk of derailment through wheel climb, rail rollover, or both.

4.2.4 Results of Curving Validation Runs

4.2.4.1 Change In Speed/Balance Condition

Figures 4.13 to 4.15 show the axle and truck lateral displacements in the 7.5 degree curve for three curving conditions. These are over-balanced, balanced, and under balanced. As the plots show, the axles and truck run smoothly down the center of the track for the initial tangent sections (the first 50 feet). As the vehicle travels through the entry spiral, the axles move out to generate a difference between their left and right rolling radii. For higher speeds (the balanced and under-balanced cases), the axle shift is greater. This generates a larger difference in the rolling radii and creates the larger lateral forces needed for turning at a faster rate. This can be seen in the increased lateral displacements for the under-balanced case (34.0 mph) compared to the lateral displacements for the balanced (24.0 mph) and over-balanced (12.0 mph) cases, which are 0.42", 0.38", and 0.32",

respectively. The outward motion of the axles causes the truck frame to initially shift outward, too, before being influenced by the balance condition of the curve. For the over-balance case, where the resultant force is directed toward the inside of the curve, the truck frame shifts to the inside rail (a negative displacement). In the balance case, the truck displacement remains positive but smaller than the displacement of the axles. At under-balance speed, the large radial acceleration due to centrifugal force pushes the truck frame to the outside of the axles.

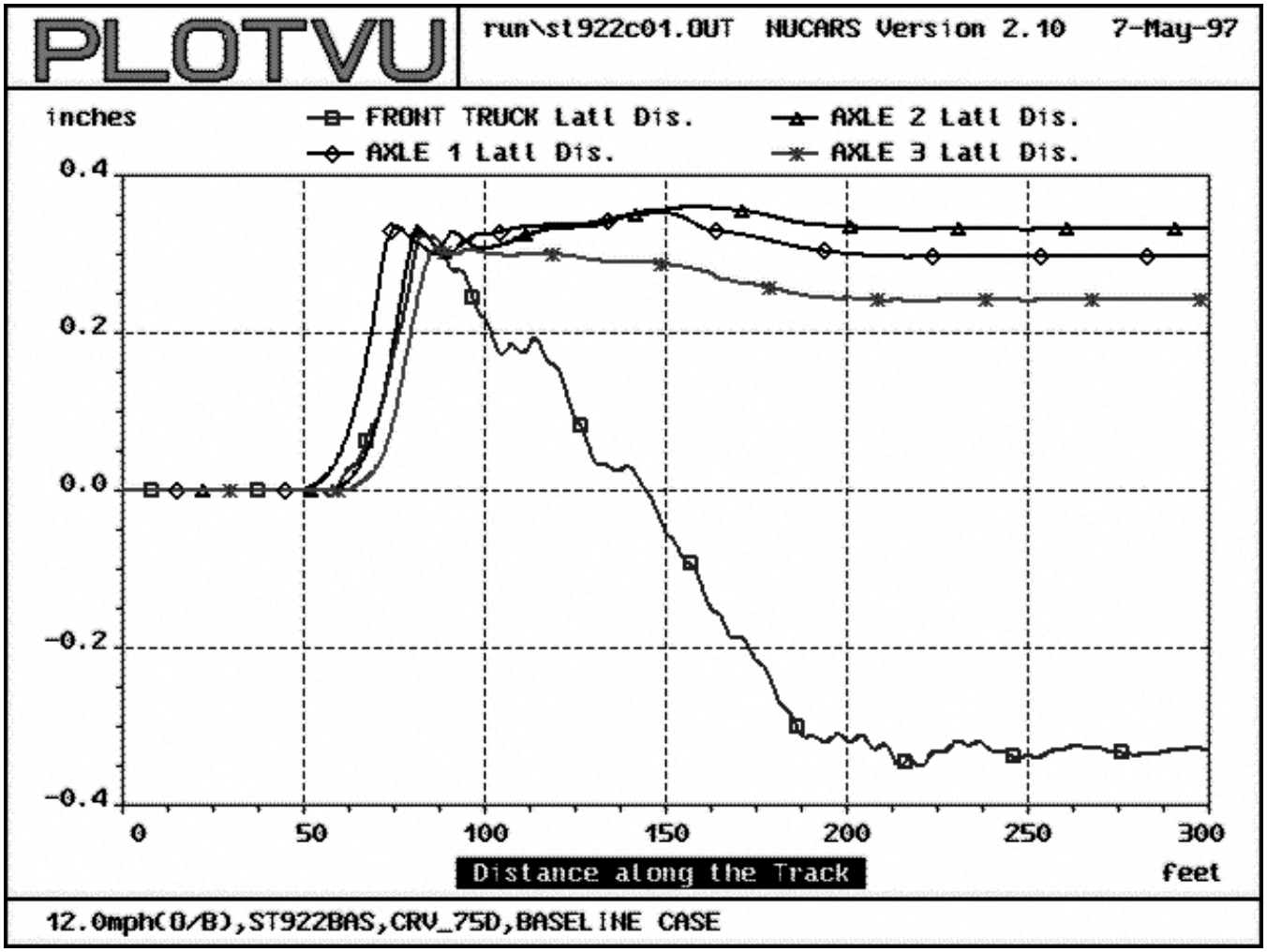

Figure 4.13 Axle lateral displacements for over-balance speed

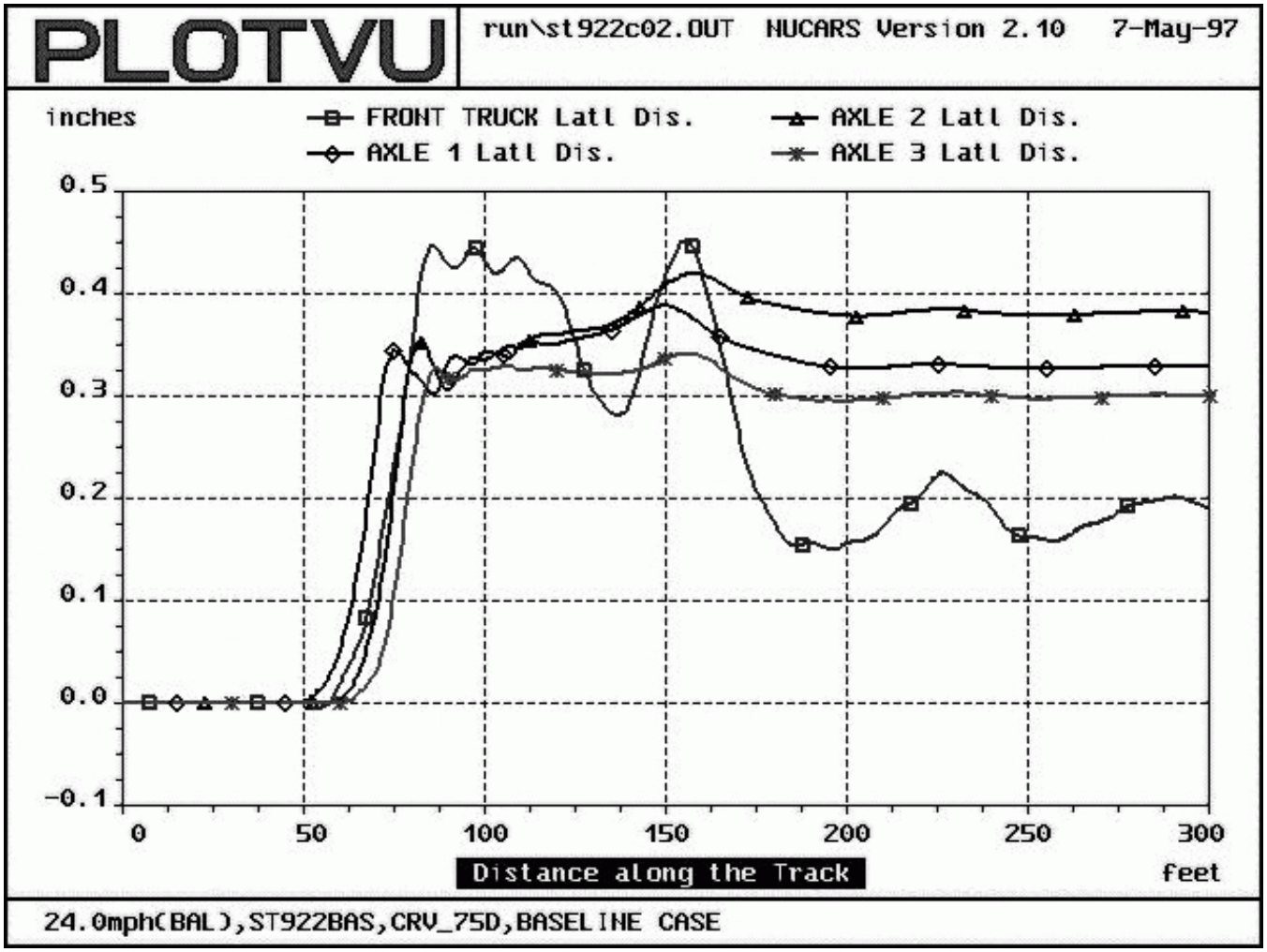

Figure 4.14 Axle lateral displacements for balance speed

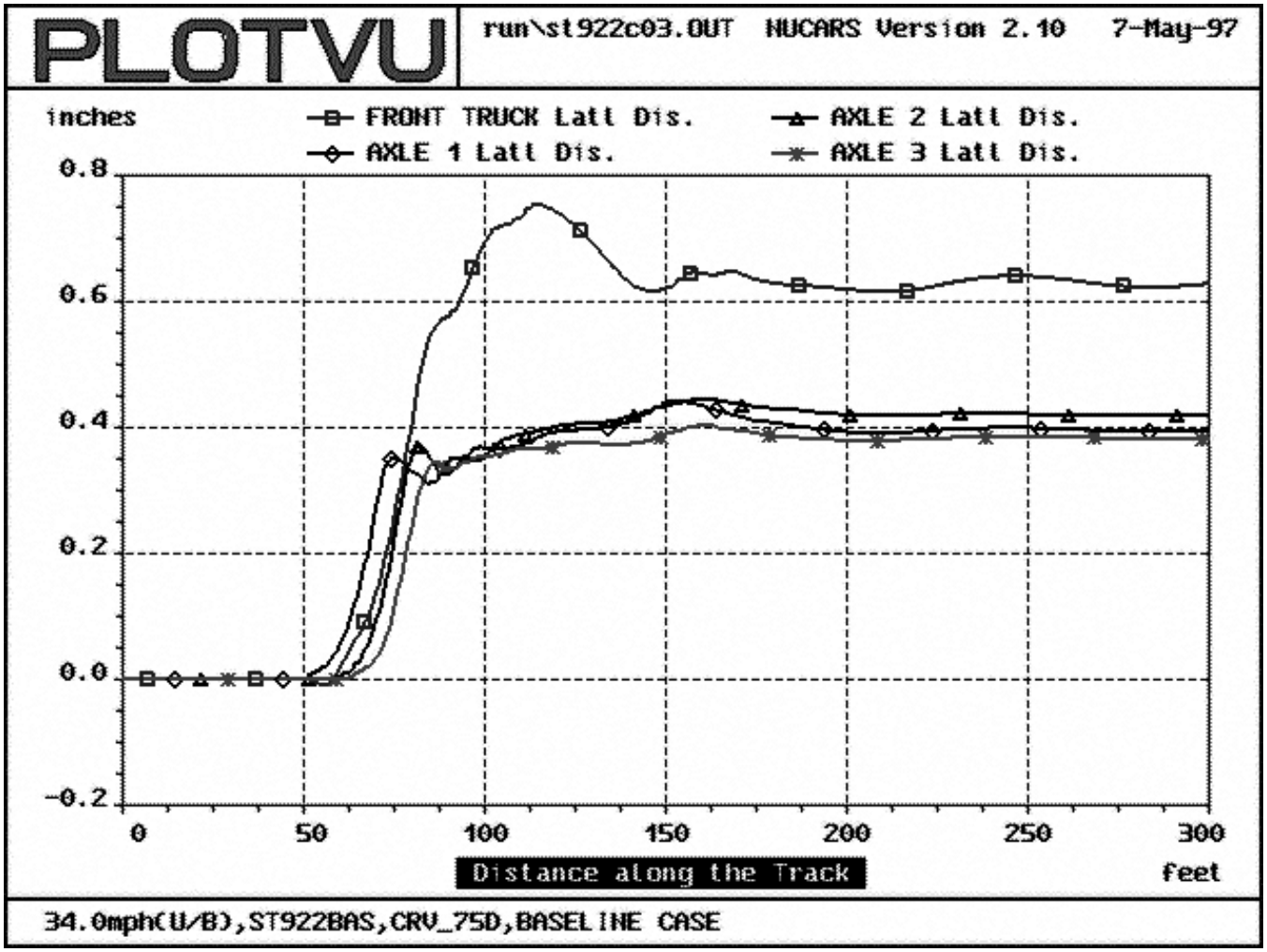

Figure 4.15 Axle lateral displacements for under-balance speed

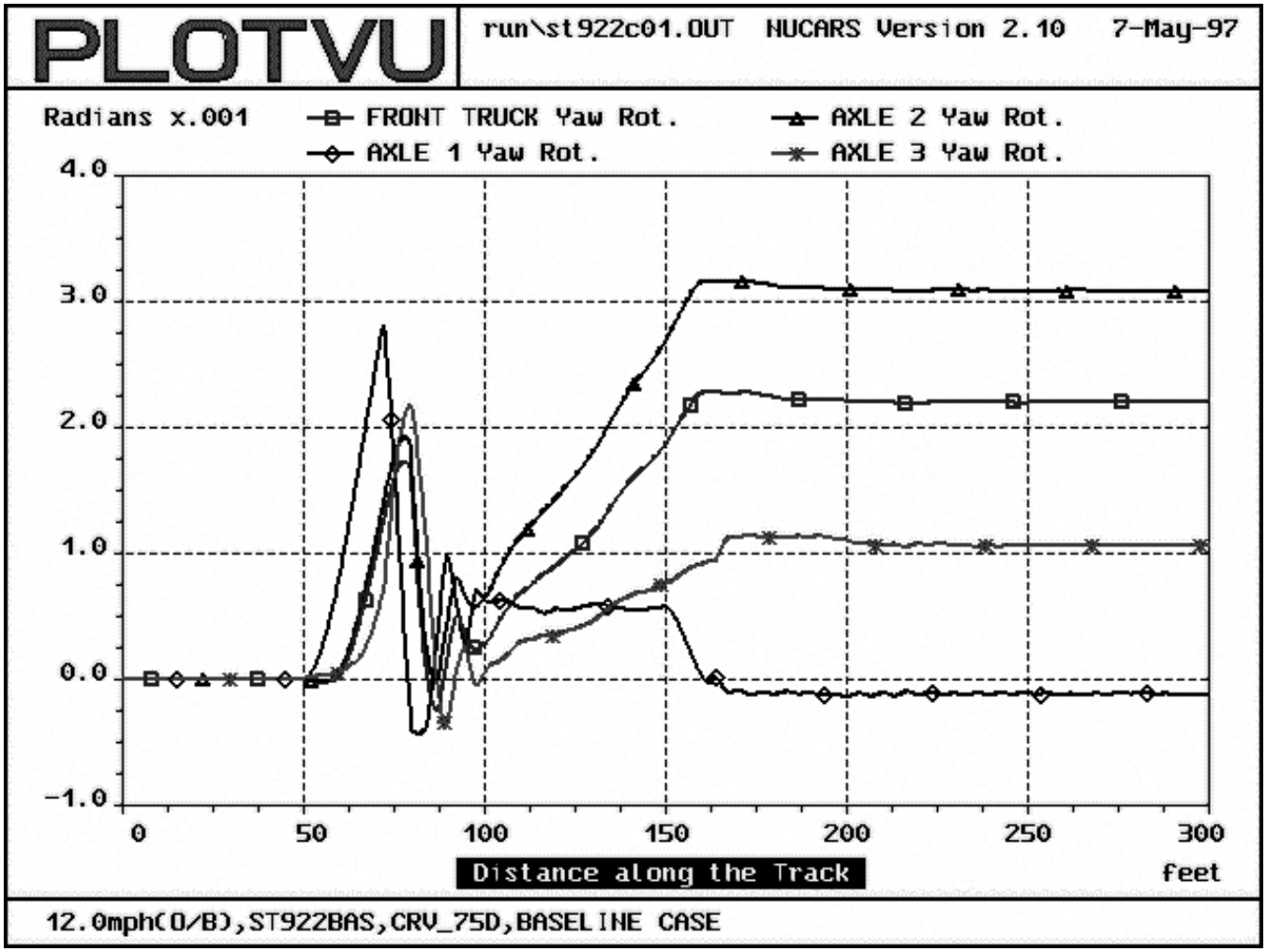

Figure 4.16 Axle yaw rotations for over-balance speed

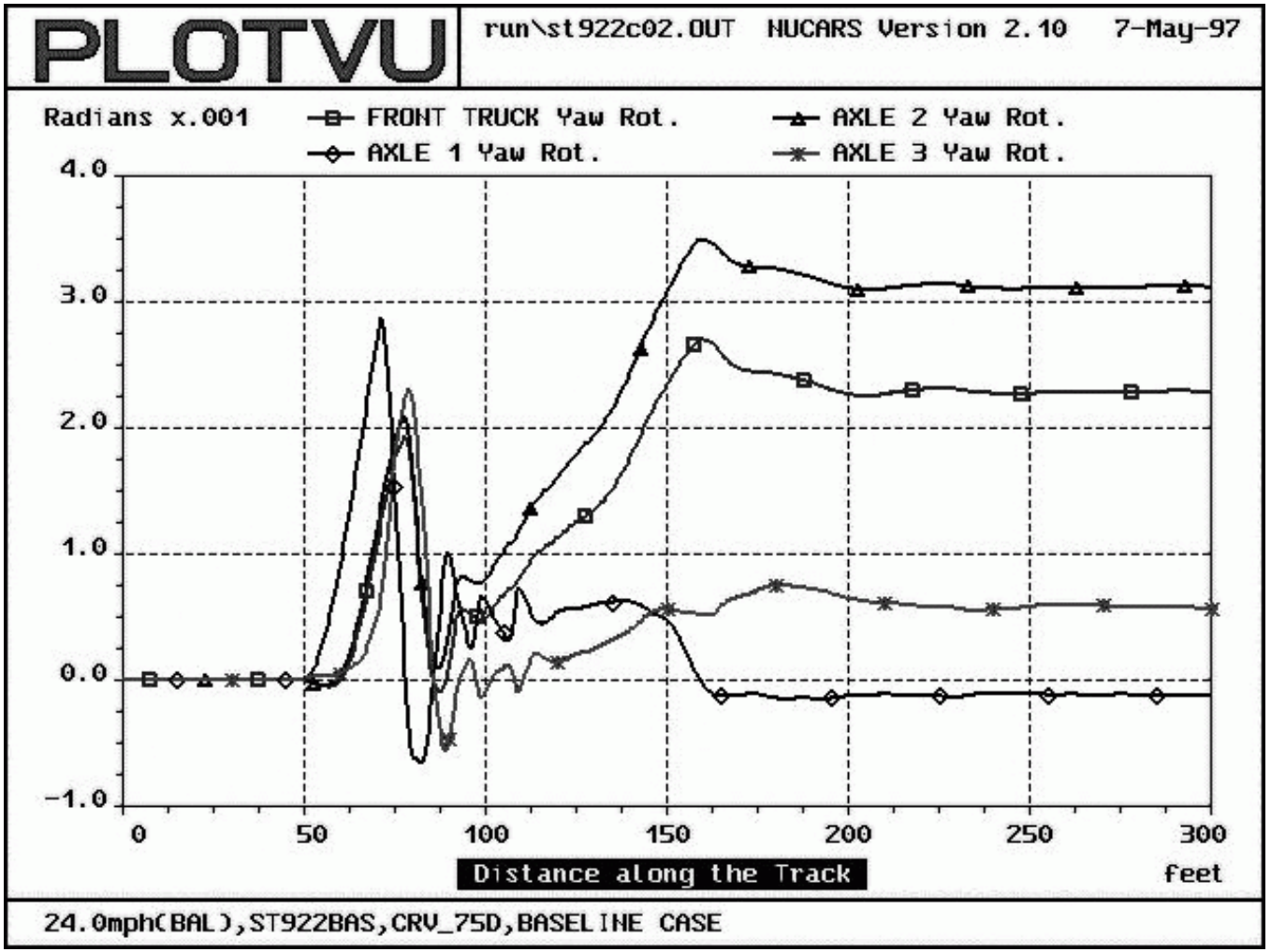

Figure 4.17 Axle yaw rotations for balance speed

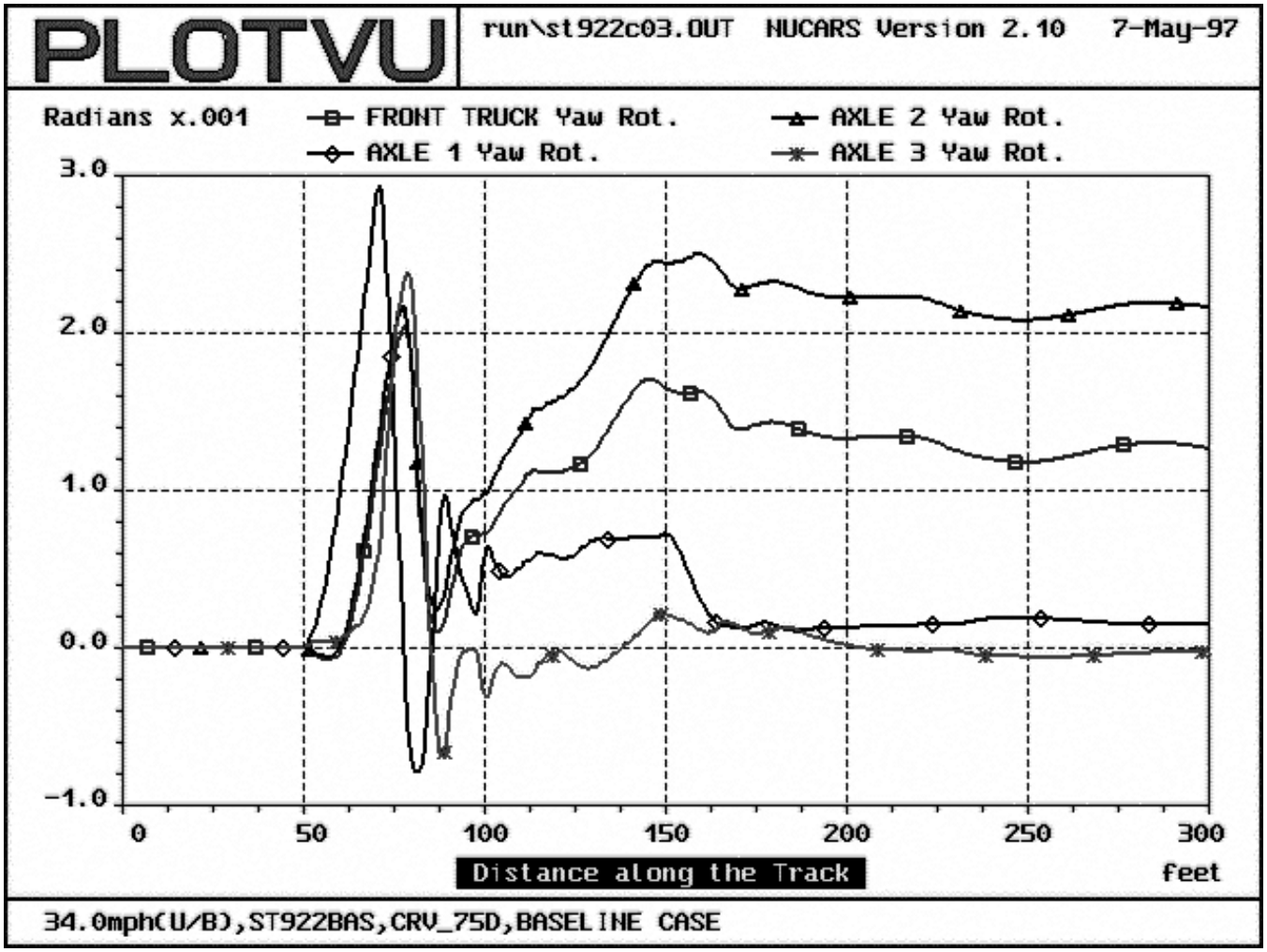

Figure 4.18 Axle yaw rotations for under-balance speed

The yaw rotation of the axles and truck frame for the three balance conditions are shown in Figures 4.16 to 4.18. The angles given in the plots are relative to the local track coordinate systems and represent the angle of attack that each axle makes with the rail. The yaw of an axle relative to the truck frame can be determined by

$$\Theta_{AXLE/TRUCK} = \Theta_{AXLE} - \Theta_{TRUCK} - \Theta_{REL} \quad \textbf{(4.4)}$$

or

$$\Theta_{AXLE/TRUCK} = \Theta_{AXLE} - \Theta_{TRUCK} - \sin^{-1}\left(D/R\right) \quad \textbf{(4.5)}$$

where

Θ_{AXLE} = **axle angle of attack with track**
Θ_{TRUCK} = **truck angle relative to track**
$\Theta_{AXLE/TRUCK}$ = **axle angle relative to truck**
Θ_{REL} = **angle between local coordinate frames for axle and truck**

as shown in Figure 4.19.

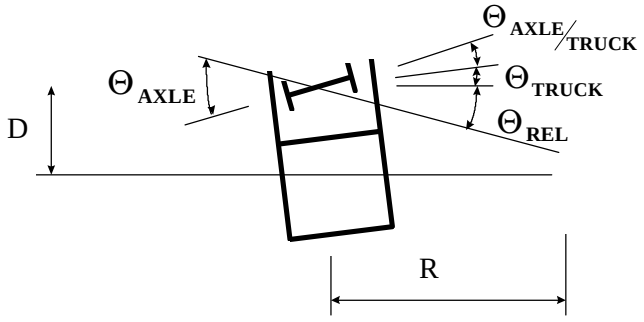

Figure 4.19 Angles due to distance between relative coordinate frames

The yaw of axle 1 relative to the truck frame varies from -0.762° for the over-balance case to -0.690° and -0.614° for the balance and under-balance cases, respectively. The lower axle yaw at higher speeds is due to the increased lateral displacement of the truck frame. For higher speeds, since the lateral displacement of the lead axle is one tenth of one inch larger and the lead axle is laterally constrained to the truck frame by traction links and inter-motor connections, the front of the truck frame is pulled to the inside of the curve, reducing its yaw angle. This can be seen in the reduced magnitude of the truck yaw angle at higher speeds.

The center links connecting the middle axle (axle 2) to the truck frame are oriented parallel to each other. This prevents the middle axle from yawing relative to the truck frame while negotiating a curve. The difference between the yaws of the truck and axle 2 in the plots is a constant 0.06°. This represents the difference in angular orientation of the local coordinate frames located at the respective centers of gravity (C.G.'s), as calculated by

$$\Theta_{REL} = \sin^{-1}\left(\frac{D}{R}\right) \qquad \textbf{(4.6)}$$

or

$$\Theta_{REL} = \sin^{-1}\left(\frac{9.26}{764*12}\right)$$
$$= 0.058^\circ$$

The variables D and R represent the distance between coordinate frames and the curve radius, as defined earlier.

The lateral-to-vertical force ratios (L/V's) on the individual wheels are similar for the three balance conditions, as depicted in Figures 4.20 to 4.22. The largest L/V occurs on the outside wheel of the middle axle for the 7.5° curve, unlike conventional trucks where the largest L/V occurs on the outside wheel of the lead axle. This is due to the larger angle of attack at the middle axle, as compared to the end axles in curving. The orientation of the traction links allows the end axles to yaw into the curve, while the center links keep the middle axle yaw fixed in relation to the truck. This can be seen by the angles of attack for the balanced case, shown in Figure 4.17, which are 0.178° for the middle axle and -0.006 and 0.040° for the lead and trail axles, respectively. As speed increases, more curving force is required and the loads on the wheels increase. As a result, the left (high) rail L/V's for both axles 1 and 2 are largest for the under-balanced run, which has the highest speed

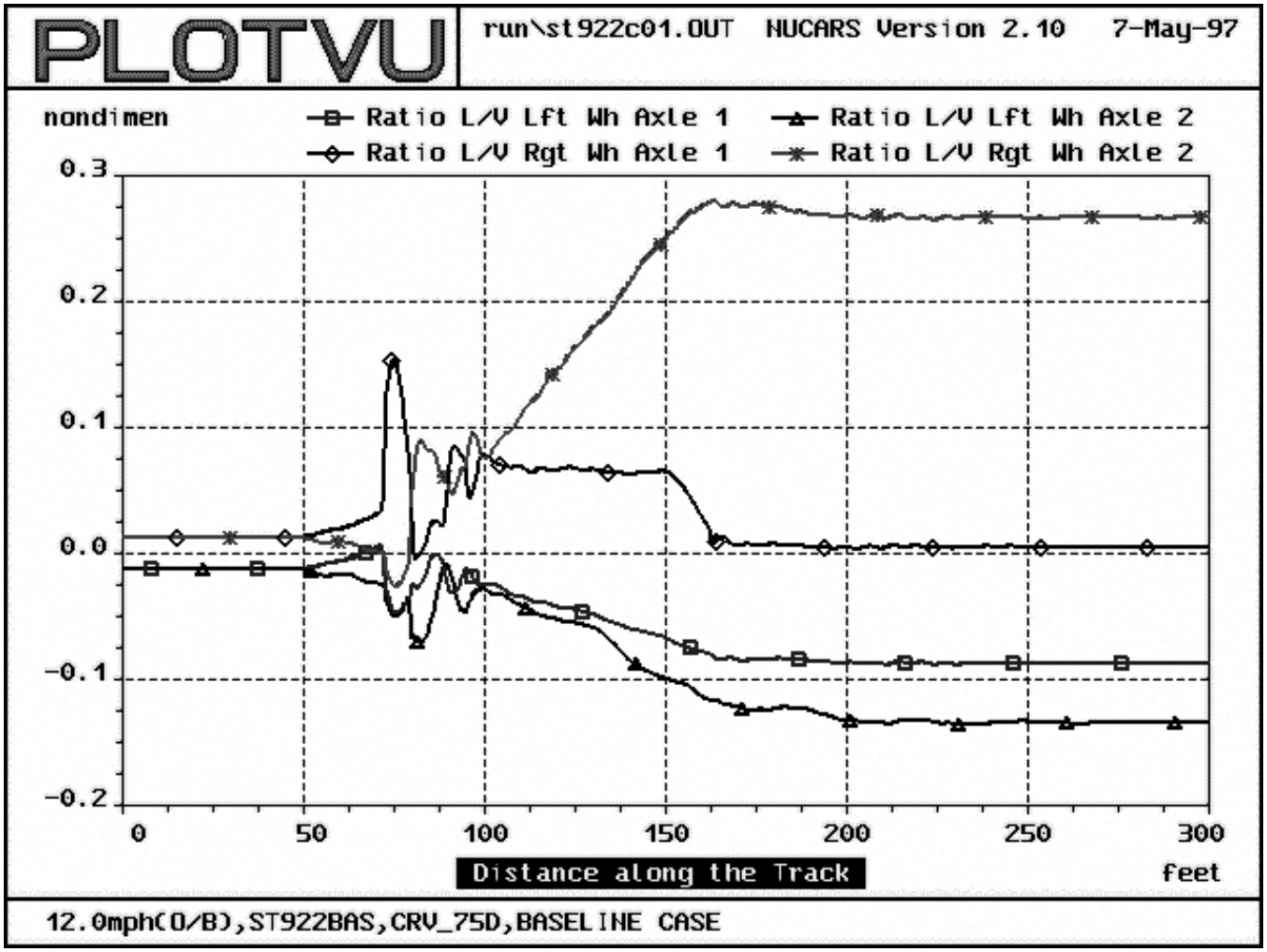

Figure 4.20 Wheel L/V ratios for axles 1 & 2 at over-balance speed

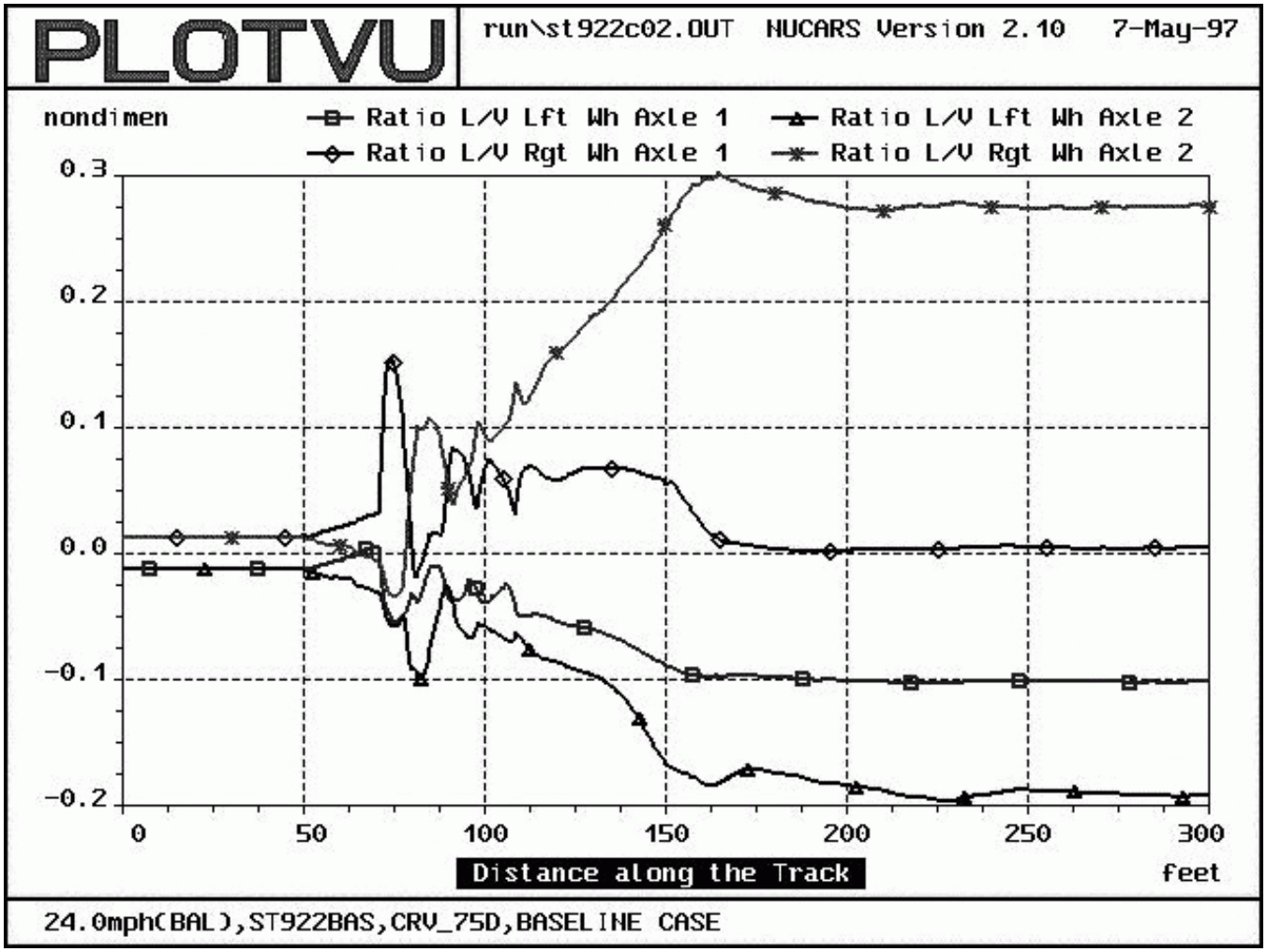

Figure 4.21 Wheel L/V ratios for axles 1 & 2 at balance speed

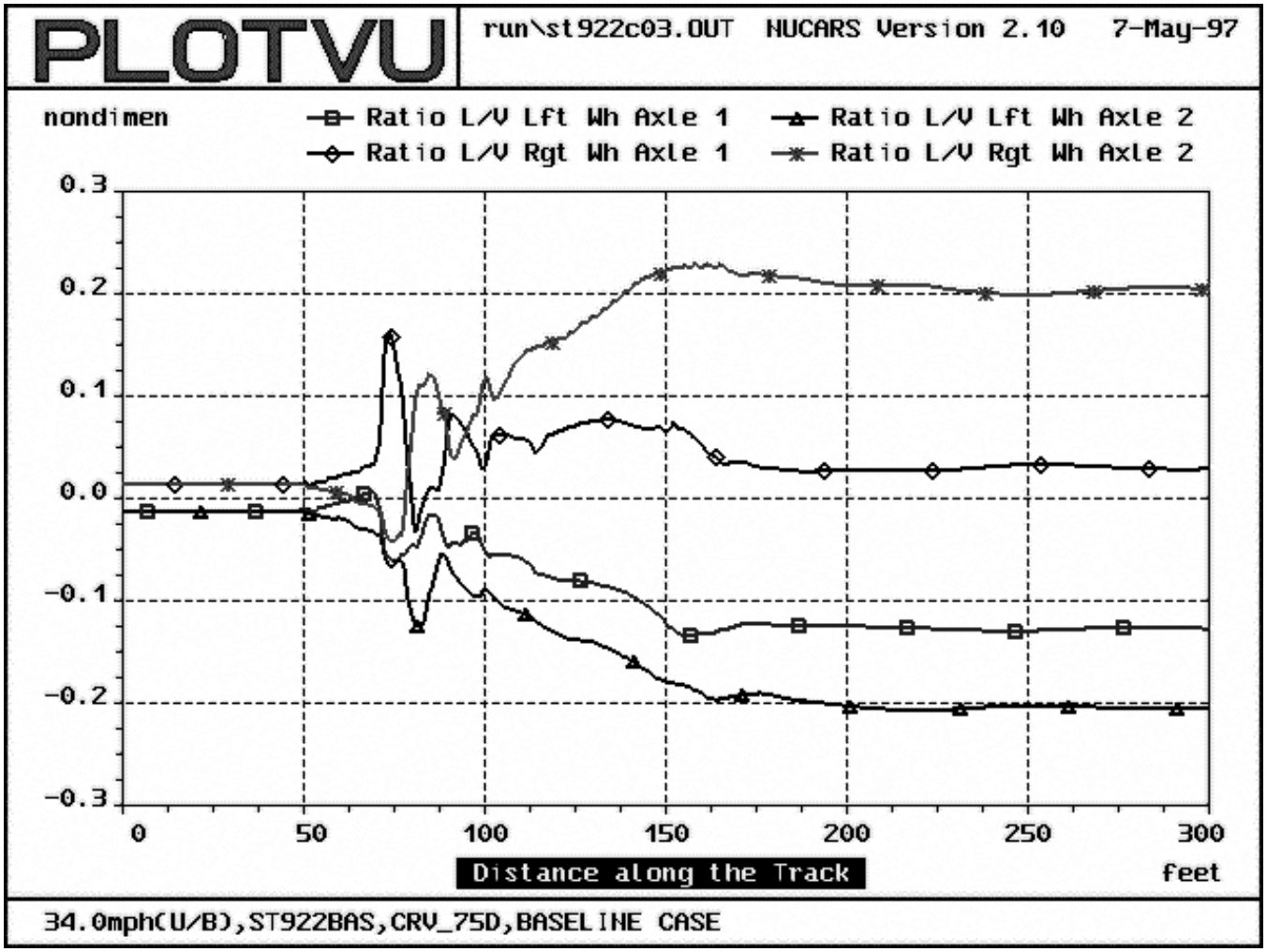

Figure 4.22 Wheel L/V ratios for axles 1 & 2 at under-balance speed

4.2.4.2 Change in Curvature

Figures 4.23 to 4.26 show the lateral displacements of the axles and truck frame for runs at balance speed on the four curved track sections. For the runs on the 7.5, 10 and 12 degree curves, the three axles all have similar relative displacements, with the magnitudes slightly increasing for higher curvatures. This indicates that the axles are able to negotiate the curve without much flanging. The yawing of the axles and radius differential between the left and right wheels (due to wheel conicity) enable the axles to curve. For higher degree curves, however, the axle constraints to the truck and the rail do not allow it to displace sufficiently to negotiate the curve. Therefore, the axles must flange to create the forces necessary for curving, as explained previously.

For instance, in a 20 degree curve, contact between the outside wheel of the lead axle and that rail produces a moment about the truck center of gravity. This moment is then transferred through the secondary suspension to the platform of the locomotive. As shown in Figure 4.34, the flange contact for the 20° curve is evident from the large jump in L/V ratio for the high-rail wheel of the lead axle, as compared to the 12° curve results in Figures 4.33.

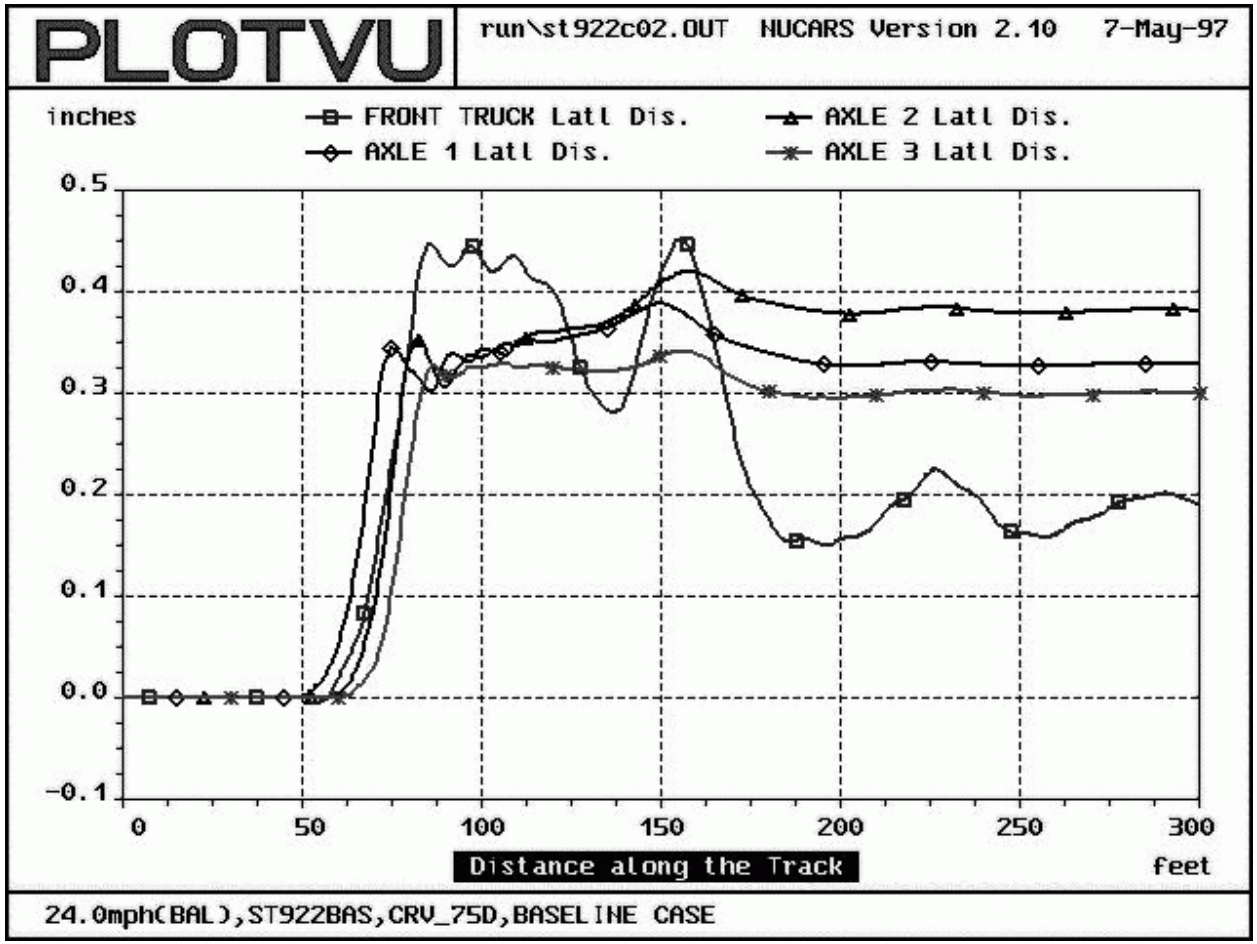

Figure 4.23 Axle lateral displacements for 7.5° curve

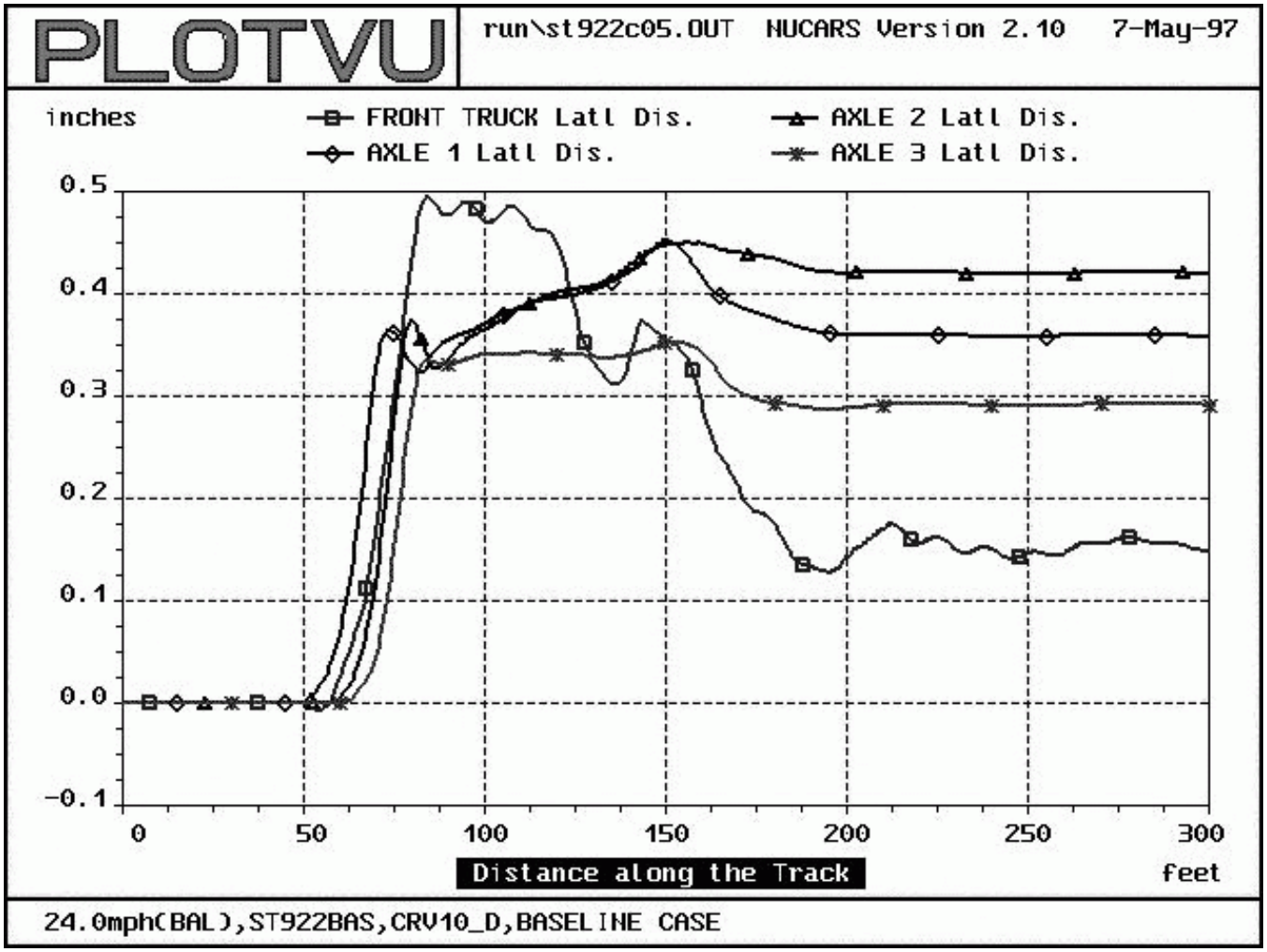

Figure 4.24 Axle lateral displacements for 10° curve

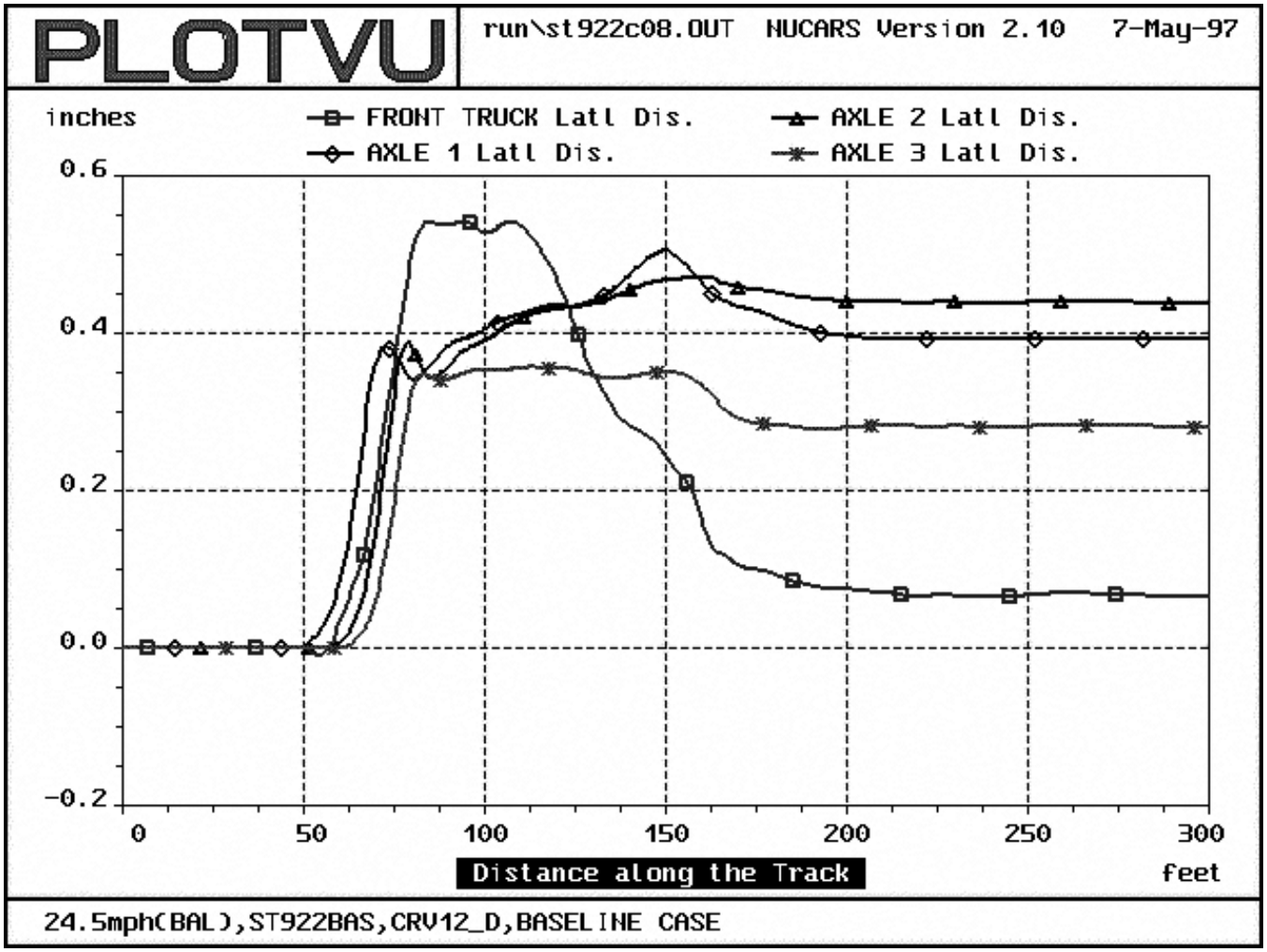

Figure 4.25 Axle lateral displacements for 12° curve

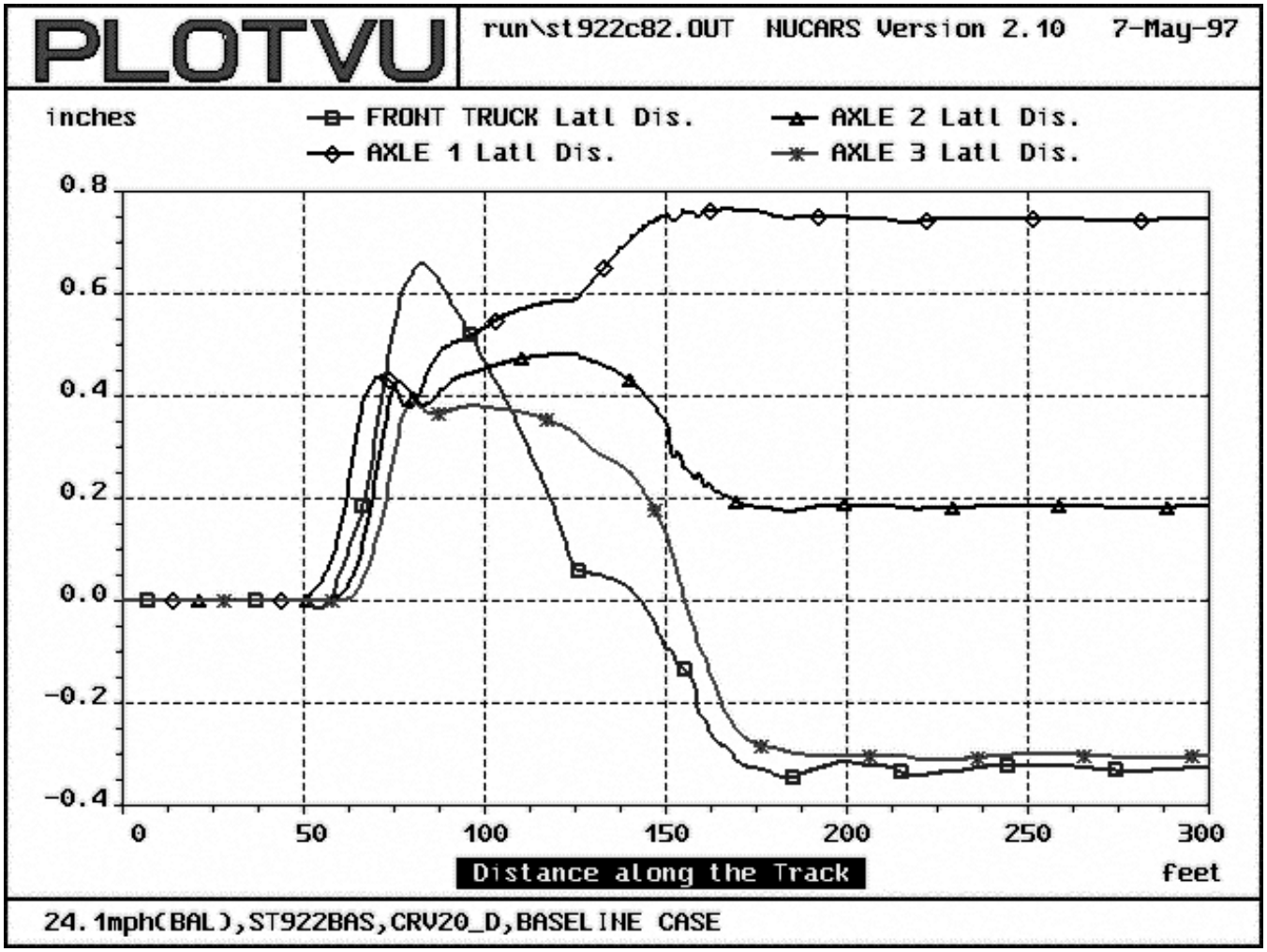

Figure 4.26 Axle lateral displacements for 20° curve

This change in curving dynamics is also shown in the plots of truck and axle yaw, shown in Figures 4.27 to 4.30. The first three plots (for 7.5, 10 and 12 degree curves) all have similar relationships between the yaw angles of the axles and truck frame, with the yaw magnitudes increasing with curvature. In the 20 degree curve, however, there is a jump in the yaw magnitude from 0.258° to 0.458°, as compared to the 12 curve. Additionally, it can be seen that axle 1 has the largest angle of attack in the 20° curve; the yaw of axle 1 is .744°, the truck frame yaw is 0.659°, and axles 2 and 3 are yawed negatively. This amounts to a yaw angle of -1.185° for axle 1 relative to the truck frame. Thus, the left rail flange contact is causing the lead axle to shift laterally, generating the large yaw angle.

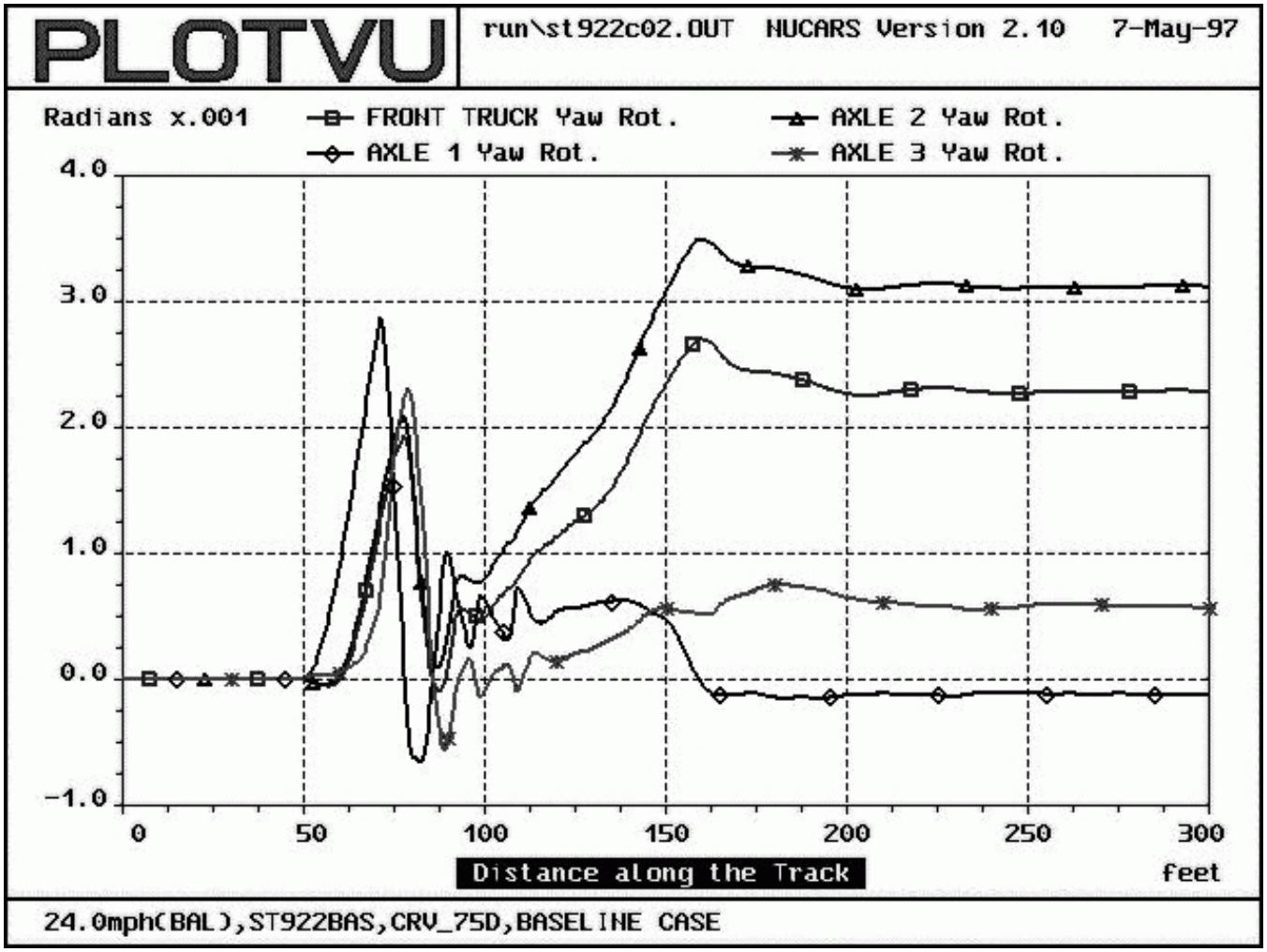

Figure 4.27 Axle yaw rotations for 7.5° curve

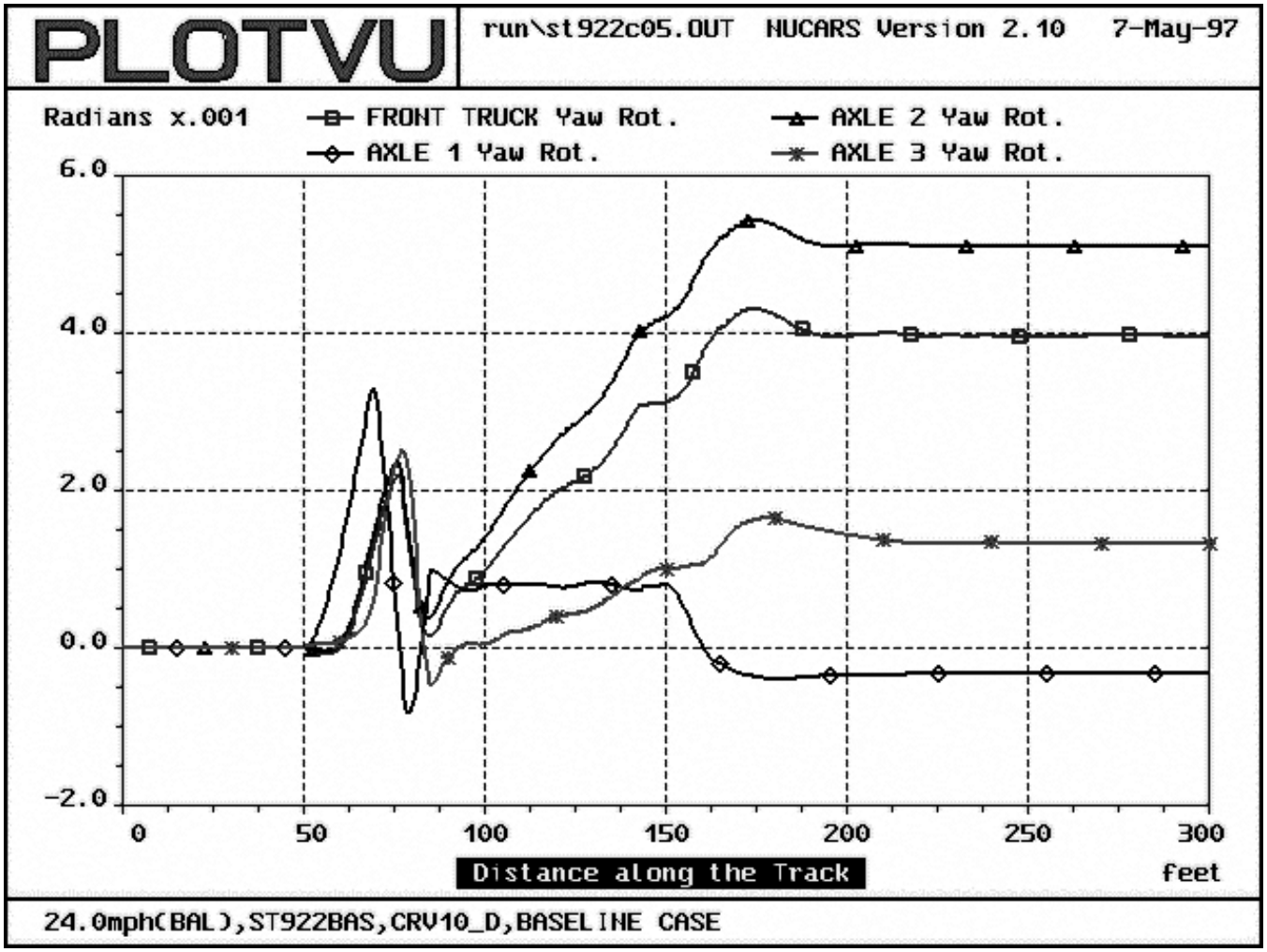

Figure 4.28 Axle yaw rotations for 10° curve

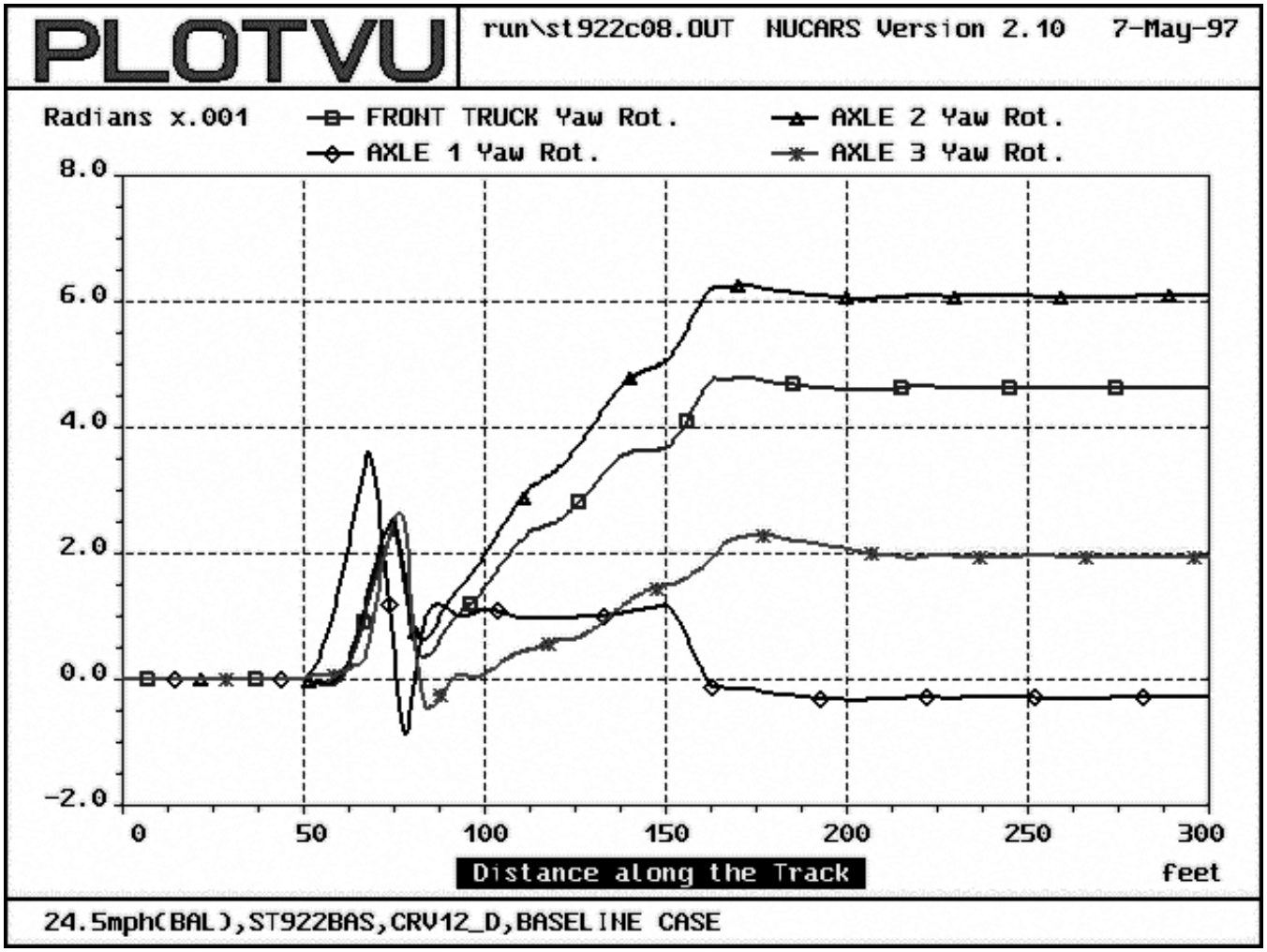

Figure 4.29 Axle yaw rotations for 12° curve

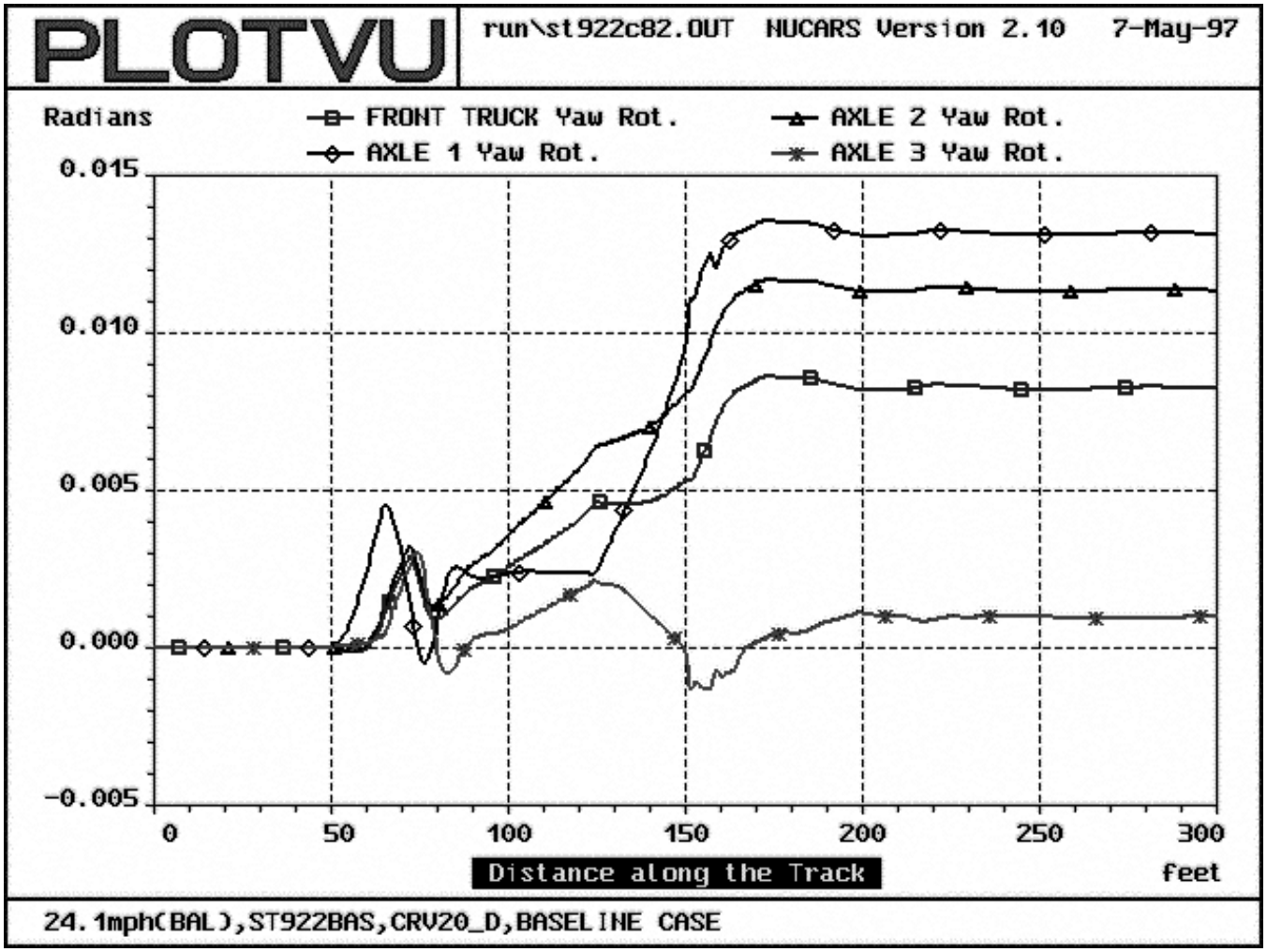

Figure 4.30 Axle yaw rotations for 20° curve

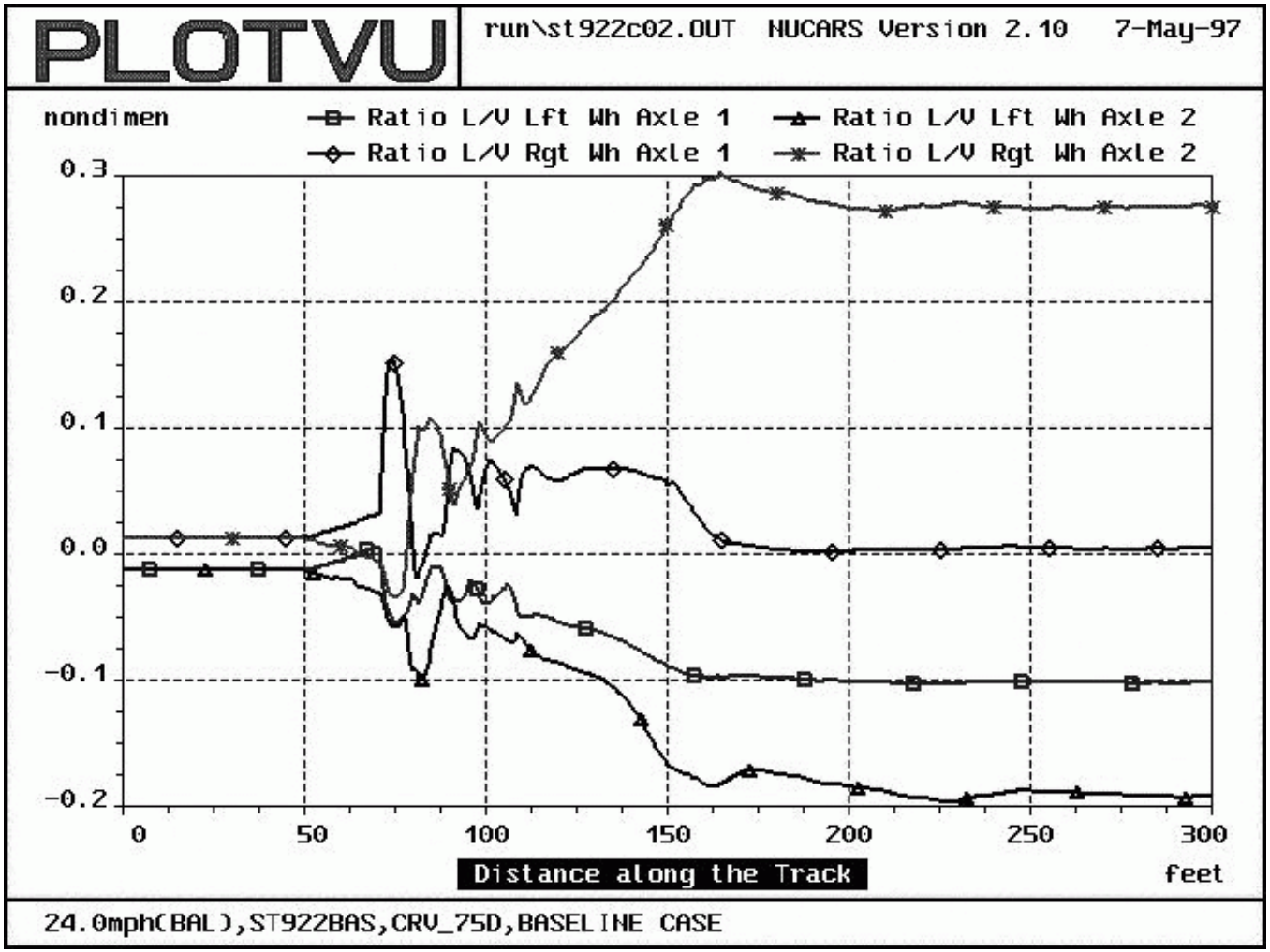

Figure 4.31 Wheel L/V ratios for axles 1 & 2 in 7.5° curve

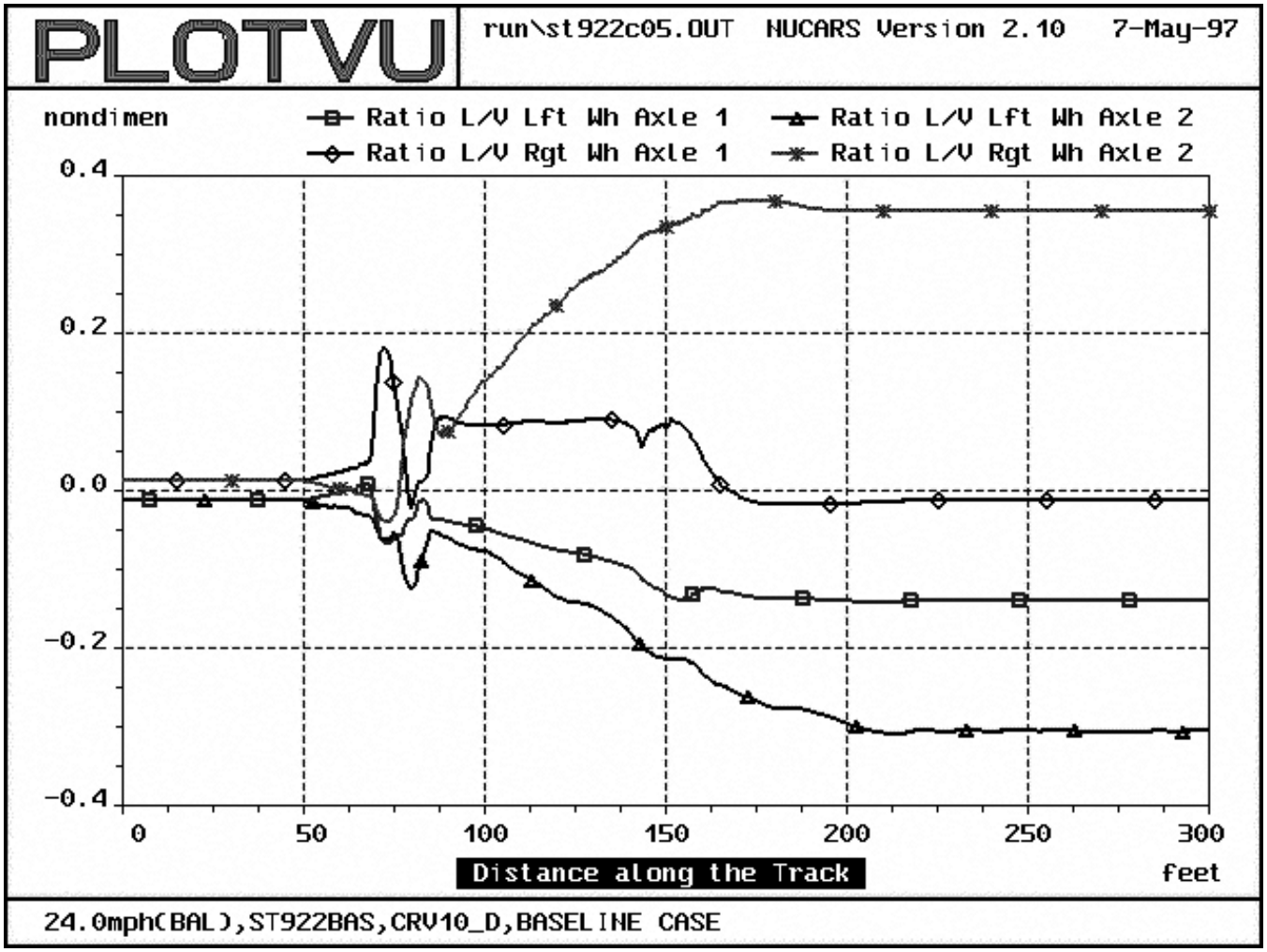

Figure 4.32 Wheel L/V ratios for axles 1 & 2 in 10° curve

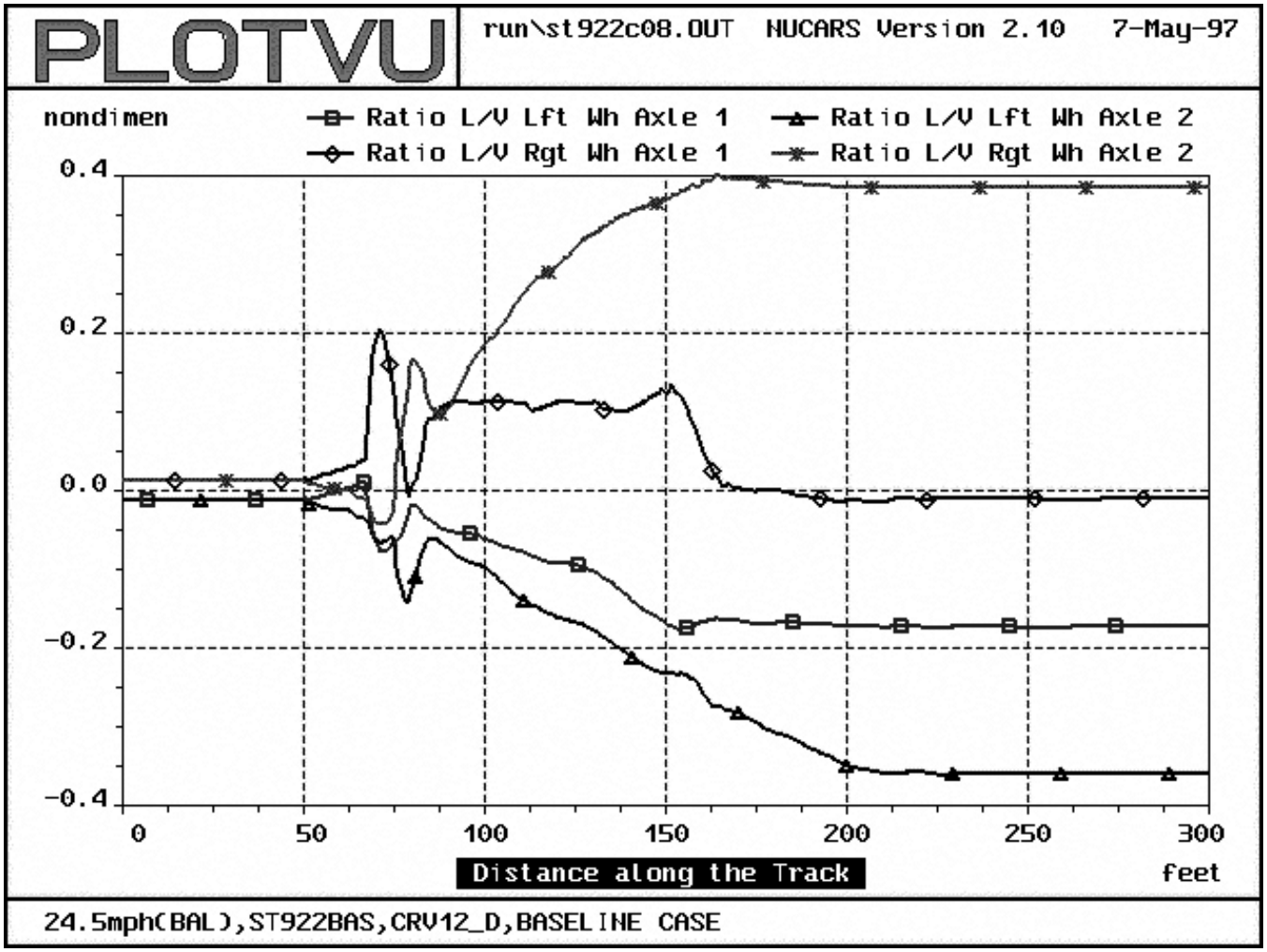

Figure 4.33 Wheel L/V ratios for axles 1 & 2 in 12° curve

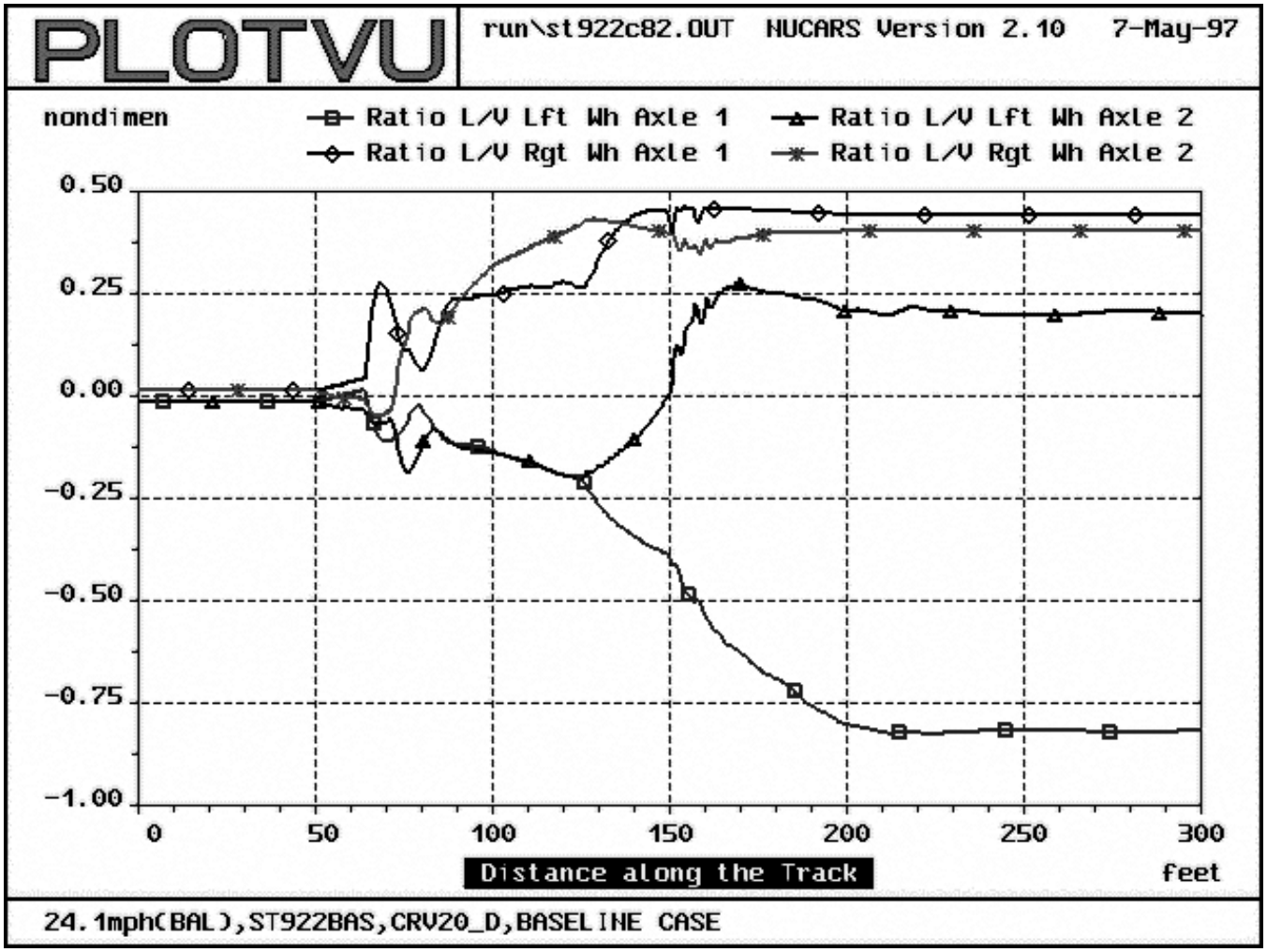

Figure 4.34 Wheel L/V ratios for axles 1 & 2 in 20° curve

4.2.4.3 Comparison with Field Test Data

To further validate the model's curving performance, the wheel L/V ratios are compared with experimental test data collected on the WRM test loop in Pueblo, Colorado. This comparison is shown in Figures 4.35 to 4.37, and includes running at over-balanced, balanced and under-balanced speeds. The test data is listed for the outside wheel of the lead axle, since this wheel typically has the highest L/V value. The outside axles of the steerable truck are able to yaw and reduce their angle of attack. This places the highest L/V ratio on the outside wheel of the center axle. The L/V ratio for the outside wheel of both the lead and center axle are compared to the test data. Since the correlation between the test data and the wheel of the center axle are close, and since the highest L/V value is typically on the lead axle, I believe that the test data is actually for the outside wheel of the center axle. If this is the case, then the model output has both similar values and similar trends. Thus the model would be a good representation of the locomotive's dynamics.

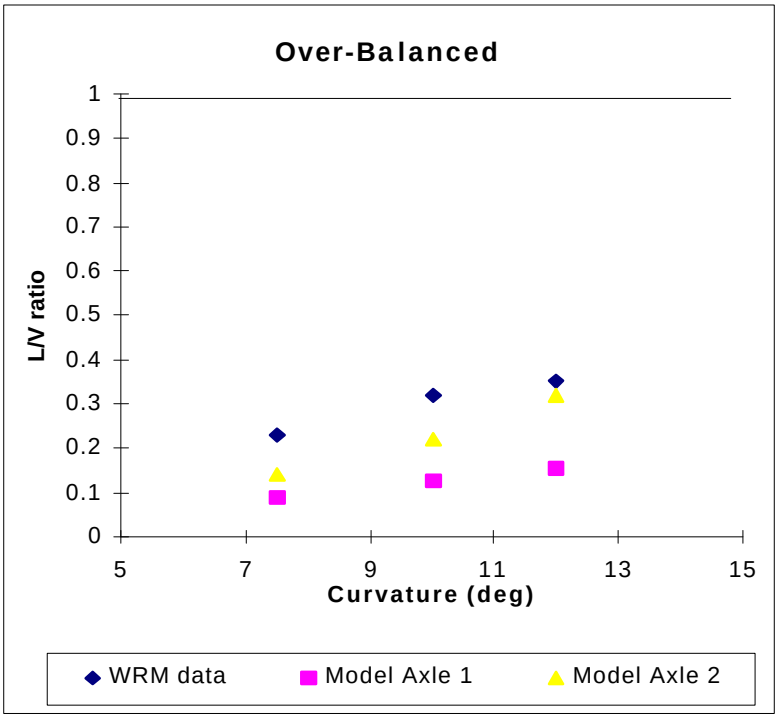

Figure 4.35 Comparison of model to experimental model at over-balance speed

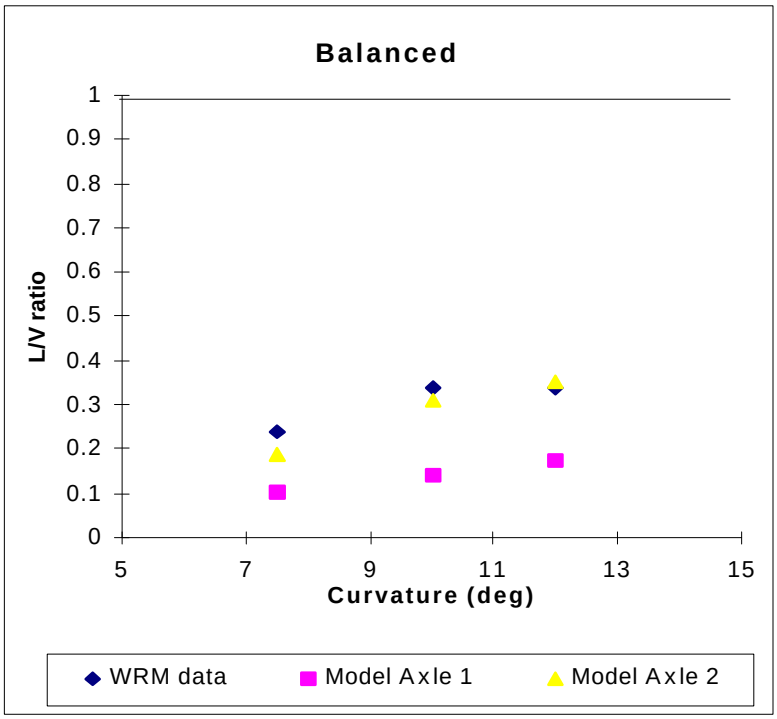

Figure 4.36 Comparison of model to experimental model at balance speed

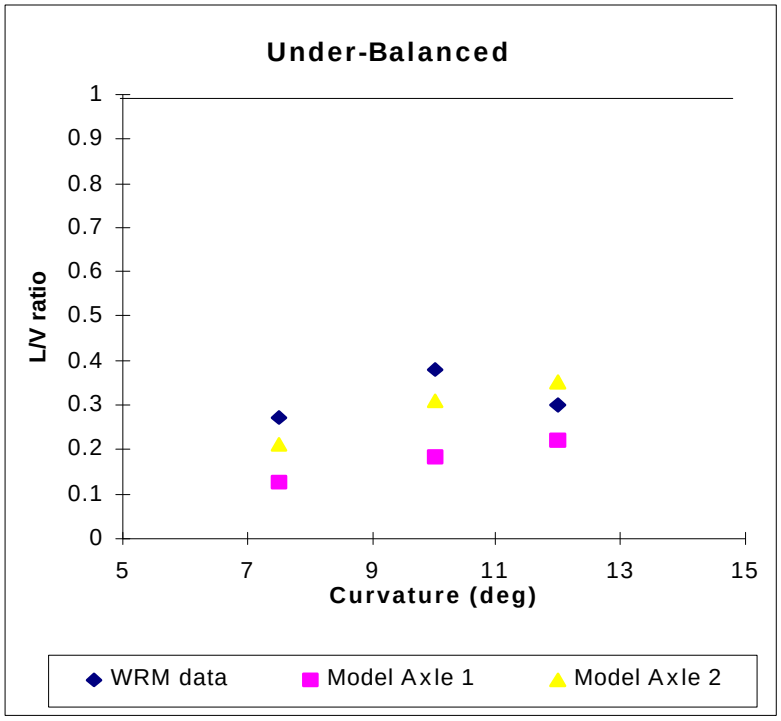

Figure 4.37 Comparison of model to experimental model at under-balance speed

Chapter 5

Parametric Sensitivity

After validation of the NUCARS model, the results from simulation runs are assumed to represent the locomotive's dynamics under the specific run conditions. This allows the locomotive to be tested through simulation to determine the effects from different components on its dynamics. These dynamics include curving performance and stability on tangent track. The curved track and tangent track tests are conducted separately and will be discussed in different sections. Some parametric configurations are tested on both the curved and tangent track sections, but most are not. This chapter will discuss the model's sensitivity to parametric variation, and will include the run conditions and a discussion of the results and their significance.

5.1 Tangent Track Tests

The tangent track parametric testing is conducted on the same track section that was used for the tangent track validation and discussed in section 5.2.1. The run conditions are also similar, except for the range of speeds used and the parametric changes. The stability speed of the baseline model occurs at 75 mph. This speed will change for different parametric configurations, so an increased range of 40 to 100 mph is used, with a difference of 10 mph between runs. The FFT's of the relative lateral displacement of the lead axle are taken for each speed and plotted together for each parametric configuration. By comparing the magnitudes of these sets of FFT plots with each other and with the FFT magnitudes for the baseline configuration (shown in Figure 5.1) it is possible to determine

whether a variation has a positive or negative effect on the model's stability. An increase in the magnitude of the FFT for a particular speed corresponds to a decrease in the stability of the model.

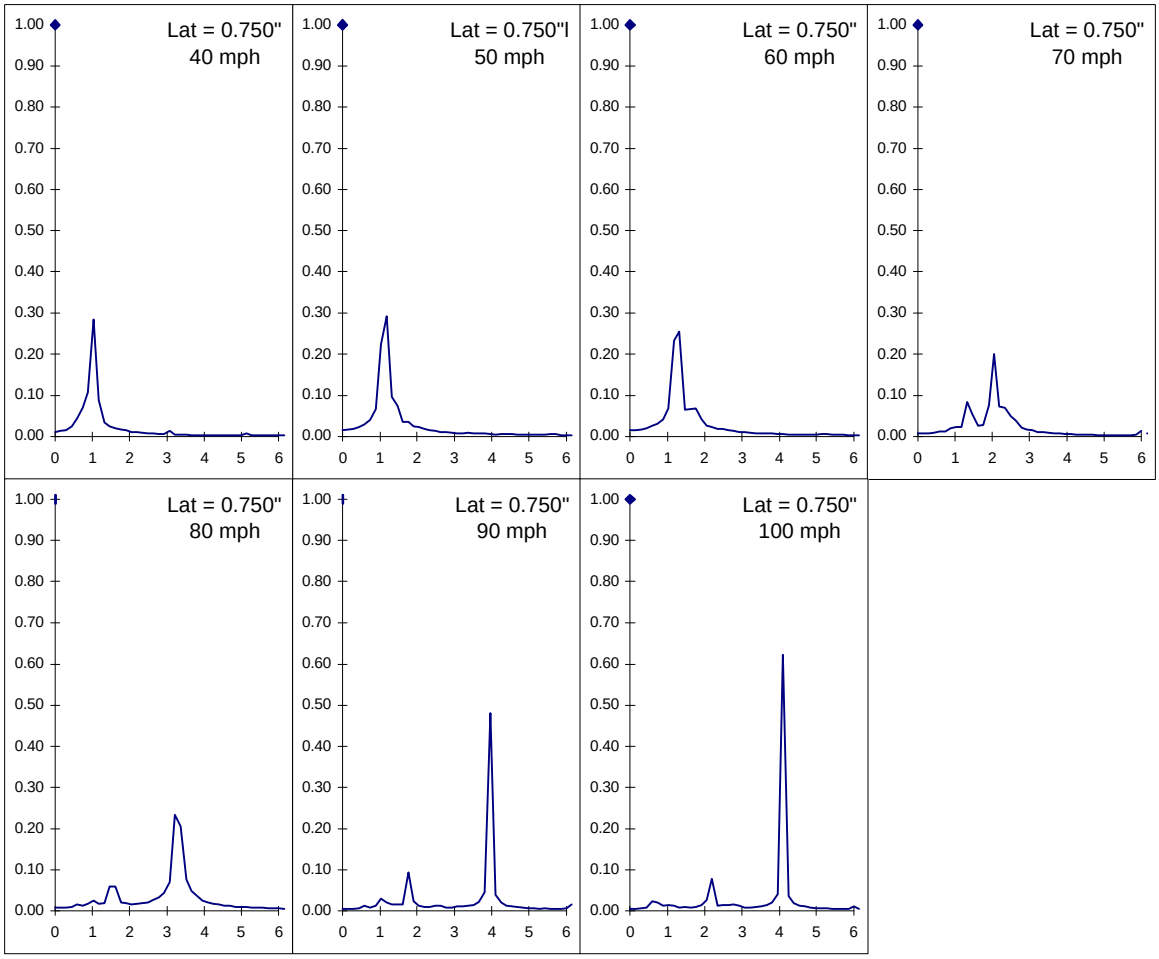

Figure 5.1 FFT's of relative lateral displacement for Baseline model

5.1.1 Inter Motor Link Lateral Stiffness

The inter motor links connect the motors in a truck together laterally. This benefits performance in shallow curves because the axles, which are rigidly connected to the motors in all direction other than in pitch, move outward on the rails together. For tangent track performance, however, the inter motor connections cause the axles to hunt together (as shown in Figure 5.2.).

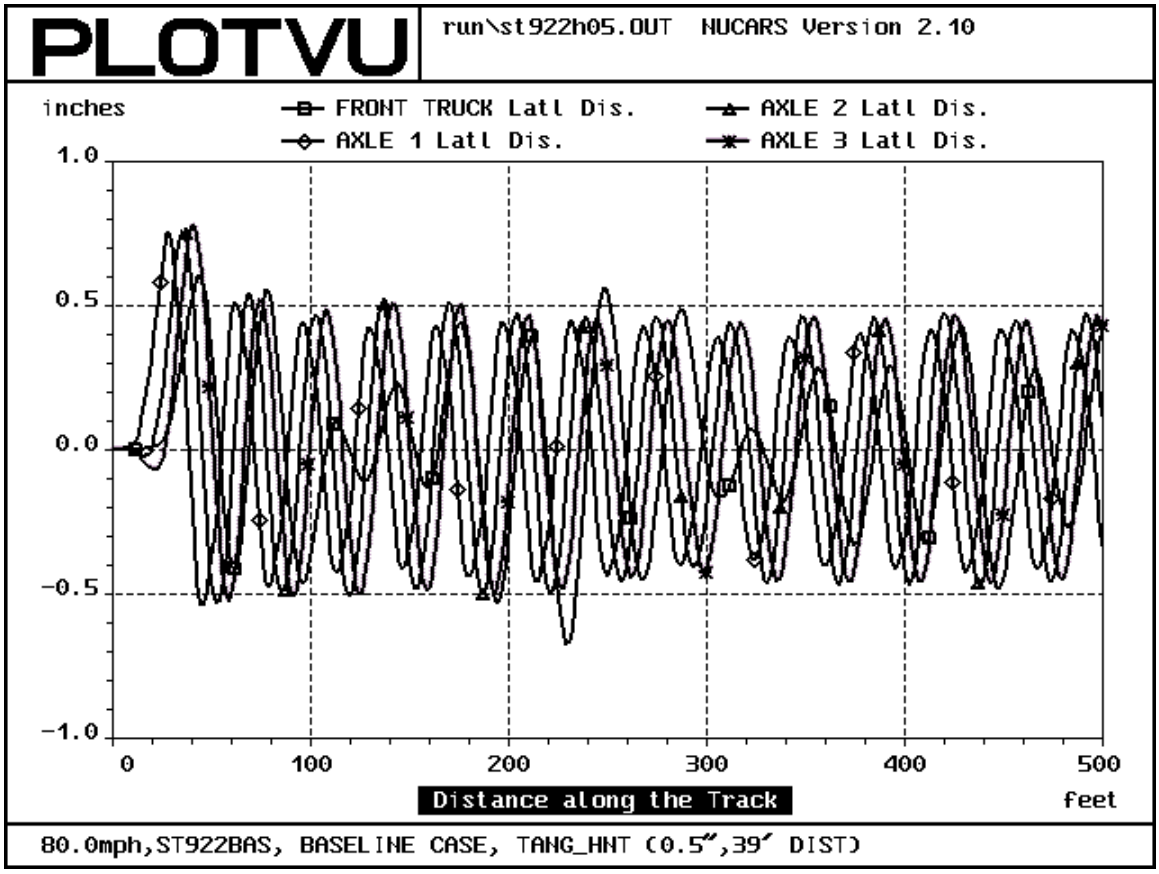

Figure 5.2 Lateral displacement of axles for Baseline model at 80 mph

The presence of lateral connections between the motors decreases the stability of the model. This is shown by the magnitudes in the FFT plots being smallest for the case with no A-frame lateral stiffness (shown in Figure 5.3). At 80 mph, the FFT magnitude is reduced from 0.23 for the baseline configuration to 0.12 for no lateral inter motor stiffness. When some stiffness is added (50% of the baseline value, shown in Figure 5.4), the FFT magnitude increases to 0.27. For even larger lateral stiffness (200%, as shown in Figure 5.5), the tangent track stability of the model is further decreased. This is shown by the magnitude of the FFT for 80 mph increasing to 0.37. So, adding lateral stiffness between the axles is harmful to tangent track stability of the steerable model.

IML=0
files: ST922HA1.OUT to ST922HA7.OUT

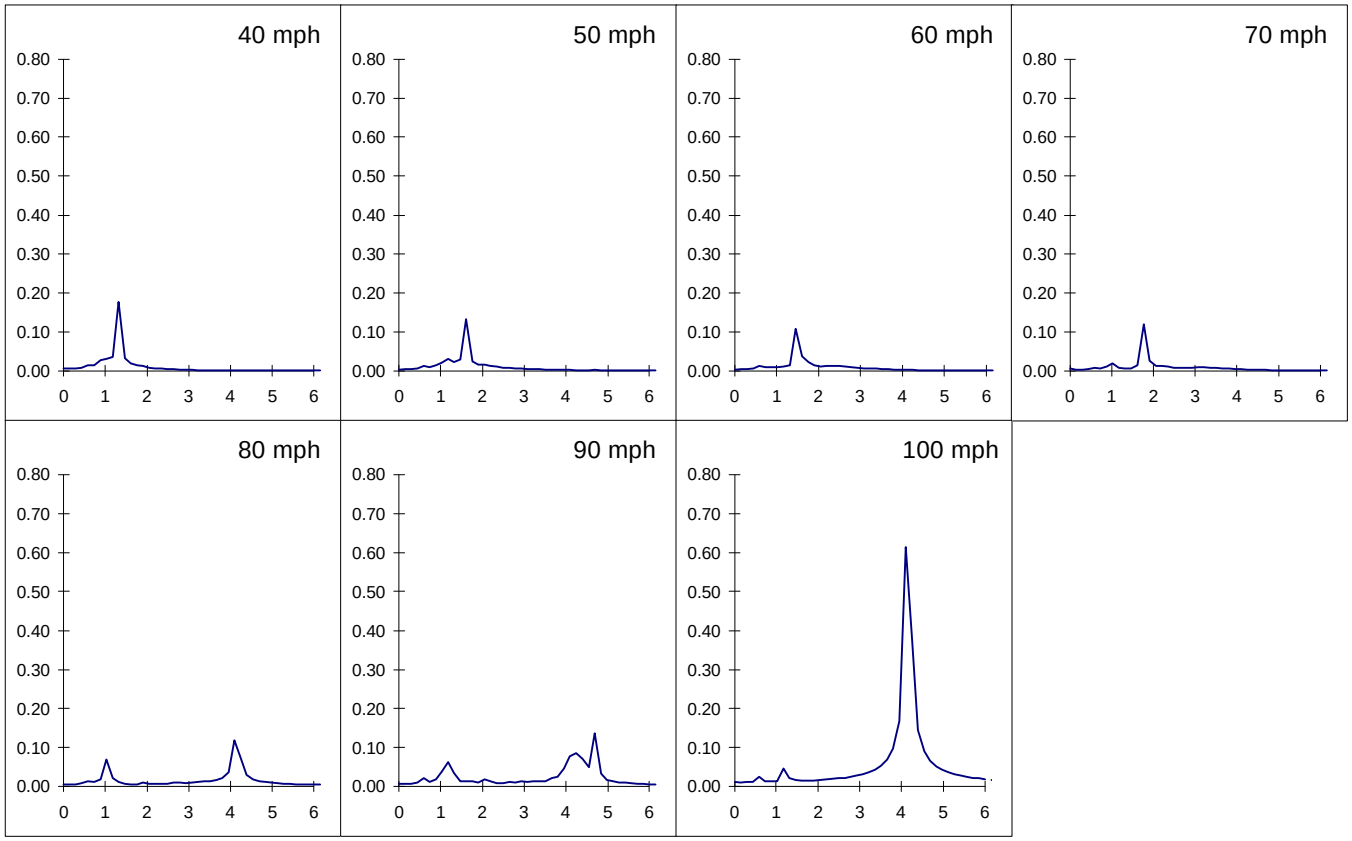

Figure 5.3 FFT's of relative lateral displacement for 0% IML lateral stiffness (0 #/in.)

IML=50% (40k #/in)
files: ST922HB1.OUT to ST922HB7.OUT

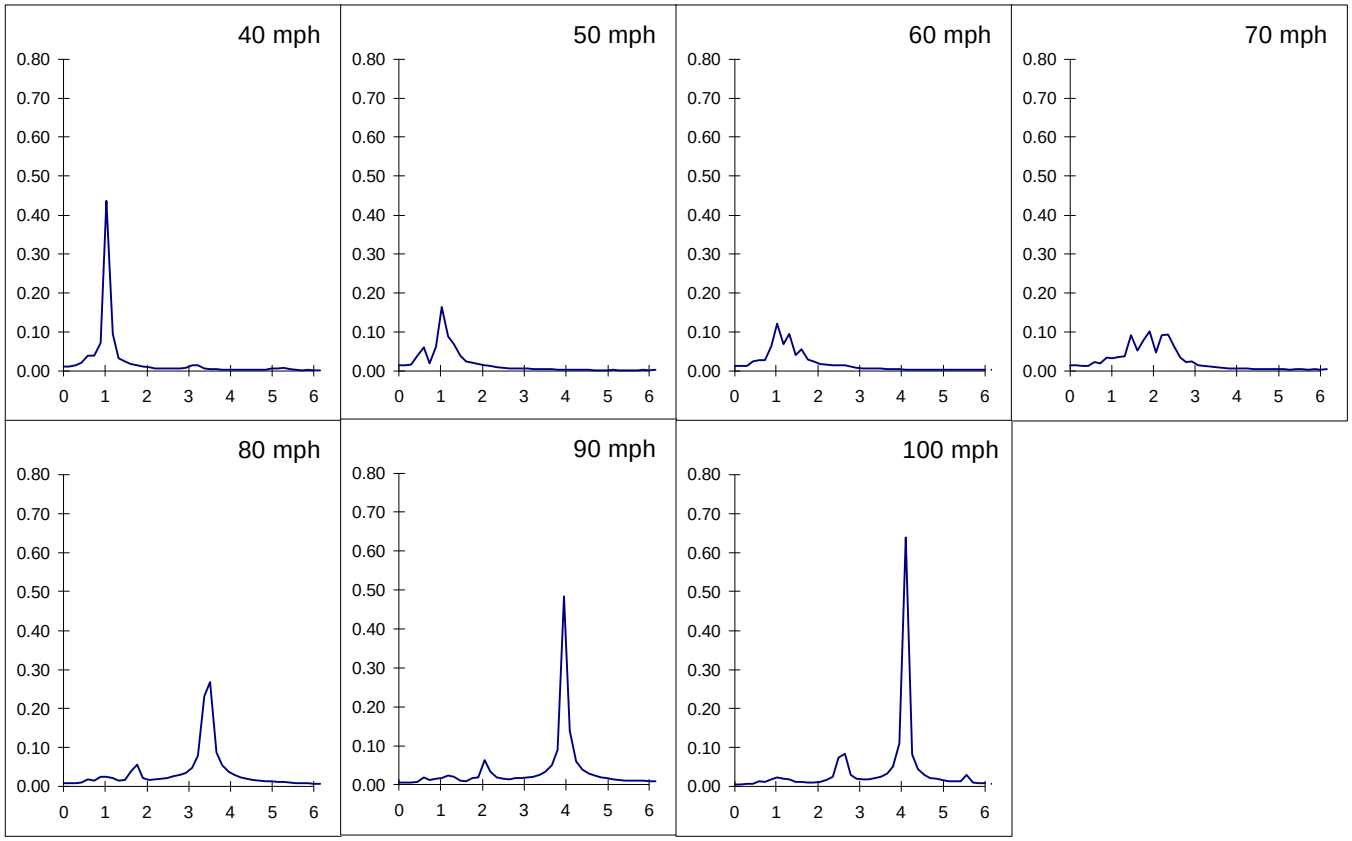

Figure 5.4 FFT's of relative lateral displacement for 50% IML lateral stiffness (40k #/in.)

IML=200% (160k/in)
files: ST922HC1.OUT to ST922HC7.OUT

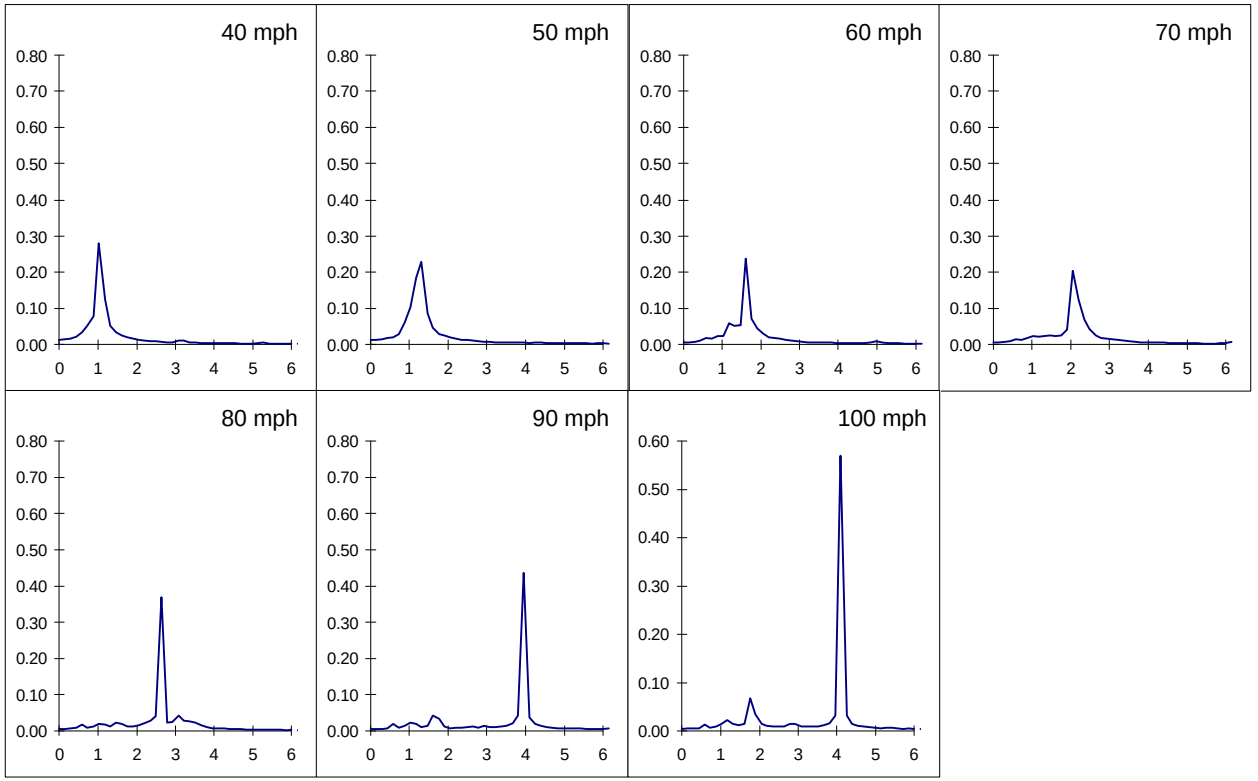

Figure 5.5 FFT's of relative lateral displacement for 200% IML lateral stiffness (160k #/in.)

5.1.2 Yaw Damping

The yaw dampers sit between the platform and truck frames to the left and right of the truck center pin and are oriented in the longitudinal direction (as shown in Figure 5.6). There is little relative longitudinal motion between the truck frames and platform, so these dampers only change length due to relative yaw displacement. Since they absorb energy from the system, the yaw dampers help the tangent track stability of the model. This is shown in the FFT's of Figure 5.7, where the yaw dampers have been removed and the magnitude of the FFT for 80 mph increases from 0.23 for the baseline case to 0.37. Adding some yaw damping (50% of the baseline value, as shown in Figure 5.8), the FFT magnitude decreases to 0.32. Still more yaw damping (the FFT's for 200% are shown in Figure 5.9) reduces the magnitude to 0.28. This increased tangent track stability comes at the price of curving performance, where increased yaw damping slows the reaction time for the truck to align itself in a curve.

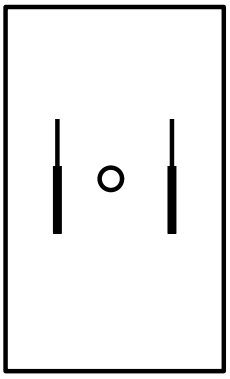

Figure 5.6 Orientation of yaw dampers

YDAMP=0
files: ST922HD1.OUT to ST922HD7.OUT

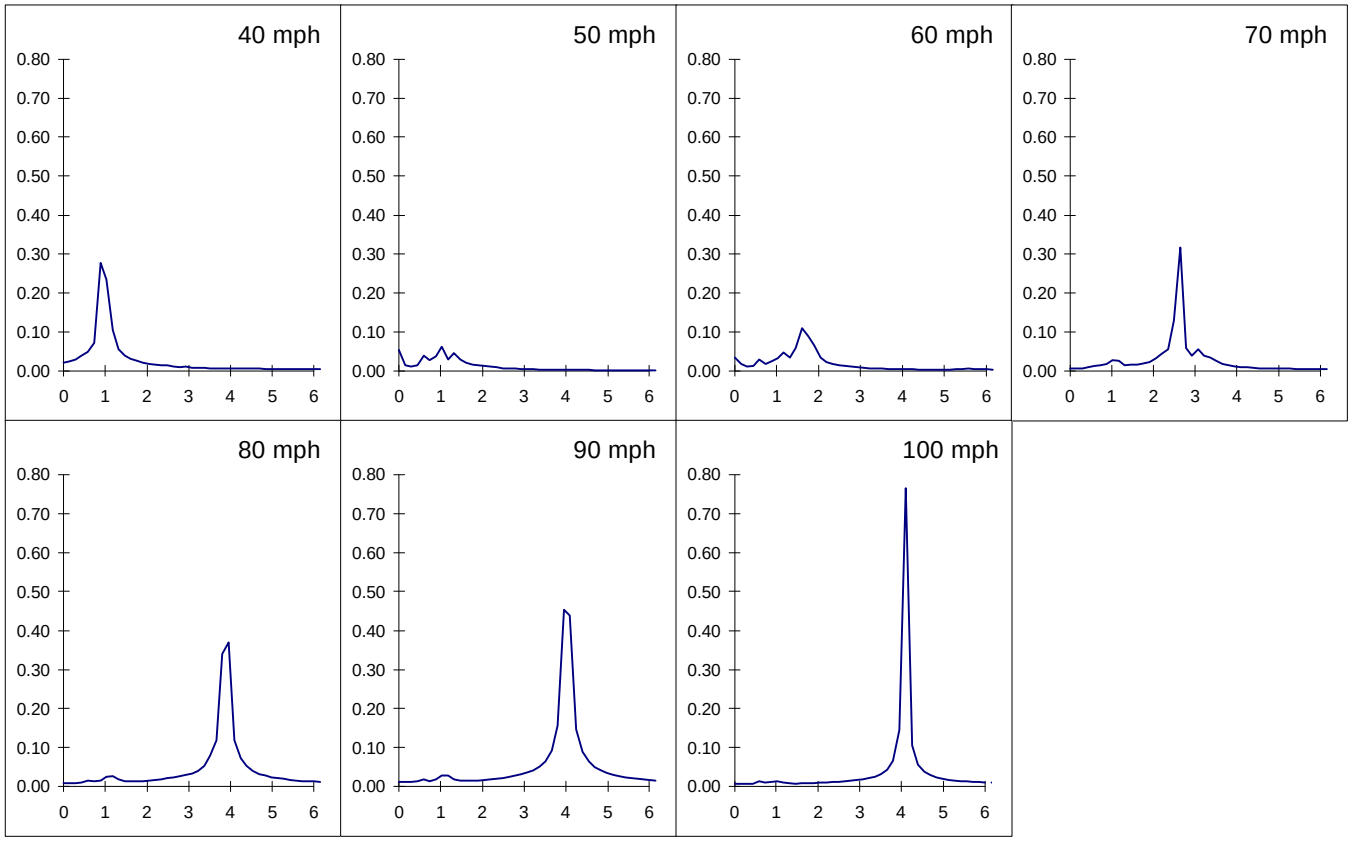

Figure 5.7 FFT's of relative lateral displacement for 0% yaw damping (0 #-s/in.)

YDAMP=50% (1800 #-s/in)
files: ST922HE1.OUT to ST922HE7.OUT

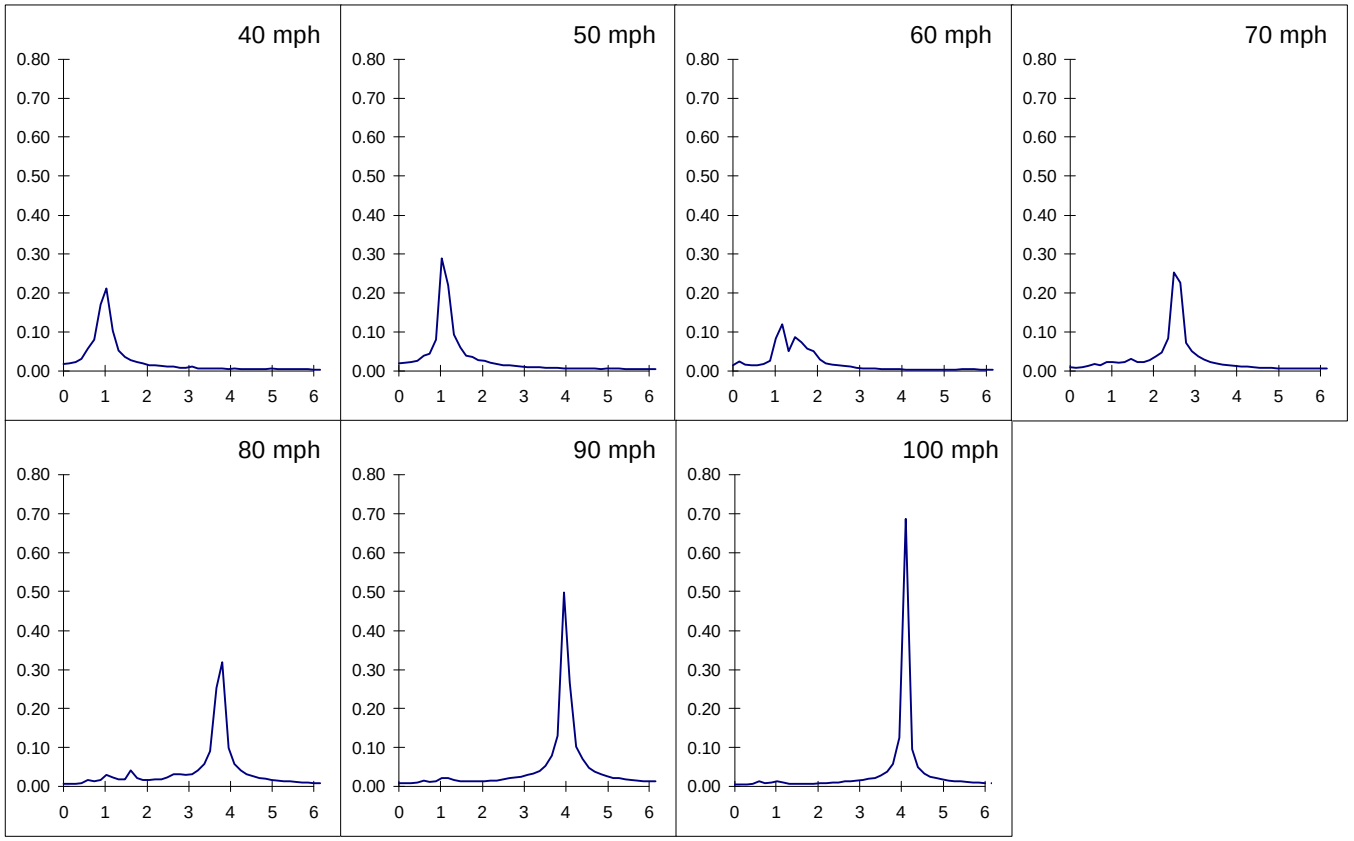

Figure 5.8 FFT's of relative lateral displacement for 50% yaw damping (1800 #-s/in.)

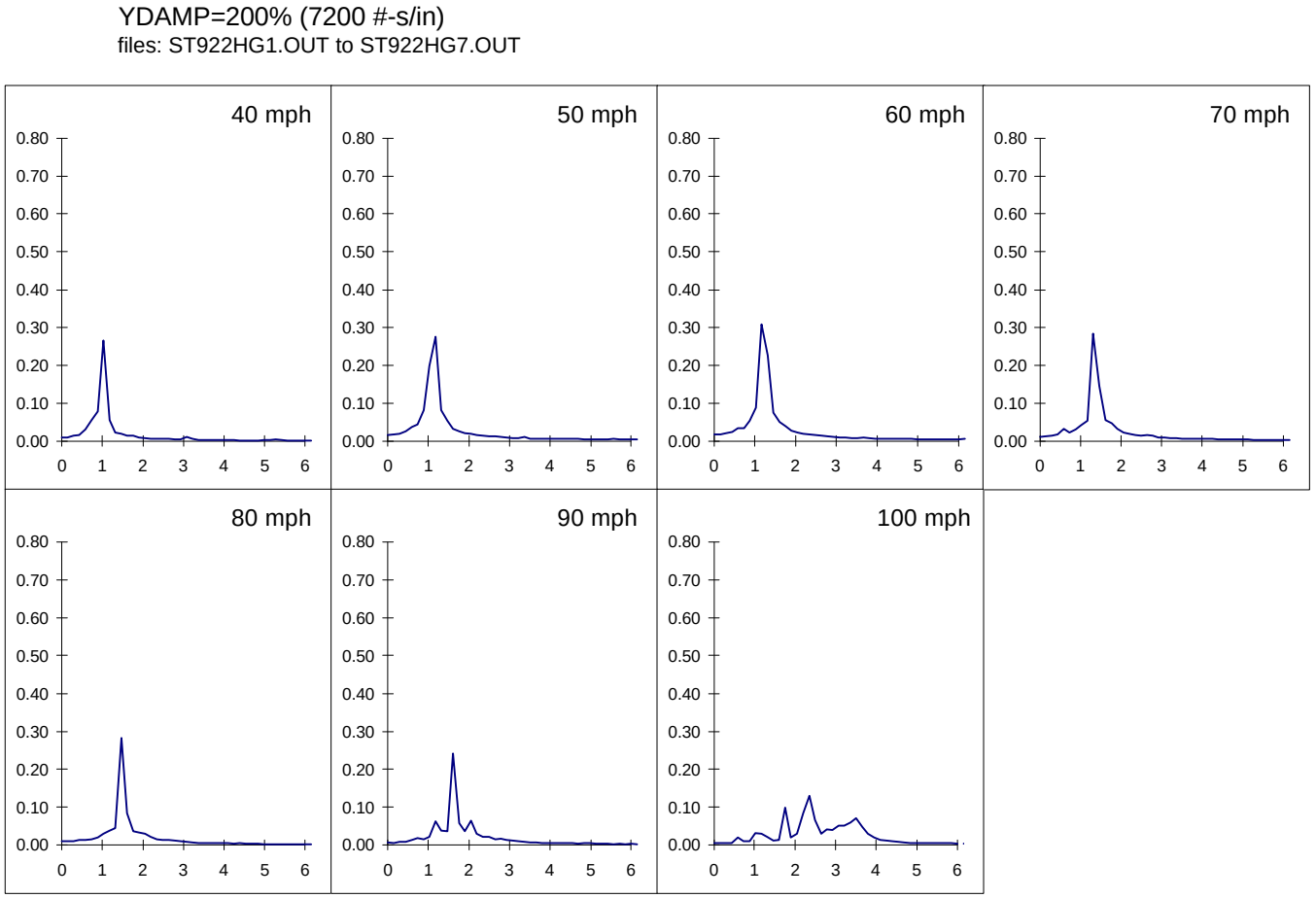

Figure 5.9 FFT's of relative lateral displacement for 200% yaw damping (7200 #-s/in.)

5.1.3 Lateral Damping

The lateral dampers sit on the centerline of the truck in front of and behind the center pin (as shown in Figure 5.10). Due to this orientation, the lateral dampers change length due to lateral and yaw displacements and absorb energy from both the lateral and yaw components of hunting. Their benefit on stability can be seen in Figure 5.11, where the lateral dampers have been effectively removed and the FFT magnitude for 80 mph has increased to 0.56. When lateral damping is added to the model, the FFT magnitude for 80 mph decreases to 0.30 and 0.28 for 150% (Figure 5.12) and 200% (Figure 5.13), respectively. Thus, the presence of lateral damping in the model is shown to be beneficial to tangent track stability.

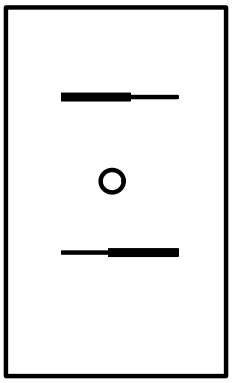

Figure 5.10 Orientation of lateral dampers

LDAMP=0
files: ST922HH1.OUT to ST922HH7.OUT

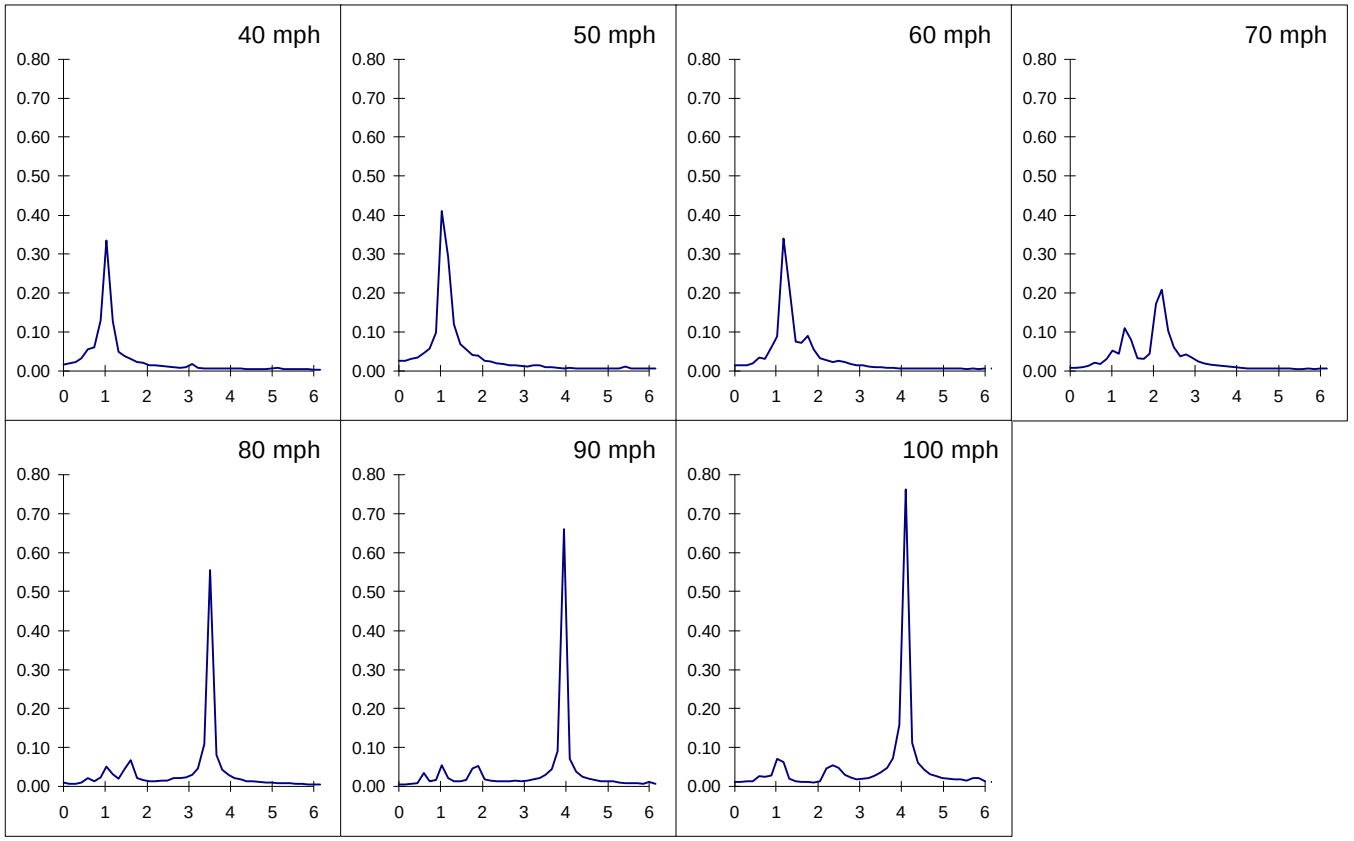

Figure 5.11 FFT's of relative lateral displacement for 0% lateral damping (0 #-s/in.)

LDAMP=150% (450 #-s/in)
files: ST922HI1.OUT to ST922HI7.OUT

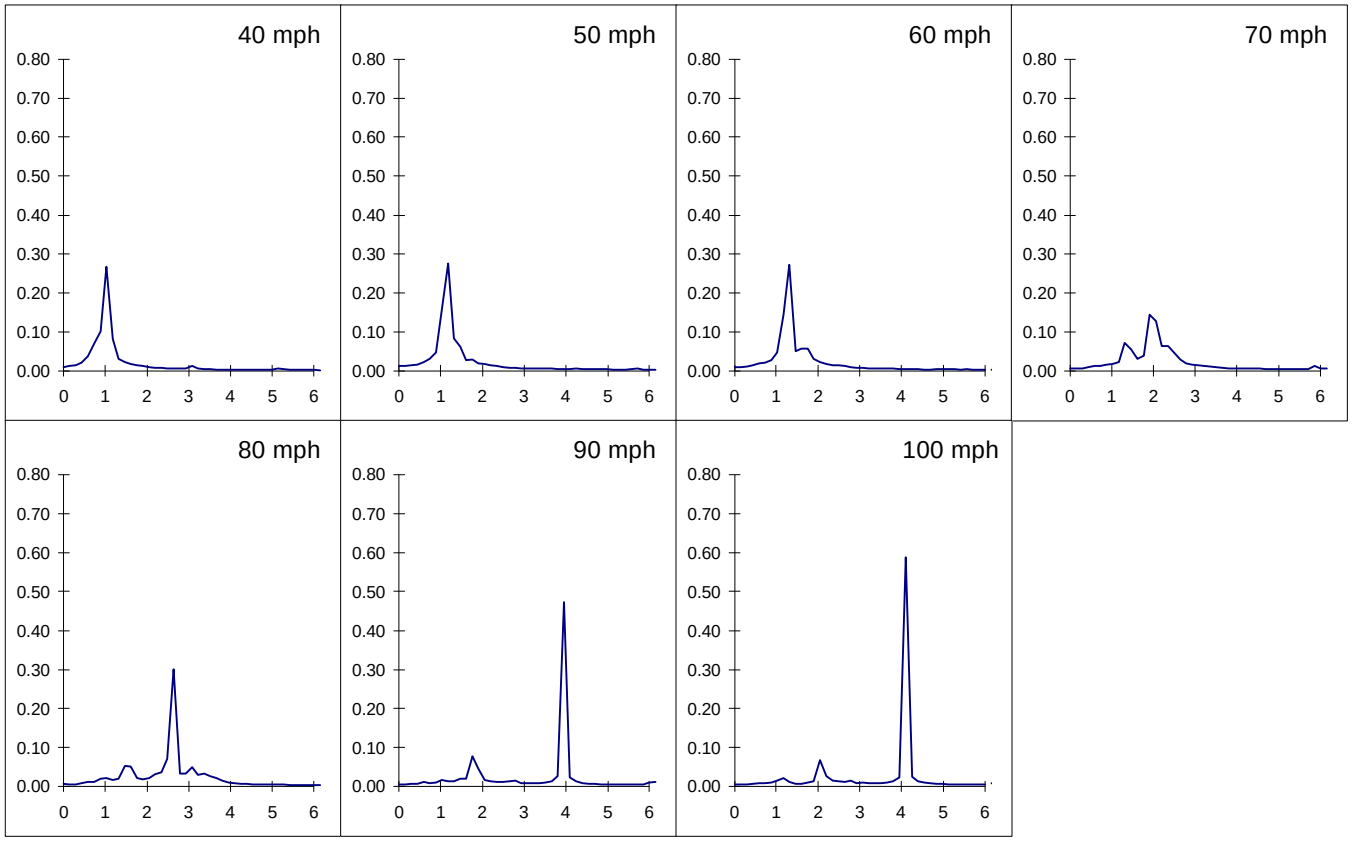

Figure 5.12 FFT's of relative lateral displacement for 150% lateral damping (450 #-s/in.)

LDAMP=200% (600 #-s/in)
files: ST922HJ1.OUT to ST922HJ7.OUT

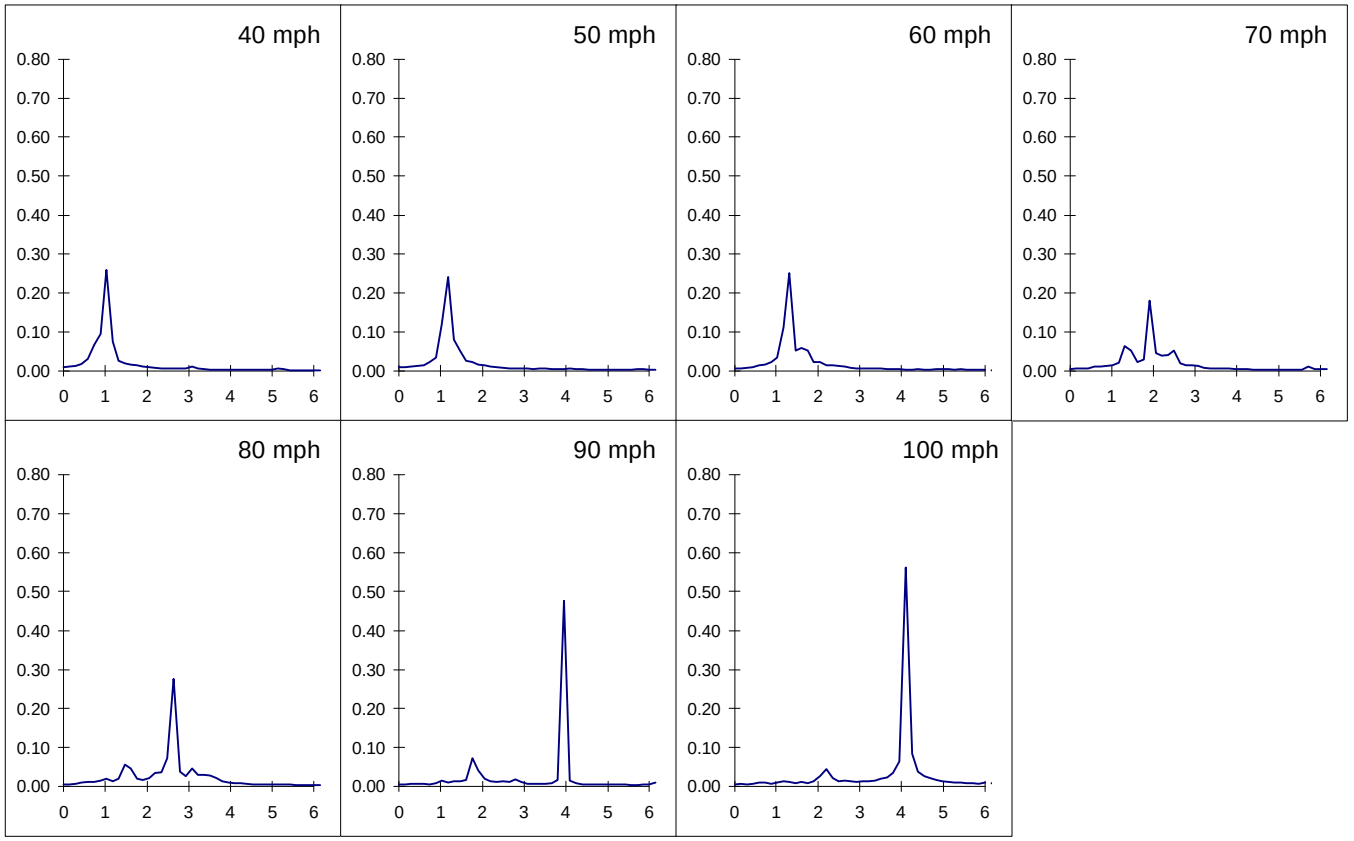

Figure 5.13 FFT's of relative lateral displacement for 200% lateral damping (600 #-s/in.)

5.1.4 Axle Primary Damping

The primary dampers are located on each end of an axle and connect the axles to the truck frame. They are oriented at an angle of 26° from vertical and are able to damp lateral motion. As a result, the presence of primary damping improves the tangent track stability of the model. Axle lateral hunting is known to occur at 1.4 Hz (as discussed in Table 5.1). The FFT's for 60 mph show that the spike at this frequency is reduced with the presence of lateral damping. With no lateral damping (as shown in Figure 5.14), the lateral axle hunting has a magnitude of 0.37. When some lateral damping is added (Figure 5.15 shows the FFT's for 50% baseline damping), this magnitude decreases to 0.33. The magnitude of the 60 mph FFT in the baseline case (Figure 5.1) is 0.25, showing further improvement in stability. Figure 5.16 shows the over-damped case, where the FFT magnitude has increased to 0.33. The presence of axle damping aids the hunting stability of the model, and the amount of damping used in the baseline case provides the greatest stability.

AXLE DAMP=0
files: ST922HK1.OUT to ST922HK7.OUT

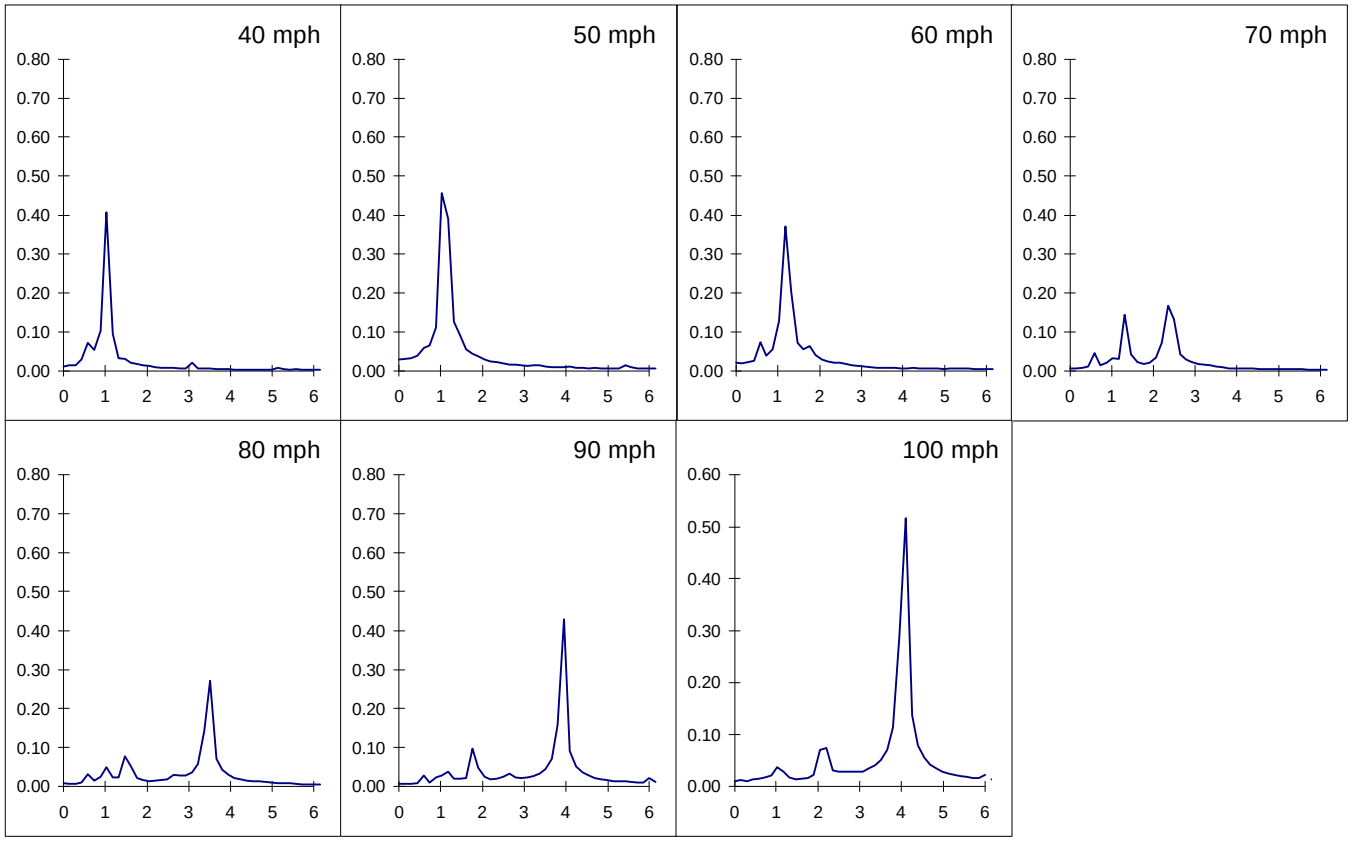

Figure 5.14 FFT's of relative lateral displacement for 0% axle damping (0 #-s/in.)

AXLE DAMP=50% (225 #-s/in)
files: ST922HL1.OUT to ST922HL7.OUT

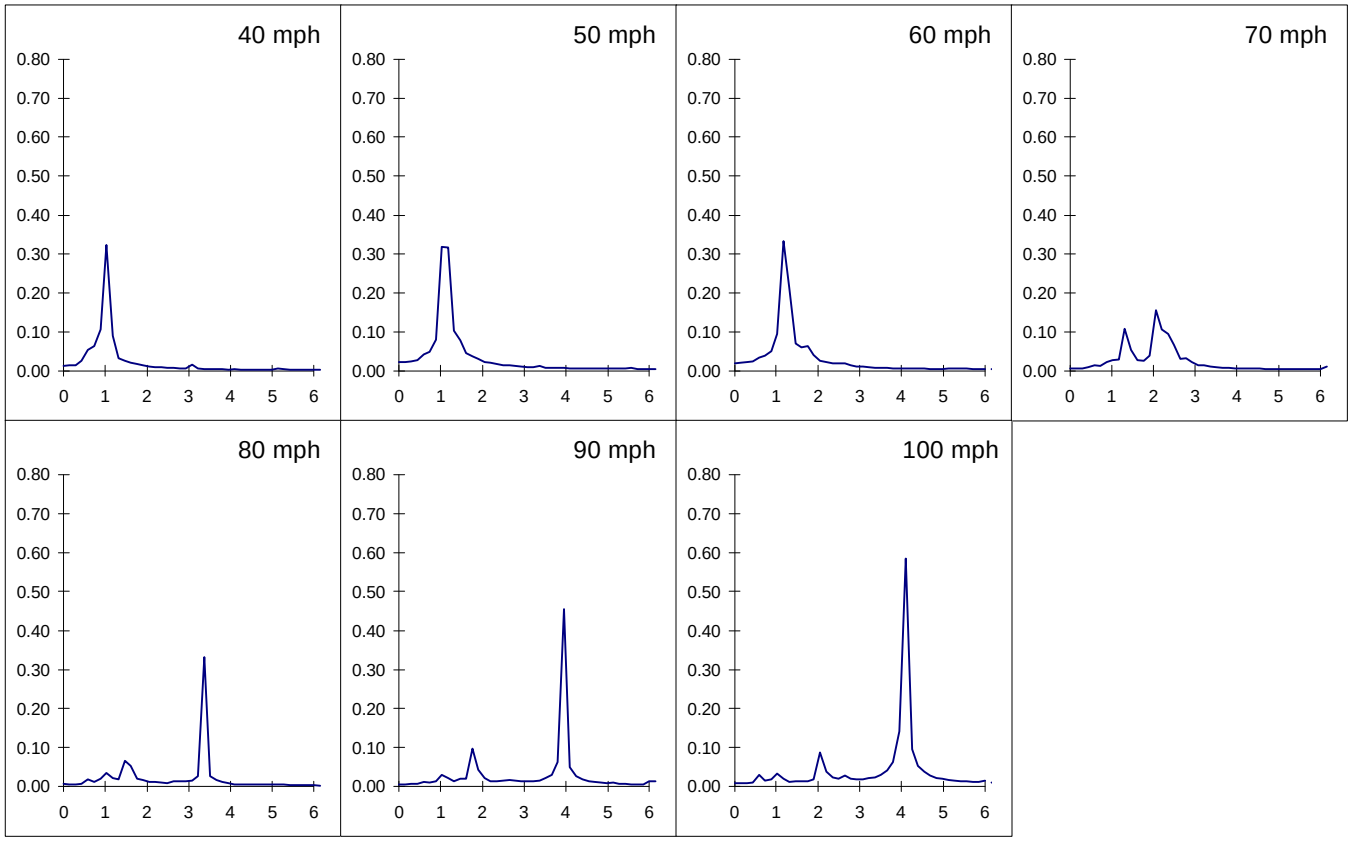

Figure 5.15 FFT's of relative lateral displacement for 50% axle damping (225 #-s/in.)

AXLE DAMP=200% (900 #-s/in)
files: ST922HN1.OUT to ST922HN7.OUT

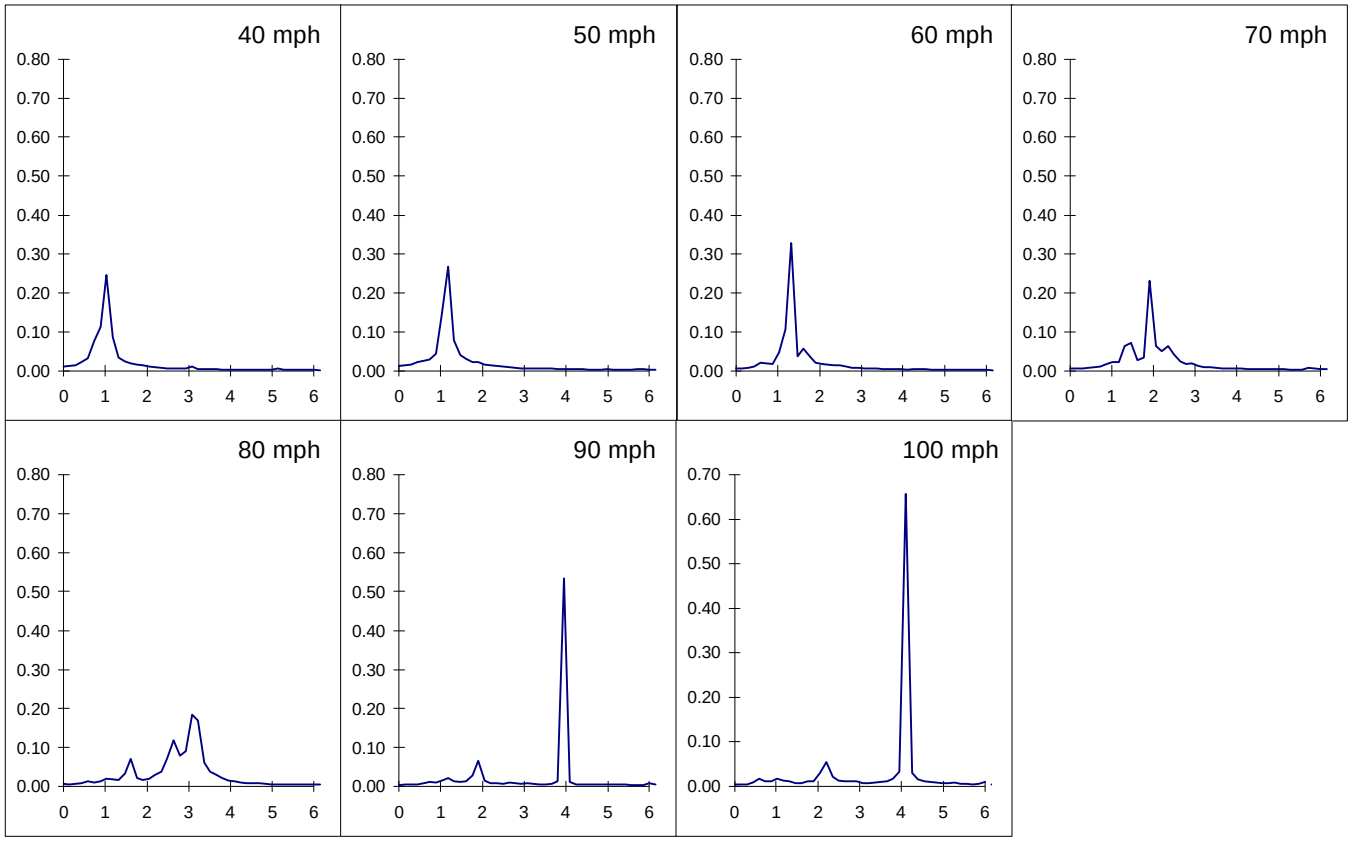

Figure 5.16 FFT's of relative lateral displacement for 200% axle damping (900 #-s/in.)

5.1.5 Axle Primary Damper Angle

To check the effect on stability of the axle damper orientation, several runs are made varying the orientation of the axle dampers from vertical to 150% of the baseline angle (0° to 39.8°). This angle affects the model's stability. For the vertically oriented dampers (Figure 5.17), the magnitude of the FFT for 60 mph is 0.38. With the axles angled by 50% of the baseline value (the FFT's for 13.3° are shown in Figure 5.18), this magnitude decreases to 0.36. For the maximum angle tested (39.8° for Figure 5.19), the magnitude is further reduced to 0.28. The FFT magnitude for the baseline configuration is 0.25 (Figure 5.1), showing that this is the best angle for the baseline amount of damping.

AXLE DAMP ANGLE=0
files: ST922HO1.OUT to ST922HO7.OUT

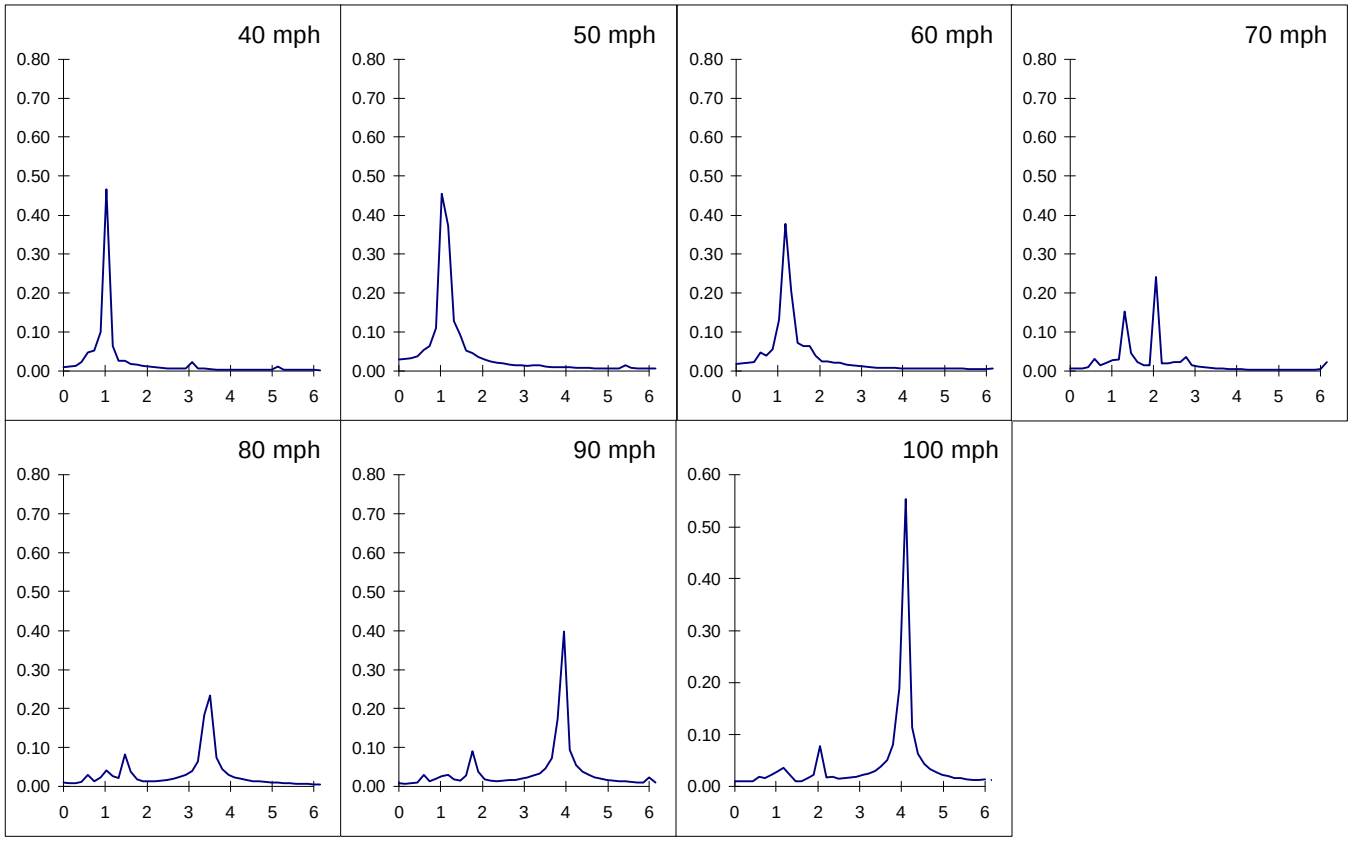

Figure 5.17 FFT's of relative lateral displacement for no axle damper angle (0°)

AXLE DAMP ANGLE=50% (13.3 deg)
files: ST922HP1.OUT to ST922HP7.OUT

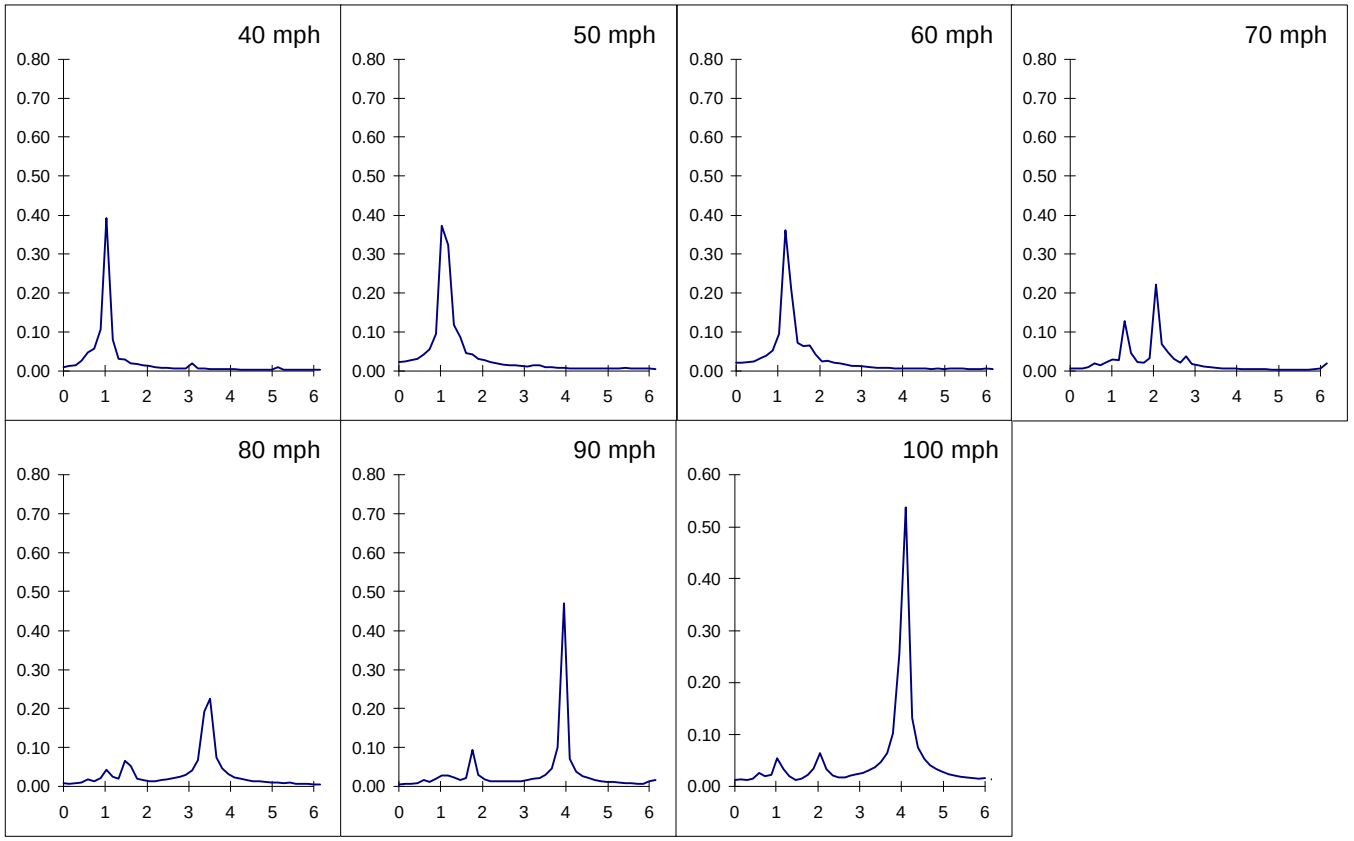

Figure 5.18 FFT's of relative lateral displacement for 50% axle damper angle (13.3°)

AXLE DAMP ANGLE=150% (39.8 deg)
files: ST922HQ1.OUT to ST922HQ7.OUT

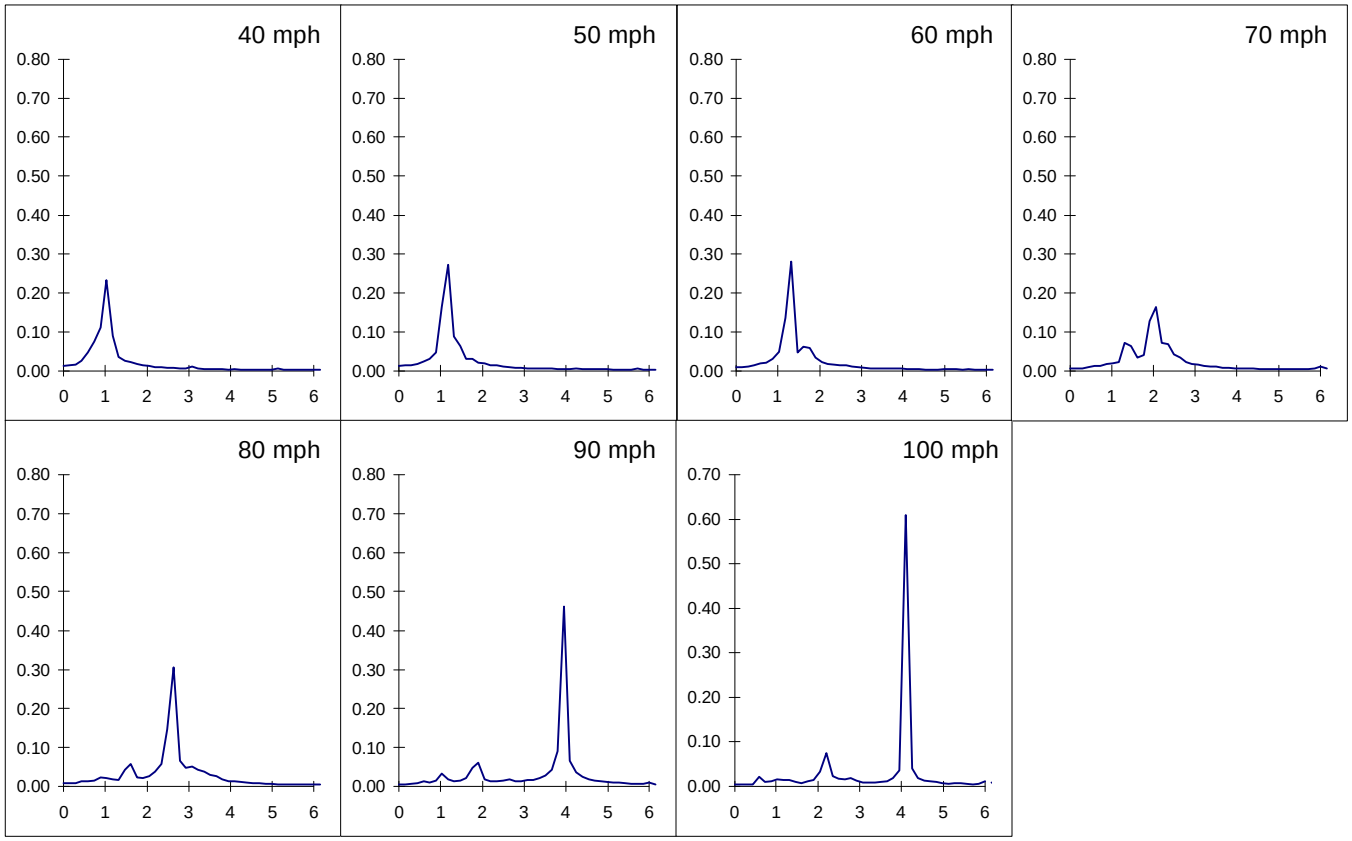

Figure 5.19 FFT's of relative lateral displacement for 150% axle damper angle (39.8°)

5.1.6 Flexicoiling Stiffness

The primary springs sit between the axles and truck frame with their axes oriented vertically. This allows them to resist vertical motion through compression or extension. Lateral and longitudinal motion between an axle and truck frame bends the springs' axes. This type of spring deformation is referred to as flexicoiling. The NUCARS model includes separate stiffness elements to account for the flexicoiling of the primary springs. To investigate its effect on stability, the flexicoiling stiffness is varied from 50% to 500% of the stiffness used in the baseline model (250 to 2500 #/in). The FFT's for these runs are shown in Figures 5.20 to 5.22.

The flexicoiling stiffness is only one component of the lateral stiffness between an axle and the truck frame and has only a minor effect on the tangent track stability of the model. The FFT magnitudes for the 80 mph runs with 50% and 200% flexicoiling stiffness are 0.34 and 0.33 respectively. When the stiffness is increased to 500% of the baseline value, the FFT magnitude changes to 0.29. This ten fold increase in the flexicoiling stiffness of the primary springs changes the FFT magnitude by only 15%, showing that it has little effect on the tangent track stability of the model.

FLEXICOILING=50% (250 #/in)
files: ST922HR1.OUT to ST922HR7.OUT

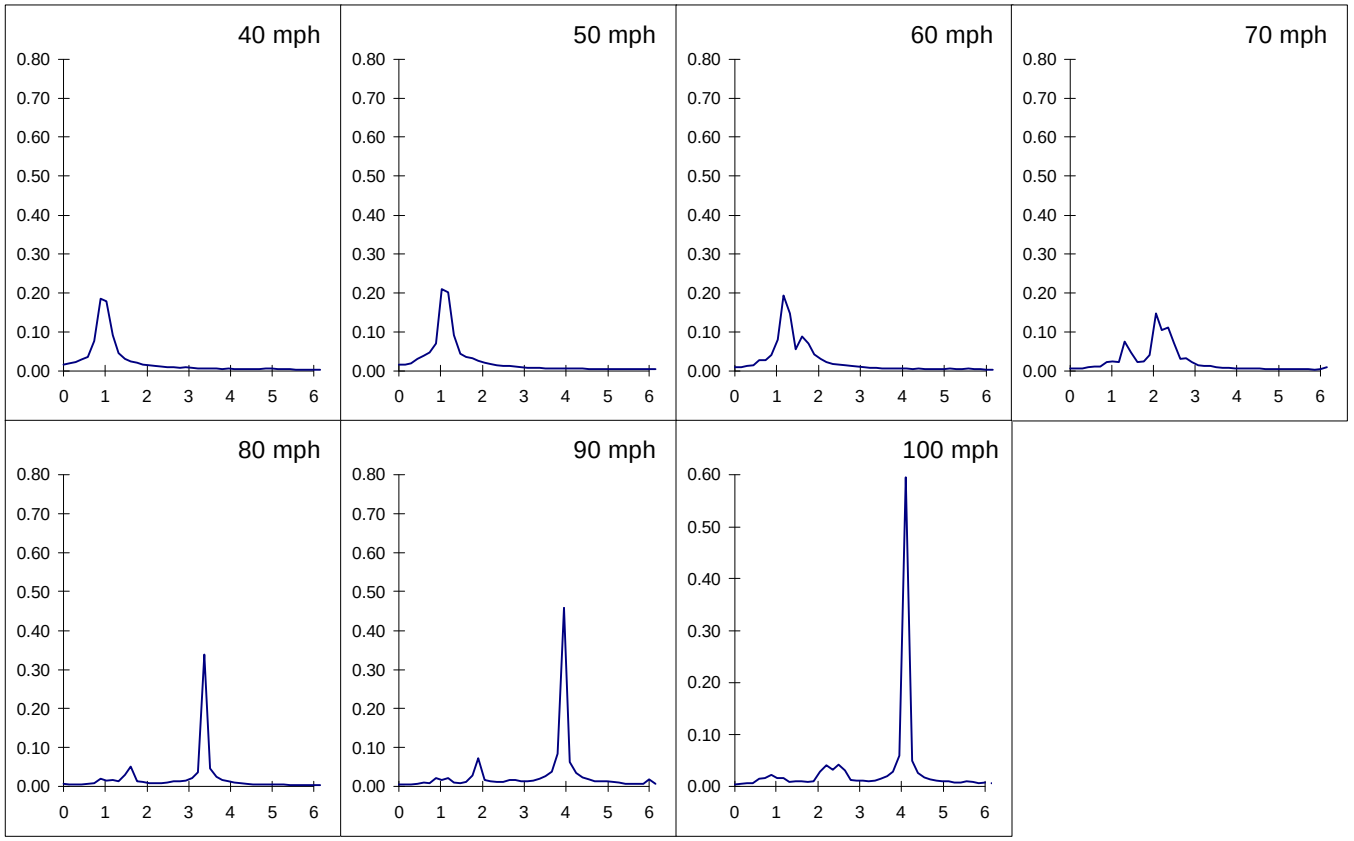

Figure 5.20 FFT's of relative lateral displacement for 50% flexicoiling stiffness (250 #/in.)

FLEXICOILING=200% (1000 #/in)
files: ST922HS1.OUT to ST922HS7.OUT

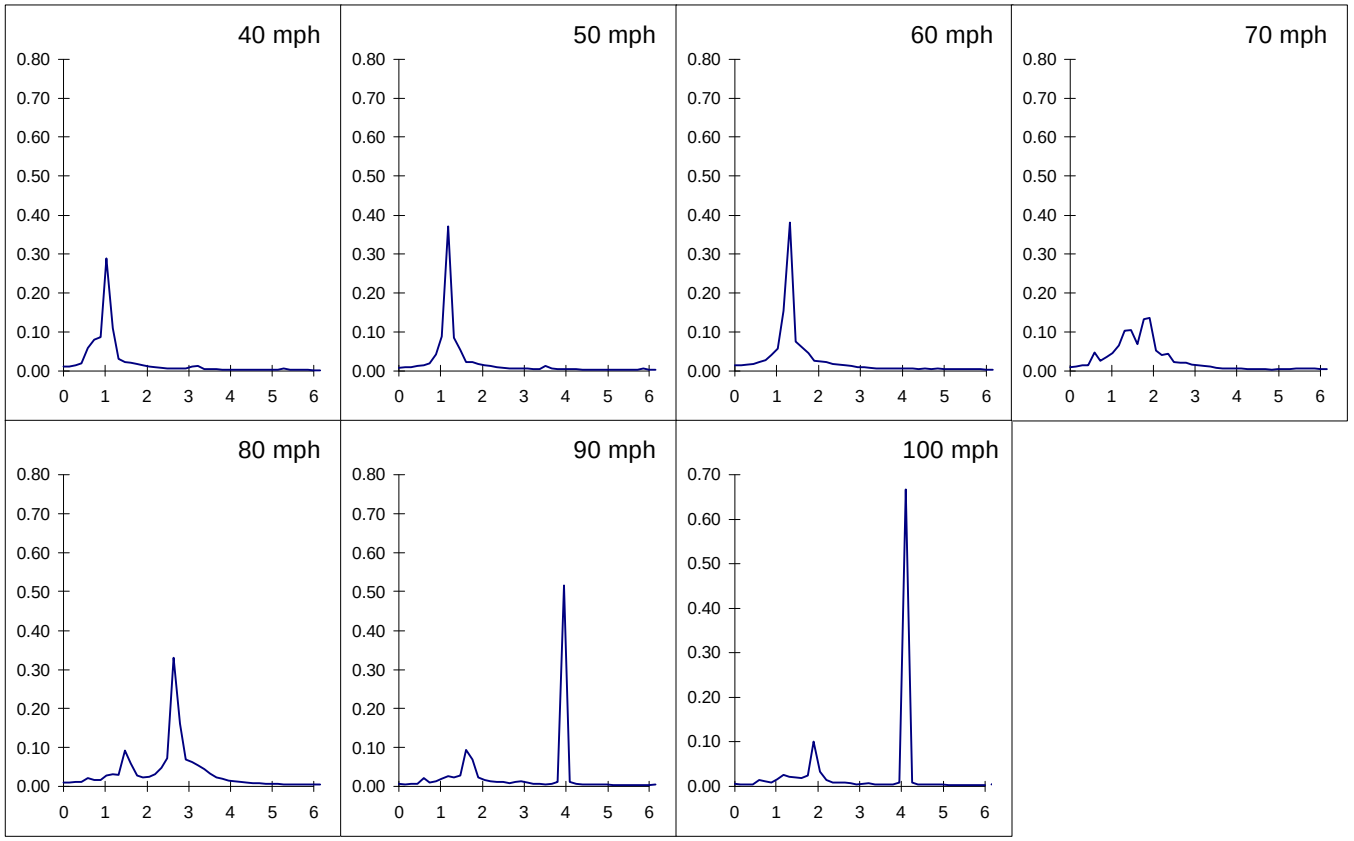

Figure 5.21 FFT's of relative lateral displacement for 200% flexicoiling stiffness (1000 #/in.)

FLEXICOILING=500% (2500 #/in)
files: ST922HU1.OUT to ST922HU7.OUT

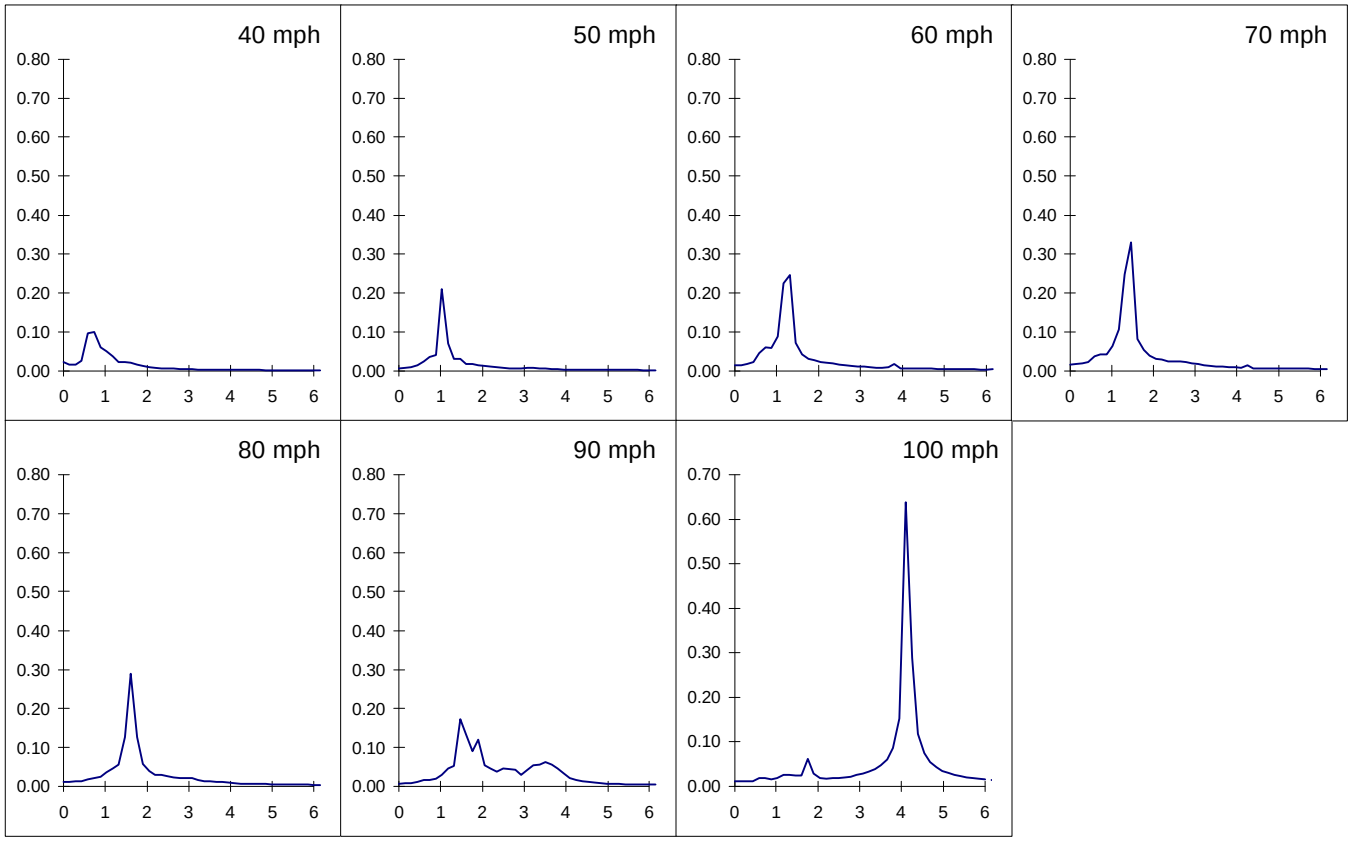

Figure 5.22 FFT's of relative lateral displacement for 500% flexicoiling stiffness (2500 #/in.)

5.1.7 Conicity

The conicity (wheel tread angle) has a dramatic effect on the tangent track stability of the NUCARS model. The lateral force that a rail exerts on a wheelset is dependent on the contact angle, which is determined by the wheel conicity. A large conicity increases the lateral rail forces on the opposing wheels of an axle, which will increase the axle's tendency to hunt. The conicity of the baseline model was 0.05 (1:20). The corresponding magnitude of the FFT for the 80 mph run is 0.24 (Figure 5.1). When the conicity is increased to 0.10 (1:10), the FFT magnitude increases to 0.47 (Figure 5.23) showing that the model is less stable. When the conicity is further increased to 0.20 (1:5), the FFT magnitude increases to 0.63 (Figure 5.24), almost three times the baseline value. Increasing the wheel conicity drastically reduces the model's tangent track stability.

CONICITY=0.1
files: ST922HW1.OUT to ST922HW7.OUT

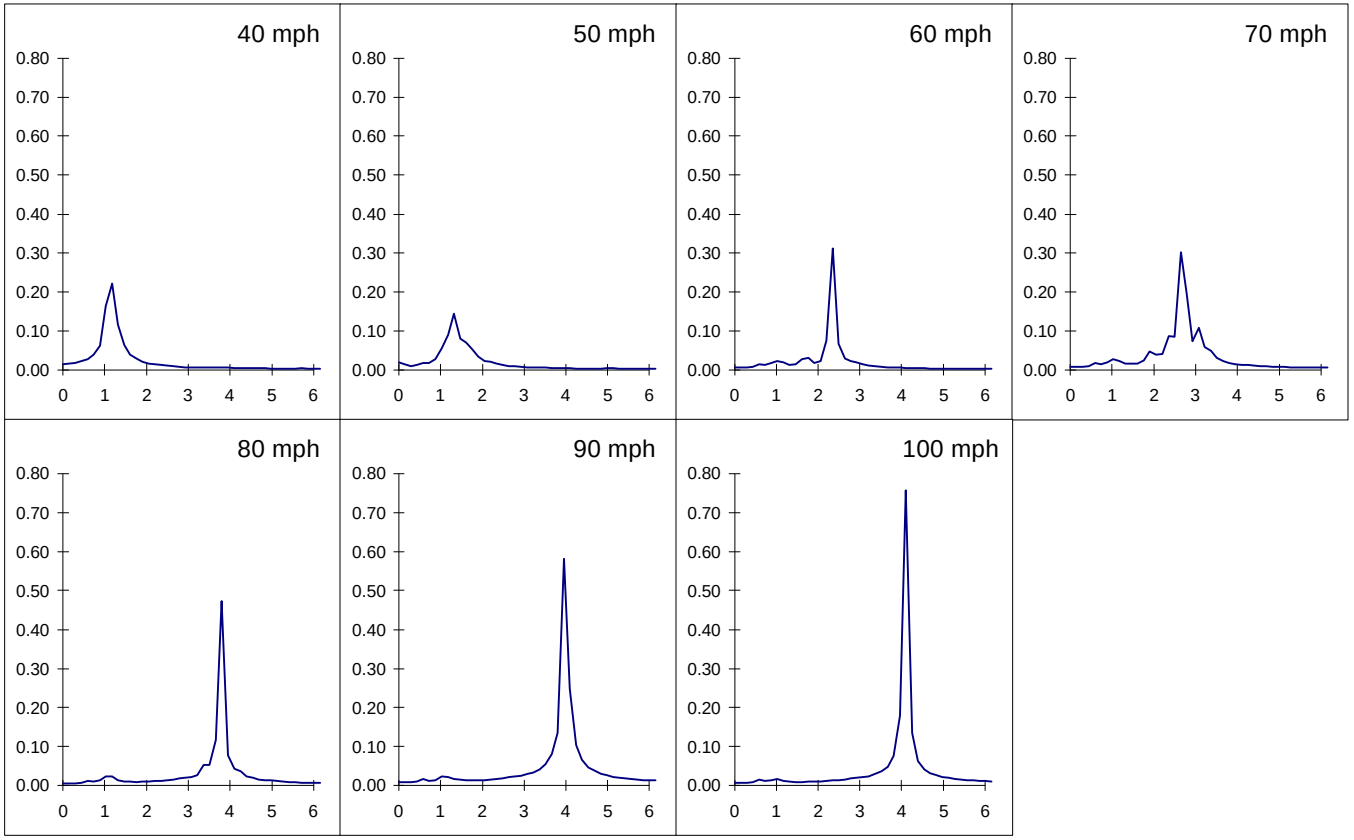

Figure 5.23 FFT's of relative lateral displacement for conicity of 0.1 (1:10)

CONICITY=0.2
files: ST922HV1.OUT to ST922HV7.OUT

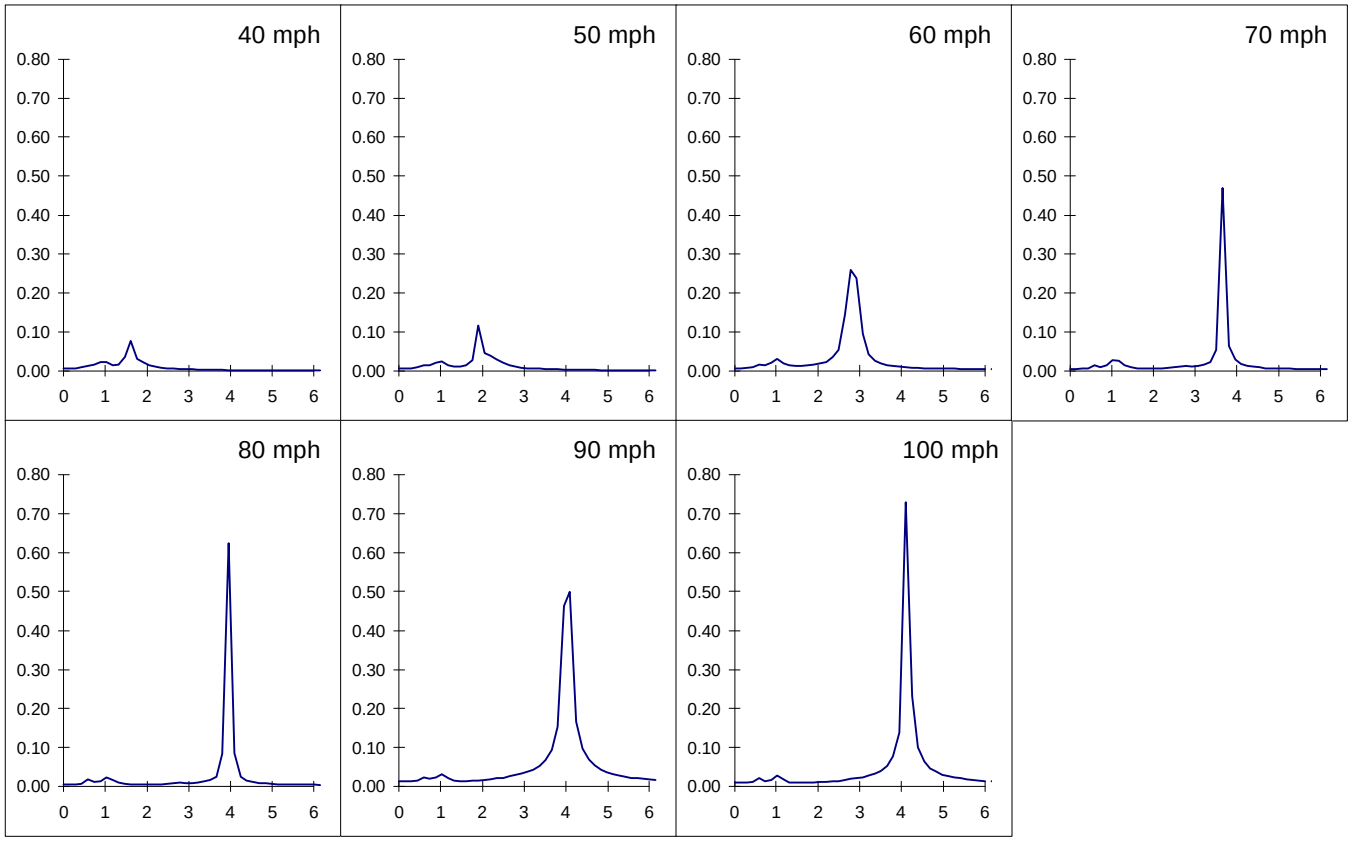

Figure 5.24 FFT's of relative lateral displacement for conicity of 0.2 (1:5)

fv5.2 Curved Track Tests

The curved parametric tests are conducted in a similar fashion to the curving validation tests. The parametric runs use the same four curved track files, and the same output values are used to evaluate curving performance, namely the lateral displacements and yaw rotations of the axles and frame and the individual L/V ratios on the wheels of the lead truck. In addition, the axle sum L/V ratio is included in the tables summarizing the parametric runs. Discussion of the curved track parametric runs will focus on the behavior in the 10° curve and, where necessary, in the 20° curve. Plots of the axle lateral displacements and the wheel L/V ratios have been included for some of the parametric tests, but comparison relies mainly on the parametric curving tables. The parametric values examined include the lateral stiffness of the inter-motor connections (IML's), the stiffness of the inter-axle steering connections (IAL's), the lateral and longitudinal clearances between the axles and the truck frames, and the wheel conicity. The parametric tests are conducted independently, and as a result, will be discussed separately in the following sections.

5.2.1 Inter Motor Link Lateral Stiffness

In negotiating a curve, the axles of the locomotive shift laterally to generate a difference in the rolling radii of the left and right wheels. This induces a yawing motion of the axles and brings the locomotive through the curve. To aid this lateral axle shift, the inter motor

links (IML's) connect the motors together laterally, which connects the axles and forces them to move together.

To investigate the effect of the IML stiffness on the model's curving performance, a comparison is made between curving runs with the baseline stiffness and runs with no IML stiffness (0%), half the baseline IML stiffness (50%), and twice the baseline IML stiffness (200%). The results of this comparison are shown in Tables 5.1 and 5.2 for the 10° and 20° curves, respectively. Additionally, Figures 5.25 through 5.30 show the axle lateral displacement and the wheel L/V ratio for the three parametric runs in the 10° curve. These figures show that the inter motor link stiffness has a small effect. Since the IML provides lateral stiffness between the axles, the lead axle (Axle 1) has its largest lateral displacement when there is no IML stiffness and displaces less as stiffness is increased. For the 10° curve, the lateral displacement is 0.365 inches for no lateral displacement and decreases to 0.359 inches and 0.358 inches for the baseline stiffness and 200% stiffness runs, respectively. This corresponds to lateral to vertical force ratios on the high rail wheel of the lead axle of 0.139, 0.140, and 0.141. In the 20° curve, the truck is pinched between the rails and the inter motor link actually forces the lead axle into the rail. For no IML stiffness, the lateral displacement is 0.583 inches. This increases to 0.597 inches for both the baseline and 200% stiffness runs. As a result of this, the ratio of lateral to vertical force on the wheels of the lead axle increases from 0.781 to 0.820 The inter motor links are intended to work in shallow curves and have little effect on performance in the 10° curve and a slightly harmful effect in the 20° curve.

Table 5.1 Results for IML lateral stiffness variation in 10° curve

	Lat Axle 1 (in.)	Angle of Attack (deg.)	Wheel L/V Axle 1 ()	Axle L/V Axle 1 ()
no IML	0.364	-0.012	0.139	0.143
50% IML	0.359	-0.018	0.140	0.152
100% IML (Baseline)	0.359	-0.018	0.140	0.153
200% IML	0.358	-0.019	0.141	0.155

Table 5.2 Results for IML lateral stiffness variation in 20° curve

	Lat Axle 1 (in.)	Angle of Attack (deg.)	Wheel L/V Axle 1 ()	Axle L/V Axle 1 ()
no IML	0.583	0.917	0.781	1.225
50% IML	0.598	0.833	0.820	1.262
100% IML (Baseline)	0.597	0.824	0.820	1.262
200% IML	0.597	0.818	0.820	1.262

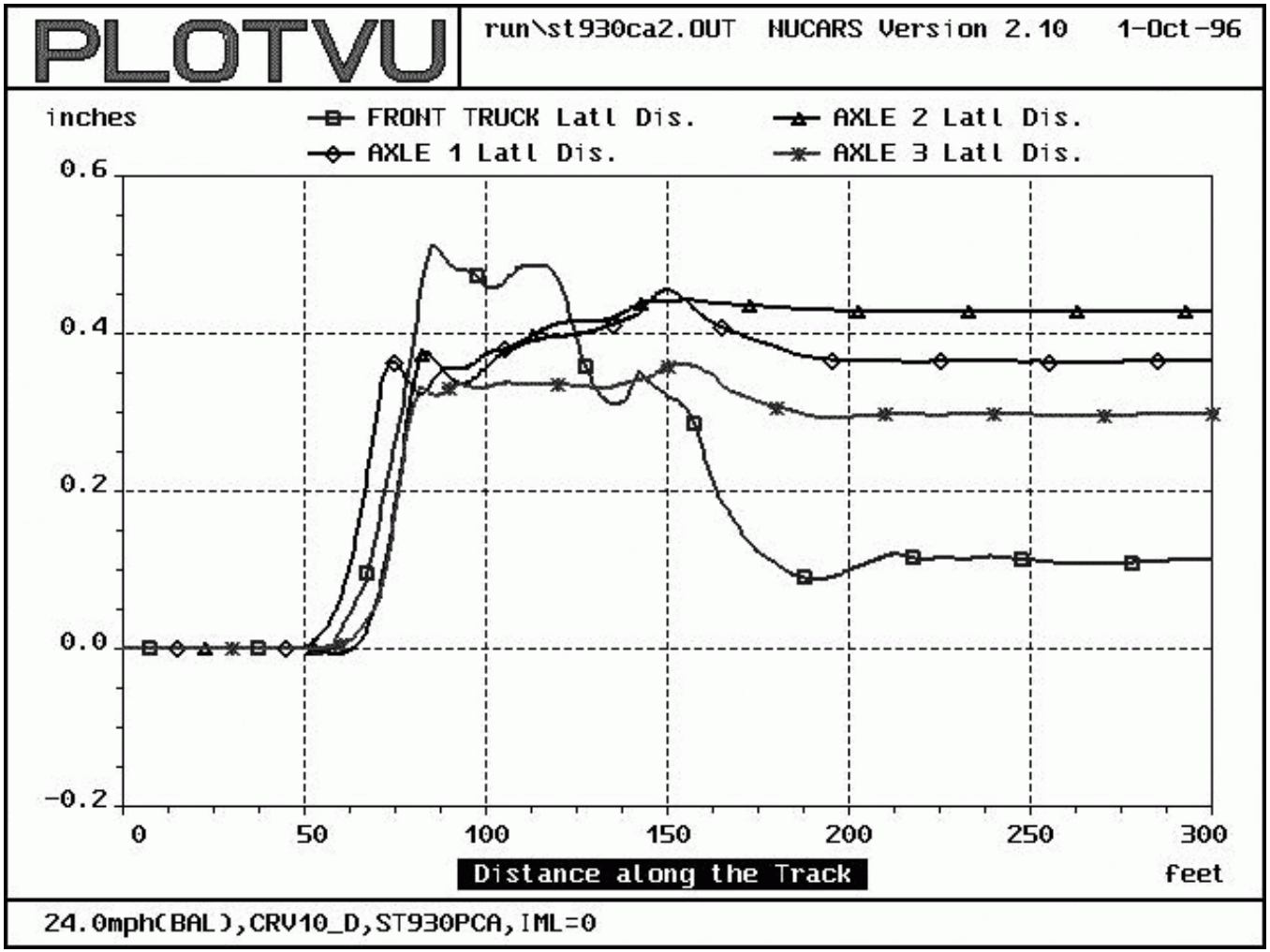

Figure 5.25 Lateral displacements in 10° curve for no IML stiffness (0 #/in.)

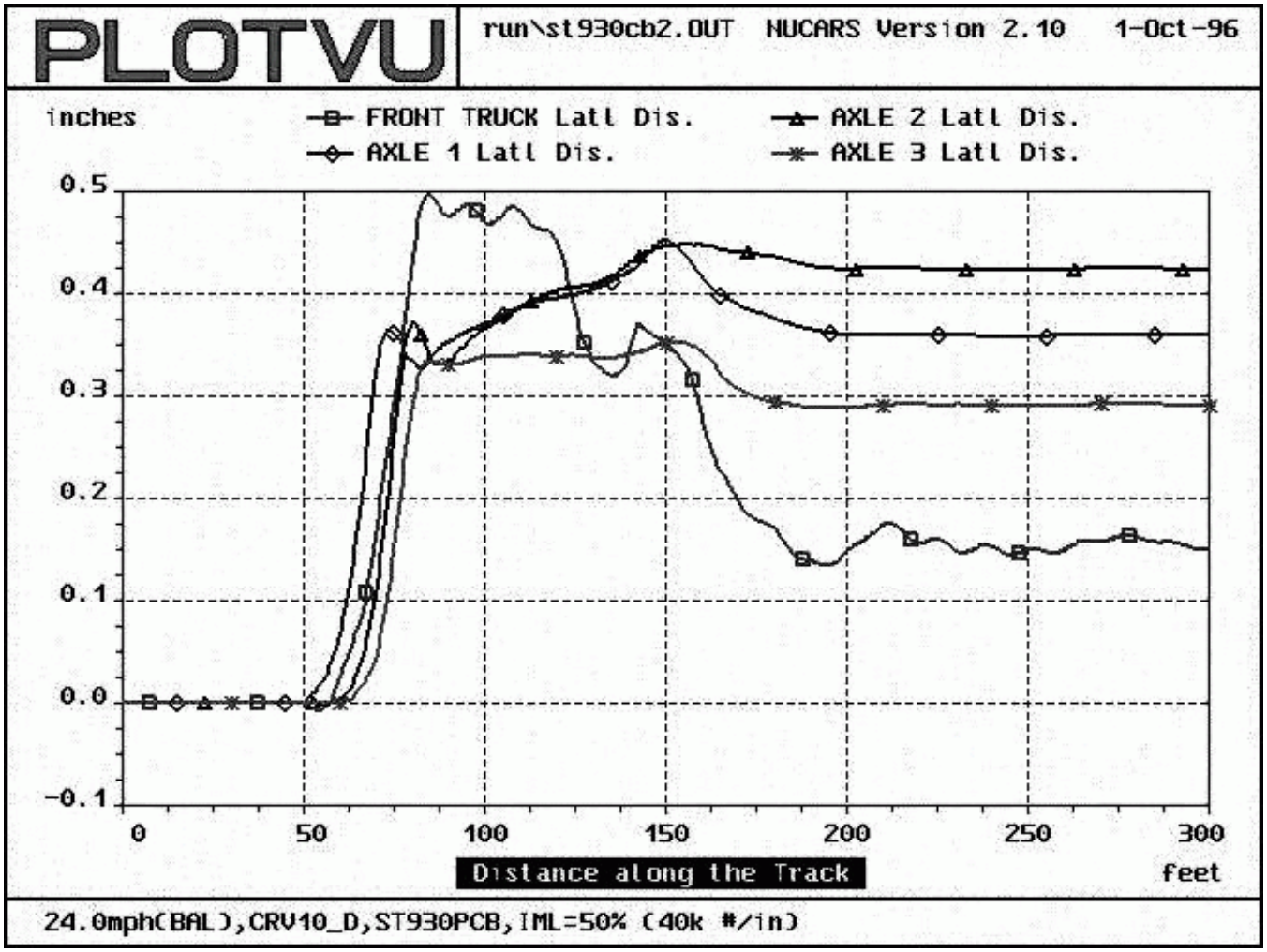

Figure 5.26 Lateral displacements in 10° curve for 50% IML stiffness (40k#/in.)

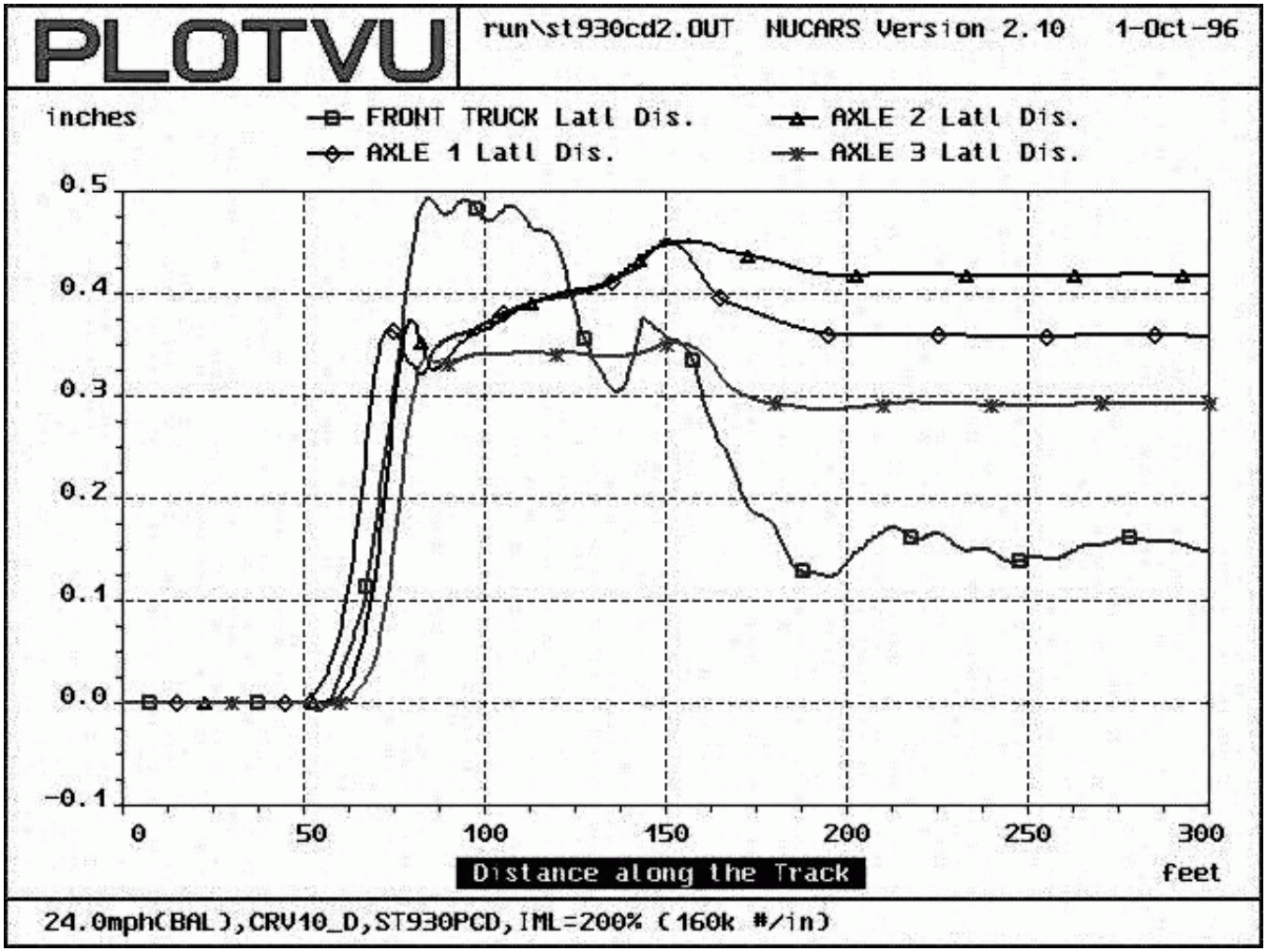

Figure 5.27 Lateral displacements in 10° curve for 200% IML stiffness (160k#/in.)

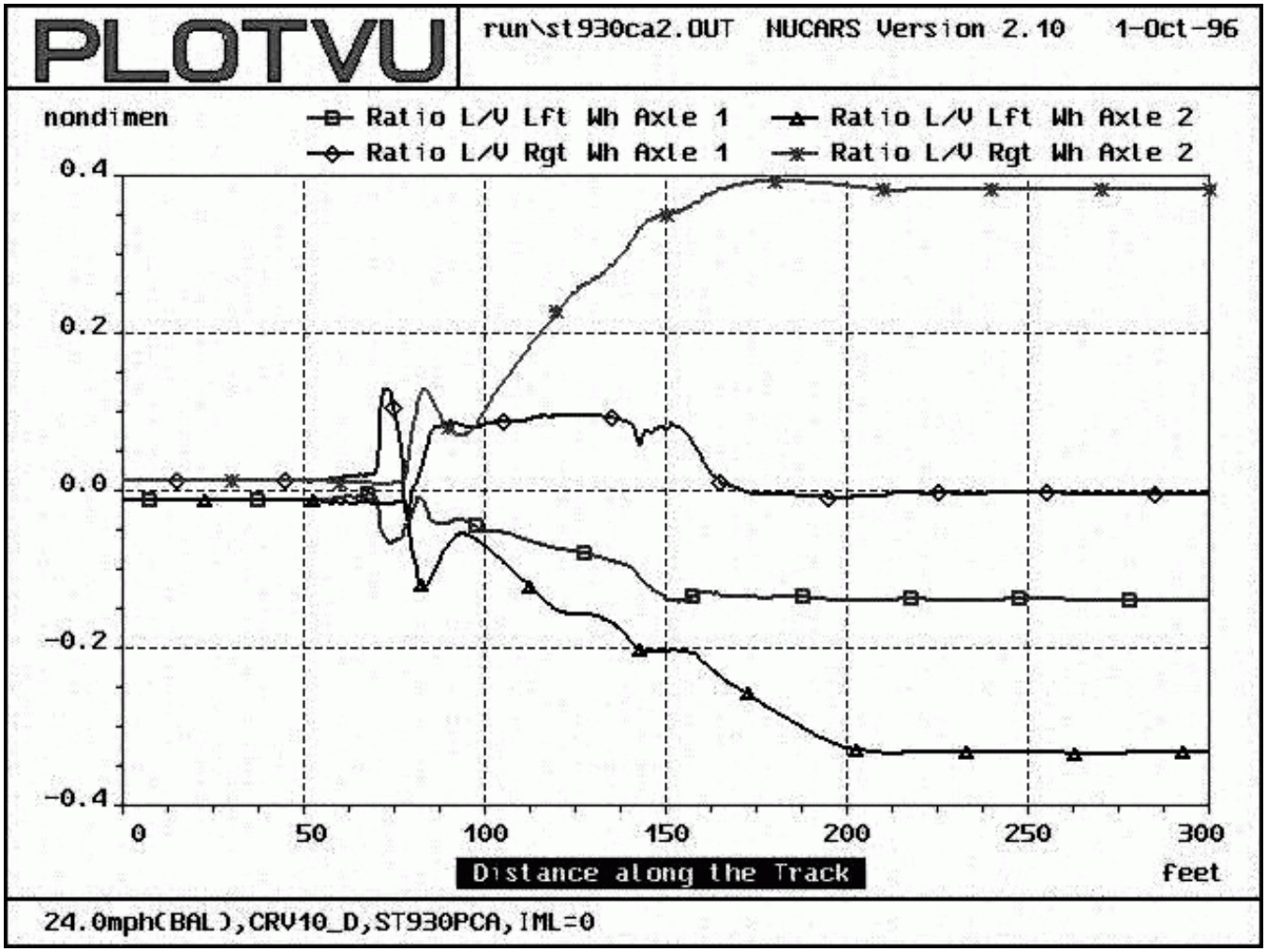

Figure 5.28 Wheel L/V ratios in 10° curve for no IML stiffness (0 #/in.)

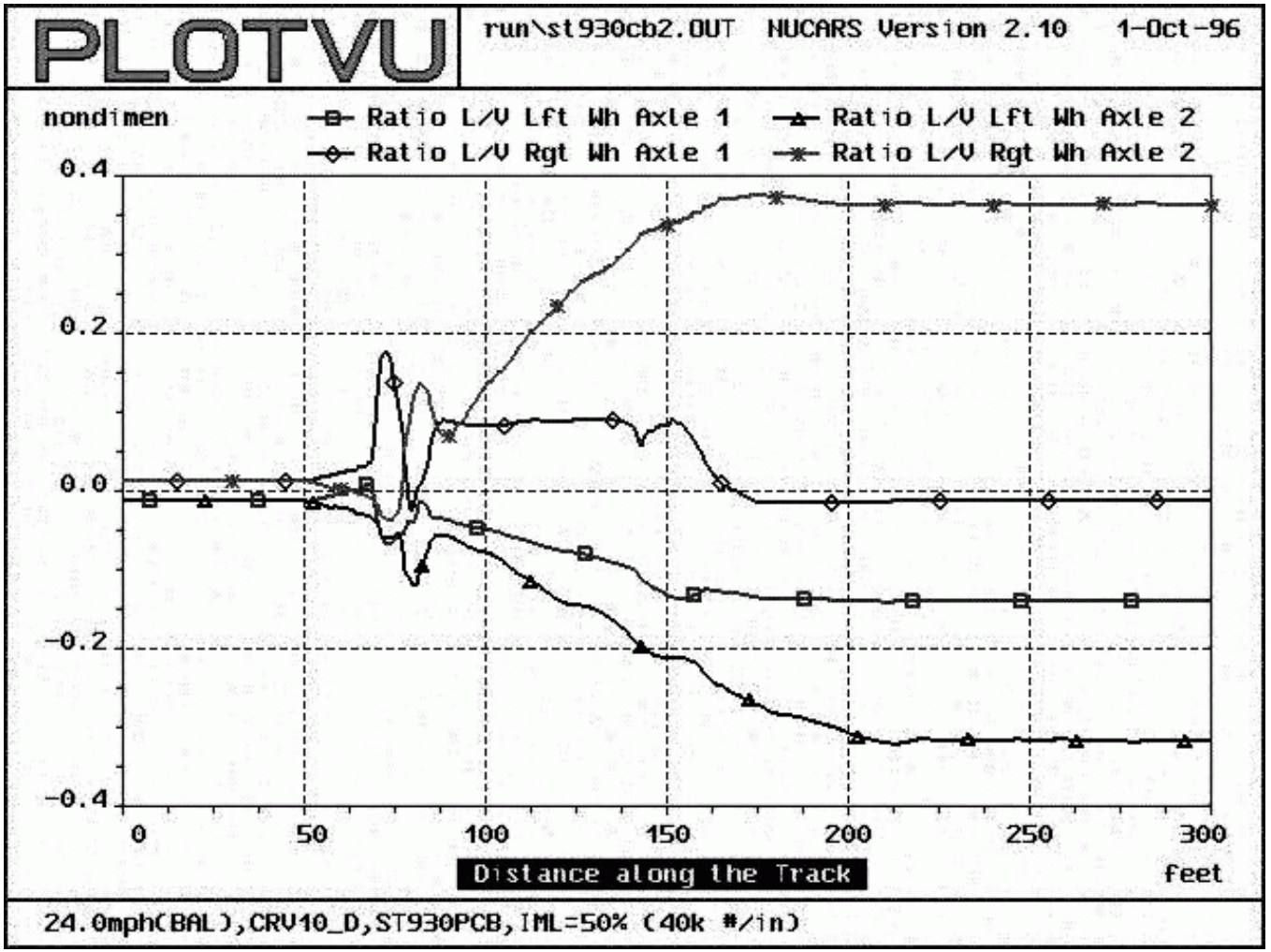

Figure 5.29 Wheel L/V ratios in 10° curve for 50% IML stiffness (40k #/in.)

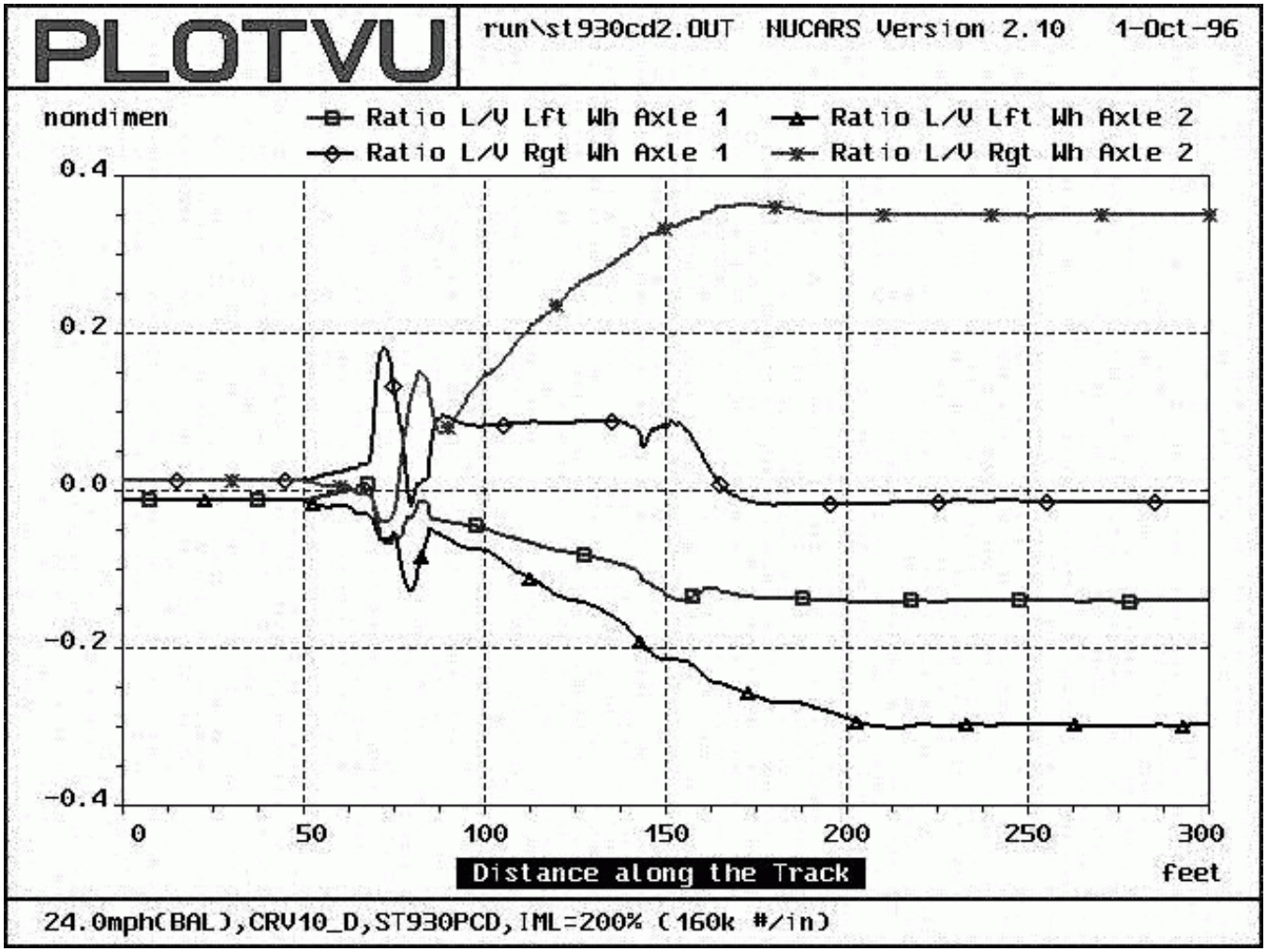

Figure 5.30 Wheel L/V ratios in 10° curve for 200% IML stiffness (160k #/in.)

5.2.2 Inter Axle Link Stiffness

The inter axle links connect the end axles of a truck together in the lateral and yaw directions. They connect them such that the axles move laterally in the same direction and yaw in opposite directions. To investigate the influence of the inter axle connections on the locomotive's curving performance, runs are made with the inter axle connection stiffness set at 50% and 200% of the baseline value (0.25E6 to 1.0E6 #/in.). The results of these runs are compared with the runs of the baseline configuration and are shown in Tables 5.3 and 5.4. The lateral axle displacements for the 50% and 200% inter axle stiffness runs are shown in Figures 5.32 and 5.32, respectively. Figures 5.33 and 5.34 show the wheel L/V force ratios for these runs.

The stiffness of the inter axle links has little effect on the curving performance of the locomotive. The results of the runs with 50% and 200% IAL stiffness are nearly identical (the lateral axle displacements and wheel L/V ratios in the 10° curve are shown in Figures 5.31 to 5.34). For the outside wheel of the lead axle, the L/V ratio changes from -0.138 to -0.142 for the 50% and 200% IAL stiffness runs, respectively, a variation of only 3%. In the 20° curve, varying the inter axle stiffness has a similar effect. The L/V ratio of the outside wheel of the lead axle changes from -0.819 to -0.820. The stiffness of the inter axle links has little effect on the curving performance of the locomotive.

Table 5.3 Results for IAL lateral stiffness variation in 10° curve

	Lat Axle 1 (in.)	Angle of Attack (deg.)	Wheel L/V Axle 1 ()	Axle L/V Axle 1 ()
50% IAL	0.359	-0.014	0.138	0.144
100% IAL (Baseline)	0.359	-0.018	0.140	0.153
200% IAL	0.358	-0.021	0.142	0.159

Table 5.4 Results for IAL lateral stiffness variation in 20° curve

	Lat Axle 1 (in.)	Angle of Attack (deg.)	Wheel L/V Axle 1 ()	Axle L/V Axle 1 ()
50% IAL	0.597	0.817	0.819	1.261
100% IAL (Baseline)	0.597	0.824	0.820	1.262
200% IAL	0.597	0.827	0.820	1.262

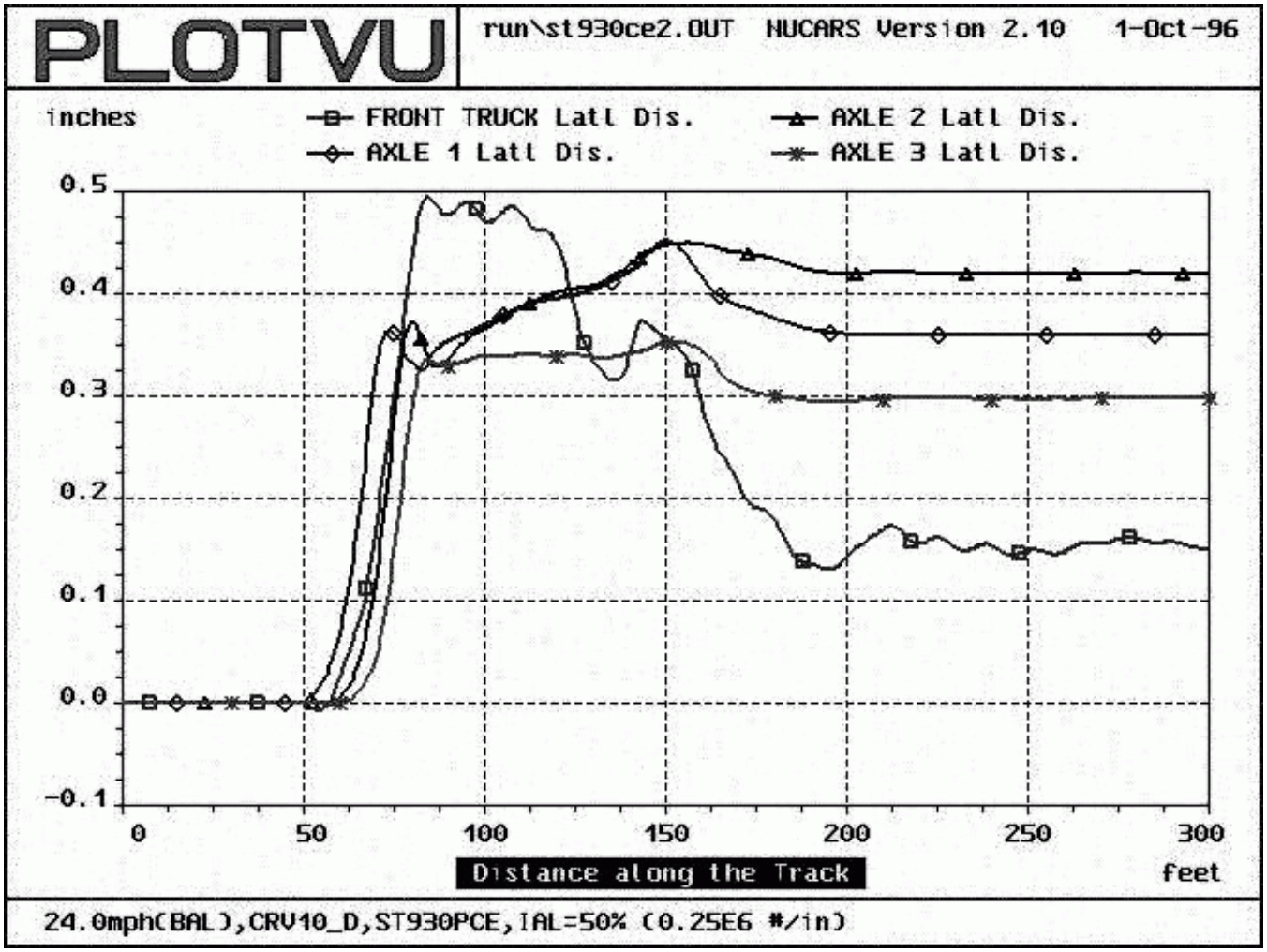

Figure 5.31 Lateral displacements in 10° curve for 50% IAL stiffness (0.25E6 #/in.)

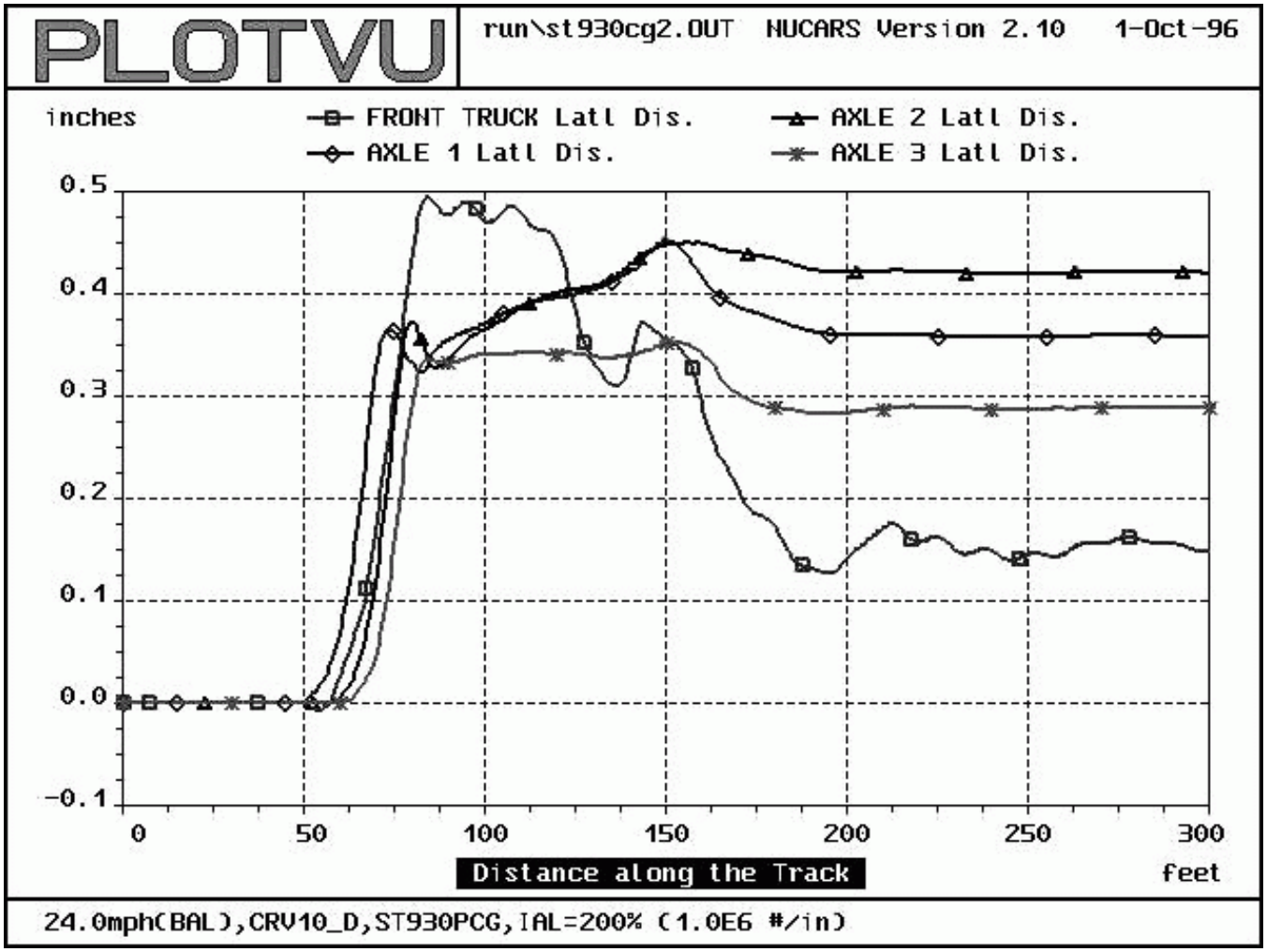

Figure 5.32 Lateral displacements in 10° curve for 200% IAL stiffness (1.0E6 #/in.)

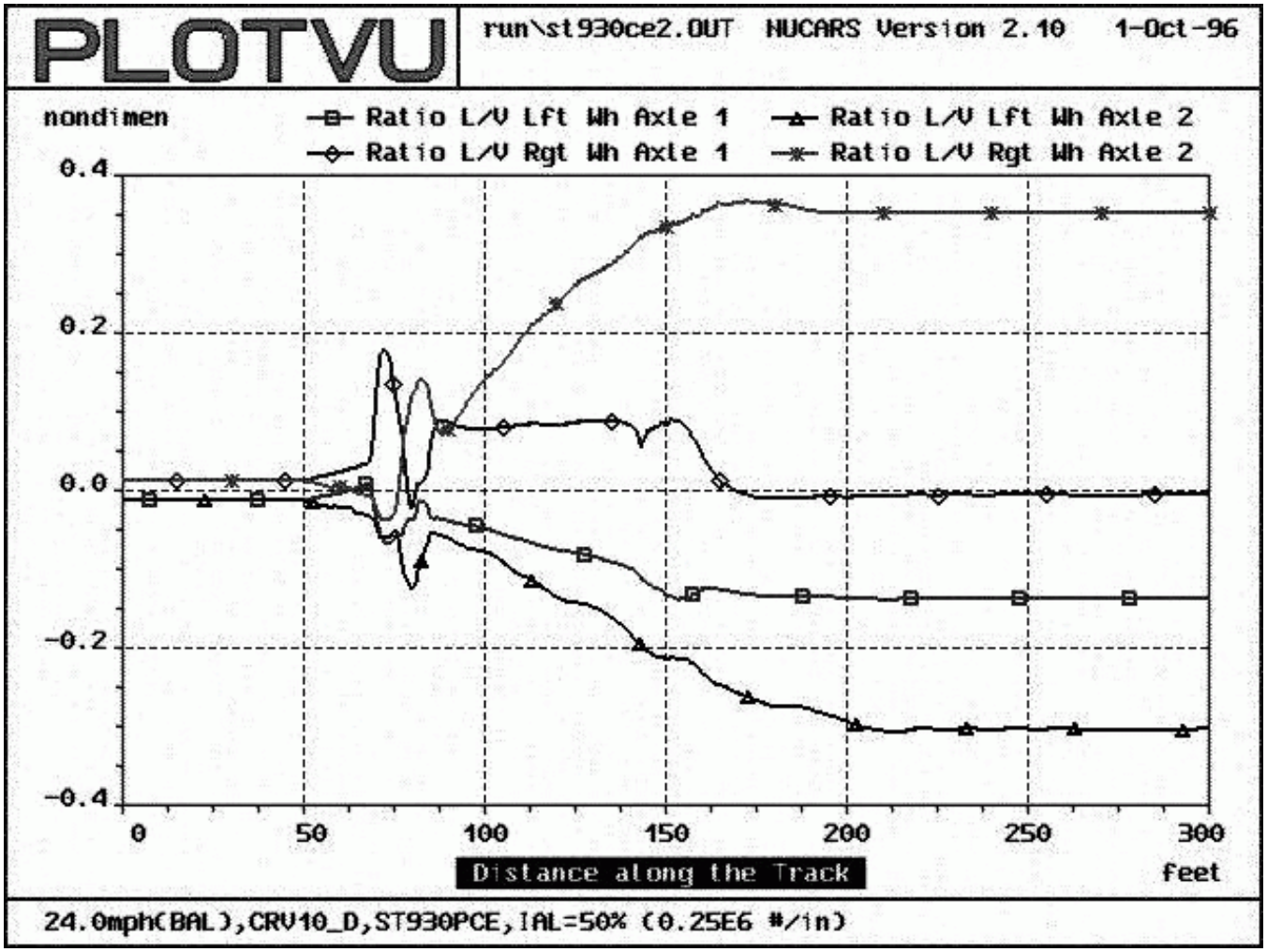

Figure 5.33 Wheel L/V ratios in 10° curve for 50% IAL stiffness (0.25E6 #/in.)

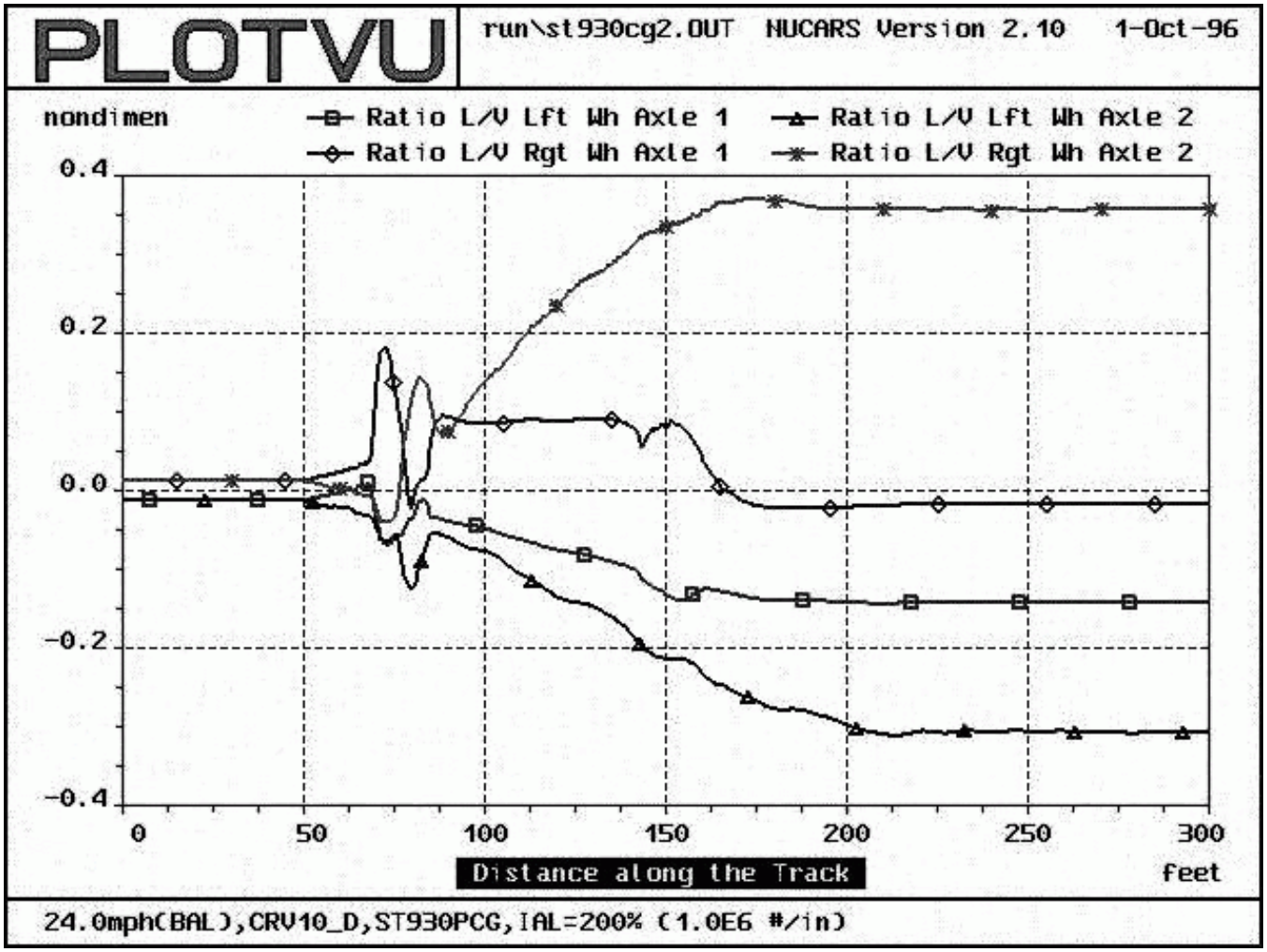

Figure 5.34 Wheel L/V ratios in 10° curve for 200% IAL stiffness (1.0E6 #/in.)

5.2.3 Lateral Clearance

Tractive effort and curving forces are transferred between the truck frame and axles through pivoting members called traction links and center links. They allow the end axles to yaw and move laterally to adjust to the shape of the track. The size of the clearance between the axle and truck frame limits the amount of lateral movement and, as a result, limits the amount of curvature that the truck can roll through smoothly. To investigate the effect of the lateral clearance on curving performance, the model is run with the coil spring lateral flexicoiling limited to 10% and 150% of the baseline value. The results of these runs are compared with the results of the baseline curving runs to show the parametric dependence. A summary of the lateral clearance parametric runs is given in Tables 5.5 and 5.6 for the 10 and 20 degree curves, respectively. Figures 5.35 to 5.38 show the lateral axle displacements and wheel L/V ratios for the 10% and 150% lateral clearance runs.

In Table 5.5, the lateral displacement of axle 1 is much larger when the lateral gap is limited to 10% of the baseline clearance than for the baseline and increased lateral gaps. The displacements are 0.580, 0.359 and 0.359 for the runs with 10%, 100% and 150% baseline gap, respectively. Additionally, limiting the lateral clearance results in a much larger angle of attack for axle 1. The angle between axle 1 and the track is 0.213°, -0.018° and -0.19° for the same runs. Limiting the lateral axle clearance causes the steerable truck curves similar to a conventional straight truck. The axles move laterally and yaw with the truck frame, as can be seen in Figures 5.35 and 5.36. In Figure 5.35, the axle clearance is limited to 10% of the baseline value, and the axles are displaced laterally due to the truck yaw. In Figure 5.36, the lateral clearance is increased to 150% of the

baseline value and the axles are able to move independently of the truck frame. As a result, they all displace positively to generate rolling radii differences and allow the locomotive to curve smoothly. In addition, limiting the axles places the highest L/V ratio on the outside wheel of axle 1, shown in Figure 5.37. When the lateral clearance is increased (Figure 5.38), the end axles are able to better align with the track and the largest L/V ratios are found on the wheels of the center axle (Axle 2) Thus, the lateral clearance between the axles and the truck frame is important to the curving performance of the steerable truck.

Table 5.5 Results for lateral gap variation in 10° curve

	Lat Axle 1 (in.)	Angle of Attack (deg.)	Wheel L/V Axle 1 ()	Axle L/V Axle 1 ()
10% Lateral Gap	0.580	0.213	0.447	0.741
100% Gap (Baseline)	0.359	-0.018	0.140	0.153
150% Lateral Gap	0.359	-0.019	0.141	0.154

Table 5.6 Results for lateral gap variation in 20° curve

	Lat Axle 1 (in.)	Angle of Attack (deg.)	Wheel L/V Axle 1 ()	Axle L/V Axle 1 ()
10% Lateral Gap	0.614	1.238	0.707	1.153
100% Gap (Baseline)	0.597	0.824	0.820	1.262
150% Lateral Gap	0.595	0.810	0.141	1.274

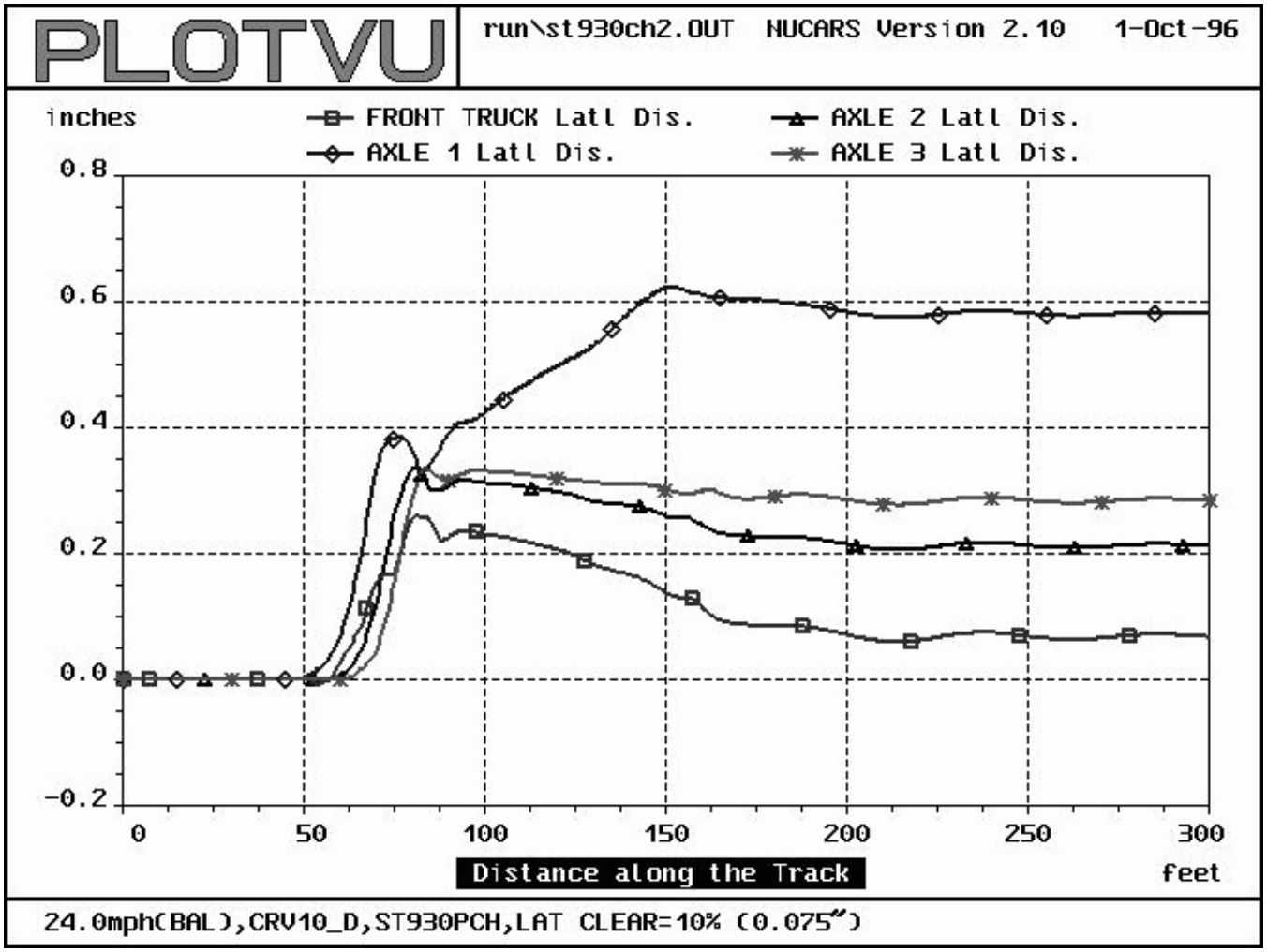

Figure 5.35 Lateral displacements in 10° curve for 10% lateral clearance (0.075")

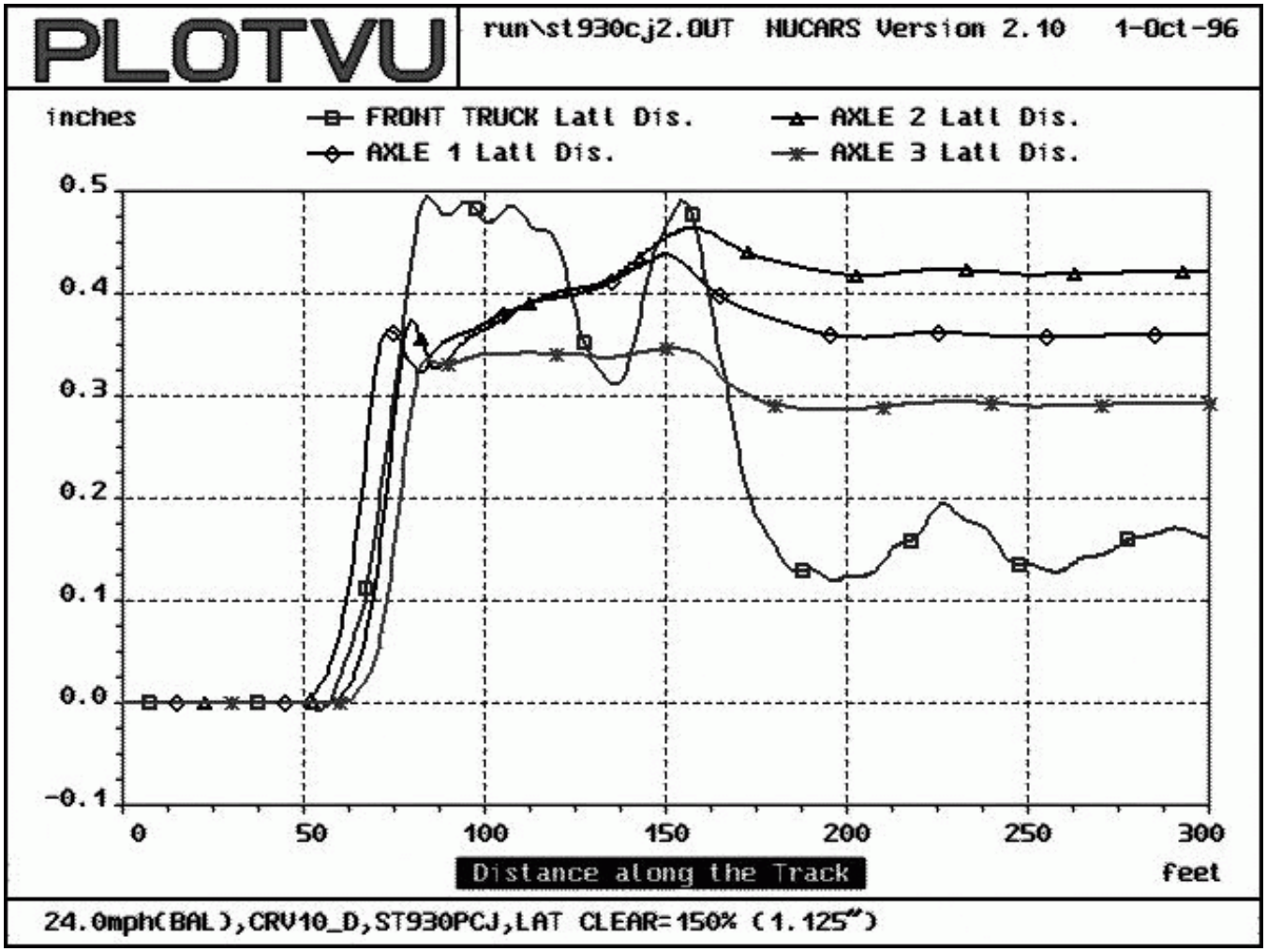

Figure 5.36 Lateral displacements in 10° curve for 150% lateral clearance (1.125")

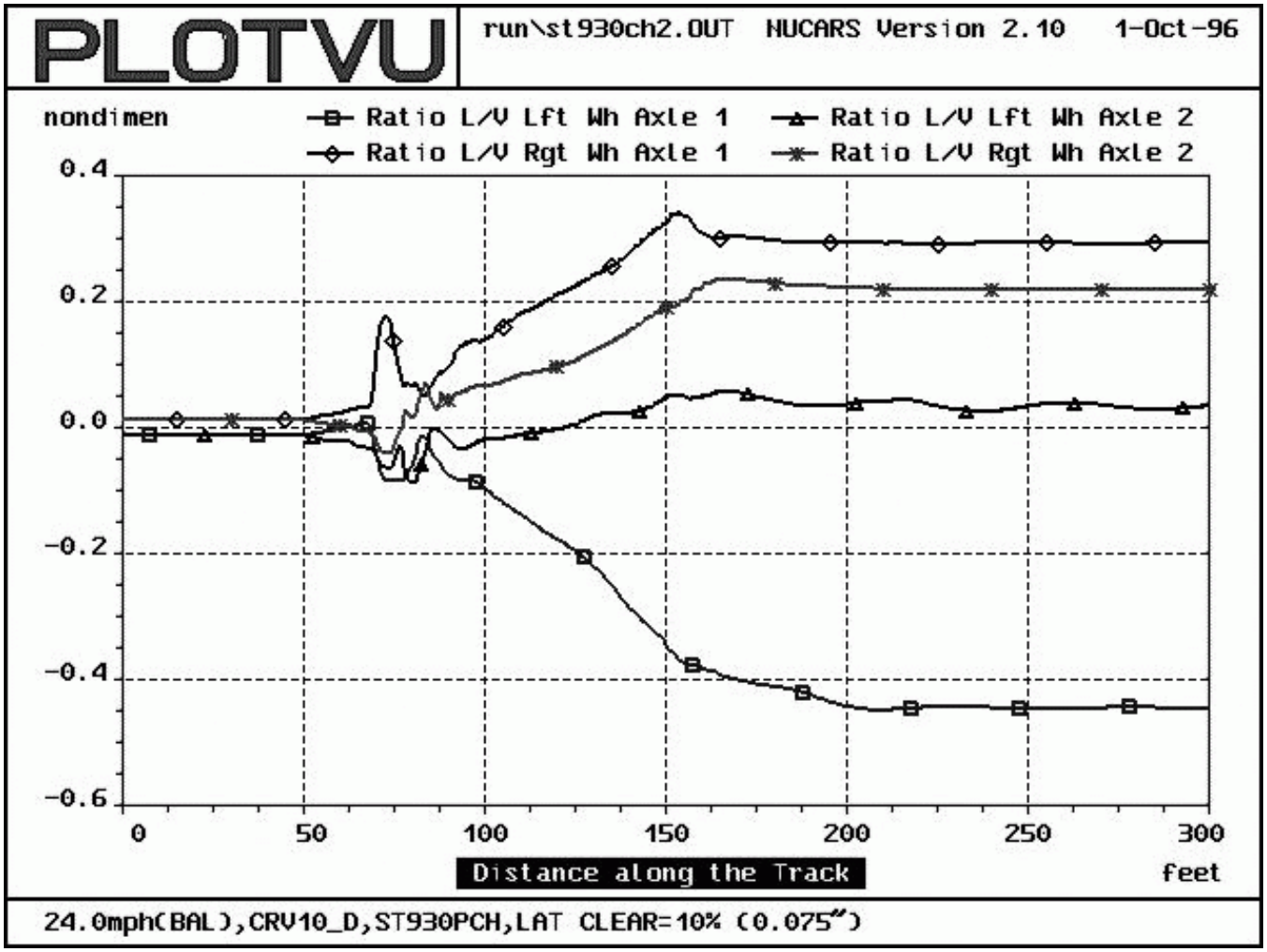

Figure 5.37 Wheel L/V ratios in 10° curve for 10% lateral clearance (0.075")

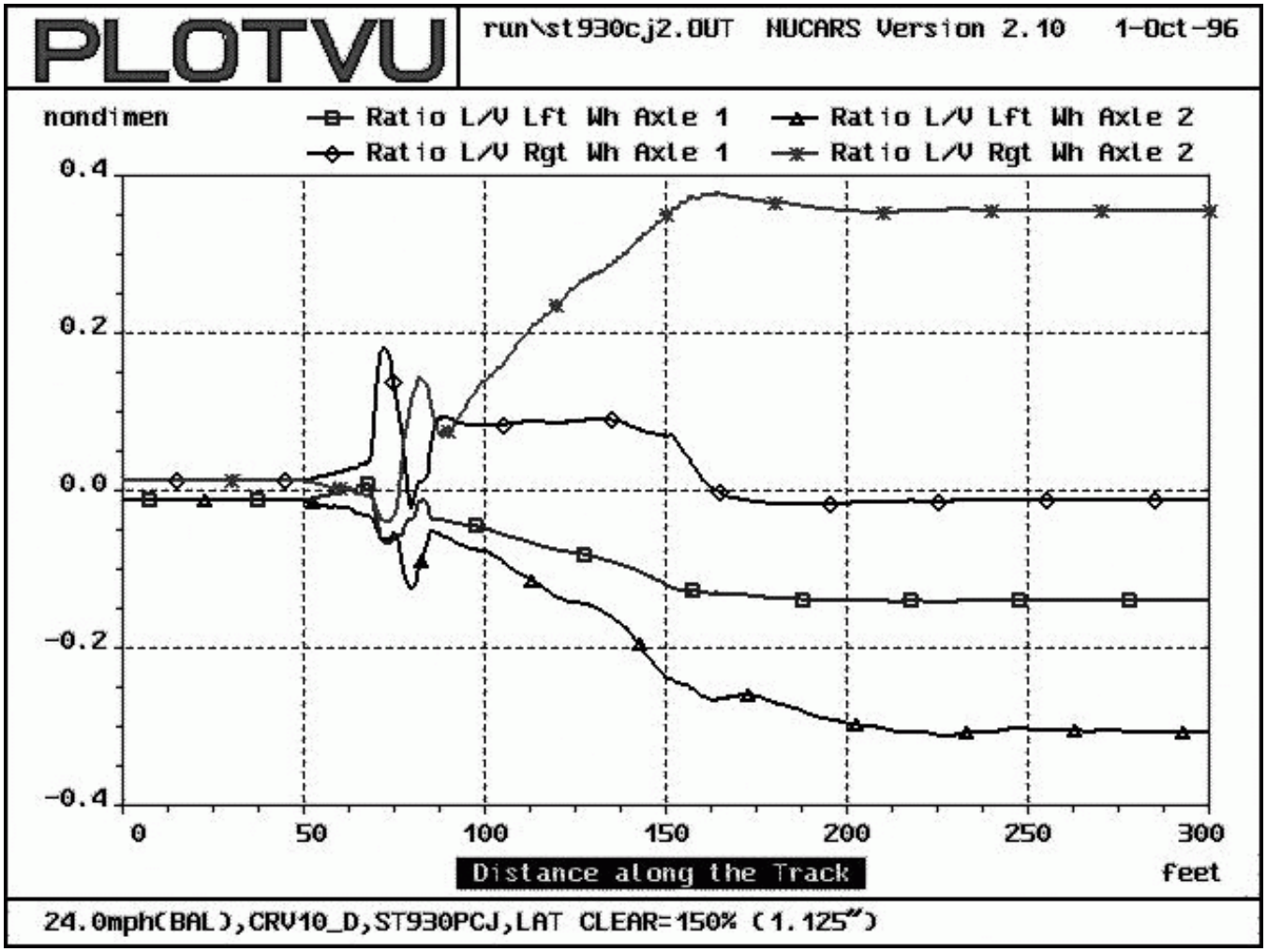

Figure 5.38 Wheel L/V ratios in 10° curve for 150% lateral clearance (1.125")

5.2.4 Longitudinal Clearance

The longitudinal clearance between the axle ends and truck frame also limits the amount of relative axle motion, which determines the maximum amount of curvature that the truck can smoothly negotiate. The effect of longitudinal clearance on curving performance is investigated by limiting the coil spring flexicoiling in the longitudinal direction and running the model through the curve sections. Tables 5.7 and 5.8 show the results for these runs, and the lateral axle displacement and the wheel L/V ratios for the 10% and 150% runs are shown in Figures 5.39 to 5.42.

Limiting the amount of longitudinal axle clearance has a similar effect to limiting the lateral axle clearance. The axles are no longer able to move independently from the truck frame, and curve similar to the axles in a straight truck. Figure 5.39 shows that the axles displace laterally due to the yaw of the truck frame, with axle 1 being pushed far to the outside of the curve, axle 2 in the center of the curve, and axle 3 to the inside of the curve. The resulting displacements are 0.686, -0001 and -0.322 inches, respectively. Figure 5.40 shows the axle displacements for the run with increased longitudinal axle clearance. When the axles are allowed to move independently of the truck frame, they move outward on the track together to generate rolling radii differences. The displacements of axles 1, 2 and 3 for the 150% longitudinal clearance run in the 10° curve are 0.359, 0.420 and 0.291 inches, respectively. This lateral motion allows the axles to better align with the track and reduces the L/V force ratios. The angle of attack of the lead axle changes from .906° to -0.018° when the axles are allowed to move independent of the truck frame. The corresponding L/V ratio of the outside wheel of the lead axle

changes from -0.750 to -0.140. Limiting the longitudinal clearance between the axles and truck frame is detrimental to curving performance.

Table 5.7 Results for longitudinal gap variation in 10° curve

	Lat Axle 1 (in.)	Angle of Attack (deg.)	Wheel L/V Axle 1 ()	Axle L/V Axle 1 ()
10% Longitudinal Gap	0.686	0.906	0.750	1.171
100% Gap (Baseline)	0.359	-0.018	0.140	0.153
150% Longitudinal Gap	0.359	-0.018	0.140	0.153

Table 5.8 Results for longitudinal gap variation in 20° curve

	Lat Axle 1 (in.)	Angle of Attack (deg.)	Wheel L/V Axle 1 ()	Axle L/V Axle 1 ()
10% Longitudinal Gap	0.625	1.627	0.882	1.321
100% Gap (Baseline)	0.597	0.824	0.820	1.262
150% Longitudinal Gap	0.509	0.215	0.563	0.868

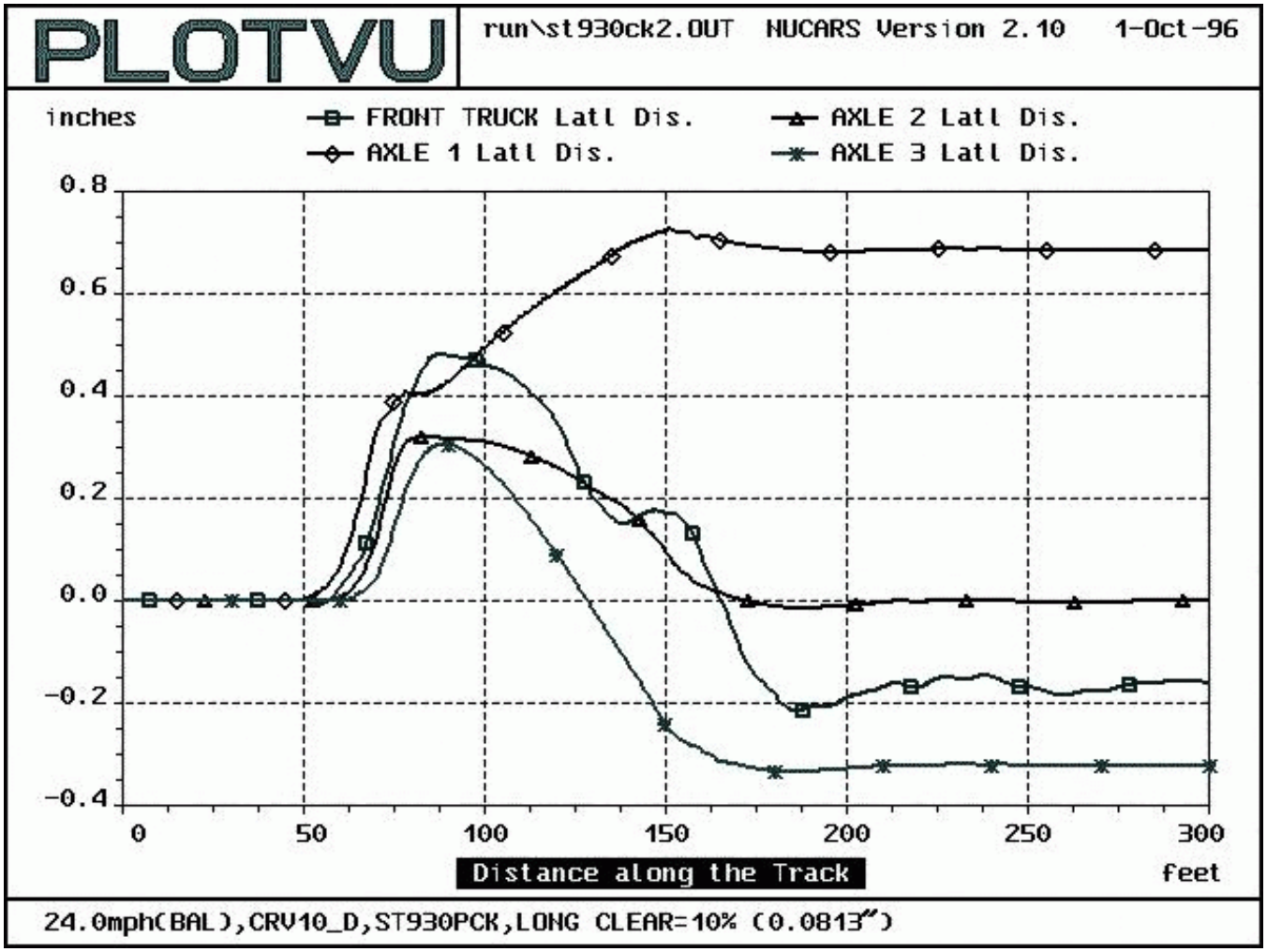

Figure 5.39 Lateral displacements in 10° curve for 10% longitudinal clearance (0.081")

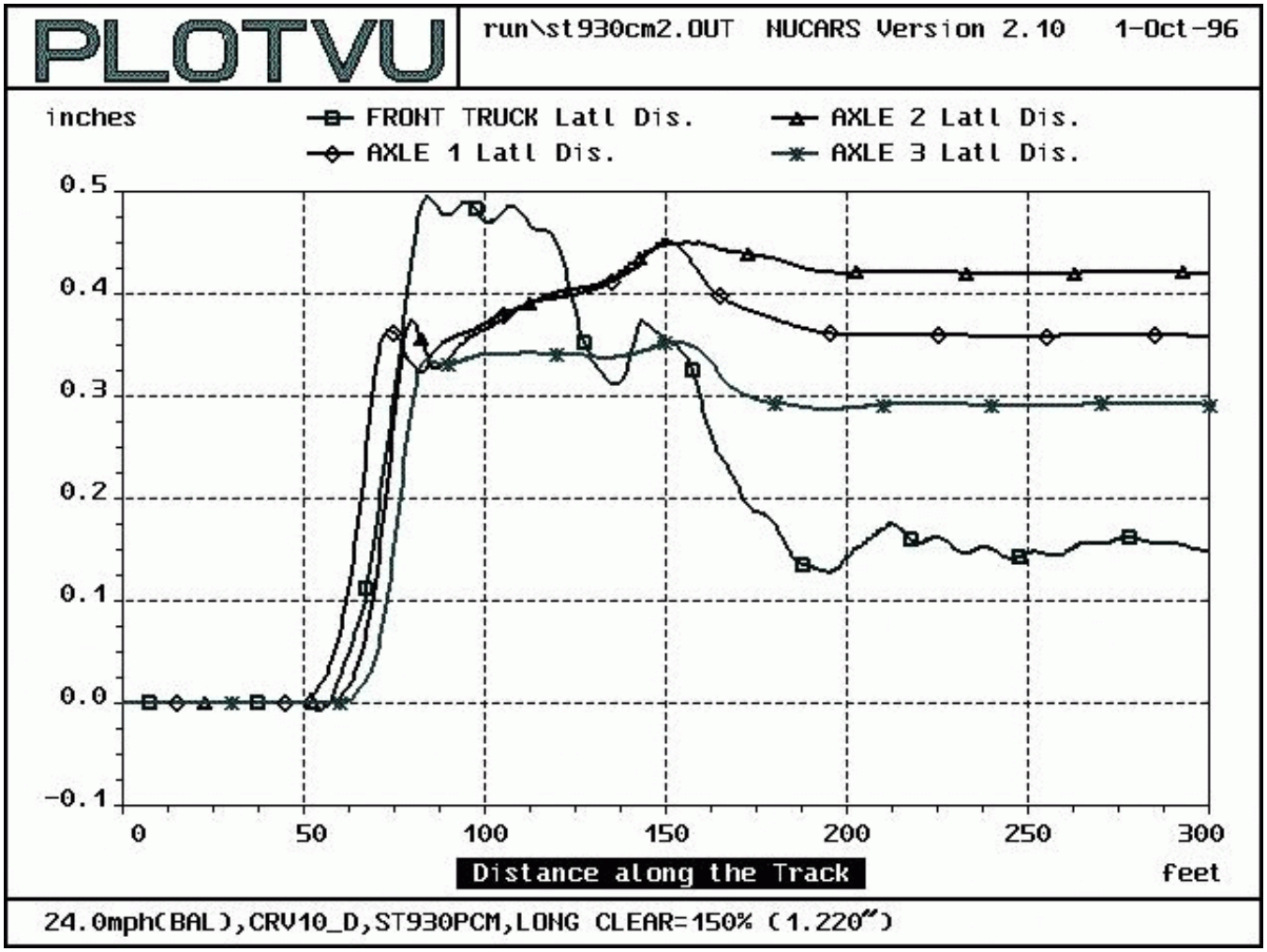

Figure 5.40 Lateral displacements in 10° curve for 150% longitudinal clearance (1.220")

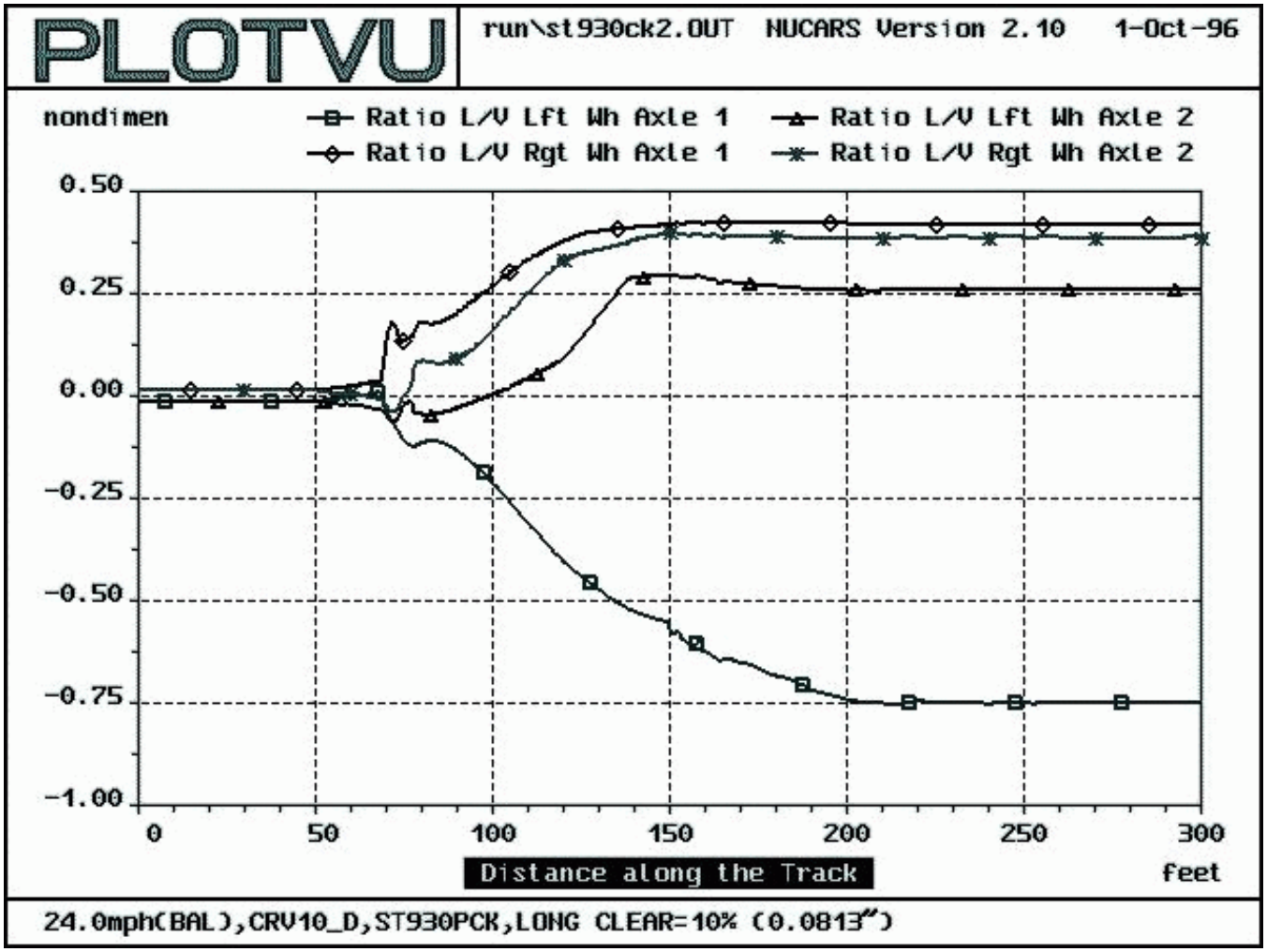

Figure 5.41 Wheel L/V ratios in 10° curve for 10% longitudinal clearance (0.081")

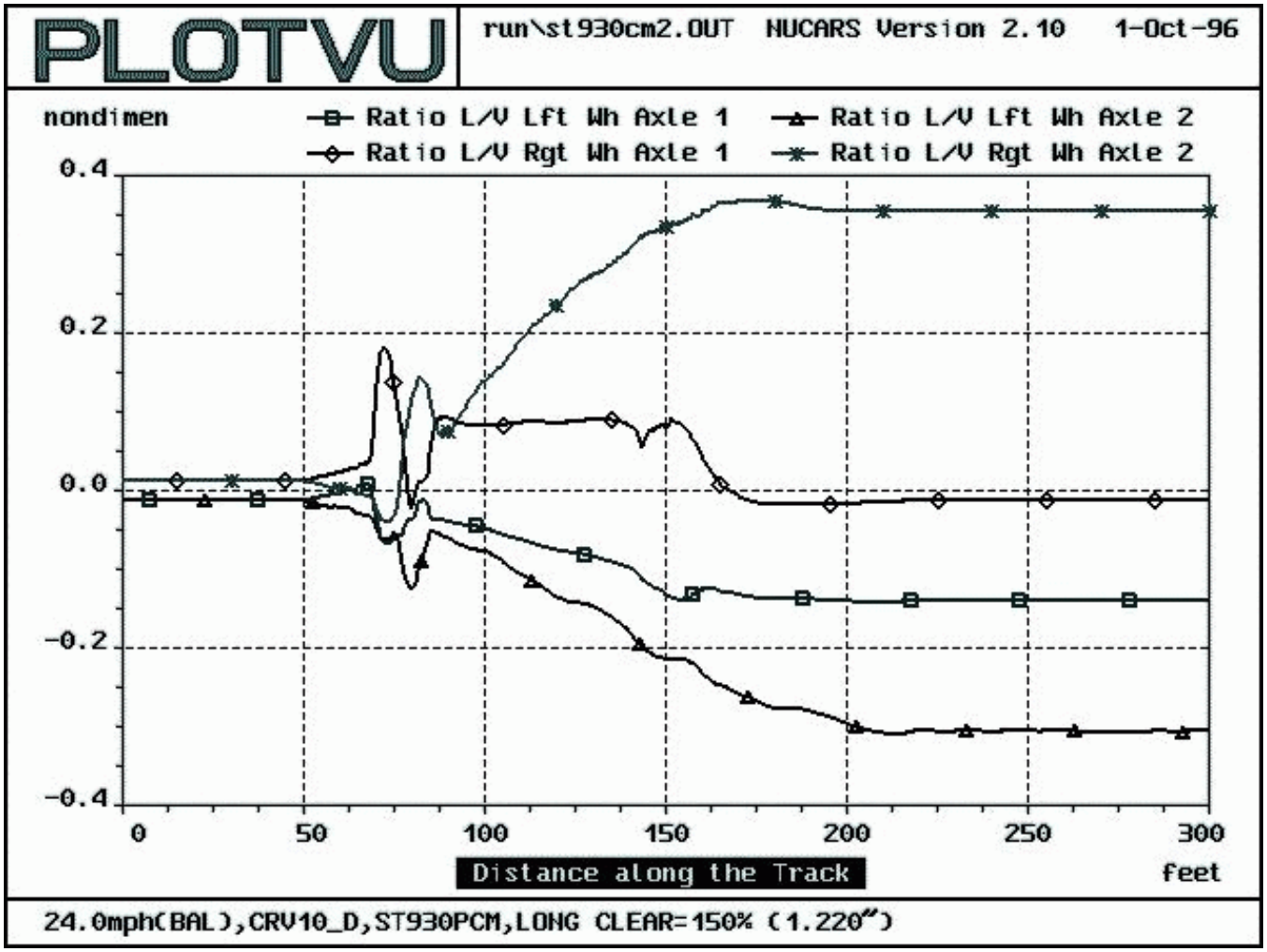

Figure 5.42 Wheel L/V ratios in 10° curve for 150% longitudinal clearance (1.220")

5.2.5 Lateral and Longitudinal Clearance

The final clearance test investigates the effect of limiting both the lateral and longitudinal clearances. This is done by limiting the lateral and longitudinal clearances to the same percentage of the baseline values and comparing these runs with the baseline curving runs. The 10 and 20 degree runs with the lateral and longitudinal clearances limited are summarized in Tables 5.9 and 5.10, and the lateral axle displacements and wheel L/V ratios for the 10° curve are shown in Figures 5.43 to 5.48.

The effect on curving performance for limiting both the lateral and longitudinal clearances is similar to limiting only the longitudinal clearances. This is due to the axle encountering the limited clearance in the longitudinal direction before it does in the lateral direction. The results of the run with the lateral and longitudinal clearances limited to 10% of the baseline values, shown in Table 5.9 are very similar to the values for the run with only the longitudinal clearance limited, shown in Table 5.7. In Table 5.5, where only the only the lateral clearance is limited, the axle is able to achieve better alignment with the track. The angle of attack for the lead axle is 0.906 degrees when both clearances are limited, and 0.906 and 0.213 when the longitudinal and lateral clearances are limited, respectively. This results in an L/V force ratio on the outside wheel of the lead axle of -0.715 for limiting both clearances and -0.750 and -0.447 for limiting the longitudinal and lateral clearance, respectively. Limiting both the lateral and longitudinal clearance is similar to limiting only the longitudinal clearance and has a similar detrimental effect on the locomotive's curving performance.

Table 5.9 Results for lateral & longitudinal gap variation in 10° curve

	Lat Axle 1 (in.)	Angle of Attack (deg.)	Wheel L/V Axle 1 ()	Axle L/V Axle 1 ()
10% Lat & Long Gap	0.689	0.906	0.715	1.136
100% Gap (Baseline)	0.359	-0.018	0.140	0.153
150% Lat & Long Gap	0.359	-0.019	0.140	0.154

Table 5.10 Results for lateral & longitudinal gap variation in 20° curve

	Lat Axle 1 (in.)	Angle of Attack (deg.)	Wheel L/V Axle 1 ()	Axle L/V Axle 1 ()
10% Lat & Long Gap	0.631	1.637	0.862	1.302
100% Gap (Baseline)	0.597	0.824	0.820	1.262
150% Lat & Long Gap	0.503	0.242	0.605	0.933

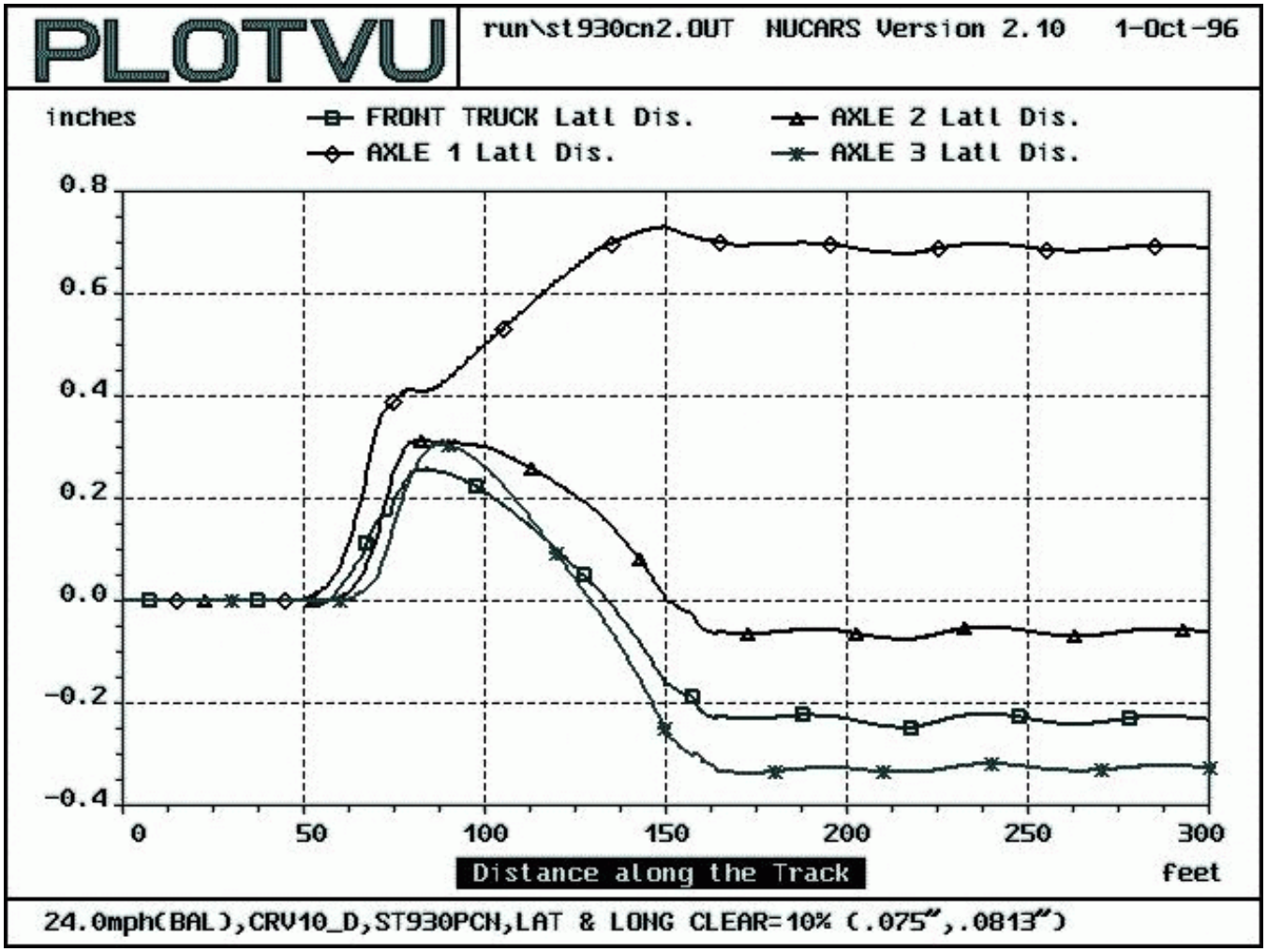

Figure 5.43 Lateral displacements in 10° curve for 10% clearances (Lat=0.075" & Long=0.081")

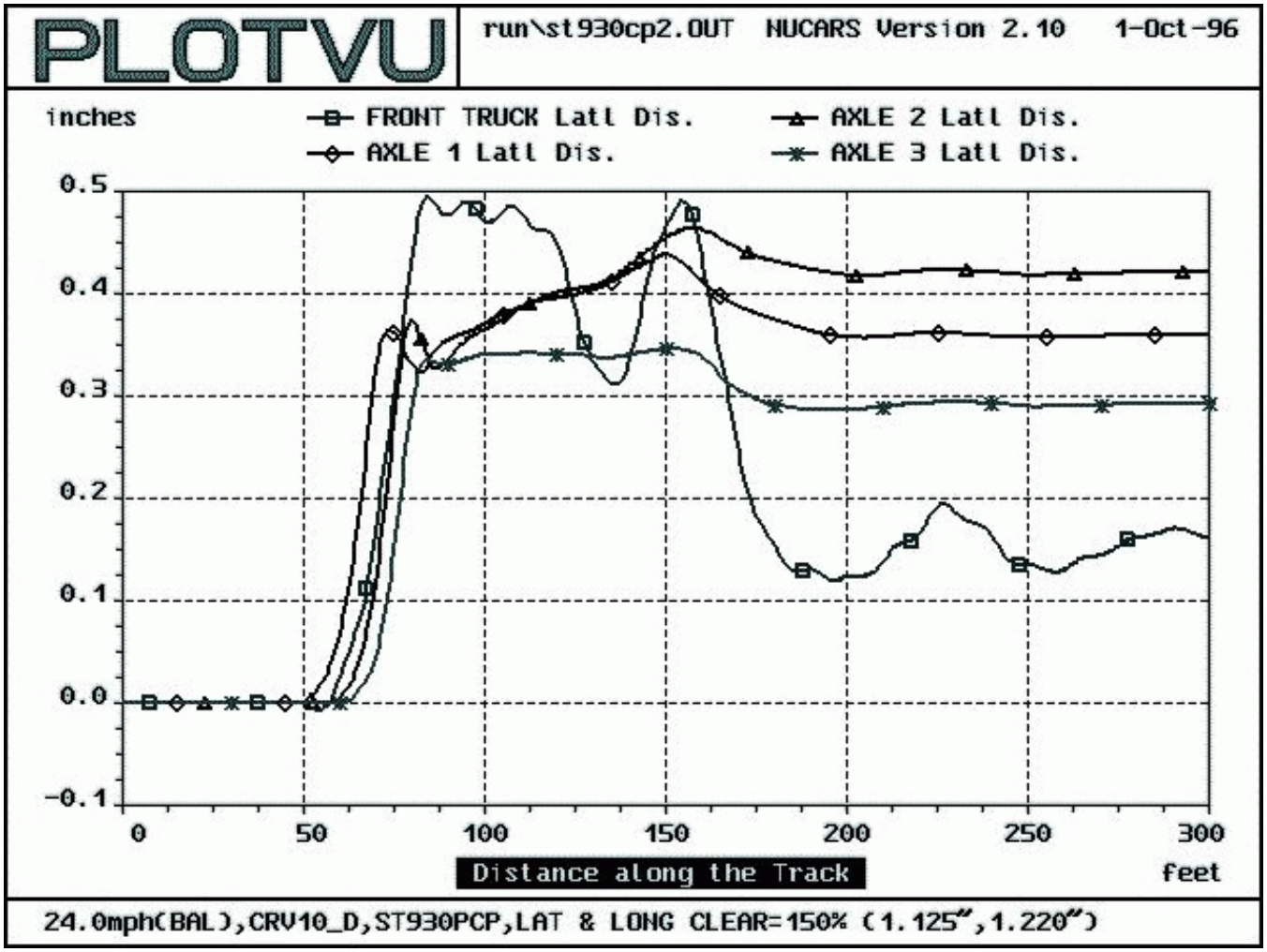

Figure 5.44 Lateral displacements in 10° curve for 150% clearances (Lat=1.125" & Long=1.220")

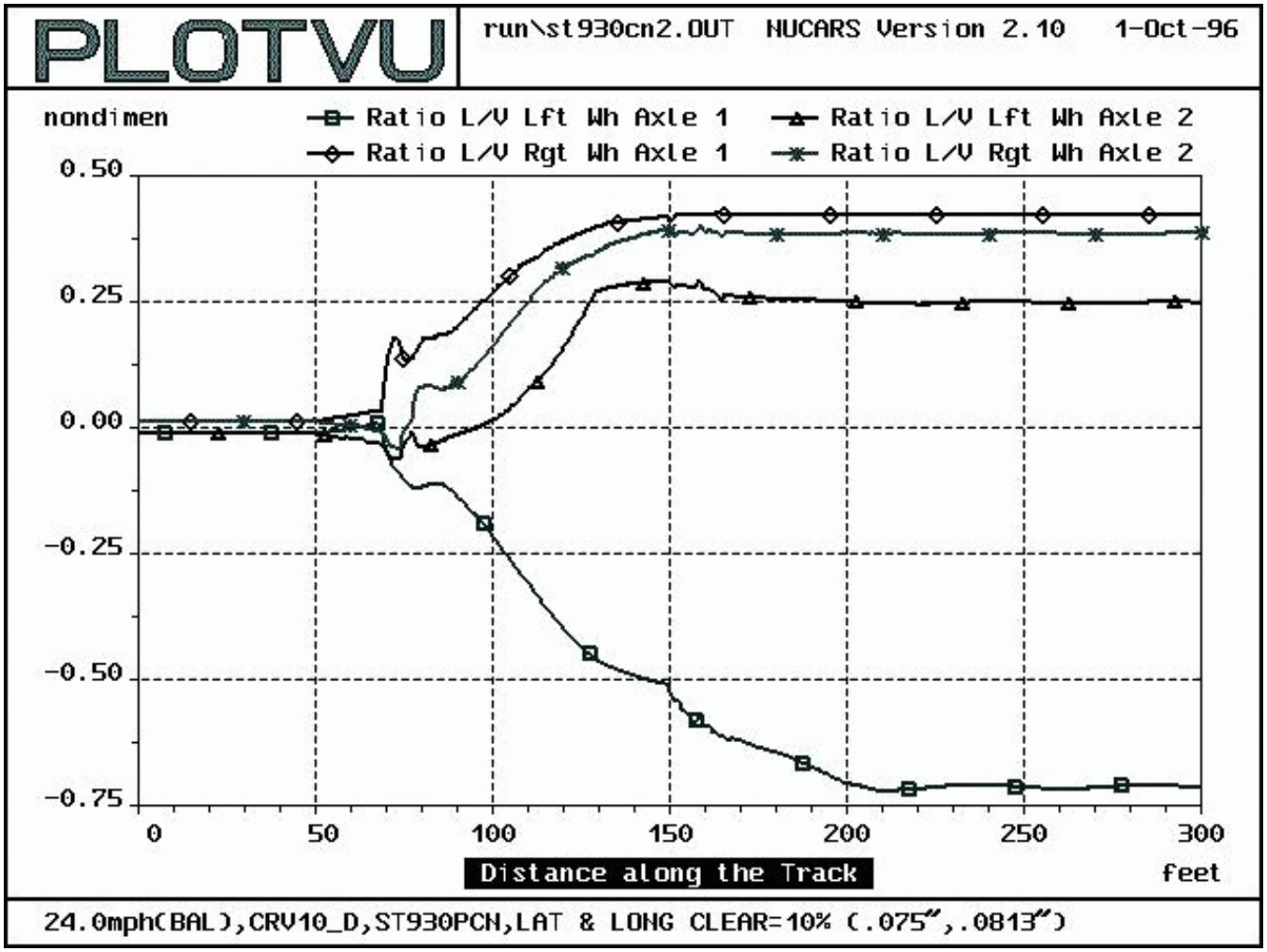

Figure 5.45 Wheel L/V ratios in 10° curve for 10% clearances (Lat=0.075" & Long=0.081")

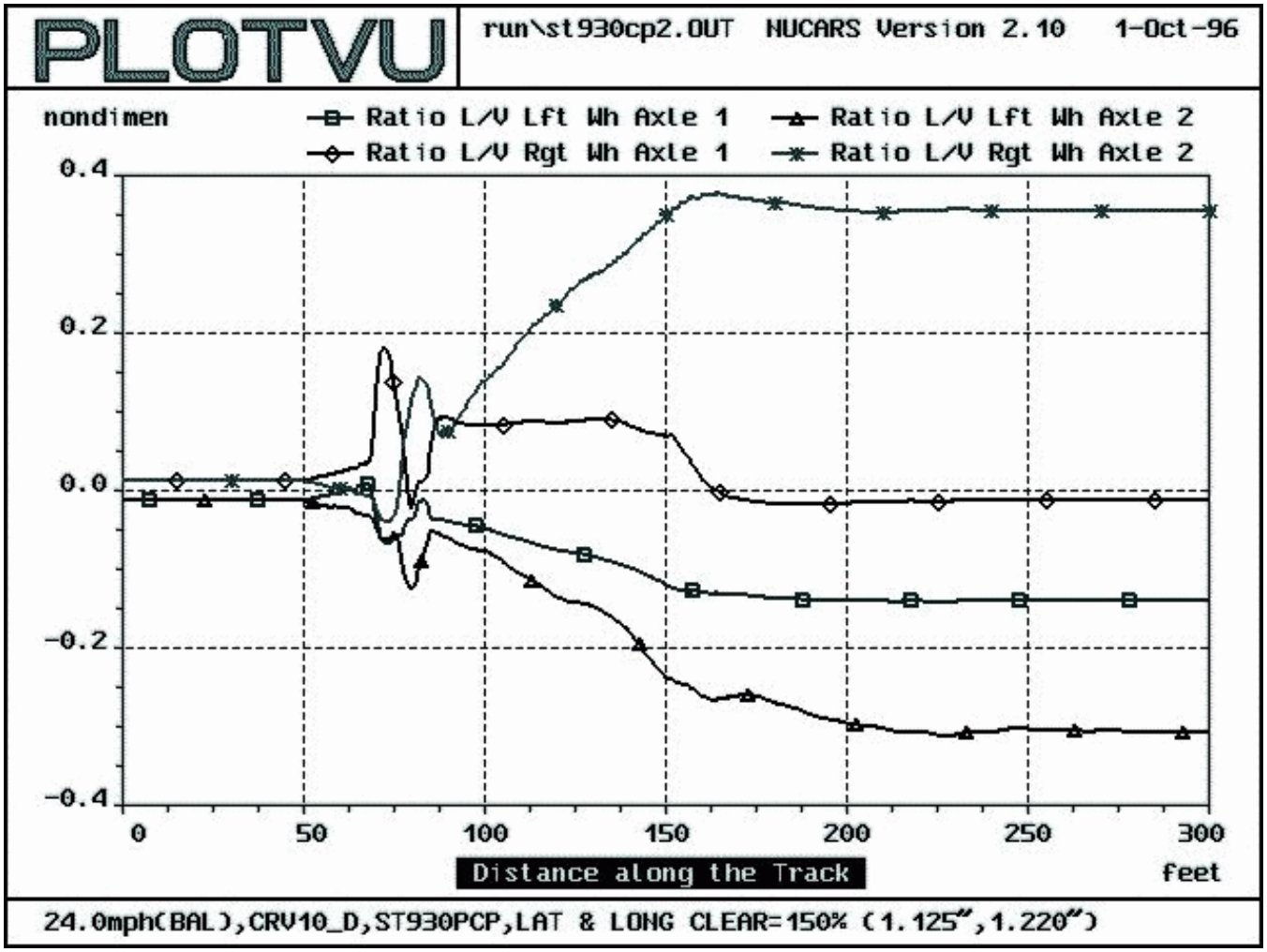

Figure 5.46 Wheel L/V ratios in 10° curve for 150% clearances (Lat=1.125" & Long=1.220")

5.2.6 Conicity

The conical wheel profile causes a wheelset to yaw about the vertical axis due to lateral motion generating a difference in the wheel rolling radii. The greater the tread angle, called conicity, the greater the radii difference for a given lateral displacement. Conversely, larger wheel conicity requires less lateral motion to generate a specific radii difference. As a result, increasing the conicity of a wheelset will improve its steering ability and improves the curving performance of a steerable truck. To test the sensitivity of the model's curving performance to wheel conicity, runs with increased conicities of 0.1 (1:10) and 0.2(1:5) are compared with runs using the baseline conicity of 0.05 (1:20). The results from these runs are summarized in Tables 5.11 and 5.12. Figures 5.47 to 5.50 show the lateral axle displacement and wheel L/V ratios for the runs with conicities of 0.1 and 0.2.

In Table 5.11, the angle of attack of the lead axle decreases with increased wheel conicity. When the wheel conicity is increased from 0.1 to 0.2, the angle of attack changes from -0.008 degrees to -0.002 degrees. This results in the L/V ratio on the outside wheel of the lead axle changing from -0.137 to -0.114. The results for the 20° curve, shown in Table 5.12, are similar. The lead axle angle of attack decreases from 0.781° to 0.751° when the conicity is increased from 0.1 to 0.2. This results in the L/V ratio on the outside wheel of the lead axle dropping from -1.037 to -1.013. This improved axle alignment and decreased L/V ratio translates to improved curving performance and a reduced likelihood of derailment. Thus, increasing the wheel conicity

has increased the curving performance of the locomotive and reduced its tendency toward derailment.

Table 5.11 Results for conicity variation in 10° curve.

	Lat Axle 1 (in.)	Angle of Attack (deg.)	Wheel L/V Axle 1 ()	Axle L/V Axle 1 ()
Conicity=0.05 (Baseline)	0.359	-0.018	0.140	0.153
Conicity=0.1	0.360	-0.008	0.137	0.183
Conicity=0.2	0.341	-0.002	0.114	0.170

Table 5.12 Results for conicity variation in 20° curve.

	Lat Axle 1 (in.)	Angle of Attack (deg.)	Wheel L/V Axle 1 ()	Axle L/V Axle 1 ()
Conicity=0.05 (Baseline)	0.597	0.824	0.820	1.262
Conicity=0.1	0.685	0.781	1.037	1.648
Conicity=0.2	0.674	0.751	1.013	1.610

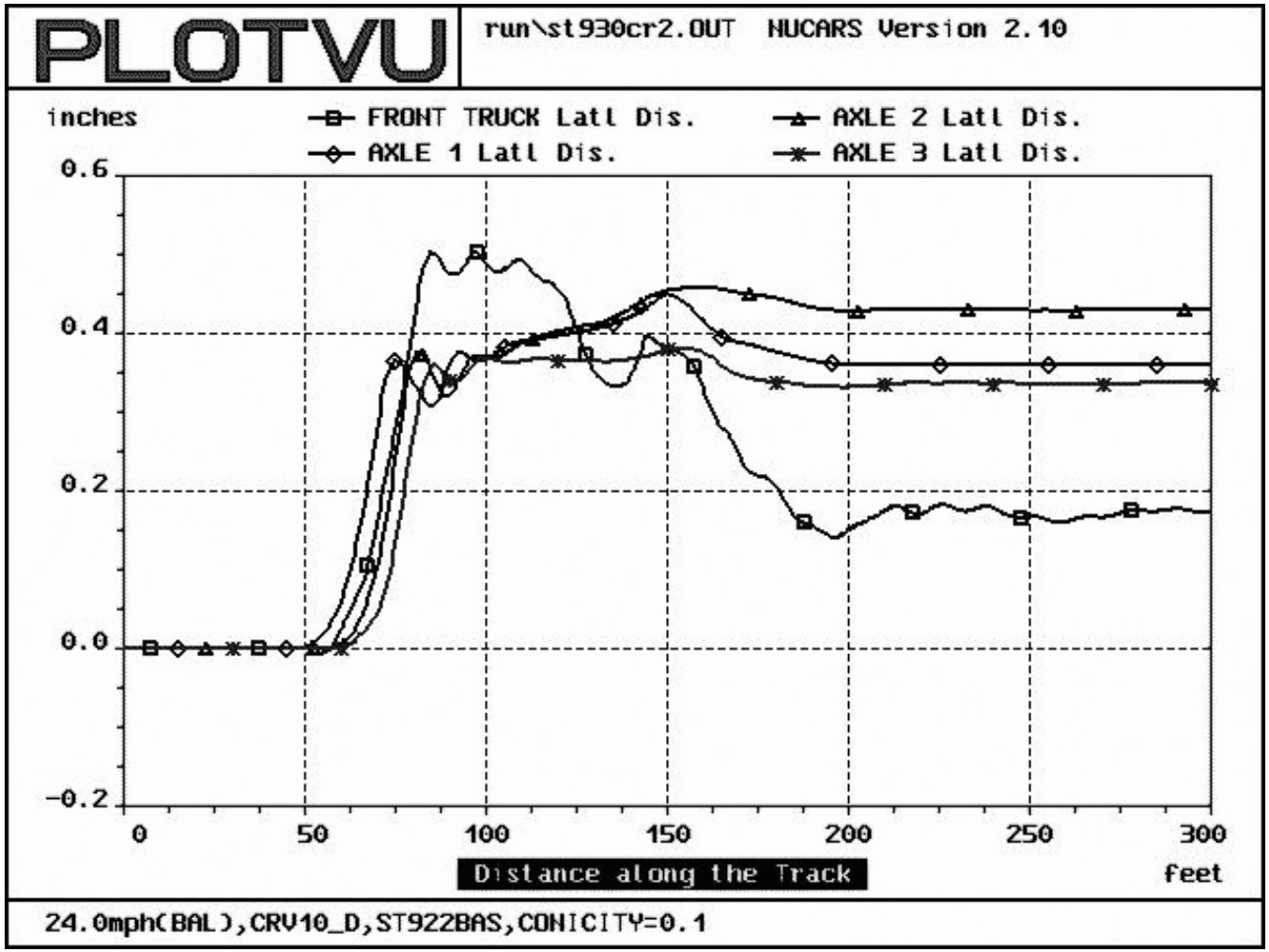

Figure 5.47 Lateral displacements in 10° curve for conicity of 0.1 (1:10)

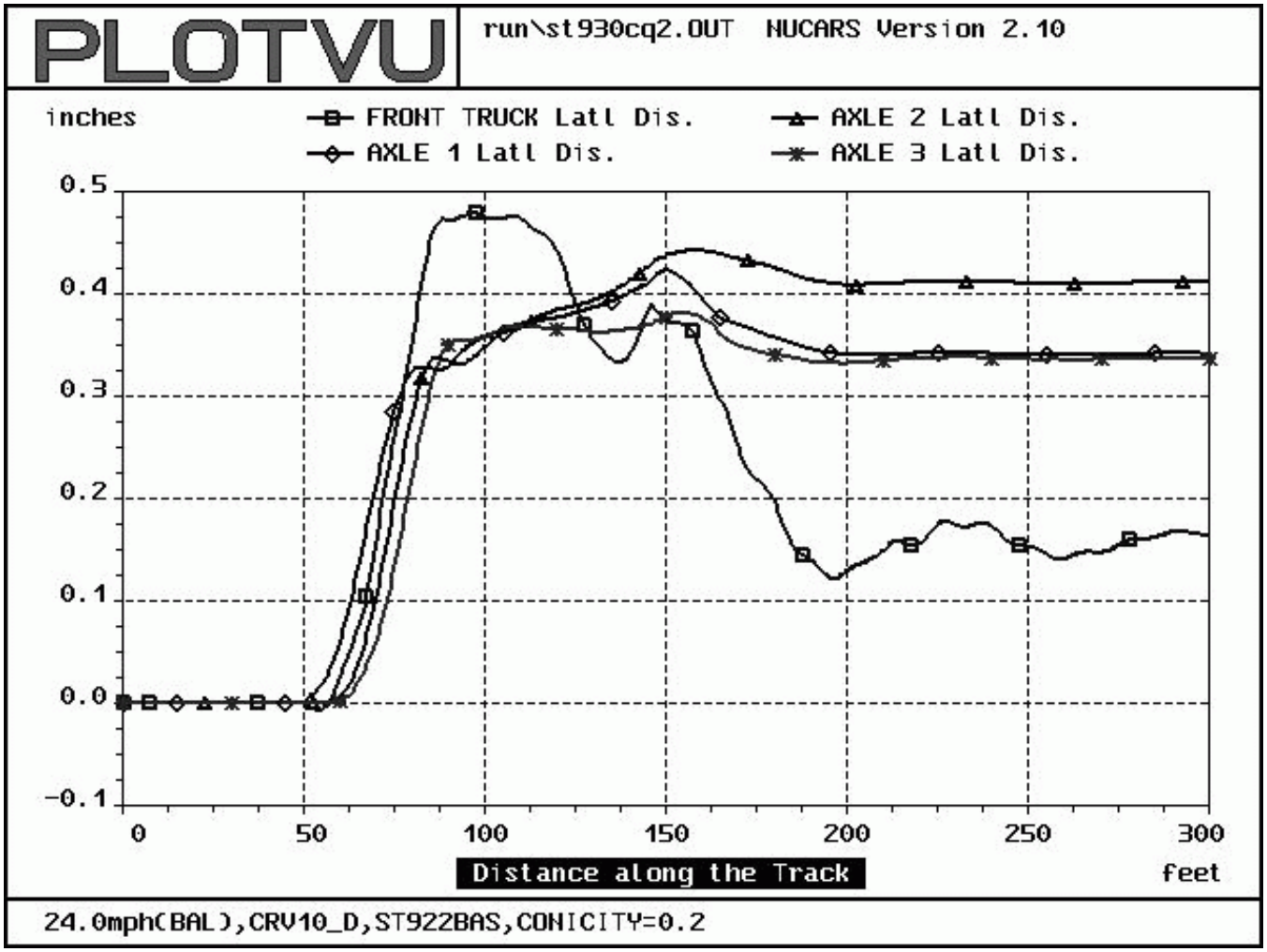

Figure 5.48 Lateral displacements in 10° curve for conicity of 0.2 (1:5)

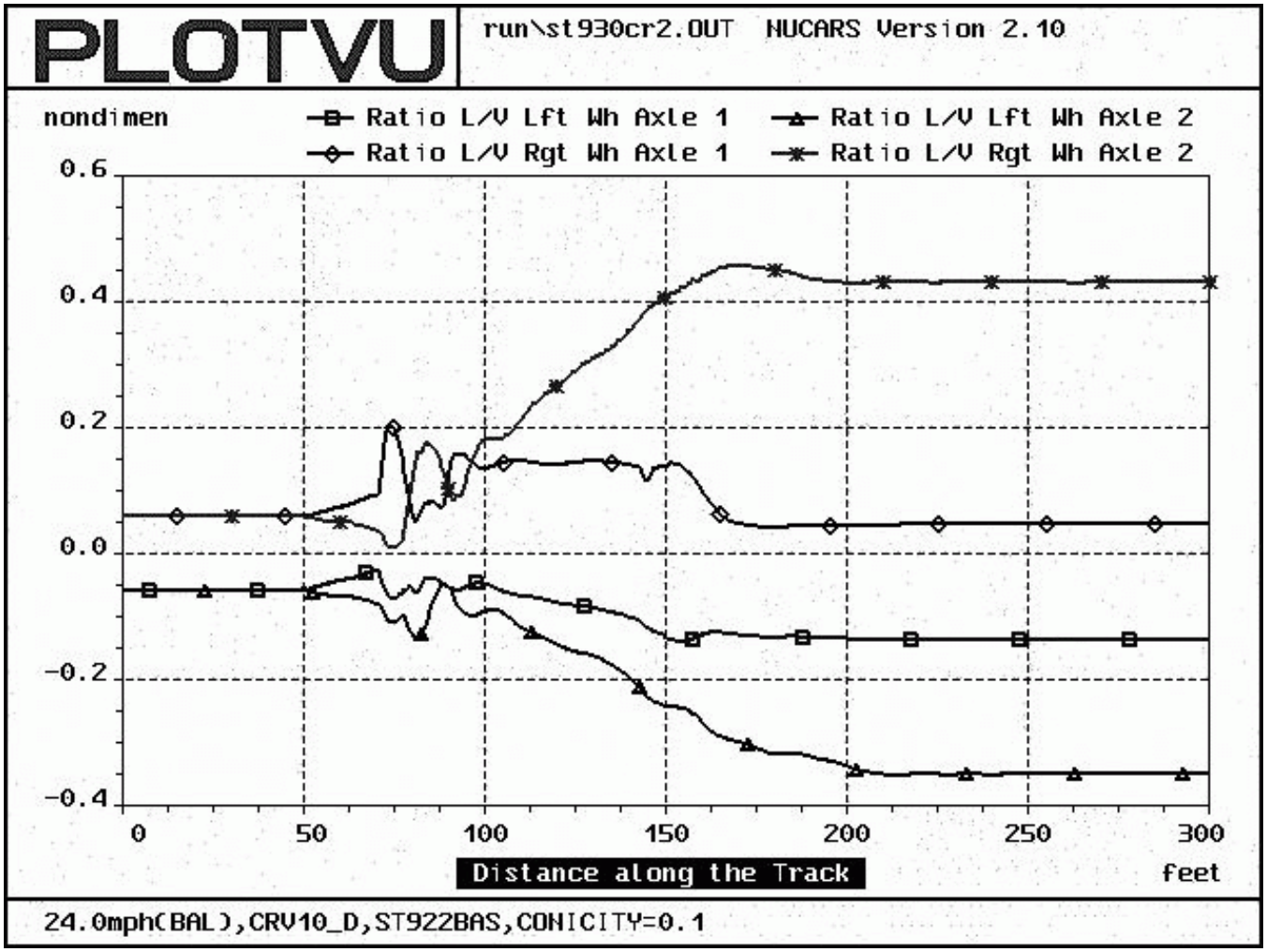

Figure 5.49 Wheel L/V ratios in 10° curve for conicity of 0.1 (1:10)

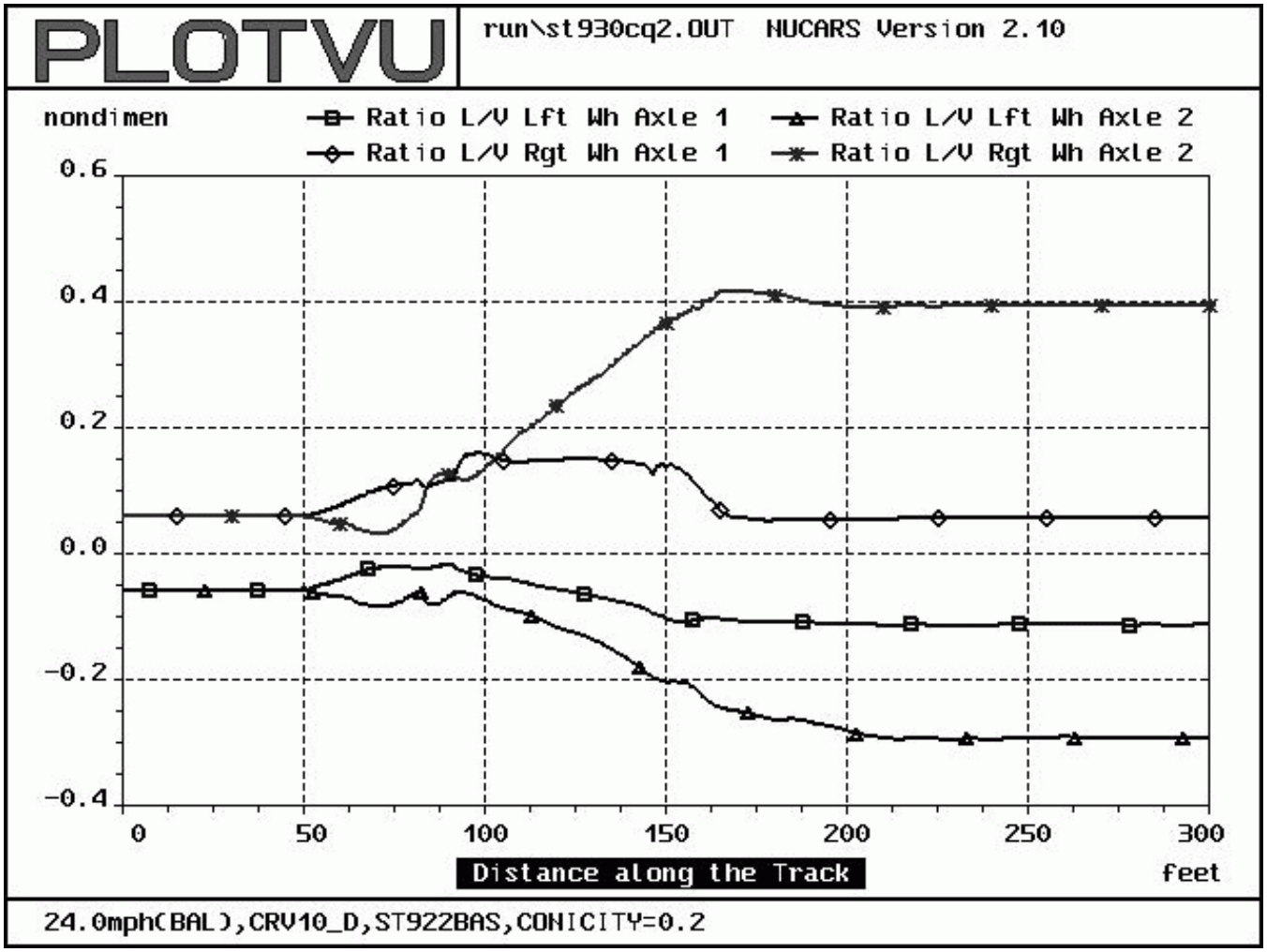

Figure 5.50 Wheel L/V ratios in 10° curve for conicity of 0.2 (1:5)

Chapter 6

Conclusions

Dynamic modeling with computers is useful to the rail industry. It reduces the costs associated with testing and allows improved performance tuning. The software package NUCARS has been used extensively to model rail freight cars, but its use on freight locomotives has been limited. A freight locomotive was effectively modeled in this project using NUCARS. The results from tangent and curved track simulation runs agree closely with a locomotive's typical behavior. Additionally, the results agree with the results obtained during experimental testing of the locomotive.

Parametric tests on tangent and curved sections of track have shown that some suspension characteristics affect the model's performance, while other characteristics have almost no effect. These tests investigated only a single parameters effect, and may not be applicable when several parameters are changed. On tangent track, the conical wheel profile leads to axle and truck hunting. This in turn can lead to rail damage, passenger discomfort, and possible derailment. Raising the critical speed for the onset of hunting lessens component and rail wear and reduces the chance of derailment. The tangent track parametric tests showed that damping is beneficial to hunting stability. Adding lateral damping and yaw damping to the locomotive increases the critical speed where hunting begins. The presence of primary damping on the axles and angling the dampers inward also increased the critical hunting speed. In both cases, the baseline values achieved the highest critical speed.

Two parameters negatively impacted hunting stability. Since wheel conicity is the cause of axle hunting, increasing the conicity increases the tendency to hunt and is harmful to the locomotive's tangent track stability. The presence of lateral stiffness between the axles due to the inter motor links causes them to hunt together. This increases the magnitude of the displacements and decreases hunting stability.

For curving, the clearance between the axles and truck frame are important. Limiting the axle clearances causes the truck to curve similarly to a conventional straight truck, with increased angles of attack and L/V forces. As a result, curving performance is degraded. Wheel conicity improves the tendency of the axles to align with the track. Increasing wheel conicity reduces the axle angle of attack and L/V ratios and aids the locomotive in curving. The lateral stiffness of the inter motor links and inter axle links has little effect for the curvatures tested.

Use of the NUCARS model to conduct parametric testing has shown which values will improve the tangent track stability and curving ability of the locomotive. It has also been substituted for costly and time consuming experimental testing. By reducing the complexity of conducting dynamic testing, NUCARS will allow more configurations to be tried. In addition, it will permit greater suspension tuning through component selection. Thus, using NUCARS to model freight locomotives, many of the same advantages found in modeling freight cars can be achieved.

Glossary

Bogie: see truck.

Bolster: a frame used above some trucks to connect to the platform and allow relative yaw between these bodies.

Center Links: rigid longitudinal links connecting the center axle to the truck frame to transmit longitudinal traction and braking forces. The center links are oriented parallel to the truck center line and prevent axle yaw while allowing lateral motion.

Center Pins: pins connecting the platform to the trucks and transferring lateral and longitudinal loads while allowing relative yaw to occur.

Coordinate Frame: reference used to describe motion. Defined as:

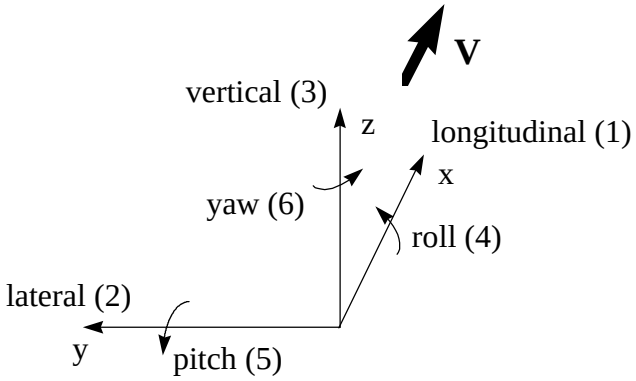

Curvature: the amount of bend in a section of track. Curvature is specified as the angle subtended by a 100' chord, as shown in Figure A2. This gives the relation between curvature, D, and curve radius, R, as:

$$\sin(D) = \frac{100'}{R} \qquad \text{(A1)}$$

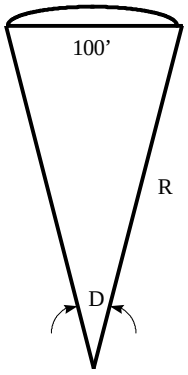

Degree of Freedom: direction along or about an axis in which motion is allowed. Degrees of freedom assigned as:

1 (longitudinal) - along x-axis
2 (lateral) - along y-axis
3 (vertical) - along z-axis
4 (roll) - about x-axis
5 (pitch) - about y-axis
6 (yaw) - about z-axis

Dog Ear: body used to mount the traction links to which is able to rotate in the yaw direction with respect to the truck frame. They change the location of the traction link ends.

Gage Clearance The clearance between a wheel flange and the rail when the wheel is rolling in its nominal position.

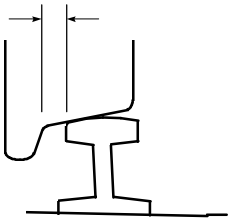

INP file: NUCARS input file, which specifies the track shape and profile.

Inter Motor Links: links that connect the motors in a truck together laterally.

Journal Box: housing for the journal bearing located at the end of an axle. The journal box is used as the connection point for axle to truck connections.

Motor Combo: an assembly composed of a motor and wheelset rigidly bolted together, with roll motion allowed between the two as the axle spins in the journal bearings.

Pedestal Leg: sliding connections between the axles and truck in a conventional truck. The pedestal legs are used to limit longitudinal motion while allowing some lateral and vertical motion.

Platform: the locomotive body including the cab and motor.

Primary Coil Springs: springs placed vertically between the axle and truck platform to transfer vertical loads between the track and bogie.

Primary Suspension: the suspension connecting the axles to the truck, composed of the axle coil springs, traction and center links, vertical dampers, and dog-bones.

RUN file: NUCARS file that specifies other files to use and the run conditions for a simulation session.

Secondary Suspension: the suspension between the trucks and the platform, composed of the center pins, lateral and yaw dampers, and side bearer pads.

Side Bearer Pad: pads which sit between the platform and truck and resist vertical motion (compression) while allowing some lateral and longitudinal motion (shear).

Steering Links: links connecting the end axles of a truck and forcing them to yaw in opposite directions to conform to the shape of a curve.

Super elevation: difference in vertical position between the right and left rails of the track. Super elevation is assigned as roll about the x-axis. A positive super elevation specifies that the left rail is higher than the right rail.

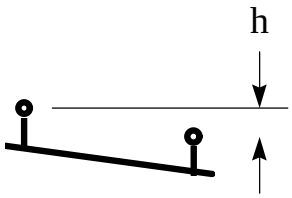

SYS file: NUCARS file which specifies the models physical configuration, including the properties of all bodies and connections.

Tangent Track: straight track with little change in the lateral direction.

Taping Line The line of rail contact on the tread of a wheel.

Track Gage: width of a track as measured between the rail heads.

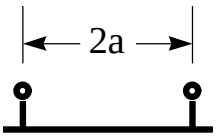

Traction Links: rigid longitudinal links used to connect the end axles to the truck to transmit longitudinal traction and braking forces. The mounting bushings on the ends of the traction links allow lateral and vertical motion while limiting motion in the longitudinal direction. The traction links can be oriented parallel to the track center line, or angle out with the axle mounts wider than the frame mounts to tie lateral and yaw motion together.

TRK file: NUCARS file used to specify the track profile through collected data.

Truck: a body composed of a frame and two or three motor combos that transmits forces between the rails and platform.

U-tube: axle housing to which the motor is rigidly bolted. The U-tube serves to protect the axle from impact damage and allows relative motion between the axle and motor.

Wheelset: unit composed of an axle and wheels rigidly mounted together and forced to spin at the same rate.

WRG file: (wheel/rail geometry file) NUCARS file which specifies the geometry of the wheel/rail contact.

Appendix A

AAR Chapter XI Criteria

TABLE 11.1
CRITERIA FOR ASSESSING THE REQUIREMENTS
FOR FIELD SERVICE

Regime	Section	Criterion	Limiting Value ****
Hunting (empty)	11.7.2	minimum critical speed (mph)	70
		maximum lateral acceleration (g)	1.5***
		standard deviation	0.26
Constant curving (empty and loaded)	11.7.3	95th percentile maximum wheel L/V	1.0
		or	
		95th percentile maximum axle sum L/V	1.5
Spiral (empty and loaded)	11.7.4	minimum vertical load (%)	10**
		maximum wheel L/V	1.0*
		or	
		maximum axle sum L/V	1.5
Twist, Roll (empty and loaded)	11.8.2	maximum roll (deg)***	6
		maximum axle sum L/V	1.5*
		minimum vertical load (%)	10**
Pitch, (loaded)	11.8.3	minimum vertical load (%)	10**
Yaw, Sway (loaded)	11.8.4	maximum L/V truck side	0.6*
		maximum axle sum L/V	1.5*
Dynamic curving (loaded)	11.8.5	maximum wheel L/V	1.0*
		or	
		maximum axle sum L/V	1.5**
		maximum roll (deg)***	6
		minimum vertical load (%)	10**
Vertical curve	11.9.2	to be added	
Horizontal curve	11.9.3	to be added	

* Not to exceed indicated value for a period greater than 50 milliseconds per exceedence.
** Not to fall below indicated value for a period greater than 50 milliseconds per exceedence.
*** Peak-to-peak.
**** See Paragraph 11.5.2.1 for allowable instrumented wheelset error bands.

Appendix B

Angle of Attack Calculations

To determine the angle of attack of the lead axle in a 20° curve for both a steerable truck and a conventional straight truck, we must first calculate the curve radius:

$$\sin 20^\circ = \frac{100 \text{ feet}}{R}$$

$$R = 287.94 \text{ ft}$$

$$= 3455.26 \text{ in}$$

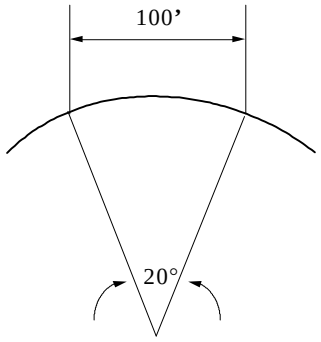

Figure A1 Definition of curvature

Next, we calculate the angle between the center of the truck and the center of the lead axle (referred to as the curve angle) of the conventional truck with pedestal liners.

For a conventional B-truck

Curve angle:

Axle lead=51"

R=3455.26"

sin(curve angle)=(Axle lead)/R

curve angle = 0.012 radians

= 0.85°

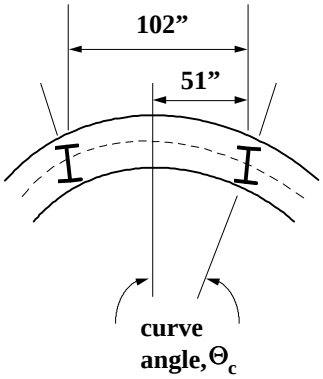

Figure A2 Angle of attack for a straight B-truck

Using the pedestal liner clearance and the truck geometry, we calculate the maximum rotation of the lead axle.

lead axle yaw:

pedestal liner clearance
new: L= 0.03”
worn: L= 0.23”
1/2 axle width, a = 39.5”

$$a = \sin^{-1}\left(\frac{\textbf{clearance}}{\textbf{39.5}}\right)$$

$$= \sin^{-1}\left(\frac{0.03}{39.5}\right) = 0.05 \quad \textbf{new pedestal liners}$$

$$= \sin^{-1}\left(\frac{0.23}{39.5}\right) = 0.34 \quad \textbf{worn pedestal liners}$$

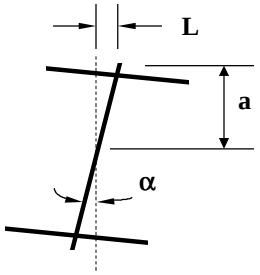

Figure A3 Conventional Axle Clearances

The minimum angle of attack of the wheels of the lead axle is then equal to the track curve angle minus the lead axle yaw rotation.

angle of attack:

angle of attack = curve angle - axle yaw
= 0.85°- 0.05°= 0.80 new pedestal liners
= 0.85°- 0.34°= 0.51 worn pedestal liners

For comparison, we calculate the yaw of the lead axle of the steerable truck, which allows us to determine the angle of attack of the wheels and rail.

For a steerable truck

curve angle:

Axle lead=79"
R=3455.26”

sin(curve angle)=(Axle lead)/R

==> curve angle = 1.31°

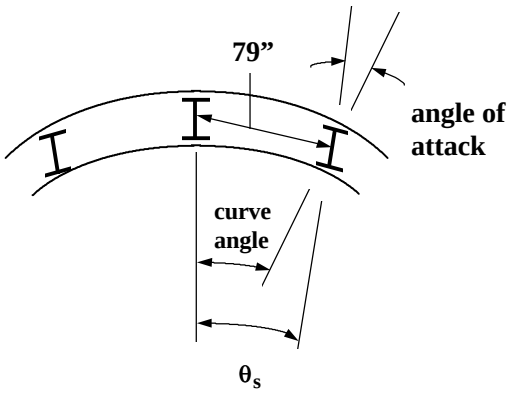

Figure A4 Angle of Attack for Steerable 3-Axle Truck

lead axle yaw:

α_u = understeering = 25% = 0.25
(according to steerable truck tests)
α = curve angle (1 - α_u)
α = 0.98°

angle of attack:

angle of attack = curve angle - axle yaw

= 1.31° - 0.98°

= 0.33°

	Angle of Attack		Critical L/V Ratio
	New Pedestal Liners	Worn Pedestal Liners	
Steerable Truck	**0.33**	**0.33**	**1.10**
B-Truck	**0.80**	**0.51**	**0.95 - 1.05**

Figure A5 Angle of attack comparison in 20° curve

References

1. de Pater, A.D., "The Equations of Motion of a Single Wheelset Moving Along a Perfect Track, Vehicle System Dynamics, Suppl. to V17, pp. 287-299, 1987

2. Knudsen, C., Slivsgaard, E., Rose, M., True, H., Feldberg, R., "Dynamics of a Model of a Railway Wheelset," Nonlinear Dynamics, V6, pp. 215-236, 1994

3. Fujioka, T., "Generic Representation of Primary Suspensions of Rail Vehicles," Proc. 11th IAVSD Symp., Vehicle 18, pp. 233-247, 1989

4. Balda, M., "Evaluation of Three-Axle Bogie Dynamics of an Electric Locomotive," Vehicle System Dynamics, Suppl. to V17, pp. 41-44, 1987

5. Arslan, A.V., "The Development and Evaluation of a Six-Axle Tangent Track Locomotive Model," Proc. 8th IAVSD Symp., pp. 15-28, 1983

6. Singh, S.P., Garg, V.K., "Nonlinear Dynamic Curving Model of a Six Axle Locomotive," Proc. 8th IAVSD Symp., pp. 606-619, 1983

7. Blader, F.B. , Elkins, J.A., Wilson, N.G., Klauser, P.E., "Development and Validation of a General Vehicle Dynamics Simulation (NUCARS)," IEEE/ASME Joint Railroad Conference, Paper # 89CH2749-0, pp. 39-46, 1989

8. Ahmadian, M.A., DeLorenzo, M.W. "NUCARS Modeling of Locomotive Bogies," Rail Transportation 1996, ASME Rail Transportation Vol. 12, pp. 49-54, 1996

9. Choromanski, W., Chudzikiewicz, A., Kisilowski, J., "Analysis of Parametric Sensitivity of the Mathematical Models that Describe Lateral Dynamics of a Railway Vehicle," Vehicle System Dynamics, Suppl. to V17, pp. 77-85, 1987

10. Richard, J.A., "Influence of Linkage Between the Front and Rear Axles on the Transversal Stability of a Railway Car with Nine Degrees of Freedom," Proc. 8th IAVSD Symp., pp. 436-448, 1983

11. Dukkipati, R.V., "Parametric Sensitivity of the Hunting of a Freight Car Truck on the NRC Curved Track Simulator,' Trans. CSME, V18, N2, pp. 147-164, 1994

12. Weinstock, H., “Wheel Climb Derailment Criteria for Evaluation of Rail Vehicle Safety,” ASME Paper #84-WA/RT-1, 1984 ASME Winter Annual Mtg.

13. Gilchrist, A.O., Brickle, B.V., “A Re-examination of the Proneness to Derailment of a Railway Wheelset,” Journal Mech. Engr. Science, v18, n3, pp. 131-141, 1976

14. Blader, F.B., “Assessing Proximity to Derailment from Wheel/Rail Forces: a Review of the State of the Art,” ASME Rail Transportation, V3, pp. 179-188, 1989

15. Garg, V.K., Dukkipati, R.V., “Vehicle Stability and Curve Negotiability Criteria” from Dynamics of Railway Vehicle Systems, Academic Press, 1984

16. Elkins, J.A., Carter, A., “Testing and Analysis Techniques for Safety Assessment of Rail Vehicles: The State of the Art,” Vehicle System Dynamics, v22, n3-4, May-July 1993, pp. 185-208

17. Elkins, J.A., Gostling, R.J., “A General Quasi-static Curving Theory for Railway Vehicles,” The Dynamics of Vehicles on Roads and on Tracks, Proceedings of the 5th VSD Symposium, Sept. 17-23, 1977, pp. 388-406

18. Chercas, D.B., “Determination of Railway Wheel Climb Probability Based on the Derailment Coefficient,” Journal of the Franklin Institute, Vol. 312, No. 1, pp.31-40, July 1981

Vita

Michael DeLorenzo was born in Chelsea, MA on May 27, 1969. After living in Connecticut and Florida, his family moved to Richland, WA in 1978. There he attended Hanford Elementary, Junior and High Schools. After graduation in 1987, he attended the University of California at Davis and completed his Bachelor of Science in Mechanical Engineering in 1994. During this time, he worked at internships at RANDEL Associates and Kaiser Engineers Hanford. In addition, he was involved in the Off-Road Bicycle Research Program, where he evaluated the performance of suspension hubs for mountain bikes. Next, he journeyed to Virginia Tech to pursue his Master of Science in Mechanical Engineering. There he focused his studies on Control Systems and Vehicle Dynamics, with his research focusing on the dynamics of rail vehicles. After receiving his degree in May 1997, he will move to northern California to work on satellite attitude control for Lockheed Martin Missiles and Space and pursue his passion for mountaineering.